Steam Generation in Line-Focus Solar Collectors: A Comparative Assessment of Thermal Performance, Operating Stability, and Cost Issues

L. M. Murphy
E. Kenneth May

April 1982

SERI ●

PREFACE

This work is part of an overall effort at the Solar Energy Research Institute (SERI) to reduce solar thermal system and component costs. The effort was carried out under Task 1006.00 and was supported by the Research and Technology Branch, Solar Thermal Division, U.S. Department of Energy (DOE), as part of the overall technology development effort in the Solar Thermal Program.

The authors would like to acknowledge Virgil Dugan, Walt Schimmel, and Mike Corradini (Sandia National Laboratories), for both encouragement in the pursuit of this research effort and for numerous helpful discussions. Special thanks are also extended to Randy Gee (SERI) for very useful comments during the preparation of the report and to Doris Gundersen, a summer intern, for valuable assistance in setting up the graphics routines. We would like to thank Ron Pederson (Texas Tech University) for his work on two-phase stability (developed during his summer stay at SERI), on which the stability analysis in this report is based. Finally, we would like to thank the numerous reviewers from various institutions who reviewed the draft report.
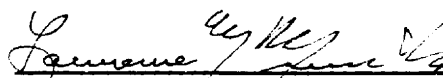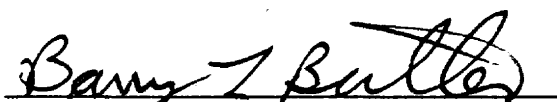
Lawrence M. Murphy, Leader
Technology Development Task

E. Kenneth May, Staff Engineer

Approved for

SOLAR ENERGY RESEARCH INSTITUTE

John Thornton, Chief (Acting)
Thermal Systems and Engineering Branch

Barry L. Butler, Manager
Solar Thermal and Materials Research Division

S≡RI ✳

SUMMARY

This report assesses the engineering and system benefits that could result from using direct steam generation (in situ boiling) in line-focus solar collector systems. In particular this work provides a systematic comparison of an in situ boiling system with the more traditional steam-flash system and with an unfired boiler system using a heat-transfer fluid. Emphasis was placed on a detailed thermal and fluid transport comparison. The report also contains a preliminary cost analysis, as well as an assessment of operational and maintenance issues such as freeze protection, scaling, control, and safety. Analytical comparisons are made for a baseline collector system with 4686 m^2 (50,420 ft^2) of aperture area.

Following a brief discussion of current technology and some specific problem areas, this study provides a review of the most current relevant research on boiling phenomena to establish guidelines for flow regimes, together with state-of-the-art correlations for boiling heat transfer and pressure drop response and for stability considerations. A description is given of the detailed, steady-state performance model, that is used to derive temperatures and pressures in the collector system and piping loops. Annual performance predictions are made using the system response characteristics defined by the steady-state model, and using an averaging technique analogous to those developed by Rabl (1981). Analytical results are presented for a wide range of insolation levels, mass flow rates, and steam delivery temperatures for each of the three types of solar systems.

The steady-state performance model has a modular format with very flexible field and collector geometry capabilities, and is capable of simulating the performance of either open or closed loop solar systems. The model uses easily modified state-of-the-art heat transfer and pressure drop correlations, and an ASME steam/water library equation of state. A detailed thermal and pressure drop analysis of the receiver tube is provided by division of the tube along its length into an arbitrary number of nodes. Two receiver models are available. One model is based upon a detailed thermal network in which only basic physical properties and dimensions of the receiver subcomponents are supplied by the user. This allows detailed analysis of conditions through the cross section of the receiver tube. The second model is based on a standard empirical efficiency curve measured for a good, state-of-the-art collector. This model provides less detail than the first, but is faster and easier to use.

Major conclusions from this study follow.

- In terms of thermal performance, direct-boiling solar steam systems appear considerably more efficient than flash or unfired boiler systems over a wide range of operating conditions. Specifically, direct-boiling systems should deliver up to 13% more net energy on an annual basis than an unfired boiler system using a heat-transfer oil, and up to 12% more net energy than a flash system. Furthermore, direct-boiling systems should typically have 5% to 10% instantaneous efficiency advantages over more conventional systems. The annual performance improvement for a north-south oriented collector field is illustrated in Fig. S-1.

SERI
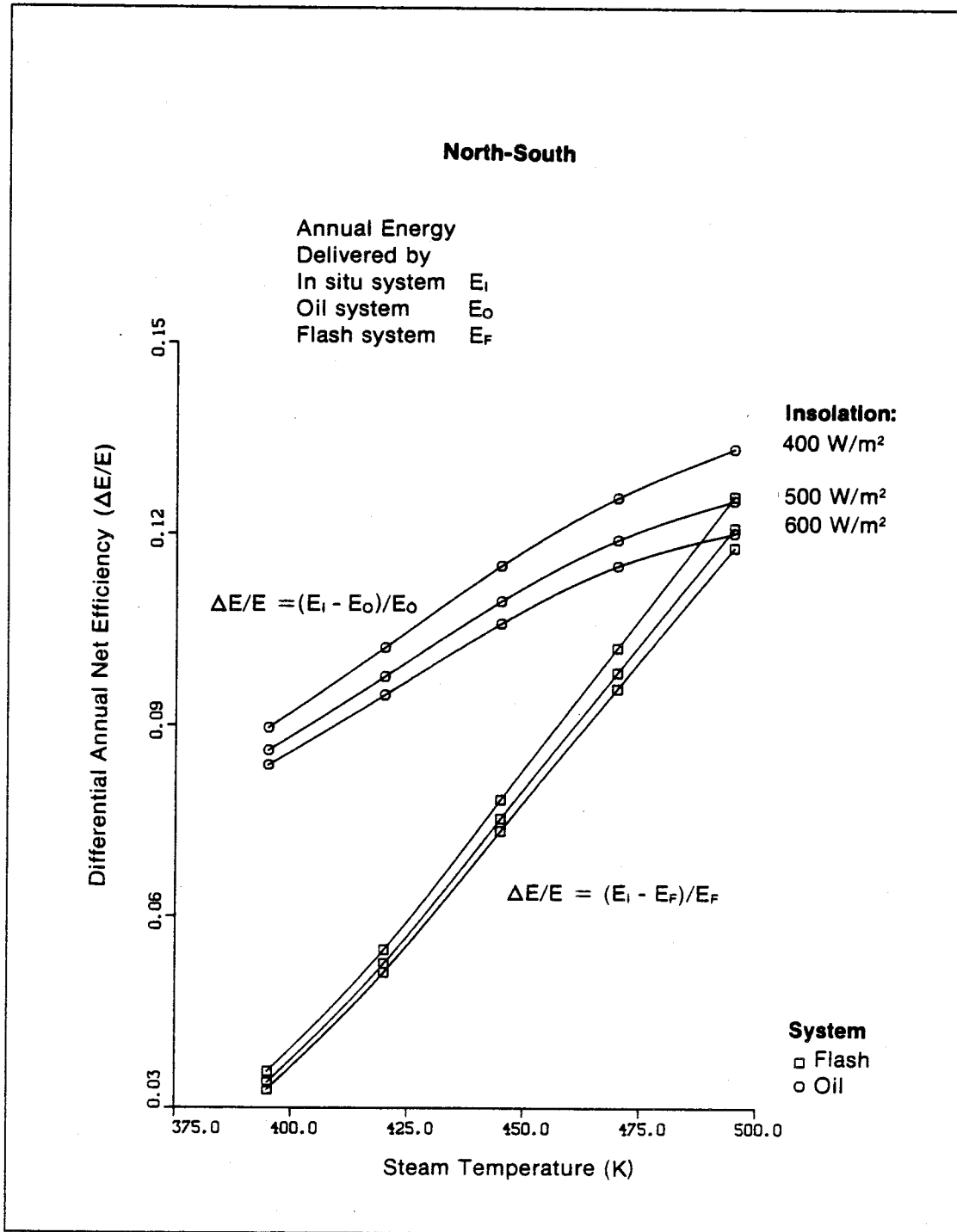
Figure S-1. Relative Annual Delivered Energy Benefit Using In Situ Boiling vs. Steam Delivery Temperature

- Predicted performance advantages of in situ systems over the more conventional systems result from the synergistic effect of a number of phenomena including differences in collector operating temperature, heat transfer coefficients, parasitic pumping power, and collector operating time. Principal reasons for the performance advantage of in situ systems over unfired boiler systems are lower collector operating temperature and a lower associated collector system cut-off temperature. Direct boiling systems are more efficient than flash systems mainly because of much lower parasitic pumping power and lower collector operating temperatures especially at high fluxes.

- Incident solar flux has a greater impact on system performance than the other two independent system variables (mass flow rate and steam delivery temperature). The efficiency of all three systems drops off dramatically at low fluxes. At high insolation levels, the differential temperature across the unfired boiler system receiver becomes quite large, and the collector outlet temperature approaches the operating limit of the heat-transfer fluid.

- System performance is always dominated by the choice and characteristics of the solar collector. The simplified collector model, based on measured experimental data, predicts performance levels that strongly agree with data predicted by the detailed collector model (within 1%).

- The relative benefit of the in situ system compared to flash and unfired boiler systems increases under conditions least favorable for solar energy collection (i.e., low insolation levels, elevated steam temperatures, increased latitude, and low ambient temperatures). This situation results because lower temperature operations reduce the collector cut-off flux (the minimum insolation level resulting in net energy collection).

The stability analysis identified five types of instability that could arise during operation of the direct-boiling system. The only instability that could occur would result from density-wave oscillations, and then only at the lowest steam-delivery temperatures. These oscillations can be eliminated by a slight increase in flow restriction at the inlet to individual collector rows. Flow restrictions required for uniform interrow flow distribution will most likely obviate any potential stability problems. Thus, the operation of a direct-boiling steam system should not produce mechanical vibrations or tube burn-out problems that could damage the selective surface of the receiver. In fact, since deterioration of the selective surface appears to be temperature dependent, degradation will probably be more rapid in higher temperature steam-flash and unfired boiler systems.

The report provides a cursory assessment of capital cost variations between the three systems, followed by a qualitative investigation of control, freeze protection, scaling, corrosion, and safety issues. Results of the cost study indicate that capital costs may be reduced by as much as 15% when compared with an unfired boiler system, primarily because the unfired boiler, expansion tank and costs for the heat-transfer fluid are eliminated. An in situ system has cost savings over a flash system because the flash valve is eliminated and a smaller pump can be used. But the initial system cost advantage does not appear as great as in the unfired boiler system. In total, an in situ steam system could reduce the cost of delivered energy by over 25% compared to an unfired boiler system.

Besides the quantitative performance benefits and the potential capital cost reductions, other advantages identified for in situ systems are: the ease of control over more conventional flash systems, the ease of heat-transfer fluid handling and safety enhancement (including the elimination of recurrent fire dangers) over unfired boiler systems, and the applicability to food processors who will not use heat-transfer fluids in systems to generate steam because of potential product contamination. The safety of high-temperature water systems can be handled by automated shutdown procedures and by the restriction of personnel access to the operating collector field, where flexhoses pose the greatest safety hazard. Corrosion and scaling problems can be controlled by conventional water treatment practices.

A major recommendation resulting from this analysis is to pursue a comprehensive costing study to more accurately estimate the economic benefit of using direct-boiling systems. In addition, simple, low-cost experiments defined as part of this study can and should be run at the Solar Energy Research and Applications in Process Heat (SERAPH) facility in FY 1982 to verify important performance and stability findings established in FY 1981, including the question of freeze protection. Based on a successful SERAPH experiment, an industrial process heat (IPH) upgrade project of an existing steam-flash system offers an excellent opportunity to further demonstrate the concept at minimal cost. This demonstration should be pursued in cooperation with industrial users and collector manufacturers.

A further extension of the study is warranted to extend the analysis beyond IPH applications. The advantages of the direct-boiling concept increase with temperature. Higher temperature operations up to the mechanical and temperature limitations of line-focus collectors would allow the production of electric power using water or another working fluid at relatively high thermodynamic efficiency.

TABLE OF CONTENTS

TABLE OF CONTENTS (Continued)

TABLE OF CONTENTS (Concluded)

LIST OF FIGURES

LIST OF FIGURES (Continued)

LIST OF FIGURES (Continued)

LIST OF FIGURES (Continued)

LIST OF FIGURES (Concluded)

LIST OF TABLES

NOMENCLATURE

A	Flow area (m^2)
A_c	Area of collectors (m^2)
C_p	Specific heat at constant pressure (J/kg K)
C_f	Fanning friction coefficient (dimensionless)
d	Pipe diameter (m)
f	Moody friction factor [dimensionless ($f = 4C_f$)]
g	Acceleration due to gravity (9.81 ms^2)
G	Mass velocity, (kg/m^2s)
Gr	Grashof number = $g\beta\Delta T\, d^3/\nu^2$ (dimensionless)
h	Heat-transfer coefficient (W/m^2K)
H	Enthalpy (J/kg)
I	Insolation (W/m^2)
k	Thermal conductivity (W/m K)
m	Mass flow rate (kg/s)
Nu	Nusselt number = hd/k (dimensionless)
P	Pressure (N/m^2)
Pr	Prandtl number = $C_p\mu/k$ (dimensionless)
Q	Volumetric flow rate (m^3/s), Internal energy (J)
Ra	Rayleigh number = GrPr (dimensionless)
Re	Reynolds number = $\rho\, du/\mu$ (dimensionless)
t	Time (s)
T	Temperature (K)
u	Velocity (m/s)
U_{SL}	Superficial liquid velocity = Qf/A_T (m/s)

v   Specific volume (m^3/kg)

W   Work (J)

x   Length (m)

x_m Mass quality = $\dfrac{\text{mass of vapor}}{\text{mass of vapor and liquid}}$ (dimensionless)

x_v Volumetric quality = $\dfrac{\text{volume of vapor}}{\text{volume of vapor and liquid}}$ (dimensionless)

Greek Letters

α Absorptivity (dimensionless)

β Coefficient of volumetric expansions (1/K)

ε Pipe relative roughness (m)

η Efficiency (dimensionless)

μ Viscosity (kg/m s)

ν Kinematic viscosity (m^2/s)

ρ Density (kg/m^3)
        Reflectivity (dimensionless)

σ Surface tension (N/m)

Subscripts

e   Exit

f   Liquid

g   Gas

i   Inlet

NS   No slip

o   Outlet

T   Total

SECTION 1.0

INTRODUCTION

This report assesses the engineering and system benefits of the direct (in situ) generation of steam in line-focus solar collectors. If realized, the expected benefits will improve the cost/performance measure of line-focus technologies to produce steam through better performance and system cost reductions. Thus, this work supports efforts to reduce the cost of solar collector systems and components to the point where the delivered cost of solar energy is competitive with conventional fuels.

1.1 THE DIRECT-BOILING CONCEPT

Allowing water to boil directly in the receiver tube of a line-focus collector constrains the maximum collector temperature to the steam delivery temperature. In contrast, the steam-flash and unfired boiler system using a heat-transfer oil currently employed to generate steam, operate at collector temperatures considerably higher than the required steam conditions. (A collector and system performance penalty is associated with increased operating temperature.) In addition, the vaporization process of the direct-boiling system can greatly reduce circulating fluid-flow rates (and hence pumping power) compared to systems based upon sensible heat transfer. Further potential benefits of direct-boiling systems include simplified system control when compared with flash systems and improved handling and safety characteristics of the working fluid when compared with heat-transfer oil systems. These benefits were recognized in a conceptual design of an industrial solar system (Gupta 1979). However at that time, the direct-boiling concept was unproven, which precluded its use in an industrial field test of a line-focus collector system. (In contrast, steam/water receivers have been successfully tested at the Sandia-Albuquerque central receiver test facility, and the concept will be employed at the Barstow "repowering" project for electric power production. However, such receivers are similar to conventional steam boilers, which operate at very high heat fluxes and are aligned vertically.) Obvious drawbacks to direct boiling in line-focus collectors include an incomplete understanding of the boiling phenomena (including stability) in horizontal tubes, the possibility of tube dryout and damage to the selective surface, the lack of freeze protection compared to heat-transfer fluid systems, and difficulty integrating thermal storage into the system.

The advantages and disadvantages of the direct-boiling concept are among those discussed in detail and quantified in this report. Future work will focus on an experimental program to demonstrate the direct-boiling concept and on the solution to the stability and freeze-protection problems, as well as on verifying the expected improvements in performance compared to existing steam-generating techniques. This evaluation is intended to assist system designers considering this concept and also to provide a basis for future programmatic efforts for line-focus collector development by DOE.

The remainder of Sec. 1.0 discusses industrial energy use and industry's predominant use of steam for low-temperature process heating. The steam-flash, unfired-boiler, and direct-generating solar steam systems are also discussed.

Section 2.0 documents the results of a literature review that was used to design the model formulated to conduct the performance comparison of the competing systems, and to analyze transport phenomena during two-phase flow of water. A detailed description of the system model is given in Appendix A. Appendix B elaborates on the literature review outlined in Section 2.0.

Section 3.0 describes the baseline solar system used for the performance comparisons. The potential benefits of the direct-boiling concept extend beyond increased performance of the solar collectors alone to the solar system as a whole. Following the system description, a brief overview of the analysis methodology is presented.

Section 4.0 gives a detailed description of the technical results of the performance analysis from both an instantaneous and long-term perspective.

Section 5.0 is a comparative analysis of the potential cost advantages in using the direct-boiling concept.

Section 6.0 discusses the potential freezing, fouling, and corrosion problems resulting from the use of water in the collector field.

Section 7.0 summarizes the analysis of the stability of two-phase flow in the collector system performed by Pederson and May (1982). Criteria developed in this report are applied to the full range of system stability operating parameters.

Conclusions and recommendations for subsequent work are provided in Sec. 8.0.

1.2 INDUSTRIAL ENERGY USE

Of the 21×10^{18} J of energy used by industry in 1976, approximately 68% was used for process heating (ITC 1977). Line-focus concentrating solar collectors operate at temperatures up to ~300°C. In this temperature range industry consumed about 4.5×10^{18} J of fuel, a major fraction of which was used to generate steam. Thus, the potential market for commercially available, line-focus solar collectors to supply steam for low-temperature industrial process heating (IPH) is very large.

A survey by Hamel and Brown (1980) compares boiler sales over the last ten years and shows that most industrial boilers that were sold operate at 0.7 to 1.4 MPa (100 to 200 psia) corresponding to steam saturation temperatures of 166° to 194°C (330° to 380°F). Such conditions permit great flexibility in supplying a variety of process temperature requirements. Fewer boilers are sold to produce steam at higher temperatures because of the rapid increase in boiler pressure at temperatures above 200°C (400°F). Above 200°C, direct process heating is generally employed, with heat-transfer oils often used for indirect heating applications.

The food industry is a major user of low-temperature IPH and is a prime candidate for the near-term, large-scale application of solar IPH systems (DeAngelis 1981). Because of the fear of product contamination, solar systems that use heat transfer oils are often eliminated from potential applications in the food industry. Solar systems using water are preferred in these applications.

2

SERI ───────────────────────────────────

1.3 CURRENT METHODS OF STEAM GENERATION IN LINE-FOCUS SOLAR COLLECTORS

To date, two methods have been employed to generate industrial process steam using line-focus solar collectors: the steam-flash concept, in which pressurized water is heated in the collector field and then flashed to steam; and the unfired-boiler concept, in which a nonfreezing, heat-transfer fluid is circulated through the collector field to generate steam through heat-exchange in an unfired boiler. Each of these systems and aspects of their operation are briefly discussed in the following subsections.

1.3.1 Steam-Flash System

A diagram of this system is shown in Fig. 1-1. Water, pressurized to prevent boiling, is circulated through the collector field and then flashed across a throttling valve into a separator. Steam is fed into the plant utility system. Boiler feedwater input maintains the level in the separator and the subcooled liquid is recirculated through the collectors. The in situ boiling concept would use a similar system configuration, without a flash valve. Subcooled water would be heated to boiling and steam would form directly in the receiver tube. System design would ensure that steam quality at the collector outlet was consistent with the operating stability of the system.

Although the steam-flash system uses water, a superior heat transport fluid, the in situ boiling system is still more advantageous. The flash system uses a sensible heat change in the working fluid, which makes the temperature differential across the collector relatively high. The rapid increase in water vapor pressure with temperature requires corresponding increases in system operating pressure to prevent boiling. Increased operating temperatures reduce the thermal efficiency of the solar collectors. Increased pressures within the system require a more robust design of collector components, such as receivers and flexhoses, and piping. The differential pressure over the delivered steam pressure required to prevent boiling is supplied by the circulation pump and is irreversibly dissipated across the flash valve. When boiling occurs in the collectors, as in an in situ boiler, the system pressure drop and consequently, electrical power consumption is greatly reduced. In addition, the latent heat-transfer process minimizes the temperature rise across the solar collector.

The flash system also presents a difficult control problem if attempts are made to reduce electric parasitic power consumption. The simplest control scheme combines a constant speed pump and a flash valve modulated to control a given pressure differential (Acurex 1980). In effect, the system pressure drop and parasitics are fixed, regardless of insolation conditions and steam production rate. A second proposed control scheme (Stauffer Chemical Co. 1979) uses a fixed control valve orifice and a measure of insolation to control pump speed. This scheme modulates system flow rate and pressure differential. Still a third design operates a constant speed pump while adjusting the modulating valve to prevent boiling through feedback control from a steam look-up table (Cherne et al. 1978). In contrast, a direct-boiling system is self-regulating; water in the receiver tube is heated to boiling and passes into the two-phase region. With a fixed pump flow rate, system pressure drop and steam quality vary directly with insolation. Collector operating temperature and pressure closely correspond to steam delivery conditions.
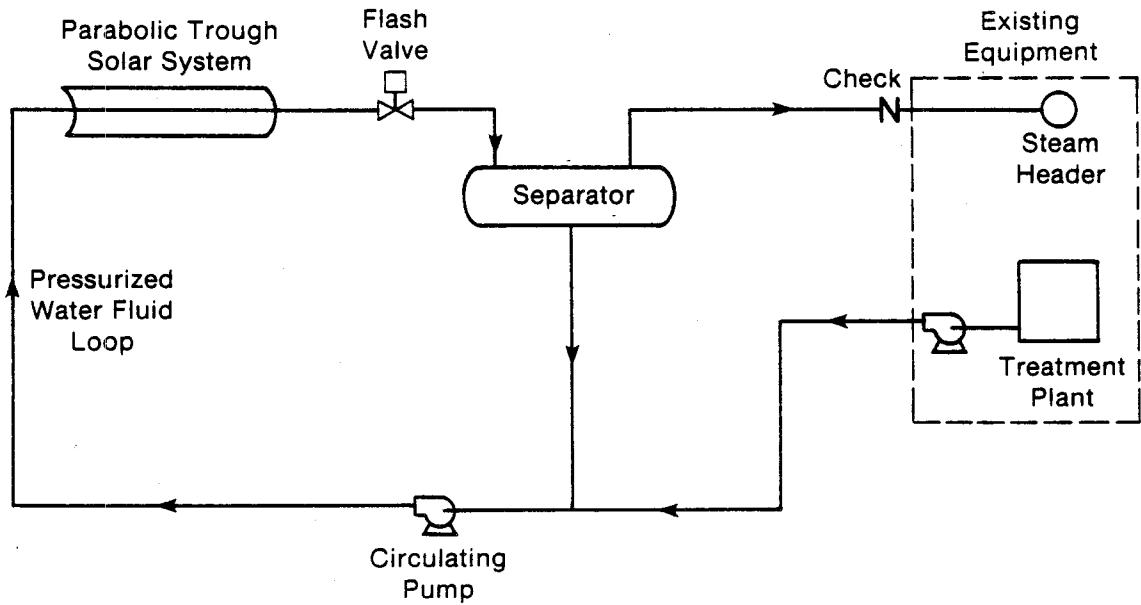
Figure 1-1. Steam Flash Generating System
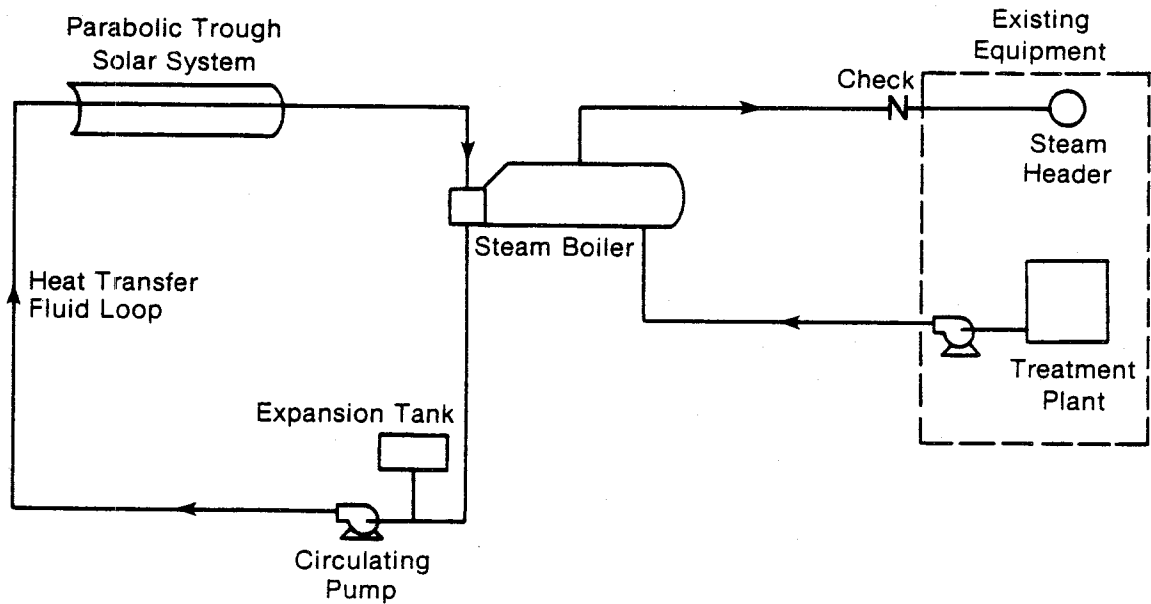
Figure 1-2. Unfired Boiler Steam Generating System

The open-loop, steam-flash, and direct-boiling systems are subject to corrosion and scaling, which can be controlled by standard industrial water treatment and maintenance techniques (see Sec. 6.0). Water systems are also subject to freezing in adverse climates; this problem is also discussed in Sec. 6.0.

1.3.2 Unfired Boiler System

A diagram of an unfired boiler solar steam system is shown in Fig. 1-2. In this system, the heat-transfer fluid can be nonfreezing and noncorrosive, system pressures are low, and control is straightforward. (A constant speed pump is generally used.) These factors largely overcome the disadvantages of water systems, and are the main reasons for the predominant use of heat-transfer oil systems in current industrial steam-generating solar systems.

The major disadvantages of the system result from the characteristics of the heat-transfer fluid. These fluids are hard to contain, and most heat-transfer fluids are flammable. Decomposition, when the fluids are exposed to air, can greatly reduce ignition-point temperatures, and leaks into certain types of insulation can cause combustion at temperatures that are considerably lower than measured autoignition temperatures. Fires have occurred in both the Willard and Coolidge irrigation solar systems, which use oil in unfired boilers, and at the Sandia Laboratories test facility. Special care must be taken in selecting gaskets, packings for valves, and mechanical seals for pumps, because at high temperatures the viscosity and surface tension of heat-transfer fluids are low, and leaks are common. Generally an all-welded system is desired; suppliers usually recomment 300-lb flanges, even though system pressures are low. A fire protection system and explosion-proof equipment may be required. Heat-transfer fluids are also relatively expensive ($2-$20/gal), a potential pollution problem, and often excluded from food industry applications.

Heat-transfer fluids have much poorer heat-transfer qualities than water. They are more viscous at ambient temperatures, are less dense, and have lower specific heats and thermal conductivities than water. These characteristics mean that larger flow rates, collector differential temperatures, and pumping power inputs are required to obtain the equivalent quantity of energy transport compared to a system using water. In addition, heat-transfer coefficients are lower, so there is a larger temperature differential between the receiver tube and the collector fluid; this effect results in reduced collector efficiency at a given fluid temperature compared with the collector efficiency at the same temperature using water.

The temperature differential required to transfer heat across the unfired-boiler heat exchanger is responsible for additional increases in collector temperatures in an unfired boiler system compared to the open-loop water systems which do not require a heat exchanger. The unfired boiler and the nitrogen-blanketed expansion tank capable of holding all of the fluid inventory generally are pressure vessels which increase costs. To prevent corrosion, steam generators use 90-10 Cu-Ni tubes. Another safety issue arises, since most failures in heat transfer fluid systems occur following cross-contamination (Dow Chemical Co. n.d.). Steam leakage into the hot oil causes a rapid increase in pressure, thus, necessitating careful sizing and venting of pressure relief valves on the solar system side of the boiler.

1.4 THERMAL STORAGE

The solar system used to compare the three steam-generating techniques includes no provision for thermal storage. The unfired-boiler system can be easily integrated into an oil/rock thermal storage system, whereas storing thermal energy as high-pressure, high-temperature water is probably more costly. However, integrating thermal storage into any collector system will greatly increase the delivered cost of solar energy. Thermal storage raises component costs and reduces performance because of the increase in collector temperatures necessary to charge storage. Initially, solar process heat systems will be economical for industrial operations that run continuously and can absorb the entire thermal output of the collector field. The number of continuously run industrial operations (such as food plants, oil refineries, and chemical plants) is sufficiently large to present a very significant market for solar steam systems. The potential reduction in delivered energy cost attainable by the application of the direct-boiling concept will reduce the time that will be required before solar steam systems can compete economically with conventional fuels. At a later date, when oil/rock storage becomes economical, other energy storage techniques (such as latent heat or chemical) that can be more efficiently integrated into a direct-boiling system may be available. Alternatively, for discontinuous industrial operations, an in situ system could be operated using a conventional steam turbine to deliver electric power to the grid when process heat is not required.

SERI ⚙ ─────────────────────────────────

SECTION 2.0

TWO-PHASE FLOW AND TRANSPORT PHENOMENA

To compare the performance of the competing solar systems and to analyze transport phenomena during two-phase water flow, a steady-state computer program was written. Independent variable inputs are system mass flow rate, insolation in the plane of the collector (shading and end effects are neglected), and steam delivery temperature.

Although the particular problem addressed here has not been studied, a considerable amount of related work is reported in the literature and was used in selecting correlations to formulate the system performance model. A short discussion of the relevant literature and its bearing on the problem is given in this section. A detailed description of the system model is provided in Appendix A. Further discussion regarding the choice of each correlation and analytical details describing their use in the system model are provided in Appendix B. Section 3.0 outlines the physical layout of the baseline solar system to complete the data inputs to the model.

2.1 FLOW REGIMES IN HORIZONTAL, TWO-PHASE FLOW

The ability to predict the distribution of liquid and gas flowing through a horizontal tube is important because the distribution affects heat-transfer rates, temperature variations, mass velocities, and system stability. To prevent damage to the selective surface, flow instabilities, and scale build-up, the surface of the receiver tube must be in contact with the liquid phase at all times. The map proposed by Taitel and Dukler (1976) (see Fig. 7-2) is used as a means to ensure that conditions within the receiver tube are within an acceptable flow regime to avoid these problems.

2.2 PRESSURE-DROP CORRELATIONS

To calculate single-phase pressure drop, the well-established and accepted Colebrook formula is used in this study (see Appendix B, Eqs. B-1 and B-2). A study of two-phase pressure drop correlations indicates, for the flow regimes and fluid properties of interest, that the Dukler "no slip" homogeneous flow model (Dukler et al. 1964) will probably give the most accurate results (see Eqs. B-3 to B-9). Using friction factors for a rough pipe surface introduces a considerable degree of conservatism into the correlation. Over the conditions studied, a rough pipe surface will increase the two-phase friction factor from 20% to 60% compared to a smooth pipe. This effect is greatest at high Reynolds numbers. The Dukler correlation is extended in a stepwise fashion to determine pressure drop in boiling flow, and the results are compared to the work of Thom (1964) for verification.

2.3 HEAT-TRANSFER CORRELATIONS

A number of correlations were studied that could be used to calculate single-phase heat-transfer coefficients inside a cylinder. Nusselt number correlations suggested by Kays and Crawford (1980) were selected for use with water (Eq. B-10) and with heat-transfer oils at higher Prandtl numbers (Eqs. B-11 and B-12). Corrections for rough surfaces are made using Eqs. B-13 and B-14. As these equations show, the effect of a given surface roughness on the Nusselt number depends upon fluid Prandtl and Reynolds numbers. The ratio of rough surface to smooth surface friction factor increases with Reynolds number and hence has greater influence on water heat-transfer coefficients since single-phase Reynolds numbers with water in the receiver tube range from about 30,000 to 130,000, whereas Reynolds numbers for the heat-transfer oil range from 10,000 to 50,000. On the other hand, the effect of the Prandtl number for oils (about 8) is greater than for water (about 1.2). Overall, surface roughness (over the appropriate range of Reynolds numbers) increases water and oil single-phase Nusselt numbers by about 15% to 25%, and 10% to 30%, respectively.

The recommendations of Bergles et al. (1981) and of Tong (1975) were followed in selecting the Chen correlation to calculate two-phase flow, boiling heat-transfer coefficients (Eqs. B-15 to B-22). An overall boiling heat-transfer coefficient is obtained by summing the components from single-phase forced convection and from microscopic convection through the liquid film by bubble nucleation.

Correlations by Morgan are used to determine both natural and forced convection heat losses from the horizontal receiver tube and from the fluid transport piping to the environment. The first Morgan correlation (Fand et al. 1977) relates a natural convection Nusselt number to the Rayleigh number of the air around the horizontal cylinder (Eq. B-23). The second Morgan correlation (Kays and Crawford 1980) relates a forced convection Nusselt number to the cylinder Reynolds number (Eq. B-24).

The final heat-transfer problem is to determine conductive and natural convective heat loss across the annular air gap between the receiver tube and surrounding glass envelope. Recent work by Kuehn and Goldstein (1978) is used for this analysis (Eqs. B-25 to B-30).

2.4 EFFECT OF NONUNIFORM FLUX ON HEAT TRANSFER

Radiative heat flux on the collector receiver tube varies because only one side of the receiver faces the reflector, because the sun is not a point source, and because of geometrical errors inherent in the collector from mechanical imperfections of components and errors in assembly. Consequently, circumferential variations in the temperature of the receiver tube will result. The model of the heat-transfer processes occurring within the receiver assumes no circumferential temperature variations. Hickox and Gartling (1977) show that even large variations in the wall temperature of an inner cylinder cause minimal changes in overall conductive and convective heat transfer to an outer cylinder compared with the changes that occur when the wall temperature of the inner cylinder is constant. The agreement is particularly close when the highest temperature is at the bottom of the inner cylinder. When the highest

SERI ✵ ————————————————————————————————

temperature in the inner cylinder is at the top, agreement is poorer, producing a slight increase in overall heat transfer. Fortunately, from simple geometrical considerations this effect will probably not occur in a parabolic trough receiver.

The receiver tube and glass envelope could become misaligned, either from poor assembly or from the effects of gravity and differential thermal expansion during normal operations. Hickox and Gartling (1977) considered a worst case when the bottom gap under the receiver is cut in half. But even then the overall heat-transfer rate increase is small. Kuehn and Goldstein (1978) also investigated the effects of eccentricity on heat transfer between concentric cylinders and came to similar conclusions. They showed that overall heat-transfer coefficients in eccentric tests, consisting of variations in both horizontal and vertical planes, were all within 10% of the values in concentric geometry. Coefficients decreased by as much as 5% when the inner cylinder was moved up, and increased by 10% when it was moved down.

Ratzel and Sisson (1980) investigated receiver tube heat transfer with circumferential temperature variations. They found that despite large circumferential temperature differences around the receiver, the one-dimensional constant-temperature receiver model predicted nearly the same heat loss as the two-dimensional model, which accounted for circumferential temperature variations. Thus, the one-dimensional model appears adequate to predict overall heat loss from the receiver tube of a parabolic trough collector.

The analysis of circumferential temperature variations does, however, provide useful information regarding heat transfer and the prevention of possible burnout conditions for direct boiling of water in the receiver tube. Ratzel and Sisson's model (1980) assumes that circumferential temperature differences in the receiver tube are transferred to the inner wall. Temperature decrease through the receiver wall is small. Using a heat-transfer oil at extreme temperature operating conditions (315°C bulk fluid temperature), they had to maintain Reynolds numbers greater than 50,000 to prevent thermal degradation of the selective heat-transfer surface and the collector heat-transfer fluid. Peak solar flux occurs at an angle of about 50° from the bottom of the receiver tube (bottom is the lowest point in the receiver tube when the collector is facing upward vertically) for a collector fabricated to attainable specifications. Ratzel (1979) shows the effects of component imperfections and misalignments on temperature distributions and collector efficiency for various receiver designs. Misalignment above the focal line produces a large increase in peak flux on the bottom of the receiver. Misalignment below the focal line produces lower peak fluxes and wider scatter of flux on the receiver perimeter. Tracking bias produces a single maximum flux more toward the bottom of the receiver than the correct tracking. Finally, misalignment to the left of the focal line produces a large increase in maximum flux on the right side of the receiver tube. To interpret these results so as to prevent possible burnout during direct steam generation, the rotation of the receiver and the alignment of the collector must be accounted for. Given the possibility that stratification or dryout could occur during two-phase flow, the peak solar flux should be focused at as low a point on the receiver wall as possible to minimize impingement of concentrated solar energy on the dry receiver wall. Consider an east-west mounted parabolic trough of the most common design with a rotating receiver. Peak solar incidence on the receiver always occurs at noon. During winter solstice, at noon for a correctly aligned

receiver, one of the two solar peak intensities would occur on the upper part of the tube. For instance, at a latitude of 40° a peak solar intensity occurs at about 115° from the bottom of the tube. In the worst case, the focus is moved further upward by horizontal misalignment in a direction that moves the receiver closer to the ground. However, it should be noted that all geometrical imperfections reduce the absolute magnitude of absorbed solar radiation. Also, absorption efficiencies would decrease with increasing incidence angles as the focus moved closer to the top of the receiver. In addition, circumferential heat transfer in the receiver tube slightly reduces peak solar fluxes.

For a north-south oriented trough, incidence angles are at a minimum (but still greater than zero) at about two hours either side of solar noon. Because solar insolation values are smaller at these times than at noon, peak solar radiation on the receiver in the north-south orientation is reduced compared with the east-west case. In addition, considering the geometry of the north-south orientation, the upper part of the receiver tube will probably never experience peak flux densities.

In summary, the one-dimensional model adequately correlates heat loss from the receiver tube. Studies indicate that Reynolds numbers greater than 50,000 are required to minimize the difference between receiver wall and bulk fluid temperatures when using a heat-transfer fluid at peak fluid operating temperatures. Reynolds numbers of this magnitude are readily achievable for water, even at low liquid velocities. The velocity of a heat-transfer oil must be two or more times greater than water to achieve the same Reynolds number. For water flow in the nucleate boiling regime, the inside film heat-transfer coefficient, and hence temperature differentials, are reduced to a low value. Horizontal misalignment, which causes the peak solar flux intensity to move further up the receiver tube, is the worst case of collector fabrication error. Under most operating conditions, peak flux intensities will occur on the underside of the receiver tube, so that even if the tube wall drys out, the selective surface will probably not be damaged since dryout occurs on the upper part of the receiver tube. Under the worst circumstances, using an east-west oriented trough in winter, flux densities can peak at a point on the upper half of the receiver. Additional safety is afforded by the north-south oriented collector field. At this orientation, peak solar fluxes cannot occur on the upper part of the receiver tube.

SECTION 3.0

BASELINE SYSTEM DESCRIPTION AND ANALYTICAL MODEL

3.1 BASELINE SYSTEM

System components and layout of the collector field used for this study are based upon existing equipment and designs. The layout of a baseline collector field is shown in Fig. 3-1. Field size is a nominal 4686 m² (50,420 ft²); collector row spacing is 6 m (19.7 ft). A single drive chain is 36.6 m (120 ft) long; the initial field design comprises three drive chains in series and 20 collector rows. Transport piping is sized to give reasonable flow velocities in Schedule 40 piping for a baseline total flow of 7.5 kg/s (16.5 lb/s).

The collector is clearly the dominant component of the system. Therefore in the system comparisons, a state-of-the-art collector was chosen for the base-line. A parabolic trough solar collector with a 2.13-m aperture and 90°-rim angle is used in the analysis. The receiver tube is made of 16-gauge steel tubing and is 0.0413 m (1.624 in.) O.D. The other inputs to the performance evaluation program are listed in Table 3-1.

The comparative performance analysis of the three competing solar systems is undertaken using two collector models. A simplified collector model uses act-ual collector test data described by the efficiency curve (Harrison 1980):

$$\eta = 0.660 - 0.233 \frac{\Delta T}{I} - 1.285 \times 10^{-3} \frac{\Delta T^2}{I} \quad . \tag{3-1}$$

The temperature differential is between ambient and the average of the inlet and outlet temperatures over each segment of the receiver tube. The receiver tube is divided into 100 segments since, for the direct-boiling case the aver-age of the inlet and outlet collector temperatures does not approximate the average collector operating temperature.

A second detailed collector model calculates thermal performance from first principles using the data presented in Table 3-1. The data inputs were selected such that the optical efficiency of the collector was the same as the collector described above. As illustrated in Appendix A.7, the results of the two models agree very closely and thus provide a check on the detailed calcu-lations. The simple model reduces computer running time, while the more detailed model accounts for the effects of heat removal efficiency of the col-lector. This is particularly important for an oil system where the tempera-ture differential between the receiver tube and the fluid is higher than for the water systems.

Besides consideration of collector performance, the system model accounts for heat and pressure drop losses in collector-field piping. Overall system per-formance and pumping power are calculated to determine the net overall effi-ciency in terms of the independent input variables. Performance is compared in terms of a steady-state model and is easily adapted to alternate solar collectors or system configurations. Some conservatism is introduced into the
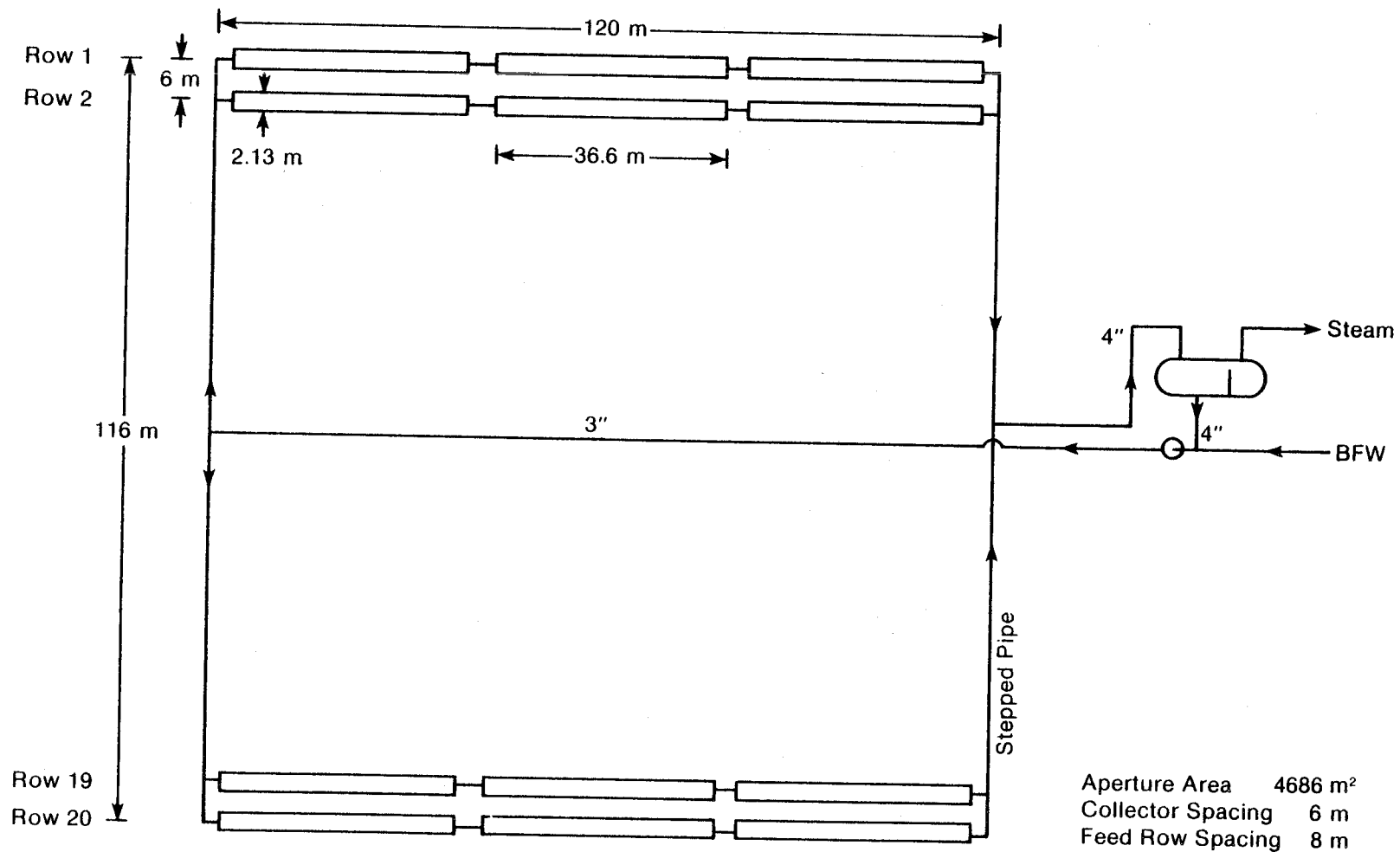
Figure 3-1. Baseline Collector Field

00099^

Table 3-1. Data Inputs for Performance Analysis

Independent variables	
Steam temperature	395-495 K (251°-431°F)
Total collector flow rate	5-15 kg/s (11-33 lb/s)
Insolation on collector aperture	0-1000 W/m^2 (0-317 Btu/ft^{2}h)
Ambient temperature	288 K
Sky temperature	282 K
Makeup water temperature	366 K
Pump efficiency	0.5
Collector	
Aperture	2.13 m (7 ft)
Reflector length per row	110 m (361 ft)
Receiver length per row	120 m (394 ft)
Number of collector rows	20
Area of collector field	4686 m^2 (50,420 ft^2)
Receiver tube (inner diameter)	0.0380 m (1.50 in.)
Receiver tube (outer diameter)	0.0413 m (1.625 in.)
Receiver tube thermal conductivity	45 W/mK (26 Btu/ft°Fh)
Glass envelope (outer diameter)	0.064 m (2.5 in.)
Glass envelope (thickness)	0.0028 m (0.11 in.)
Reflectivity of mirror	0.78
Transmissivity of envelope	0.9
Emissivity of envelope	0.92
Absorbtivity of envelope	0.02
Absorbtivity of receiver	0.94
Emissivity of receiver	0.18
Inlet line	
Inner diameter	0.0779 m (3.08 in.)
Outer diameter	0.0889 m (3.5 in.)
Equivalent length	170 m (558 ft)
Pipe roughness	0.457 × 10^{-4} m (1.80 × 10^{-3} in.)
Insulation (outer diameter)	0.195 m (7.68 in.)
Insulation thermal conductivity	0.047 W/mK (0.027 Btu/ft°Fh)
Insulation jacket emissivity	0.22
Outlet line	
Inner diameter	0.1023 m (4.03 in.)
Outer diameter	0.1143 m (4.5 in.)
Equivalent length	50 m (164 ft)
Insulation (outer diameter)	0.268 m (10.6 in.)
Manifolds	
Effective length for heat loss (inlet and outlet)	200 m (656 ft)
Pressure drop coefficients (see Eqs. A-5 and A-6)	
k_1	25
k_2	5
k_3	5
k_4	5
Unfired boiler	
Heat transfer area	110 m^2 (1184 ft^2)
Heat transfer coefficient (preheater)	625 W/m^2 K (149 Btu/ft^2°Fh)
Heat transfer coefficient (reboiler)	766 W/m^2 K (133 Btu/ft^2°Fh)

comparison through the choice of assumptions. Thus, Therminol 60 was selected as a representative heat-transfer oil for the unfired boiler system. This fluid has improved heat-transfer characteristics over oils such as Therminol 66, which have been used for higher temperature solar systems. The area of the unfired boiler heat exchanger is comparable with the area calculated for a similar solar system design (Stearns-Roger 1981); it is also consistent with the optimization criteria presented by DeWinter (1975) for exchanger costs similar to collector costs on a unit area basis. In addition, the model of the unfired boiler assumes perfect countercurrent flow. The heat-exchanger surface area greatly influences the collector operating temperature and efficiency. Determination of the true optimum size of an exchanger would involve a rigorous economic analysis and annual performance calculation. However the range of boiler and preheater effectivenesses, up to 99.5% and never below 95% except for the highest insolation level, suggests that the selected area is not too small and may in fact be oversized.

The control scheme for the flash system is somewhat idealized in that the upstream pressure of the flash value is maintained at only 3000 Pa (4.35 psi) above the saturation pressure of water. In practice, this is a difficult control problem; but the assumption minimizes electrical power inputs to the flash system and therefore allows a conservative comparison to the in situ system.

3.2 SYSTEM ANALYSIS MODEL

The system simulation model developed for the detailed performance comparisons and sensitivity studies is discussed at length in Appendix A. The model is a steady-state analysis and has significant flexibility beyond that needed for the specific systems studied in this report. With this model, easily adaptable field and collector geometry capabilities are available, and both open- and closed-loop field systems can be analyzed. The model solution, given in terms of temperature, pressure, and thermodynamic properties at both the input and output of each system component (including both piping and manifold elements), is obtained using an energy, temperature, and pressure balance convergence procedure. In addition, conditions are determined at an arbitrary number of nodes along the receiver tube to investigate detailed receiver response, and special provisions are incorporated into the system to model manifold pressure drops and heat losses. The modularity extends beyond components to pressure-drop and heat-transfer correlations, as well as the choice of collector working fluid. An ASME steam/water library computer routine was used to determine thermodynamic properties of water. The model, in addition to being used for a comprehensive steady-state comparison, was also used to define the overall system response characteristics that were needed to calculate annual system performance.

Long-term performance comparisons were made using these characteristics together with an averaging methodology explained in Appendix E. The averaging methodology is based on long-term weather data as well as system characteristics for each particular system, including the location, orientation, and steam-delivery temperature.

SECTION 4.0

RESULTS OF THE THERMAL PERFORMANCE ANALYSIS

Results of the system performance analysis are most easily assessed in terms of instantaneous and long-term performance. The detailed model described earlier provides considerable insight into instantaneous or steady-state system efficiency. This section summarizes the results obtained using the detailed model to compare the in situ, flash, and unfired boiler systems. All results are discussed relative to the baseline system configuration described in Sec. 3.0 and shown in Fig. 3-1.

Long-term and instantaneous performance measures are considered in terms of gross and net system efficiencies. Gross system efficiency is the net thermal system efficiency. In terms of system internal energy delivery rate (U), enthalpy added to the circulating fluid by the compressive action of the pump (P_{pump}), and the total solar radiation power incident on the system (I_{total}), the instantaneous gross efficiency is defined as

$$\eta_{gross} = \frac{U_{steam} - U_{water} - P_{pump}}{I_{total}} \, , \qquad (4-1)$$

where U_{steam} and U_{water} are the internal energy rates of the delivered steam and the makeup water, respectively. The net efficiency measure, which accounts for the thermal energy expended in generating electric pumping power, is defined as

$$\eta_{net} = \eta_{gross} - \frac{3 \times P_{pump}}{I_{total} \, \eta_{pump}} \, , \qquad (4-2)$$

where η_{pump} is the electromechanical efficiency of the pump (assumed equal to 0.5 in the analysis). The factor of 3 accounts for thermal to electric power conversion losses. Long-term efficiencies are defined by equations similar to Eqs. 4-1 and 4-2, except that the energy rates are integrated over time.

4.1 SYSTEM STEADY-STATE THERMAL PERFORMANCE

A wide range of parametric variations were used with the steady-state model. For each of the three system types, steady-state system performance characteristics were determined for steam delivery temperatures ranging from 395 K (251°F) to 495 K (432°F), total mass flows ranging from 5 kg/s (11 lb/s) to 20 kg/s (44 lb/s), and incident solar fluxes ranging from 200 to 1000 W/m² (64 to 317 Btu/h ft²). Results from varying each of the above parameters and discussion on pumping power are described in the following subsections.

SERI ⚜ _____

4.1.1 Mass Flow Rate Variations

The effect of mass flow rate on system efficiency is not dramatic, but is significant especially when the net efficiency measure is used. Considering first the gross efficiency measure, the effect of mass flow rate on steady-state system efficiency is illustrated in Figs. 4-1 to 4-3. The data indicate that with increasing mass flow rates, there is an increase in gross efficiency in both flash and unfired boiler (oil) systems, but the in situ system shows a slight decrease in efficiency.

The effect of flow rate on measures of efficiency is most apparent for the oil system. A number of interrelated factors cause these results. Since collector performance is the major determinant of gross system efficiency, the trend in gross efficiency can be correlated in terms of average receiver temperature*. Receiver tube temperature is plotted versus mass flow rate in Figs. 4-4 to 4-7. These data show a rapid reduction and then a gradual leveling off of average collector temperature with increased flow for the oil and steam-flash systems (which are based on sensible heat transfer). In contrast, the in situ system is almost isothermal; the temperature level is dependent only on steam temperature. In absolute terms, the receiver temperature can increase or decrease depending on operating conditions.

Increasing mass flow rate reduces the collector temperature differential, and thus tends to improve collector performance. At the same time, however, reducing steam quality for the water systems raises the collector inlet temperature by diluting the effect of adding cold boiler makeup water. This has a negative effect on collector performance and explains why the in situ system average collector temperature increases with mass flow rate. Table 4-1 lists maximum steam qualities of the water systems for each steam temperature.

Table 4-1. **Maximum Steam Qualities Predicted for Baseline System**

Insolation = 1000 W/m^2
Mass Flow Rate = 7.5 kg/s

Steam Temperature (K)	Steam Quality (%)	
	In Situ	Flash
395	16.1	15.7
420	15.6	15.2
445	15.2	14.8
470	14.8	14.3
495	14.3	13.9

_____

*Average receiver temperature in this study is the numerical average of 100 temperatures on the outer surface along the length of the tube. Thus, the nonlinear variations of temperature with length are adequately accounted for.

SERI ●
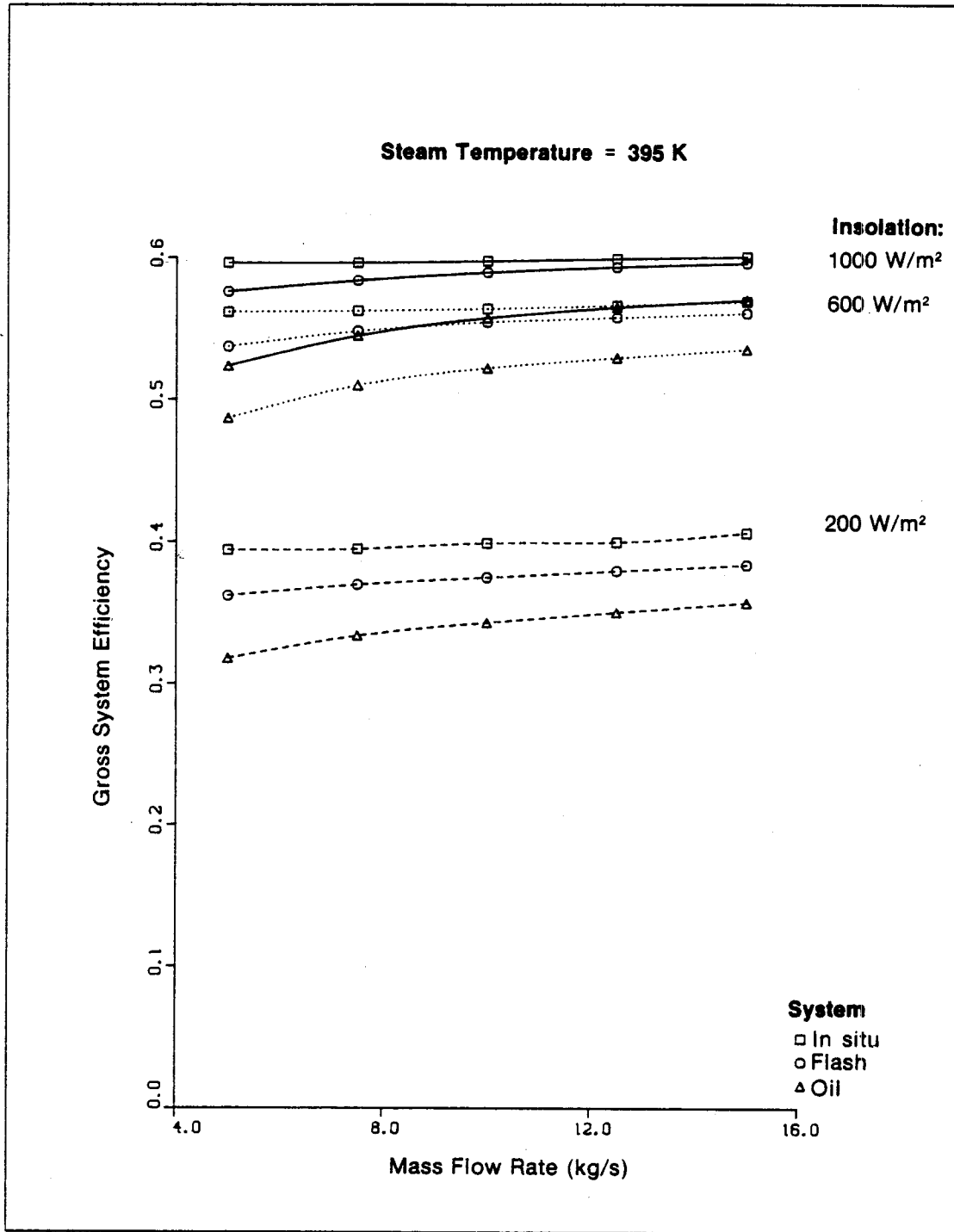
Figure 4-1. Gross System Efficiency vs. Mass Flow Rate (T_s = 395 K)
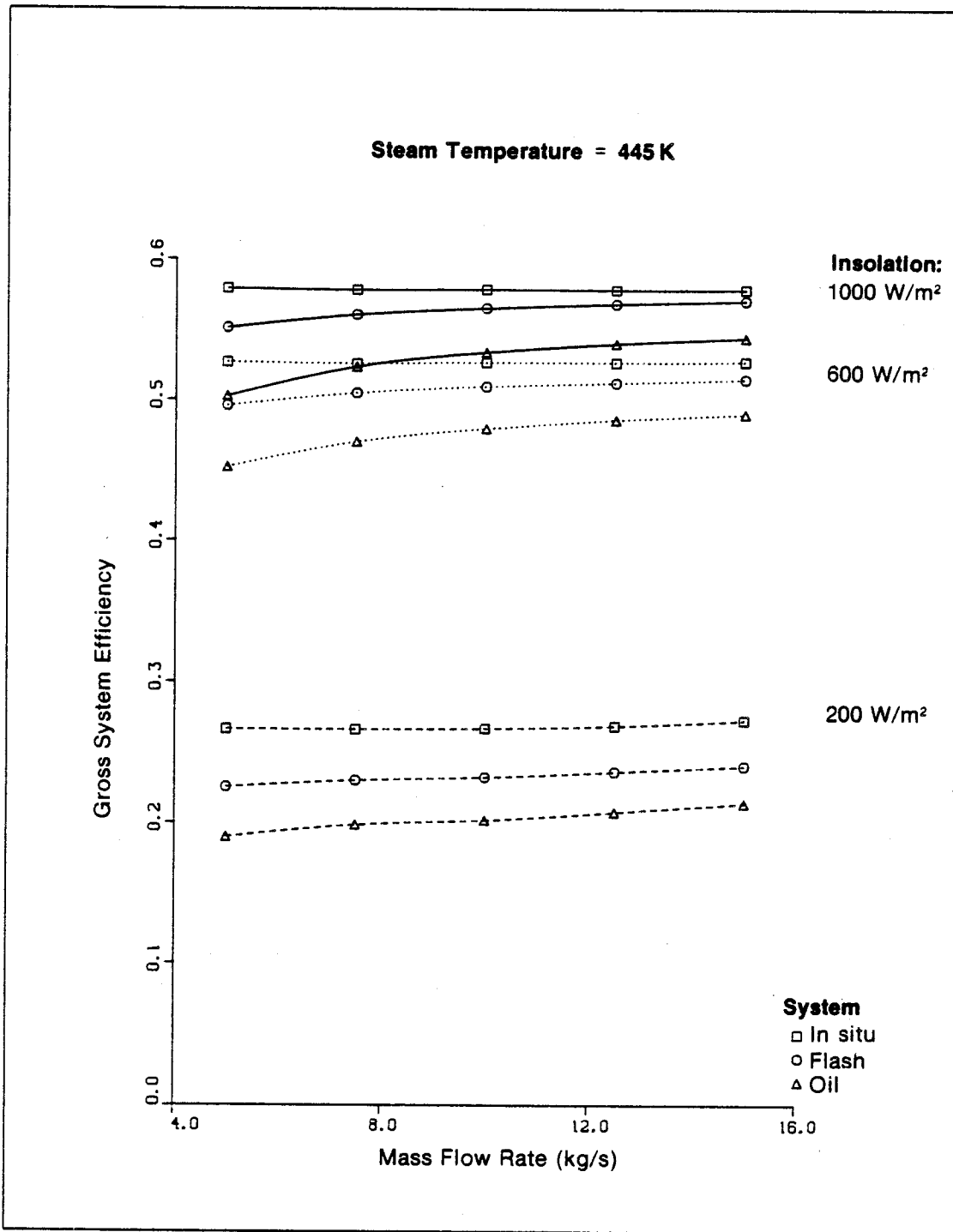
Figure 4-2. Gross System Efficiency vs. Mass Flow Rate (T_s = 445 K)
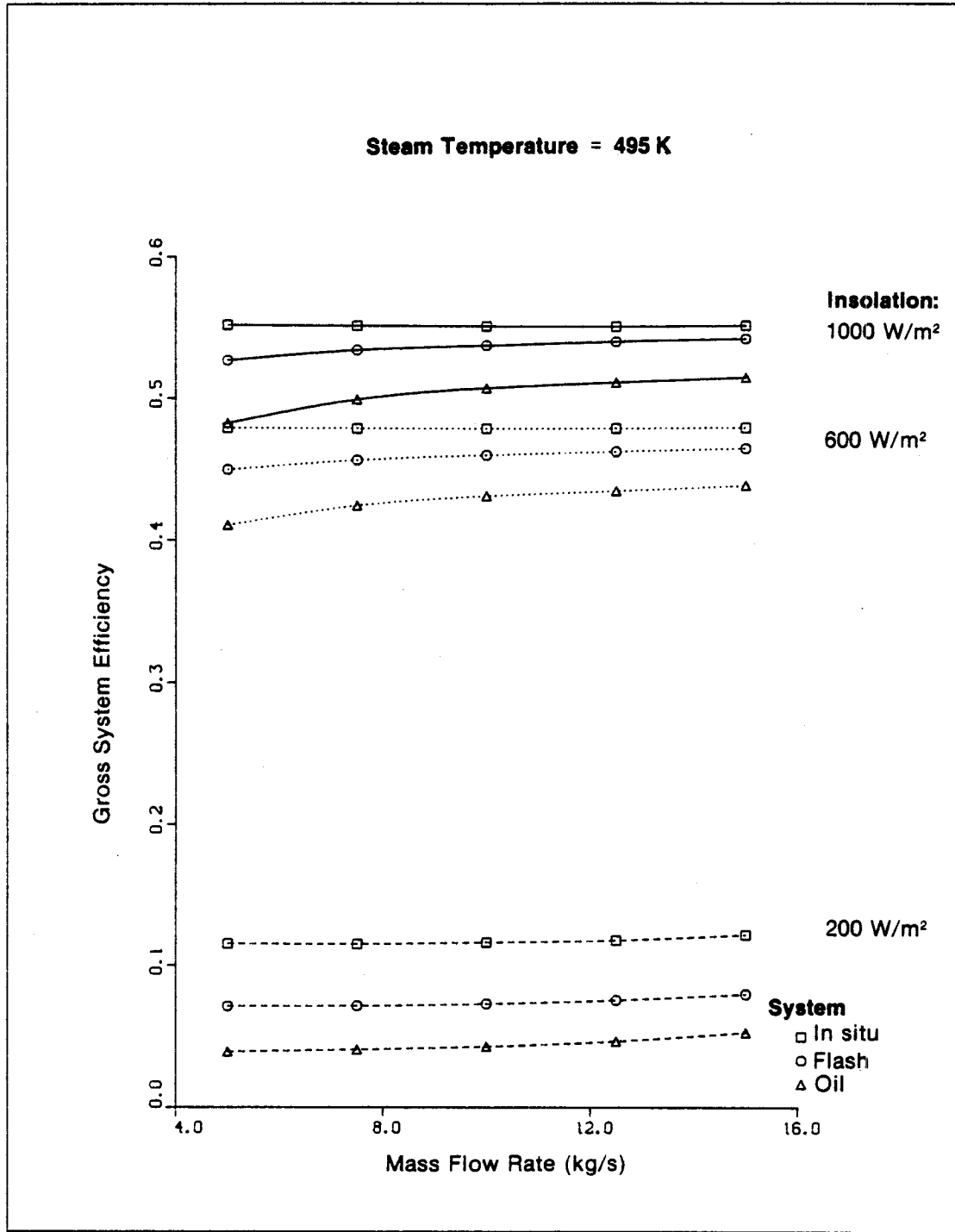
Figure 4-3. Gross System Efficiency vs. Mass Flow Rate (T_s = 495 K)
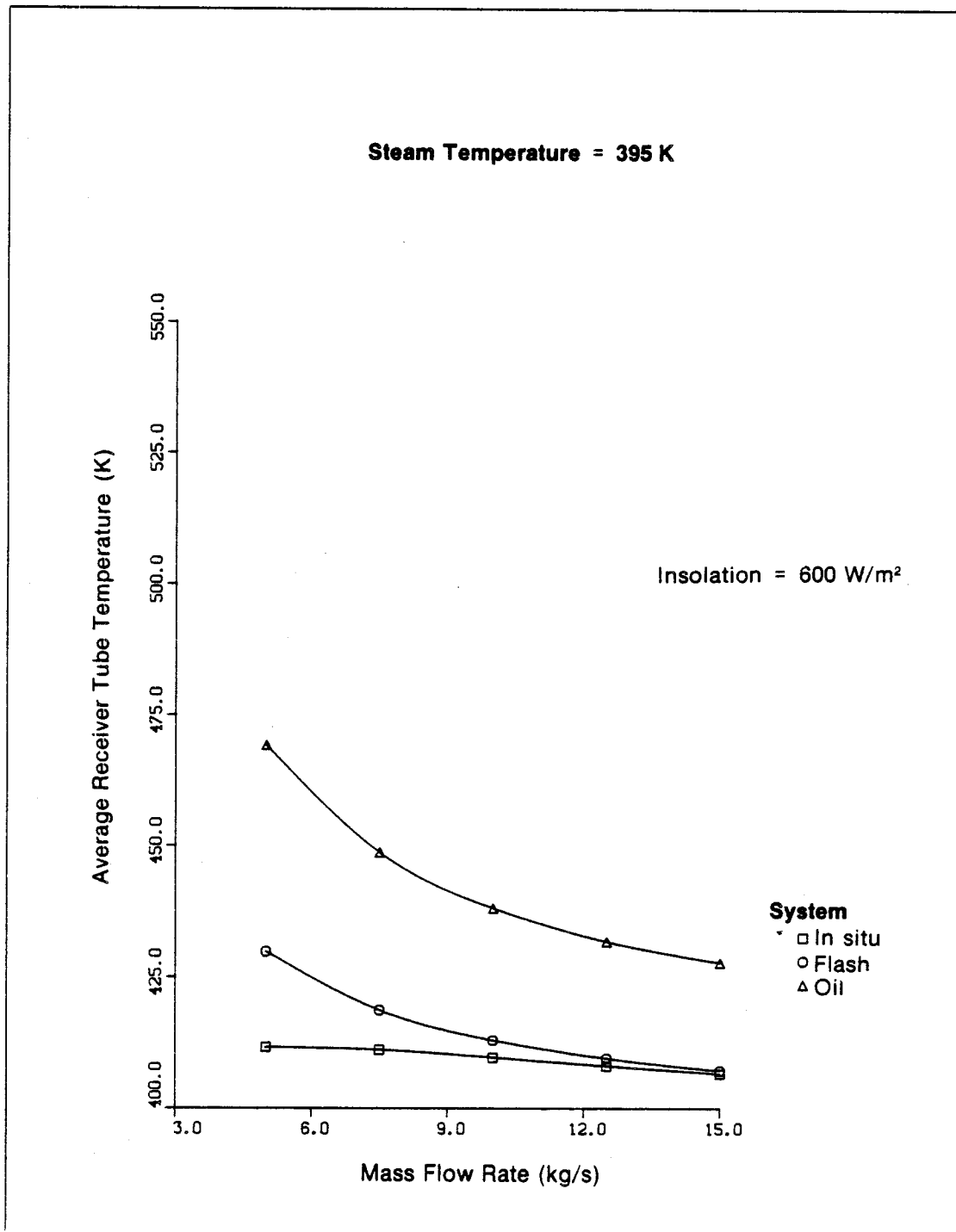
Figure 4-4. Average Receiver Tube Temperature vs. Mass Flow Rate
(T_s = 395 K, I = 600 W/m^2)

SERI ●
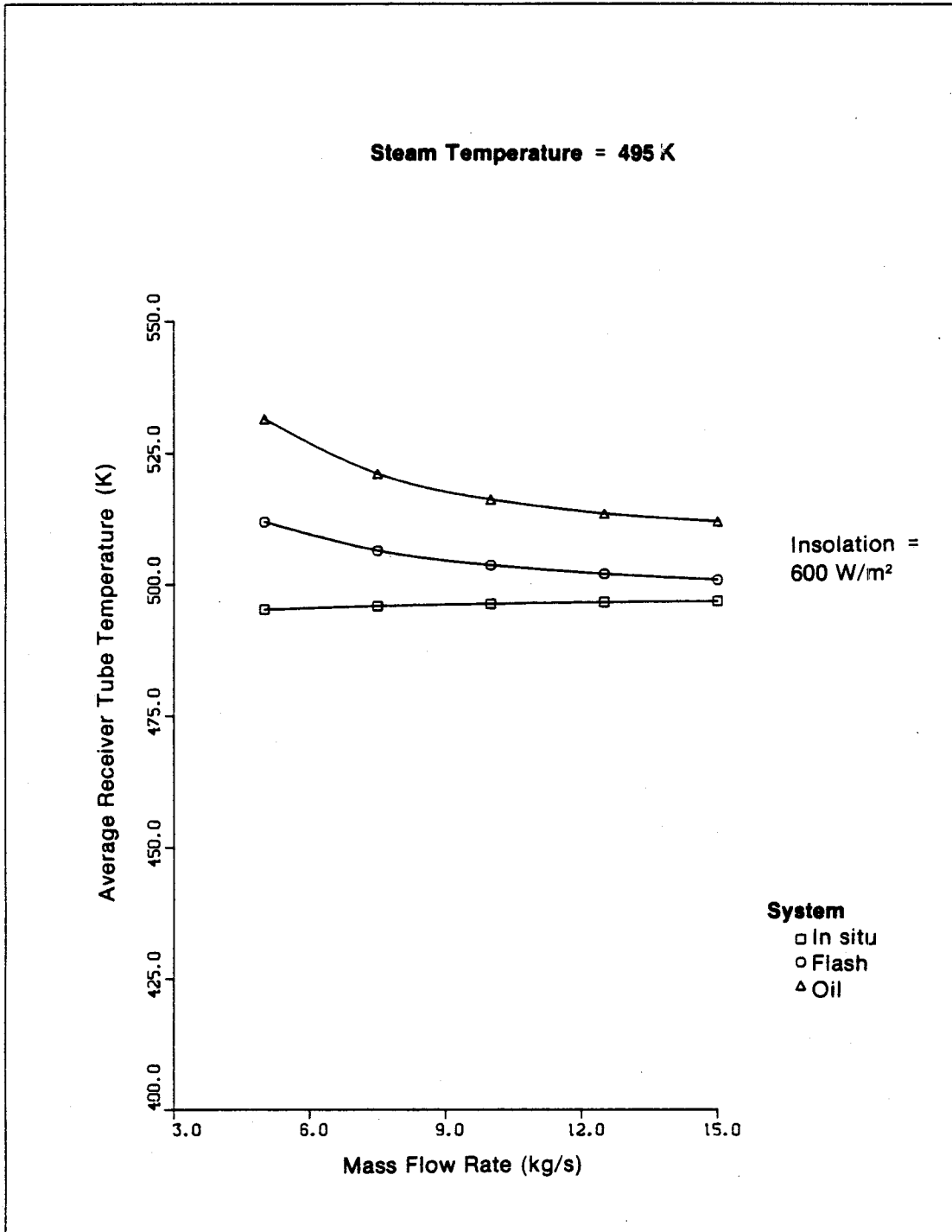
Figure 4-5. Average Receiver Tube Temperature vs. Mass Flow Rate (T_s = 495 K, I = 600 W/m^2)
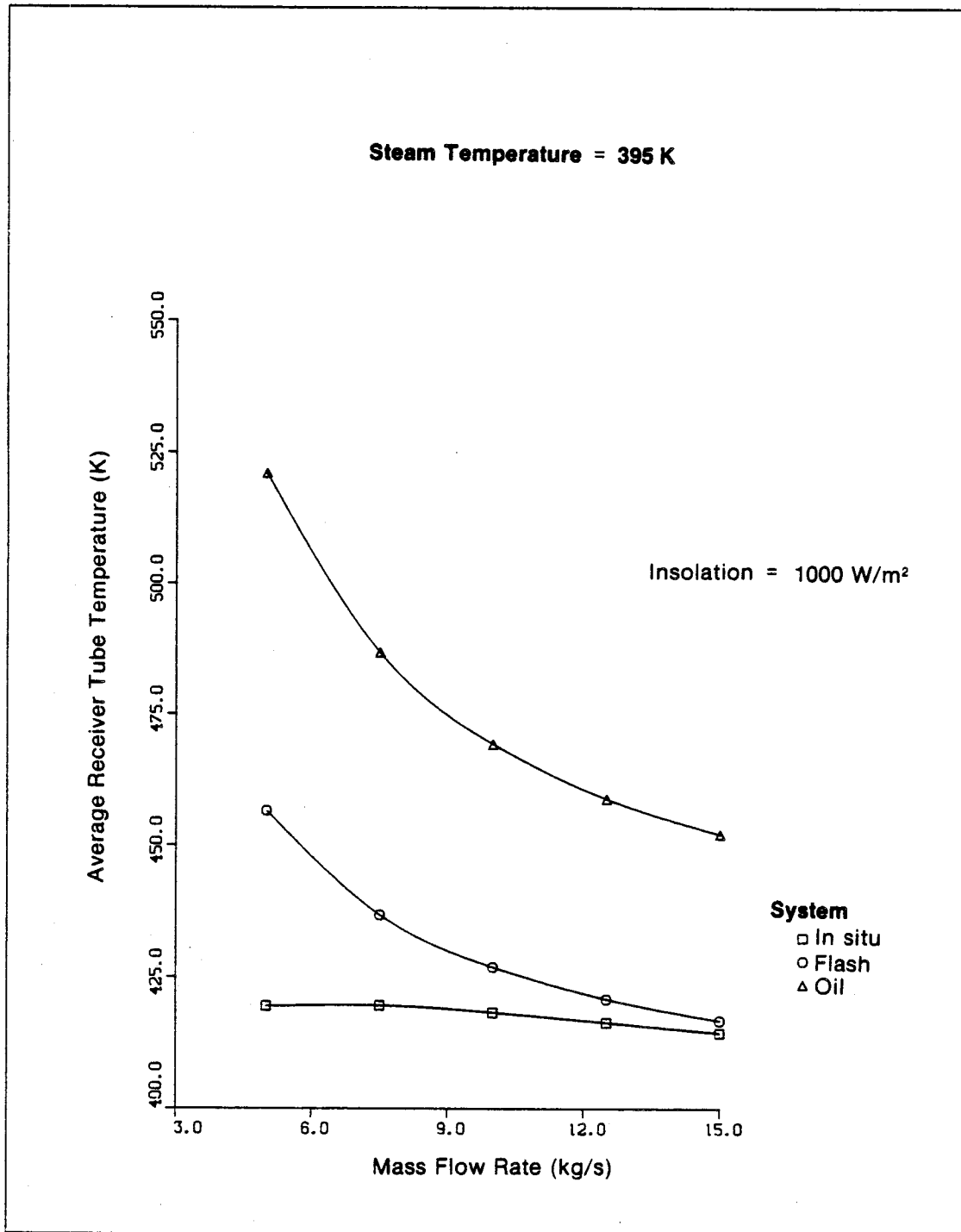
Figure 4-6. Average Receiver Tube Temperature vs. Mass Flow Rate
(T_s = 395 K, I = 1000 W/m^2)
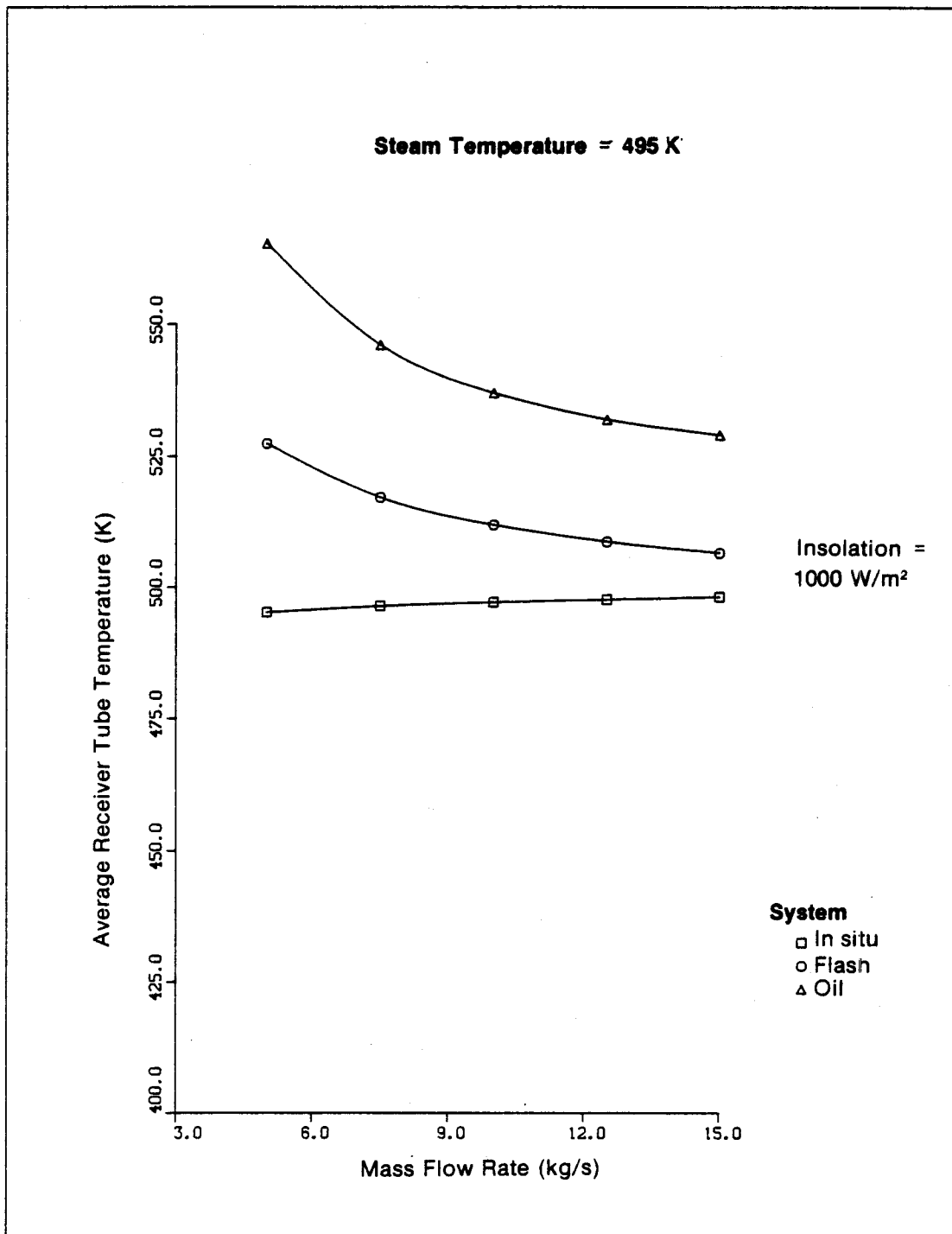
Figure 4-7. Average Receiver Tube Temperature vs. Mass Flow Rate
(T_s = 495 K, I = 1000 W/m^2)

Flow rate also affects the heat transfer coefficients inside the receiver tube. In the in situ system, increasing flow rates decrease the relative length of collector tube in which boiling occurs. Since nucleate boiling heat-transfer coefficients are greater than those associated with single-phase flow, the effective overall heat-transfer coefficient for the collector decreases, and the mean collector temperature rises slightly with increased flow. However, single- and two-phase heat-transfer coefficients of water are so high over the range of flow rates considered, that the collector performance of both the in situ and flash systems is increased only marginally by a reduction in the temperature differential across the liquid film at increased flow rates. For the oil system, typical liquid film heat-transfer coefficients compared to water at the same flow rate are lower by a factor of four. Consequently, the effect of increased oil flow rate on reducing the film temperature differential has a more pronounced effect on collector performance.

The presence of a heat exchanger in the oil system is a major factor in increased collector temperature and reduced performance. This effect indicates that the optimization of the exchanger area is a major component in the design of an oil system. However, the performance of the flash system can be used to place a bound on the performance of an unfired boiler system. In effect, a flash system is equivalent to an unfired boiler system using water as the heat transfer fluid with an exchanger of infinite area. The difference in gross performance between the steam-flash and oil systems can be attributed to the use of an exchanger of finite size and to the use of an oil with much poorer heat transport properties than water (illustrated in Figs. 4-4 to 4-7). The receiver temperatures for the steam-flash and oil systems largely parallel one another, a consequence of the impact of the heat exchanger. The variation in absolute difference in the curves is due to the exchanger and the effect of fluid properties.

Net system efficiency versus mass flow rate is illustrated in Figs. 4-8 to 4-10. Net system efficiency accounts for the impact of electrical pumping power. Maximum net efficiency for oil and flash systems occurs at about 10 kg/s. At low mass flow rates, the net efficiency increases with mass flow rate for the same reasons as mentioned above. However, as the mass flow rate increases beyond about 10 kg/s for all but the lowest fluxes, the increase in thermal efficiency is more than offset by the increased pumping power required. For the in situ system, the effect of increased pumping power with increased flow rates reinforces the decline in net efficiency as was already noted for gross efficiency. A direct-boiling system should therefore operate with the lowest possible flow rate that is consistent with system stability. Reducing the flow rate of a direct-boiling system increases steam quality and two-phase velocities. High exit qualities, particularly at lower steam pressures, can possibly lead to stability problems (see Sec. 7.0), although such problems can always be eliminated by an appropriate increase in pressure drop at the inlet to the collector rows.
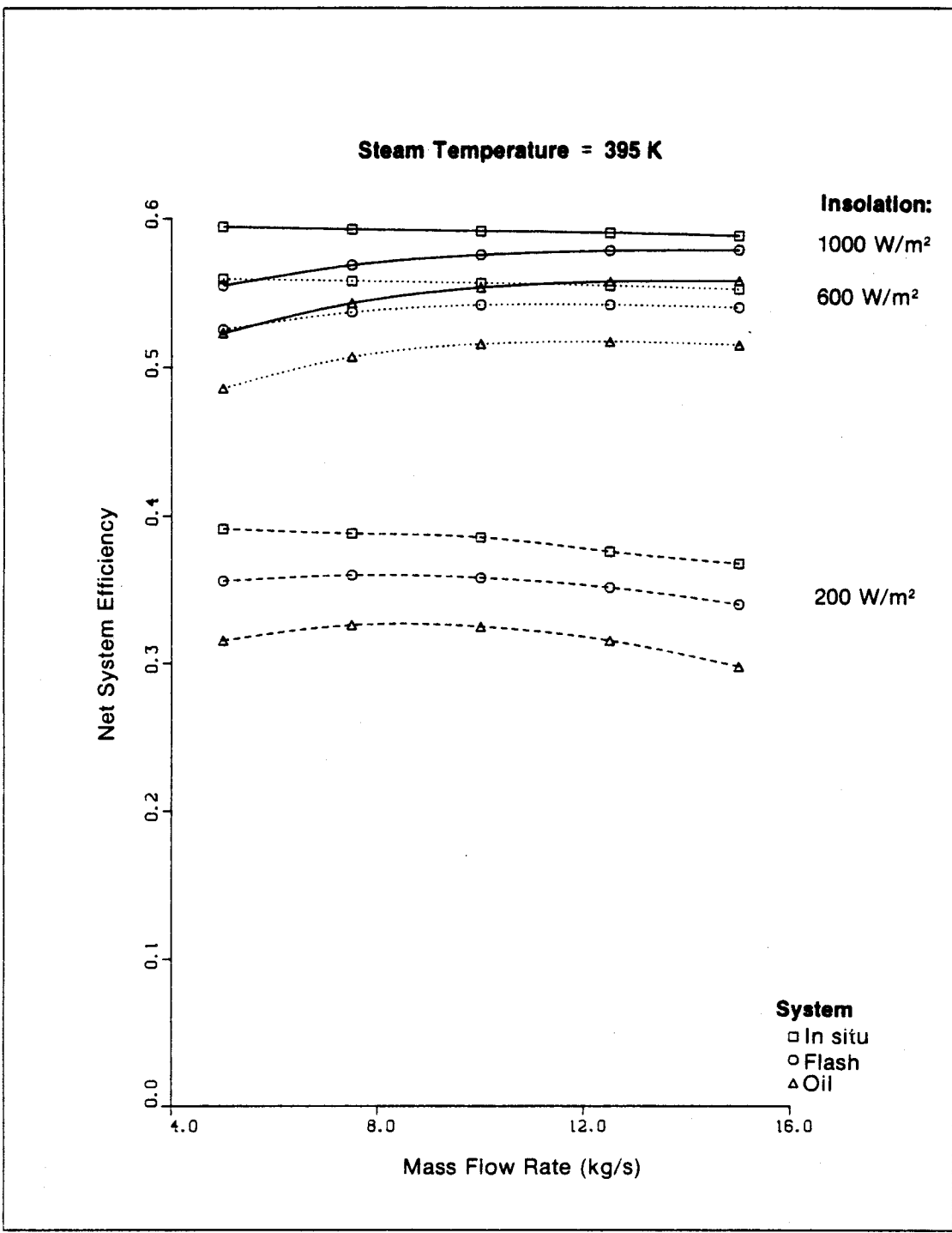
Figure 4-8. Net System Efficiency vs. Mass Flow Rate (T_s = 395 K)
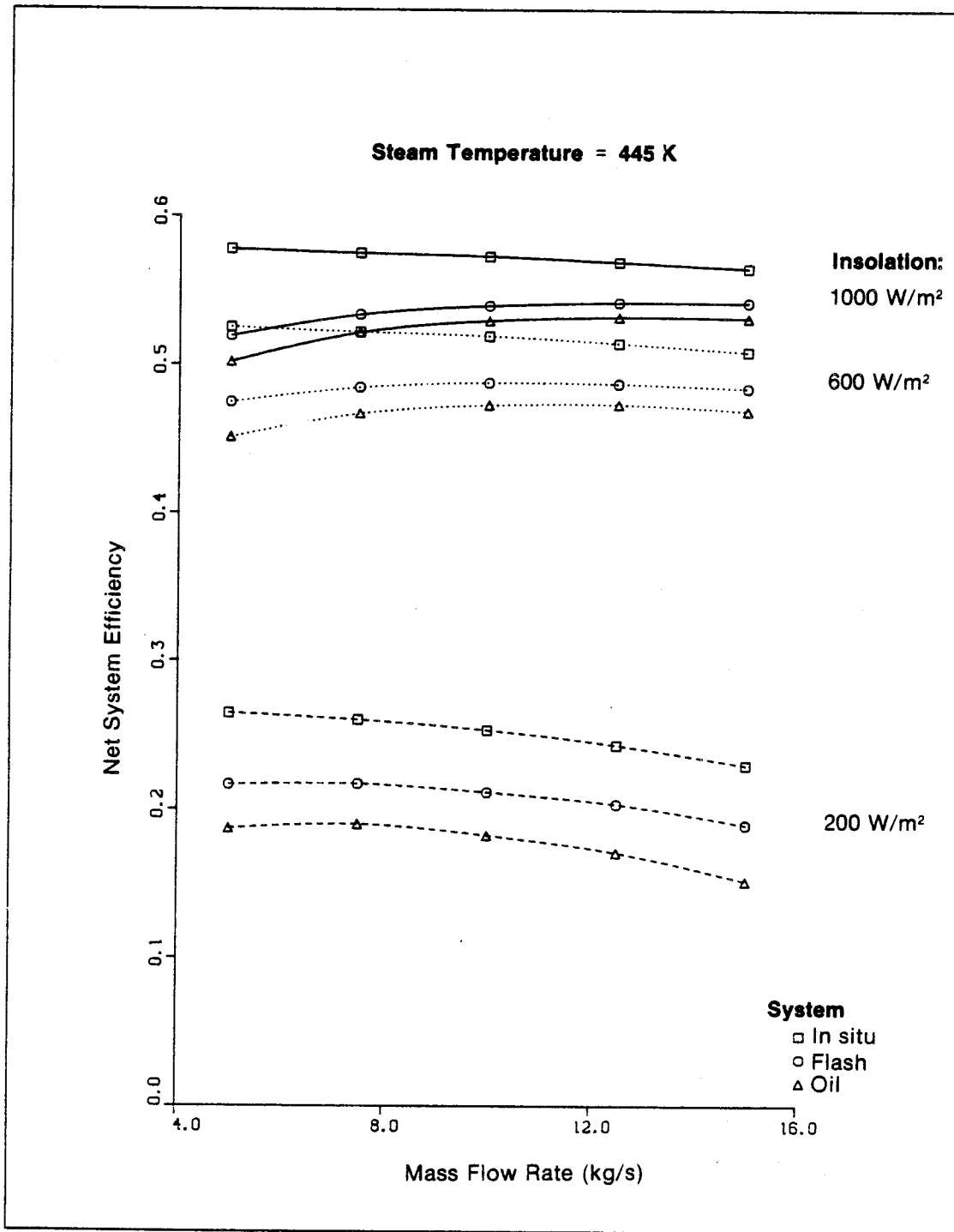
Figure 4-9. Net System Efficiency vs. Mass Flow Rate (T_s = 445 K)
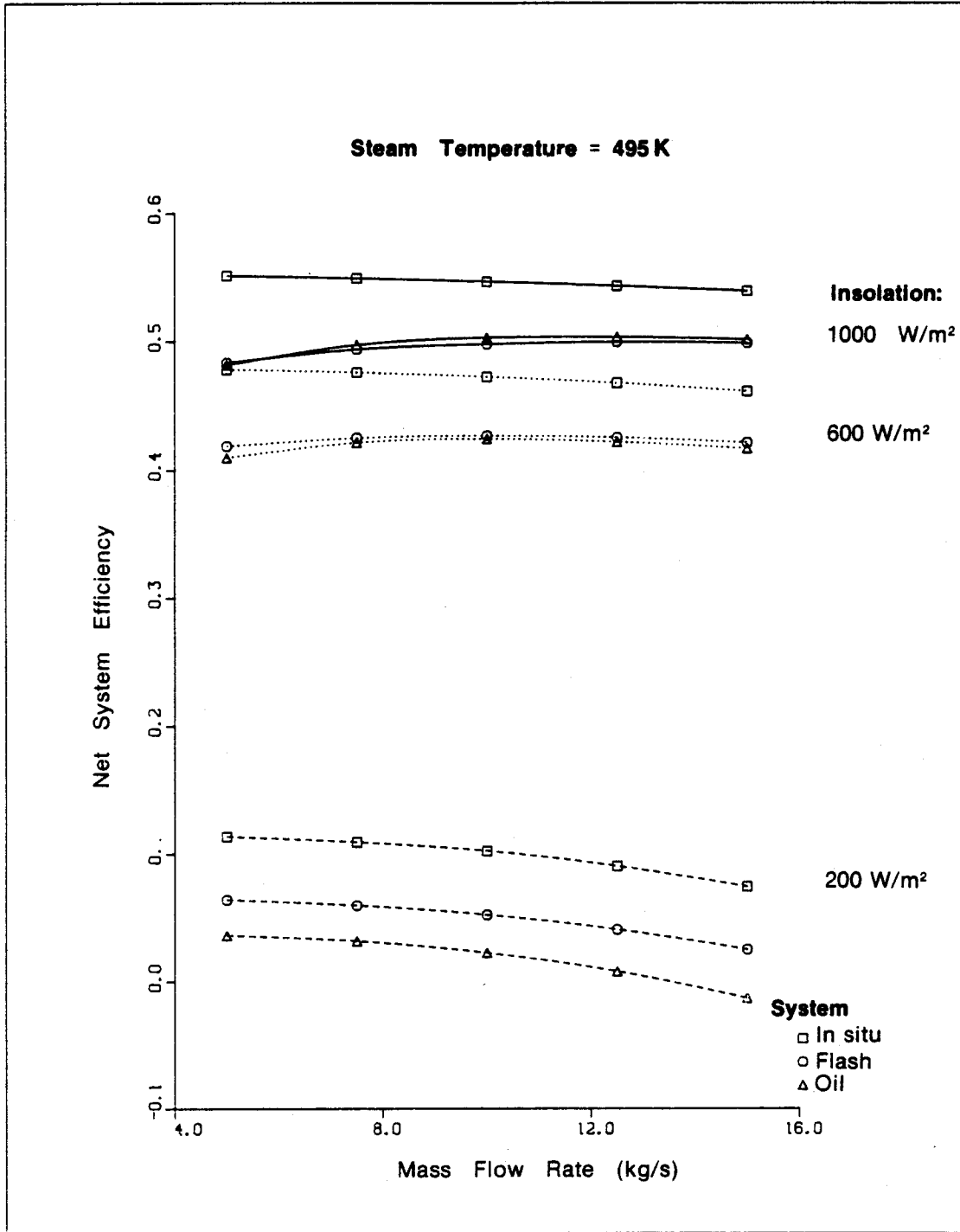
Figure 4-10. Net System Efficiency vs. Mass Flow Rate (T_s = 495 K)

In subsequent parameter variations considered in this discussion, a constant mass flow rate of 7.5 kg/s for the in situ system and 10 kg/s for the flash and oil systems are used. These mass flow rates were selected for two reasons. First, further consideration of mass flow rate does not add much insight into the subsequent discussion of other parametric variations. Second, these mass flow rates are almost optimal values from a net energy delivery perspective (although a lower flow rate could be selected for the in situ system) and therefore were used as the basis for the annual calculations.

4.1.2 Flux Intensity Variations

As expected, system efficiency is very dependent on solar flux because of the various thermal loss mechanisms and because in a gross sense, the systems are isothermal for a given steam temperature. (An isothermal condition at approximately the steam delivery temperature is a very good approximation for an in situ system.) Changes are most dramatic when the collector system cutoff* is approached. Further, Figs. 4-11 to 4-16 illustrate that efficiency drops off more rapidly with decreasing flux at higher steam delivery temperatures. At these lower flux levels, thermal losses that are dominated by the radiation loss component approach the flux gain of the collector. The curves corresponding to the gross and net efficiency measures appear quite similar for all of the systems; however the in situ system always exhibits the greatest efficiency for a given flux. The relative advantage of the direct-boiling system increases with increasing steam delivery temperature and decreasing radiative flux. The advantage of the in situ system over the oil system is quite pronounced in all cases and is explained by the thermal performance arguments presented earlier. As a rough measure, the efficiency of an in situ system at an insolation level of 600 W/m^2 equals or exceeds the efficiency of an oil system at an insolation level of 1000 W/m^2. Compared to the flash system, the advantage is more clearly distinguished when the net efficiency measure is used and the effect of parasitic pumping power is considered.

The effect of incident radiation levels on the average receiver temperature is shown in Figs. 4-17 to 4-19 where comparisons are made for three steam delivery temperatures at optimal mass flow rates. At higher steam delivery temperatures for the in situ system, the average receiver tube temperature declines slightly with increased insolation resulting from the diluting effect of large volumes of makeup water. Pressure must also be considered. Higher pressures result in reduced frictional pressure drop in the two-phase region compared to conditions at 395 K (250°F) where receiver exit velocities are extremely high. The frictional back pressure in the exit lines to the steam separator at high, two-phase velocities causes an elevation of saturation pressure and thus an elevation of temperature in the receiver tubes. Consequently, as illustrated in Fig. 4-17, at low pressure the receiver temperature increases with increasing flux for the in situ system.

---

*"Cutoff" here refers to that radiation flux below which the system makes no net energy contribution. This effect will be discussed more in connection with the annual energy calculations.
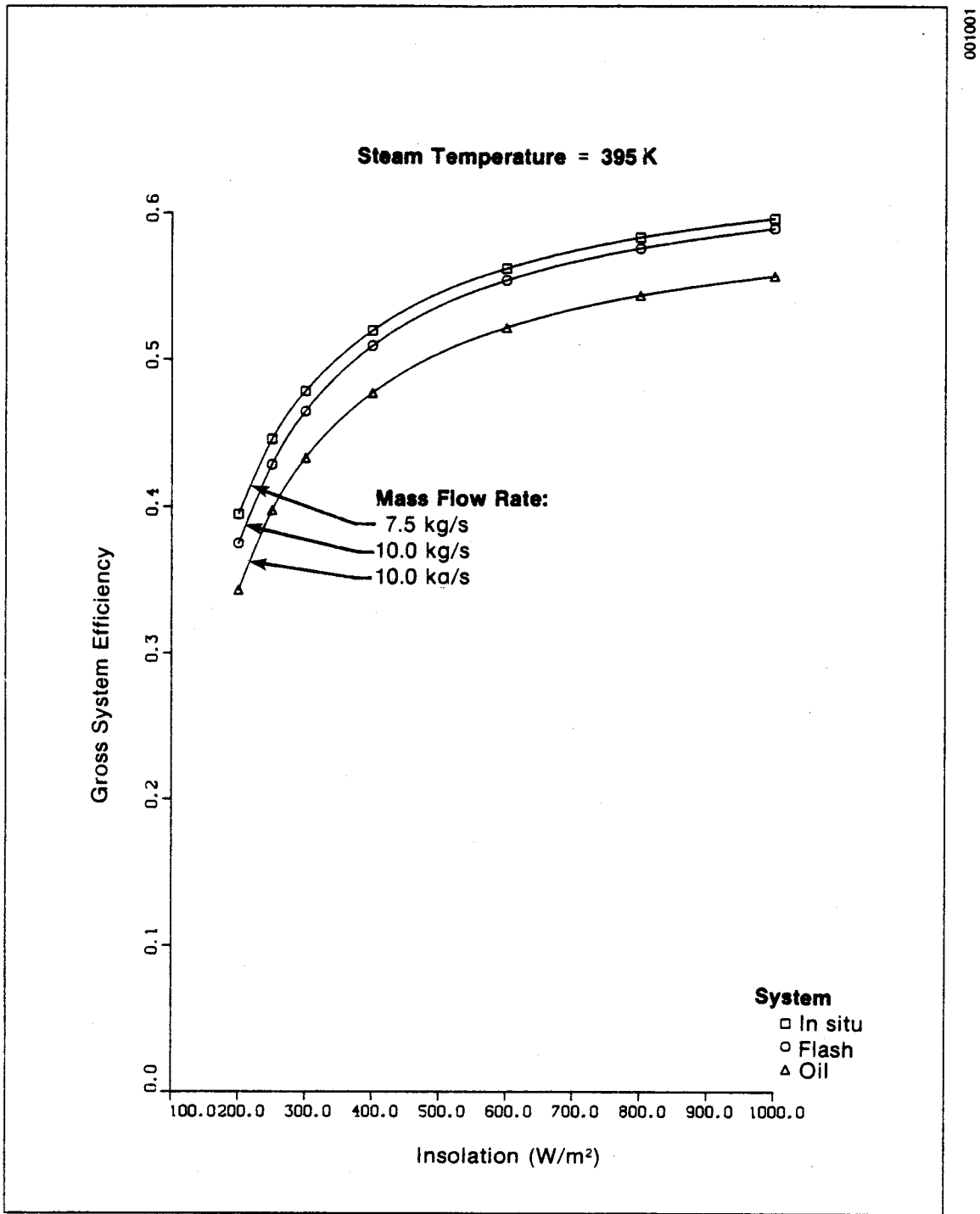
Figure 4-11. Gross System Efficiency vs. Incident Solar Flux (T_s = 395 K)
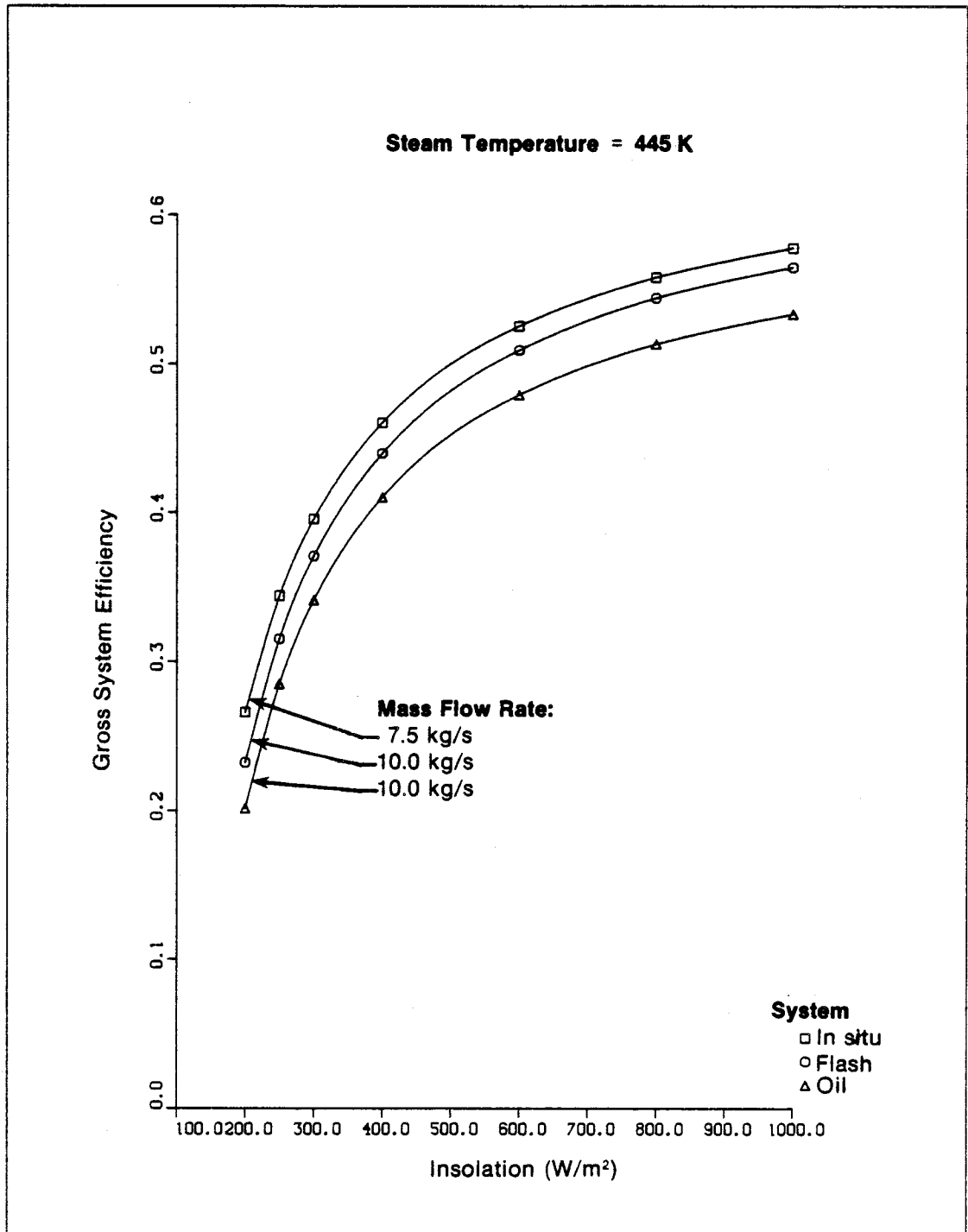
Figure 4-12. Gross System Efficiency vs. Incident Solar Flux (T_s = 445 K)

SERI
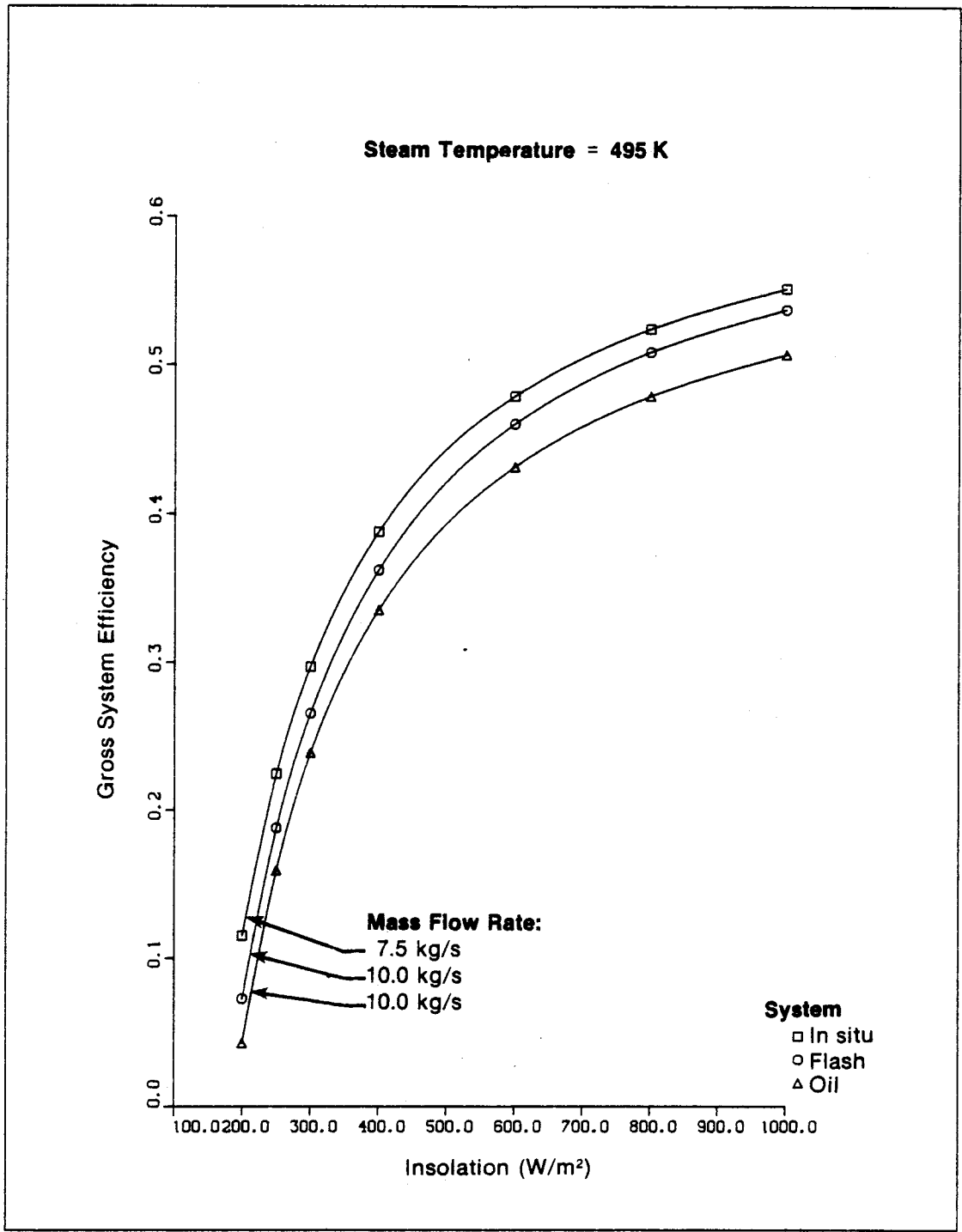
Figure 4-13. Gross System Efficiency vs. Incident Solar Flux (T_s = 495 K)
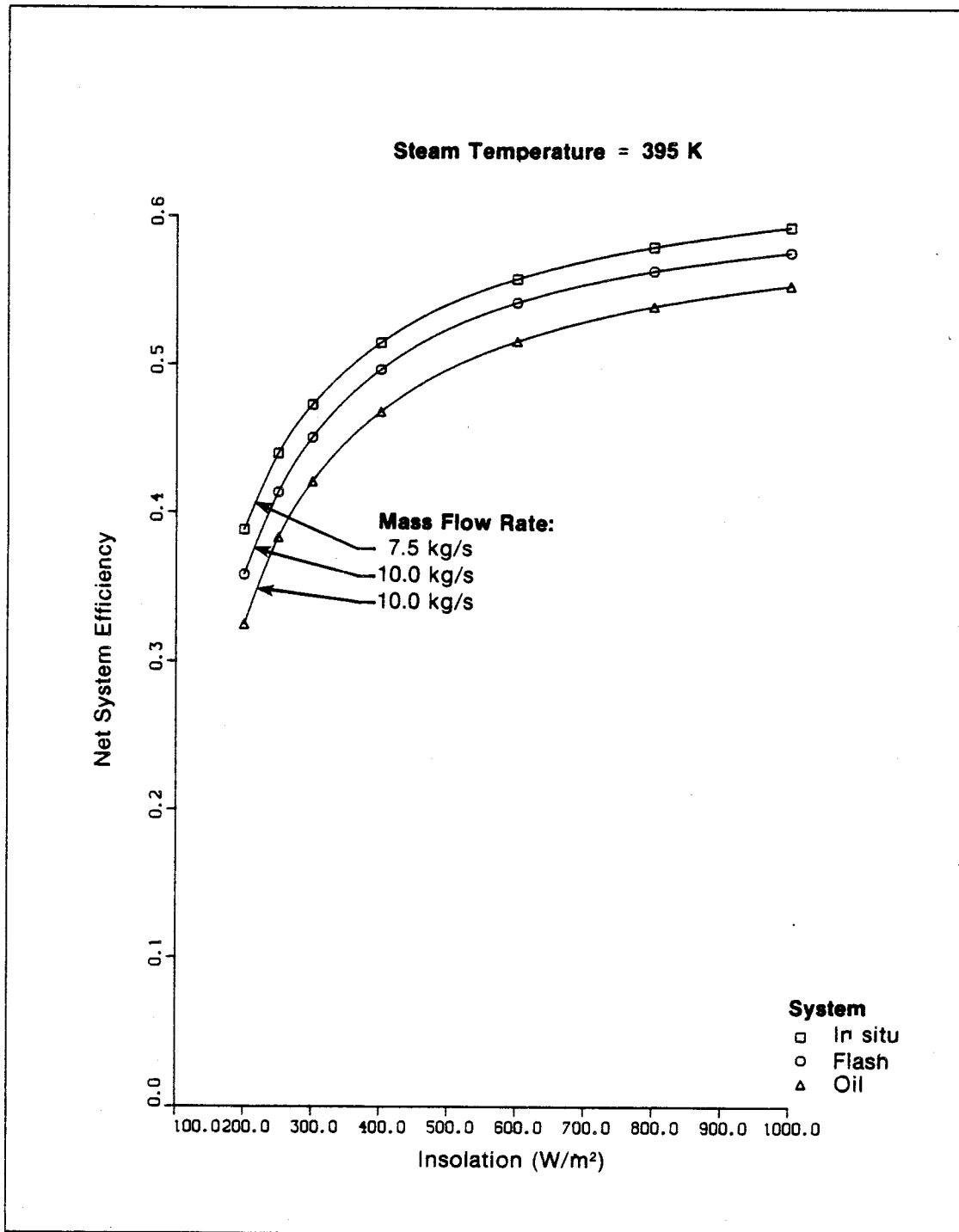
001004

Figure 4-14. Net System Efficiency vs. Incident Solar Flux (T_s = 395 K)
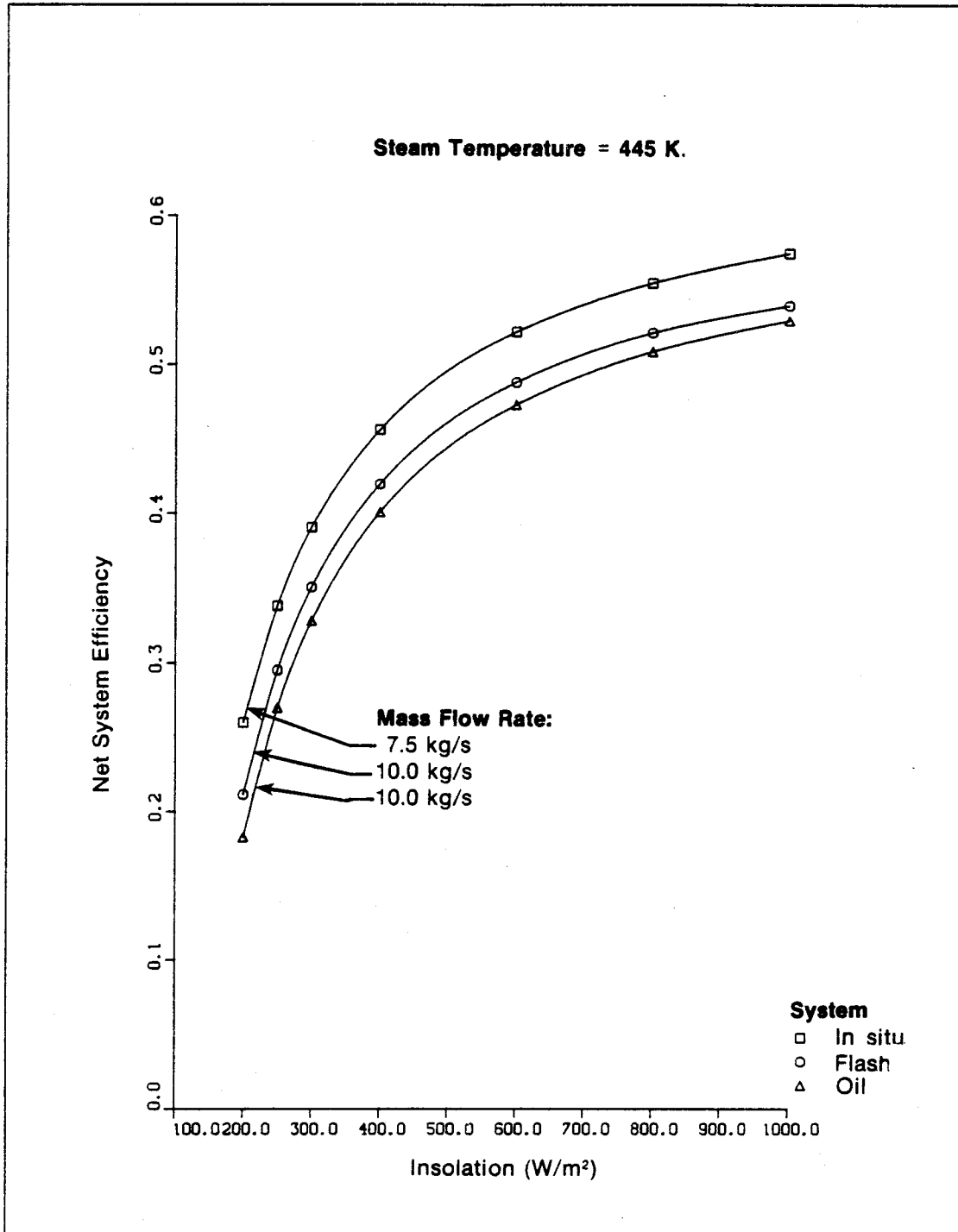
Figure 4-15. Net System Efficiency vs. Incident Solar Flux (T_s = 445 K)
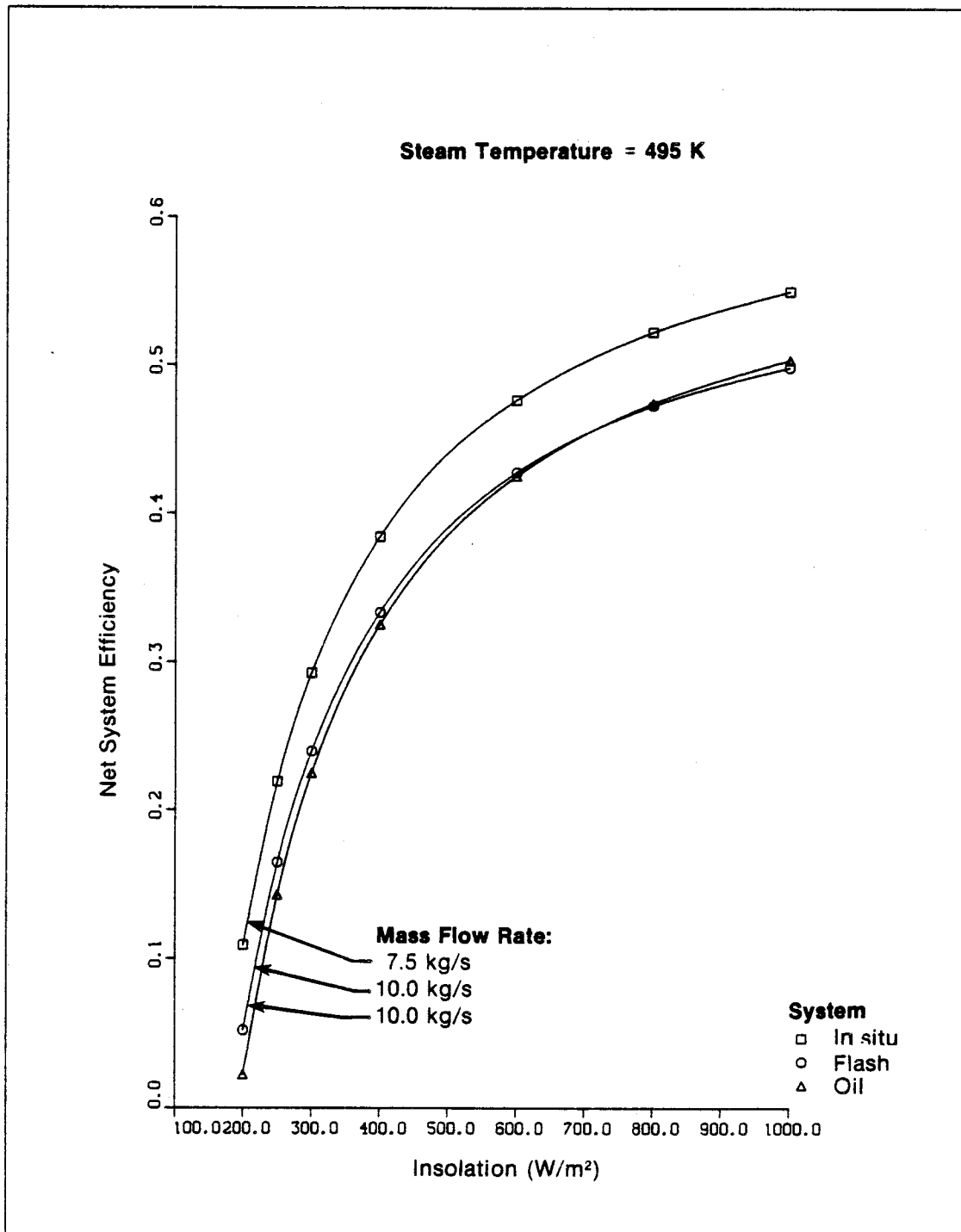
Figure 4-16. Net System Efficiency vs. Incident Solar Flux (T_s = 495 K)
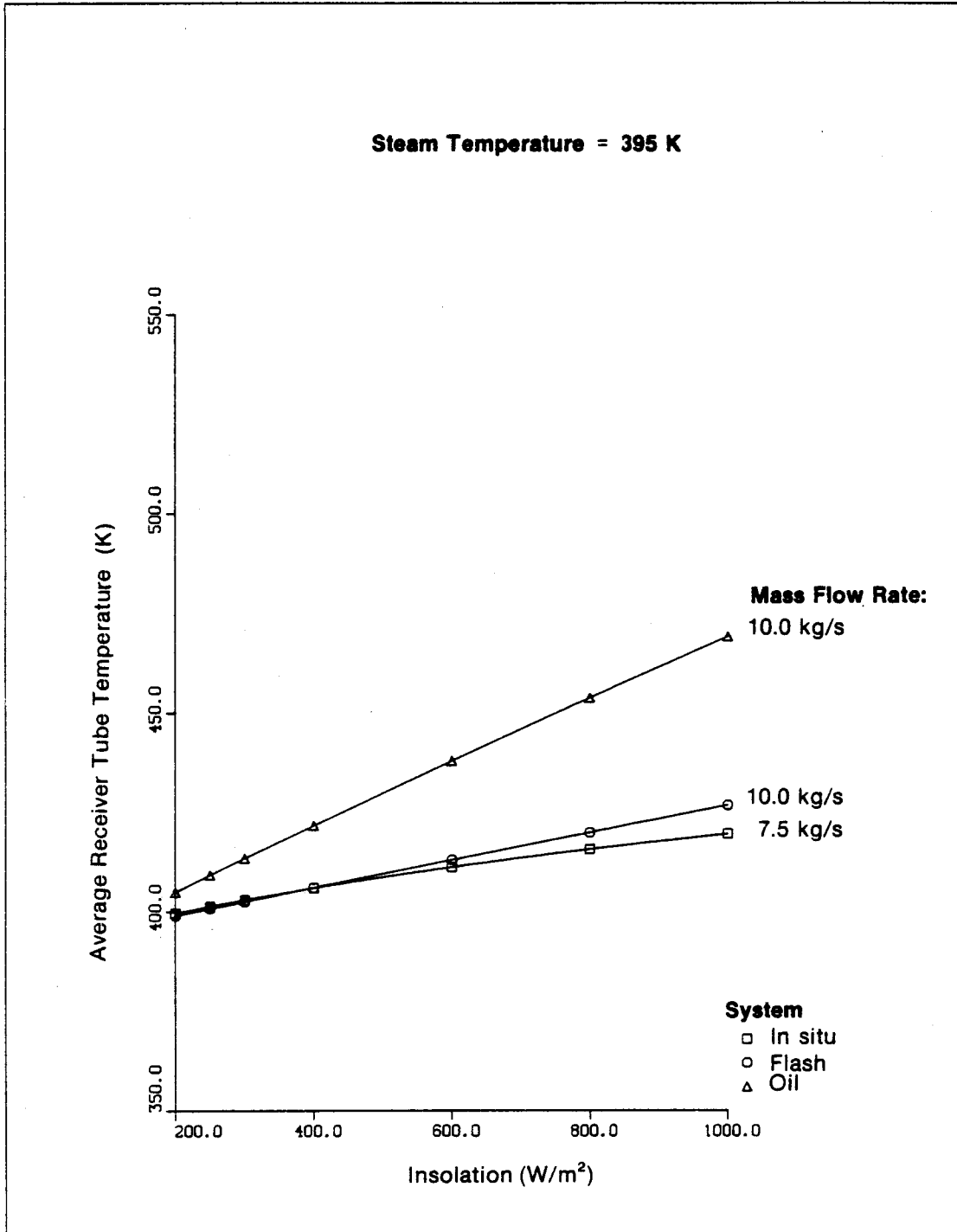
Figure 4-17. Average Receiver Tube Temperature vs. Incident Solar Flux
(T_s = 395 K)
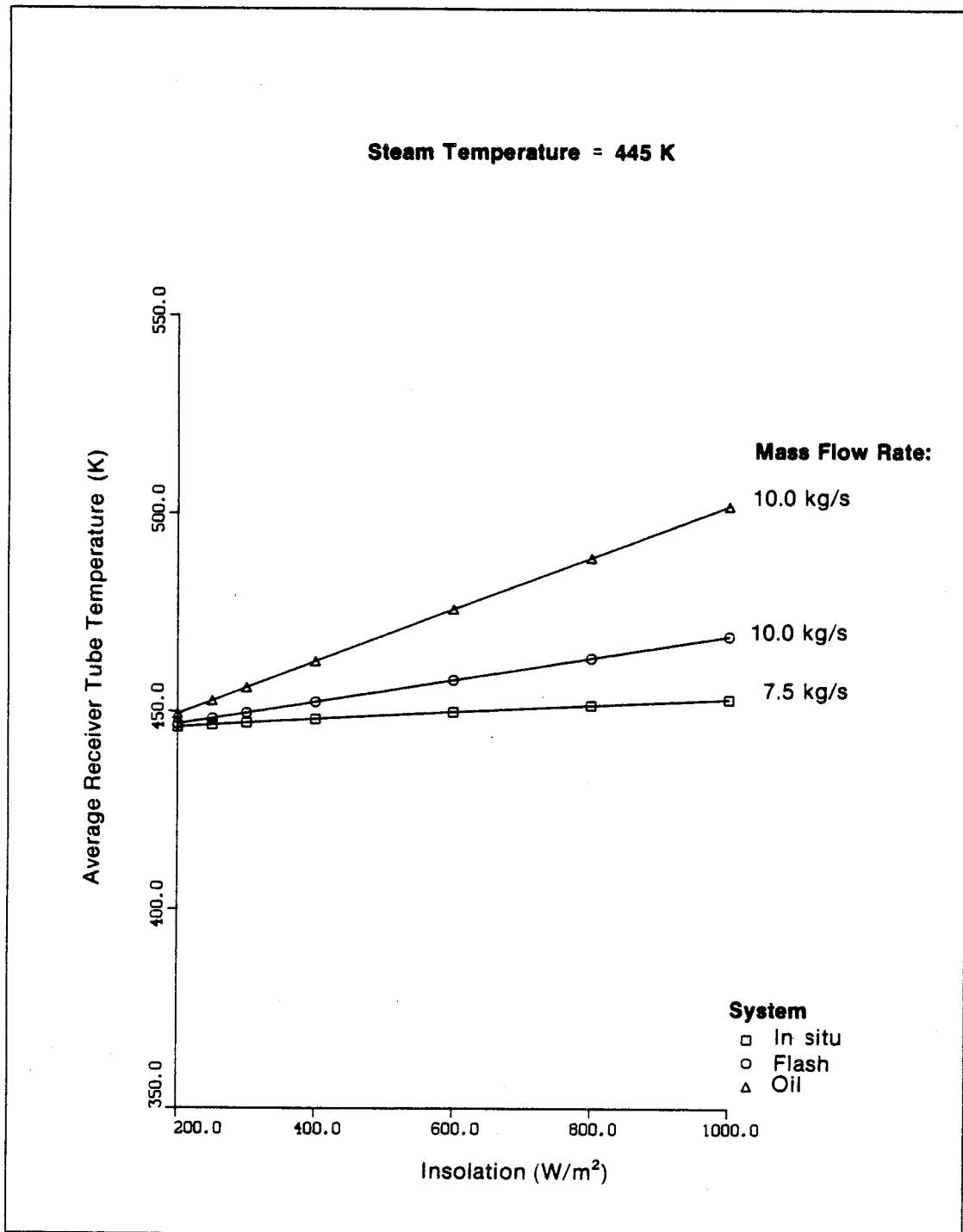
Figure 4-18. Average Receiver Tube Temperature vs. Incident Solar Flux (T_s = 445 K)

SERI ✸
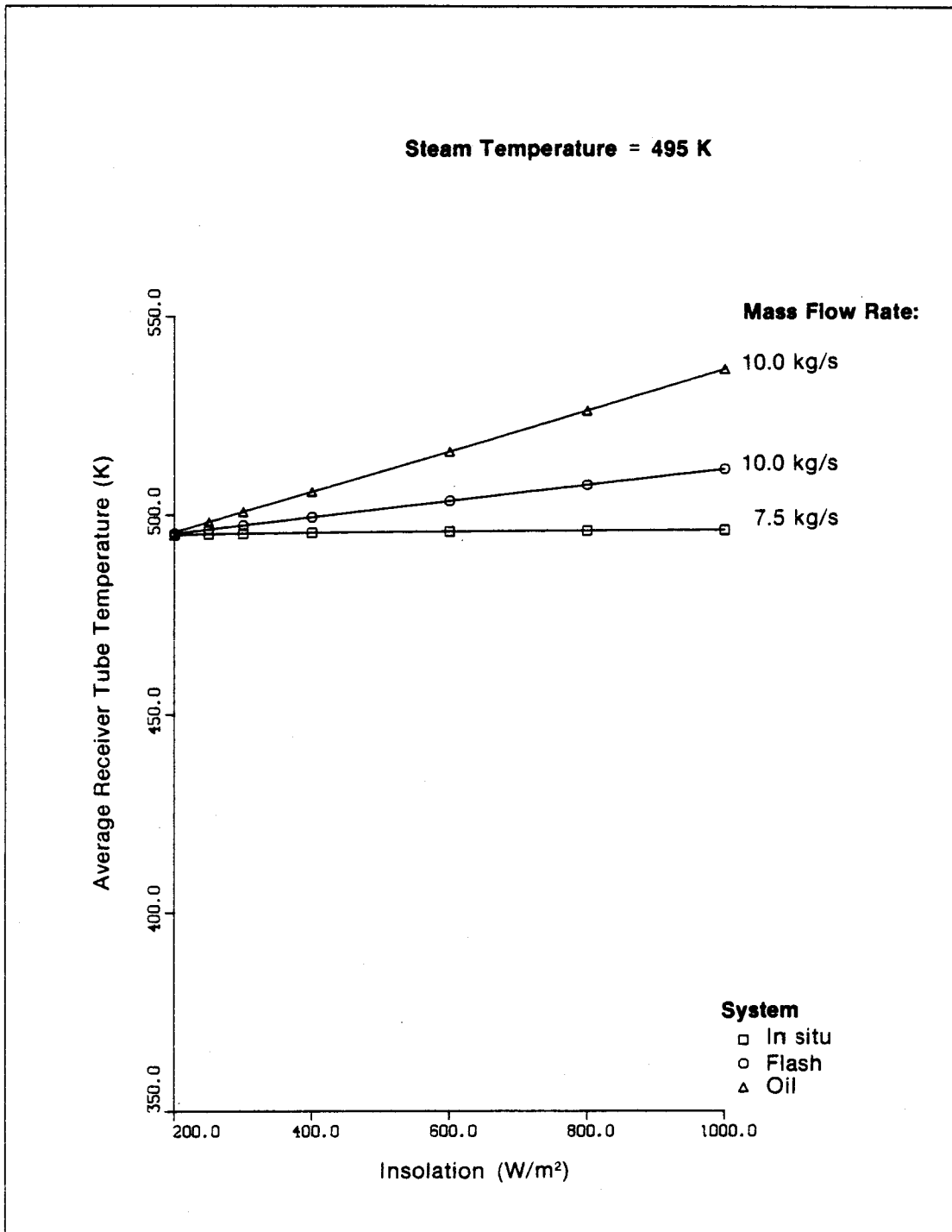
Figure 4-19. Average Receiver Tube Temperature vs. Incident Solar Flux
(T_s = 495 K)

The increase in steam quality with insolation and the decrease in temperature from the makeup water also constrain the temperature rise in the flash system receiver as flux levels are increased. A similar effect occurs in the oil system as increased steam production is made up by increased water flow through the heat exchanger. However, the effect is not as dramatic because of the inefficiencies of the heat exchange process. In addition, the low specific heat of a heat-transfer oil causes a much greater rise in collector temperature differential at a given insolation level than it would in a water system. This effect diminishes somewhat at higher temperatures (as illustrated by the difference in receiver temperature between the steam-flash and oil systems at different conditions) due to the fairly rapid increase in the specific heat of the heat-transfer fluid.

Again, these curves illustrate the point made earlier. At a given steam delivery temperature an in situ system is, for all practical purposes, isothermal at a temperature that is very close to the required steam delivery temperature regardless of mass flow and insolation. Furthermore, an approximation of isothermal operation is considerably less valid when the other systems are considered, especially the oil system where the average receiver tube temperature can vary as much as 60 K over the full range of insolation levels.

4.1.3 Steam Delivery Temperature Variations

Figures 4-20 through 4-22 and 4-23 through 4-25 illustrate variations in system net efficiency and average receiver tube temperature, respectively, as a function of steam delivery temperature. Since heat losses at a given steam temperature are fairly constant, steam delivery temperature has the greatest impact on the efficiency of various systems at lower flux levels. Also, the in situ system shows the least response to steam delivery temperature variations, and its benefit relative to the other systems increases with steam delivery temperature. At a steam temperature of 495 K and solar radiation of 200 W/m^2, the net efficiency of the oil system approaches zero.

Figures 4-23 to 4-25 illustrate that at low flux levels, the collector temperature differentials are so small that the temperatures of the receivers for all three systems tend to converge. However, as illustrated in the previous three graphs, similar receiver temperatures for each of the three competing solar systems do not correspond to similar performance. The oil system must work at some temperature higher than the steam delivery temperature for net heat exchange. Similarly, the flash system converts sensible heat change above the steam delivery temperature into latent heat of steam. In contrast, the direct boiling system will deliver energy when the average receiver tube temperature is at or below the delivered steam temperature.

In Figs. 4-23 to 4-25, the slopes of the curves are nearly constant with steam temperature at a given insolation level. Pressure effects tend to increase the temperature of the in situ system at low steam temperatures.

001010

Insolation = 200 W/m²
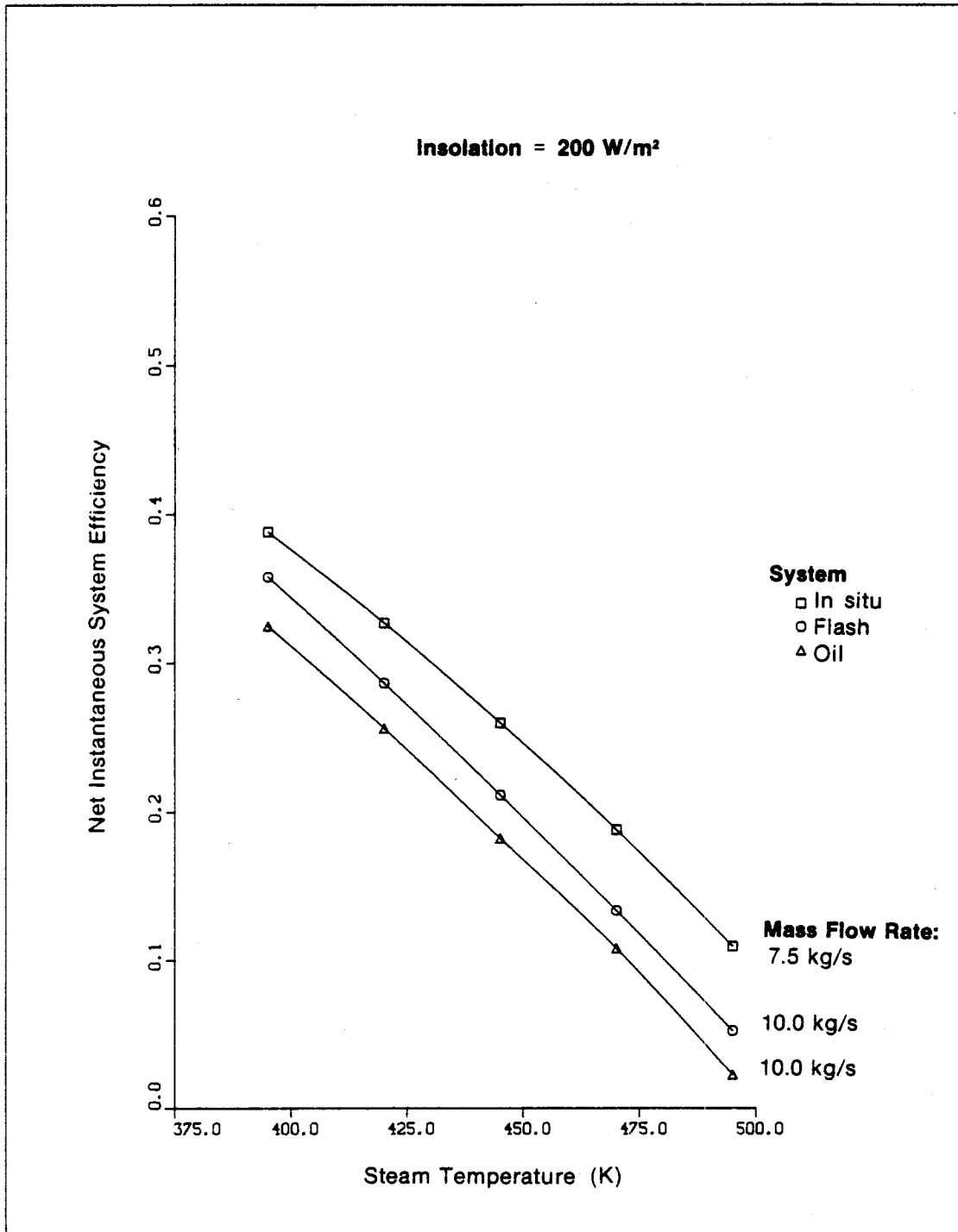
Figure 4-20. Net Instantaneous System Efficiency vs. Steam Temperature
$(I = 200 \ W/m^2)$
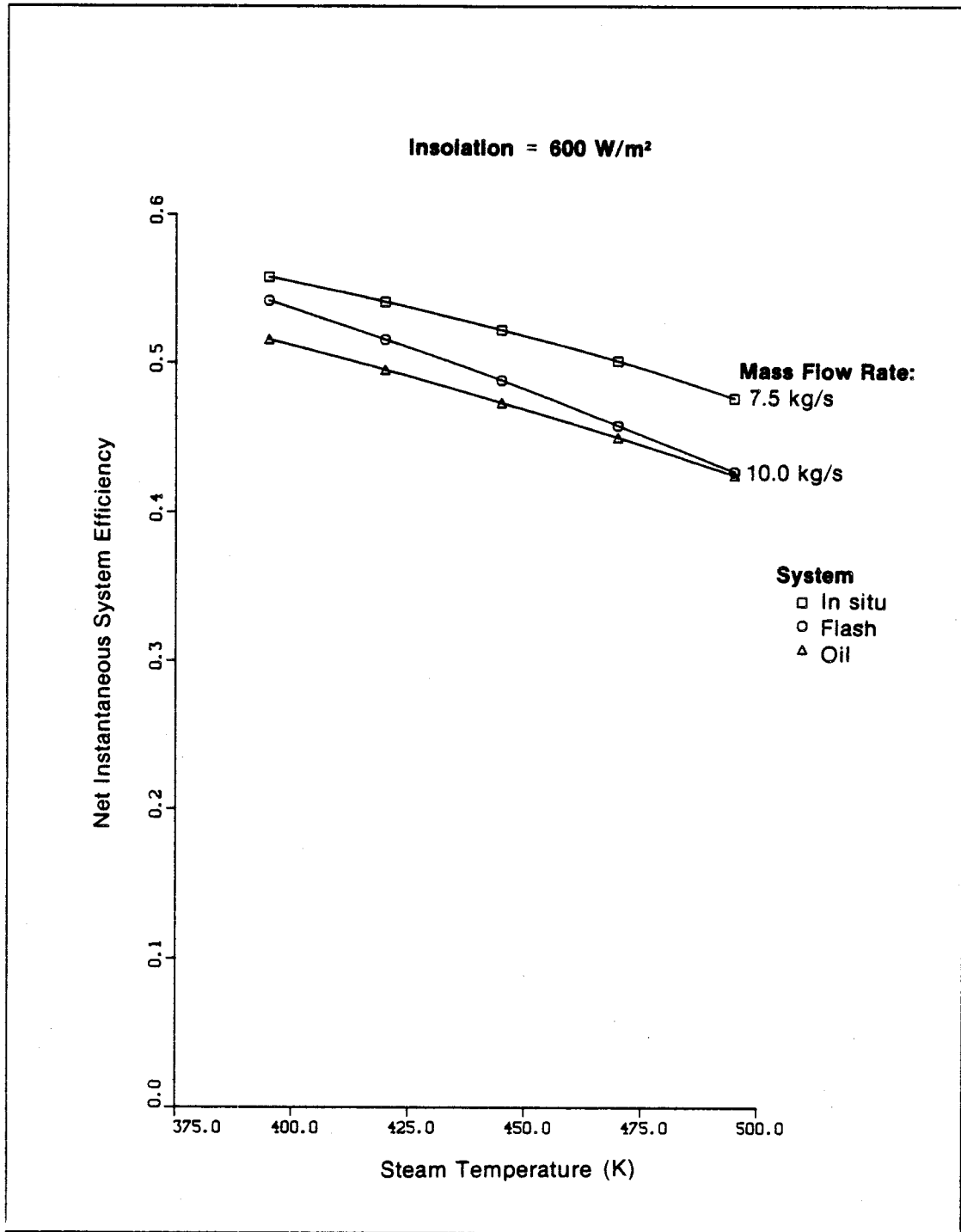
001011

Figure 4-21.   Net Instantaneous System Efficiency vs. Steam Temperature
                $(I = 600 \ W/m^2)$
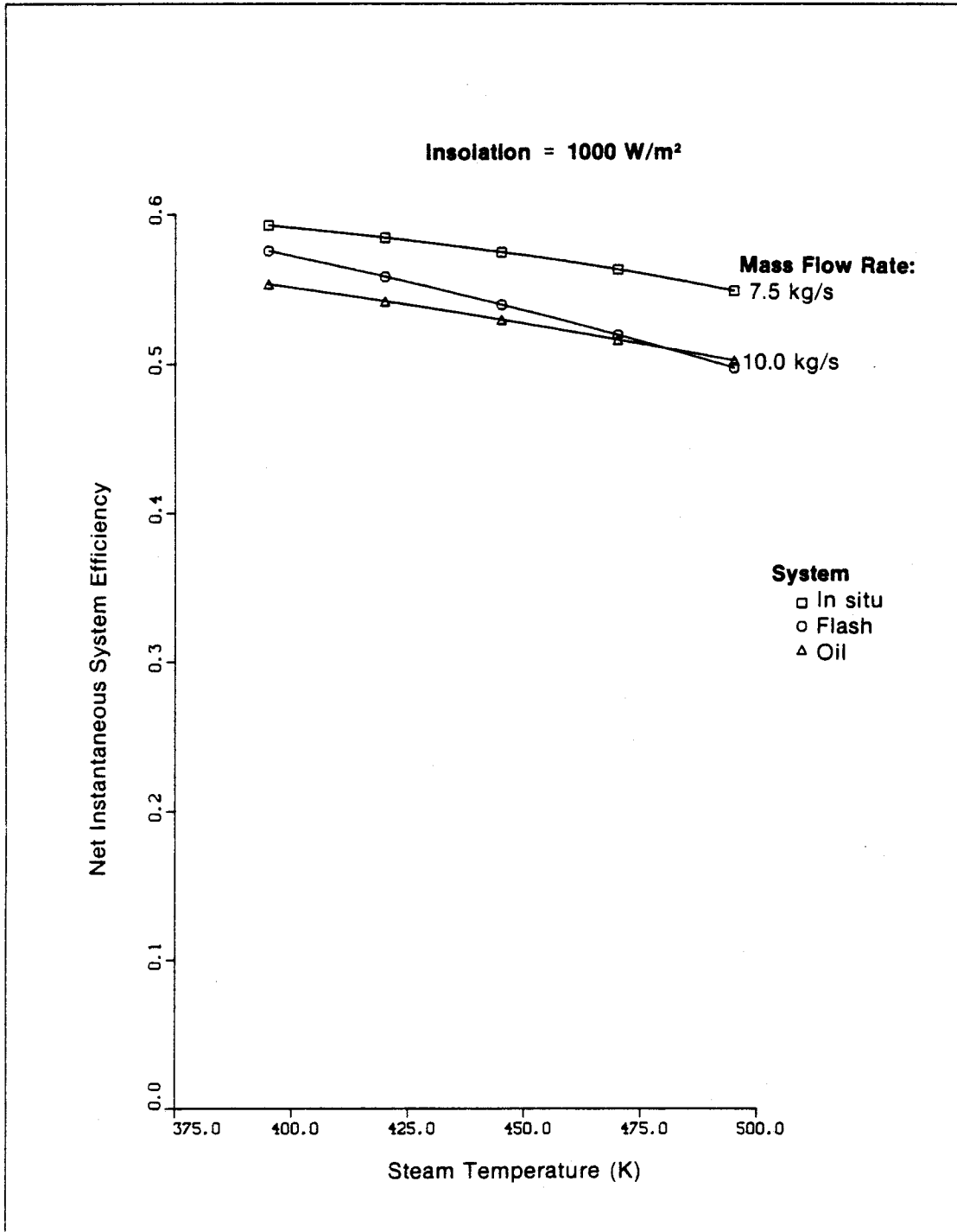
Figure 4-22. Net Instantaneous System Efficiency vs. Steam Temperature
(I = 1000 W/m^2)
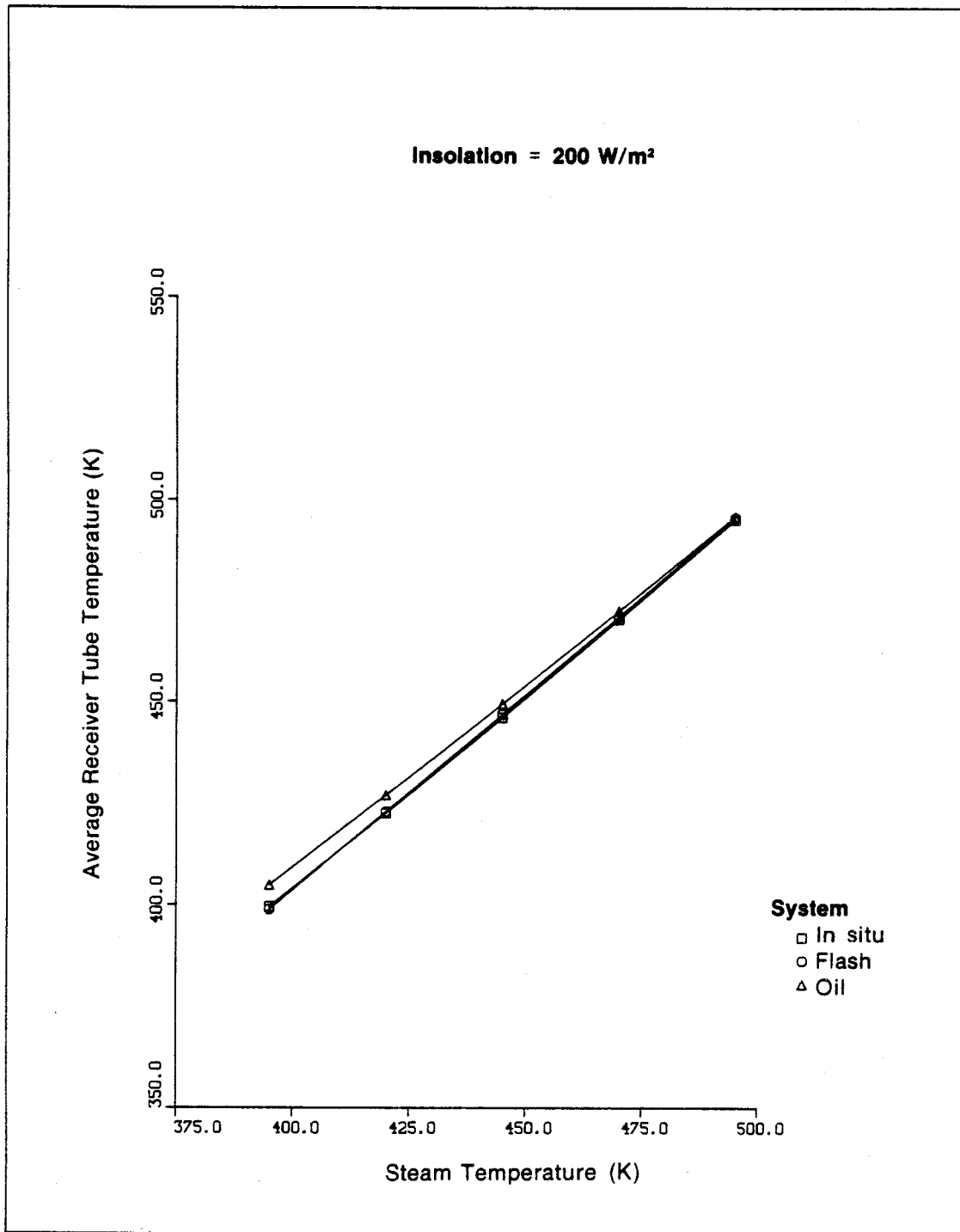
Figure 4-23. Average Receiver Tube Temperature vs. Steam Temperature
(I = 200 W/m^2)
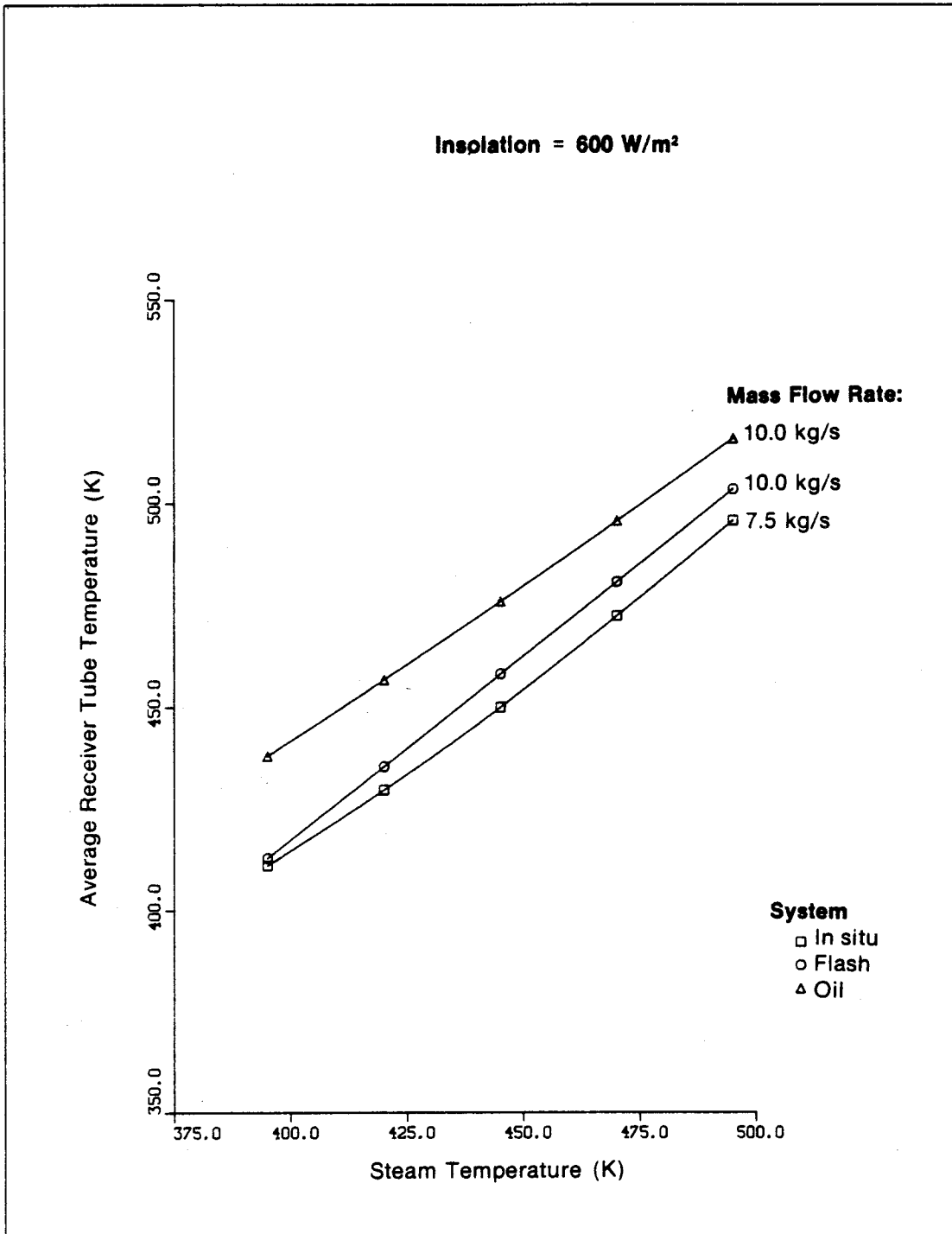
Figure 4-24.   Average Receiver Tube Temperature vs. Steam Temperature ($I = 600 \text{ W/m}^2$)
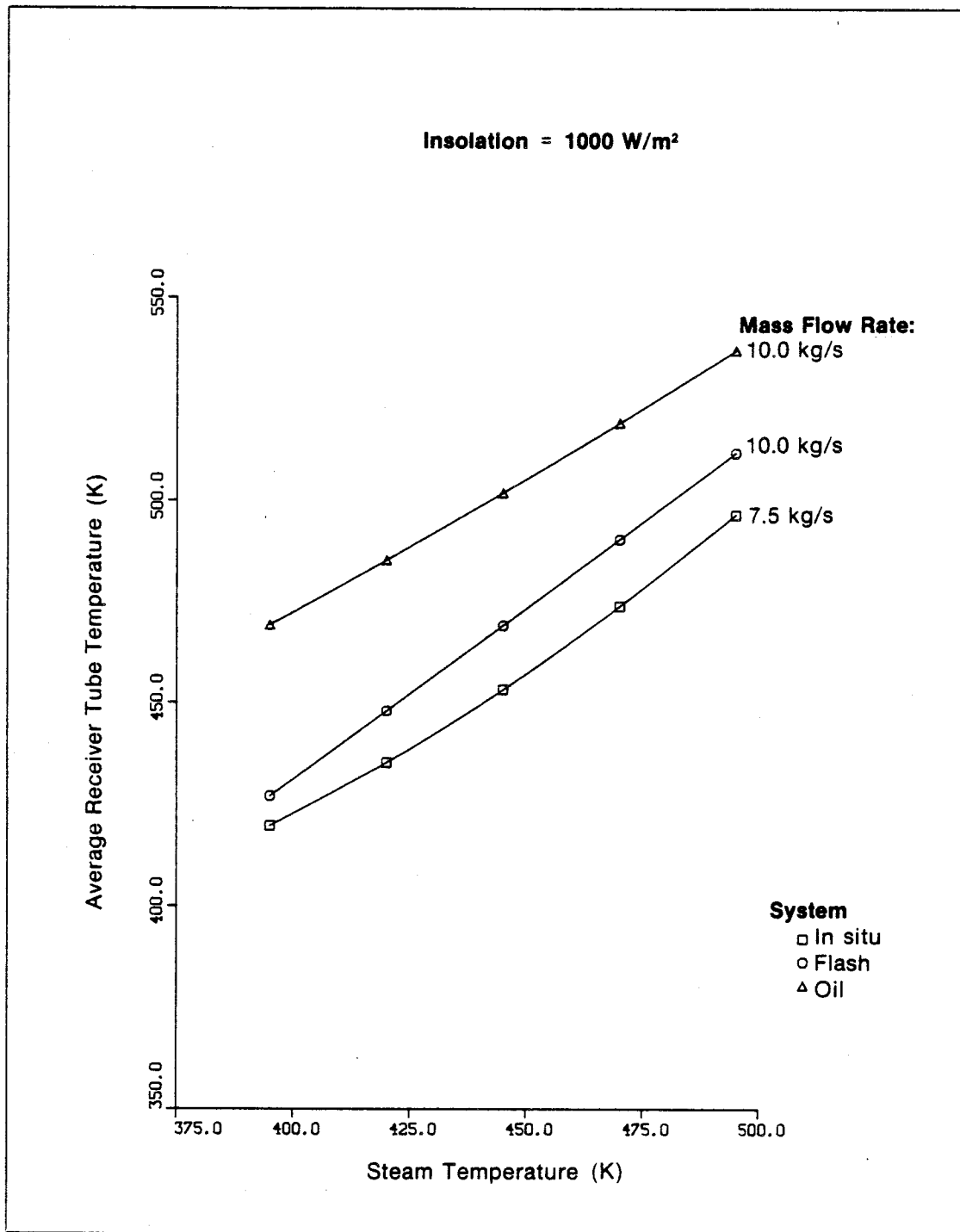
Figure 4-25. Average Receiver Tube Temperature vs. Steam Temperature
(I = 1000 W/m^2)

4.1.4 Pumping Power Effects

Pumping power has a significant impact on overall system efficiency especially when long-term performance is considered. Although pumping power at medium to high fluxes represents a relatively small negative contribution to the system efficiency, at low fluxes its effect on system efficiency can rise dramatically. Furthermore, the pumping power requirements of the steam flash system are up to 70 kW for high flux levels and high mass flow rates. Predicted pumping power versus mass flow rate is illustrated in Figs. 4-26 through 4-31 for a number of different fluxes and steam temperatures.

For the analysis, the electromechanical efficiency of the pump was assumed to be 50%. This discussion on pumping power is limited to steady-state conditions; hence, additional power required for cold start-up and field circulation to prevent freezing are not considered and are not included in the long-term analyses. The cold start-up problem with oils may have a significant impact because of their high viscosity at low temperatures.

Pumping power is proportional to differential pressure multiplied by volumetric flow rate. Since the change in volumetric flow through the pump is small, pumping power is proportional to the volumetric flow times the pressure differential ($V\Delta P$). The variation of pumping power over the range of operating variables can be analyzed in terms of a trade-off between changes in flow rate and system pressure drop.

For the oil and in situ systems, pumping power requirements are similar at similar flow rates, and mass flow rate is the primary determinant of pumping power. The curves in Figs. 4-26 through 4-31 illustrate the typical velocity-cubed dependence of system pumping power (as well as the velocity-squared pressure dependence). This is the case also for the flash system at low insolation levels where frictional effects dominate the total system pressure drop. At higher insolation levels, however, the elevation of pressure required to suppress boiling and the work dissipated across the flash valve become significant; this effect is more pronounced at low mass flow rates when collector outlet temperatures are highest. Thus, pumping power for the flash system goes through a minimum for higher insolation levels at a mass flow rate of about 10 kg/s for the baseline system described in this report. However, some mechanical component limitations could require that flow rates be increased beyond the optimum level if the flash system were used to generate high pressure steam. For instance, at a mass flow rate of 10 kg/s and an insolation level of 1000 W/m^2, system pressures will exceed 3.6 MPa (520 psia) for steam delivery temperatures in excess of 470 K (386°F).

Figs. 4-32 and 4-33 show the effect of delivered steam temperature on pumping power. The large increase in flash system pumping power reflects the increase in water saturation pressure at increased temperature. For the oil system, two competing effects are at work. First, reduced viscosity at higher temperatures reduces frictional effects. Second, the large volumetric expansion coefficient of the oil increases fluid velocities and increases frictional pressure drop. Thus when correlated in terms of mass flow rate, pumping power increases slightly with temperature. Pumping power of the in situ system declines with increasing steam pressure because the reduction in two-phase velocities reduces frictional pressure drop.
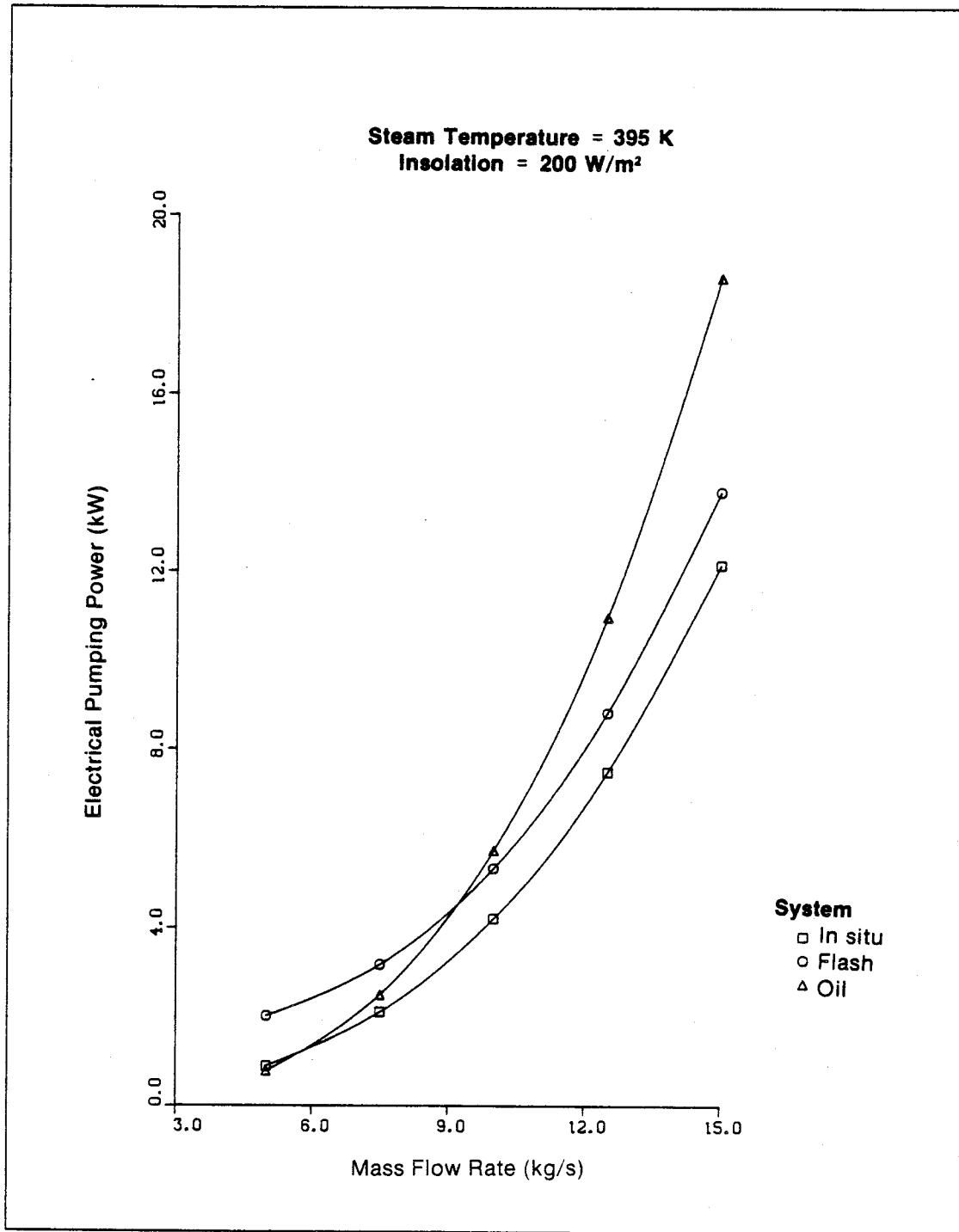
Figure 4-26. Electrical Pumping Power vs. Mass Flow Rate ($I = 200$ W/m^2, $T_s = 395$ K)
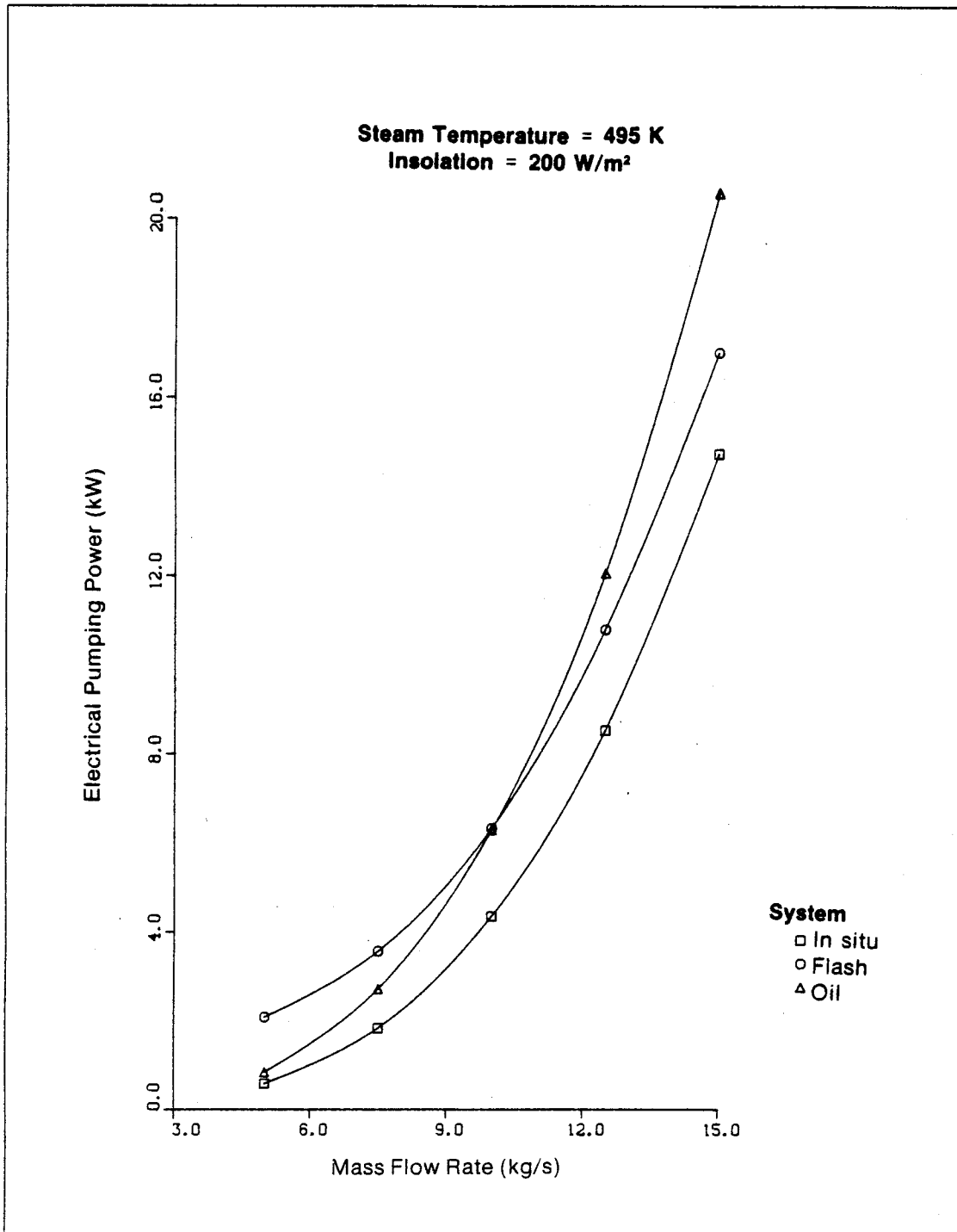
Figure 4-27. Electrical Pumping Power vs. Mass Flow Rate (I = 200 W/m^2, T$_s$ = 495 K)
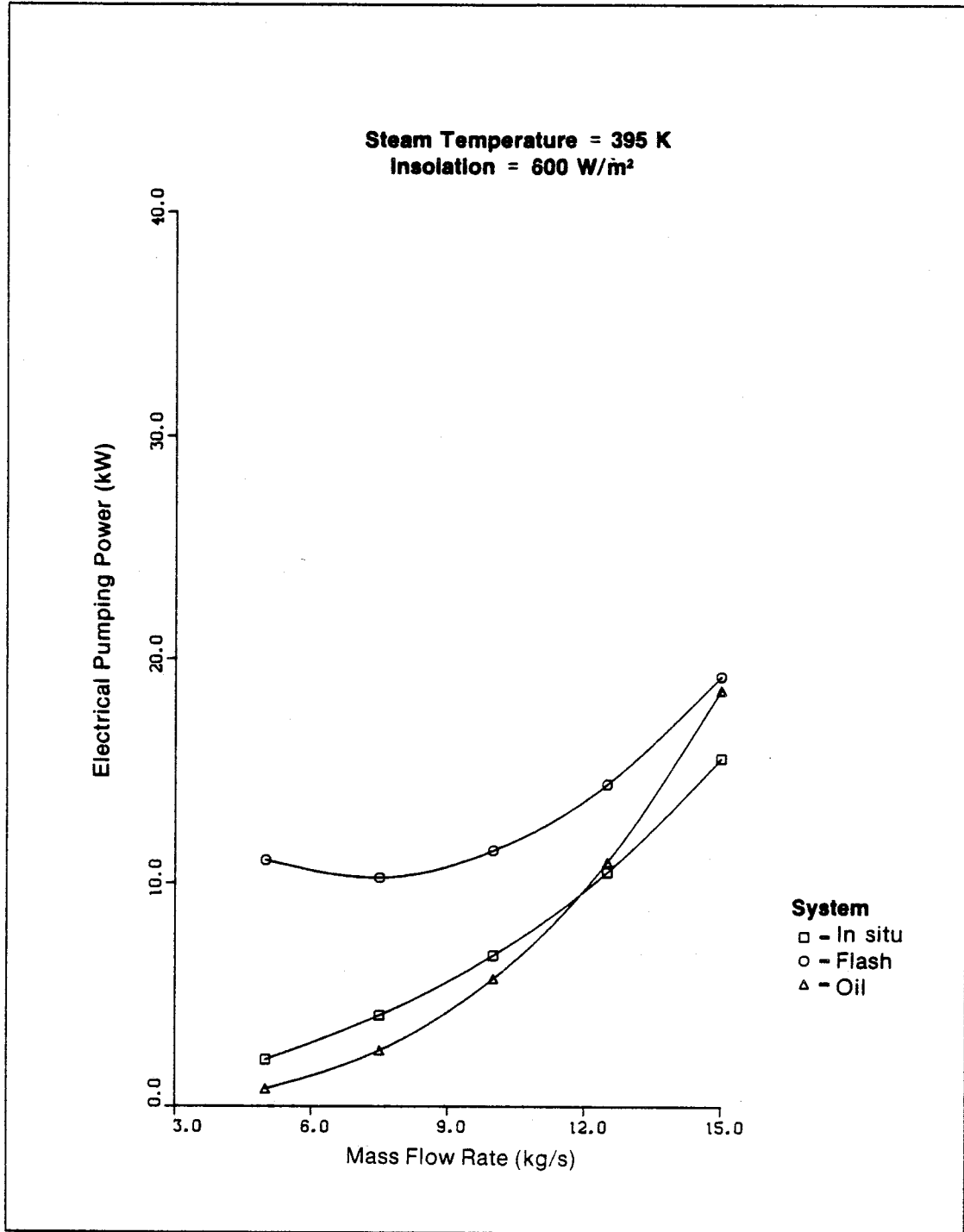
Figure 4-28. Electrical Pumping Power vs. Mass Flow Rate (I = 600 W/m^2, T$_s$ = 395 K)
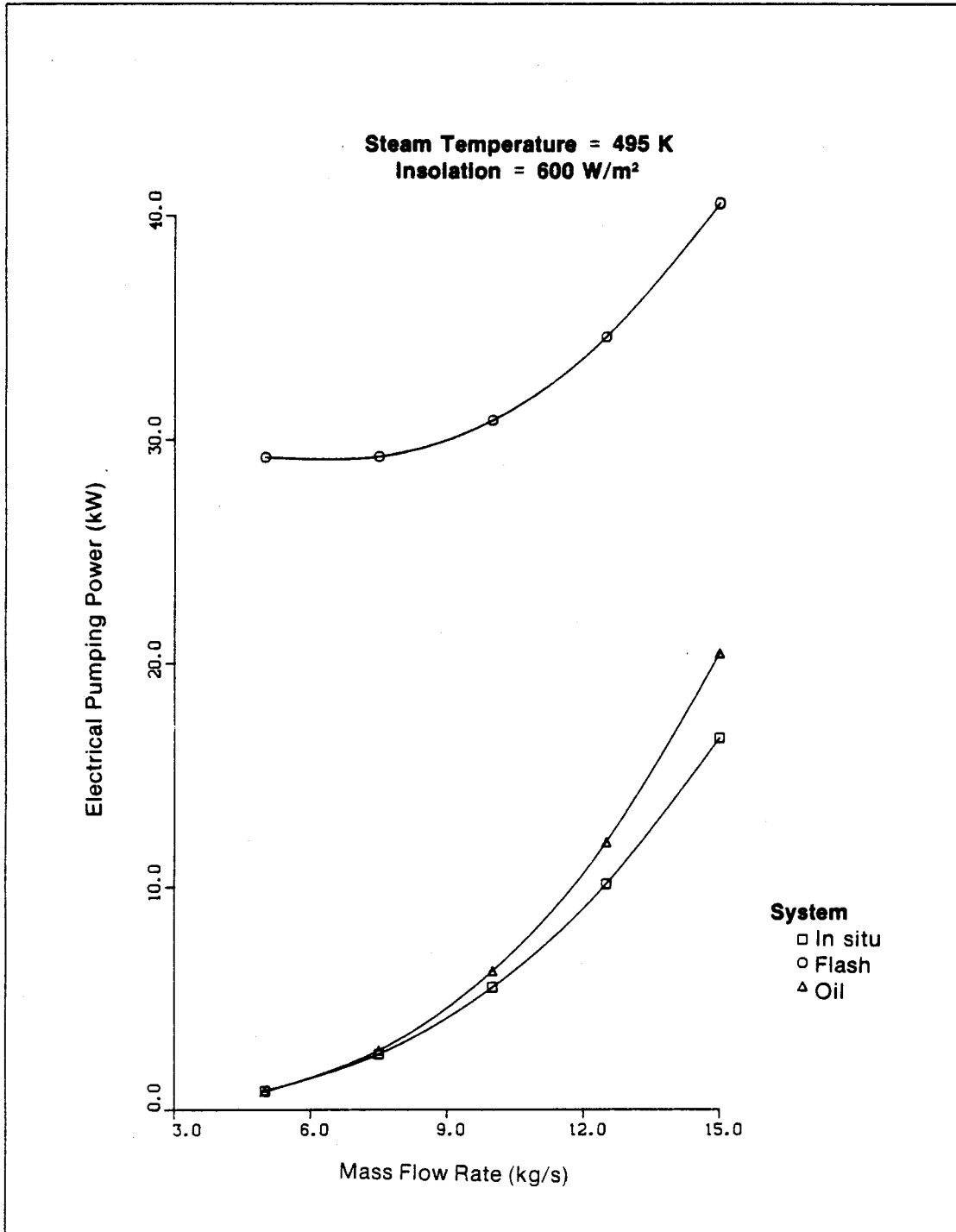
Figure 4-29. Electrical Pumping Power vs. Mass Flow Rate (I = 600 W/m², T_s = 495 K)

001020

Steam Temperature = 395 K

Insolation = 1000 W/m²
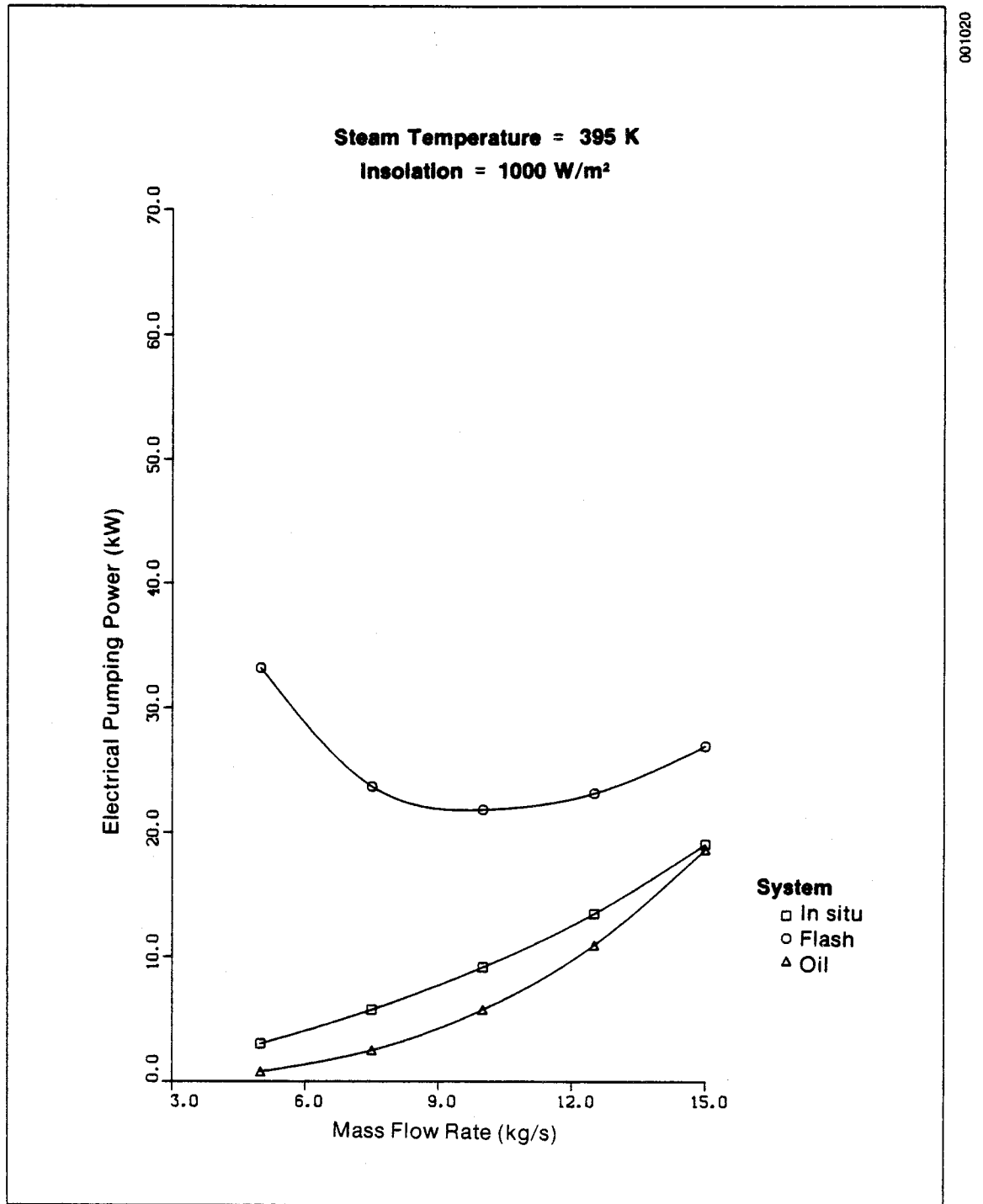
Figure 4-30.   Electrical Pumping Power vs. Mass Flow Rate (I = 1000 W/m²,
T$_s$ = 395 K)
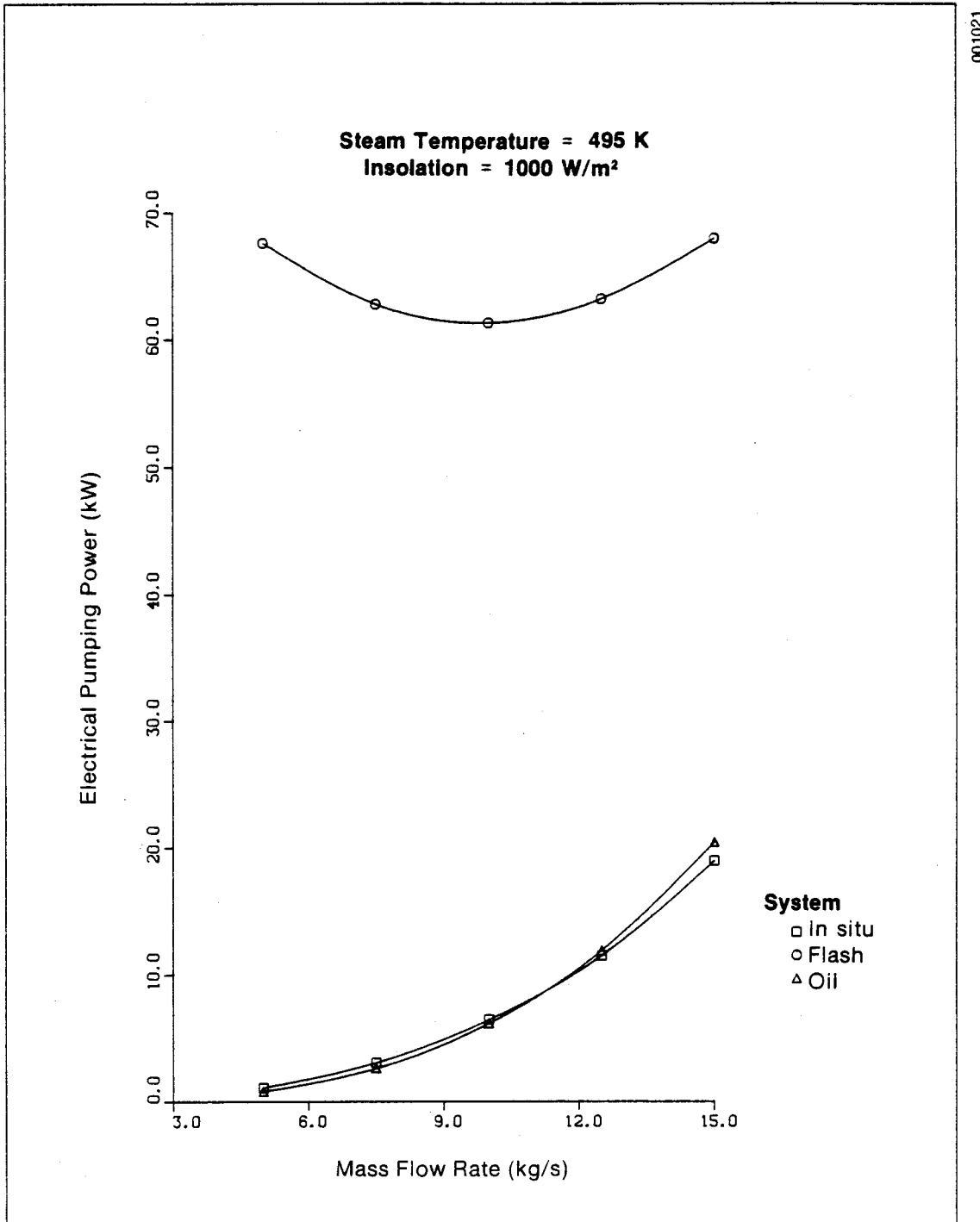
Figure 4-31. Electrical Pumping Power vs. Mass Flow Rate (I = 1000 W/m^2, T$_s$ = 495 K)

001022
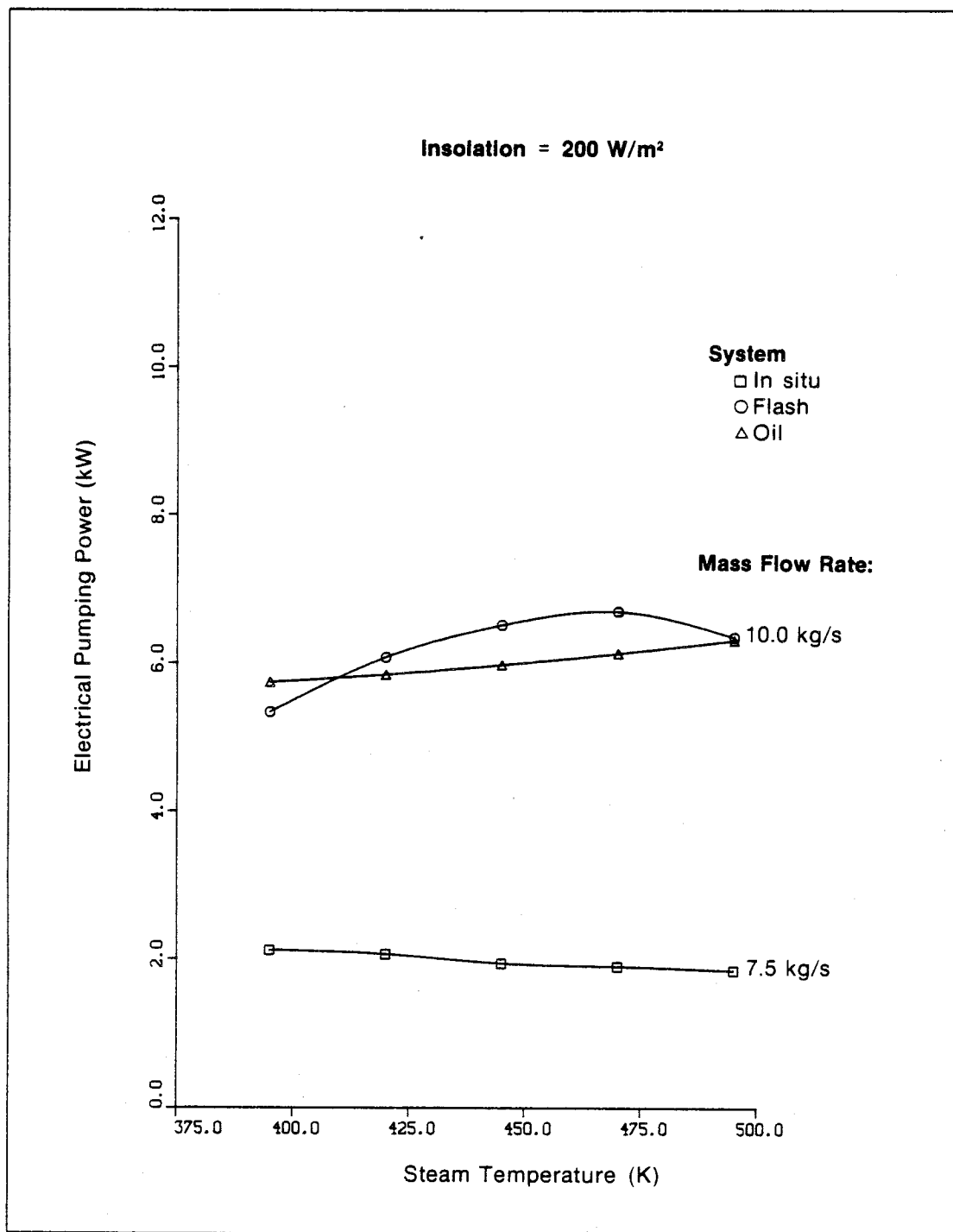
Figure 4-32. Electrical Pumping Power vs. Steam Temperature
(I = 200 W/m^2)

52
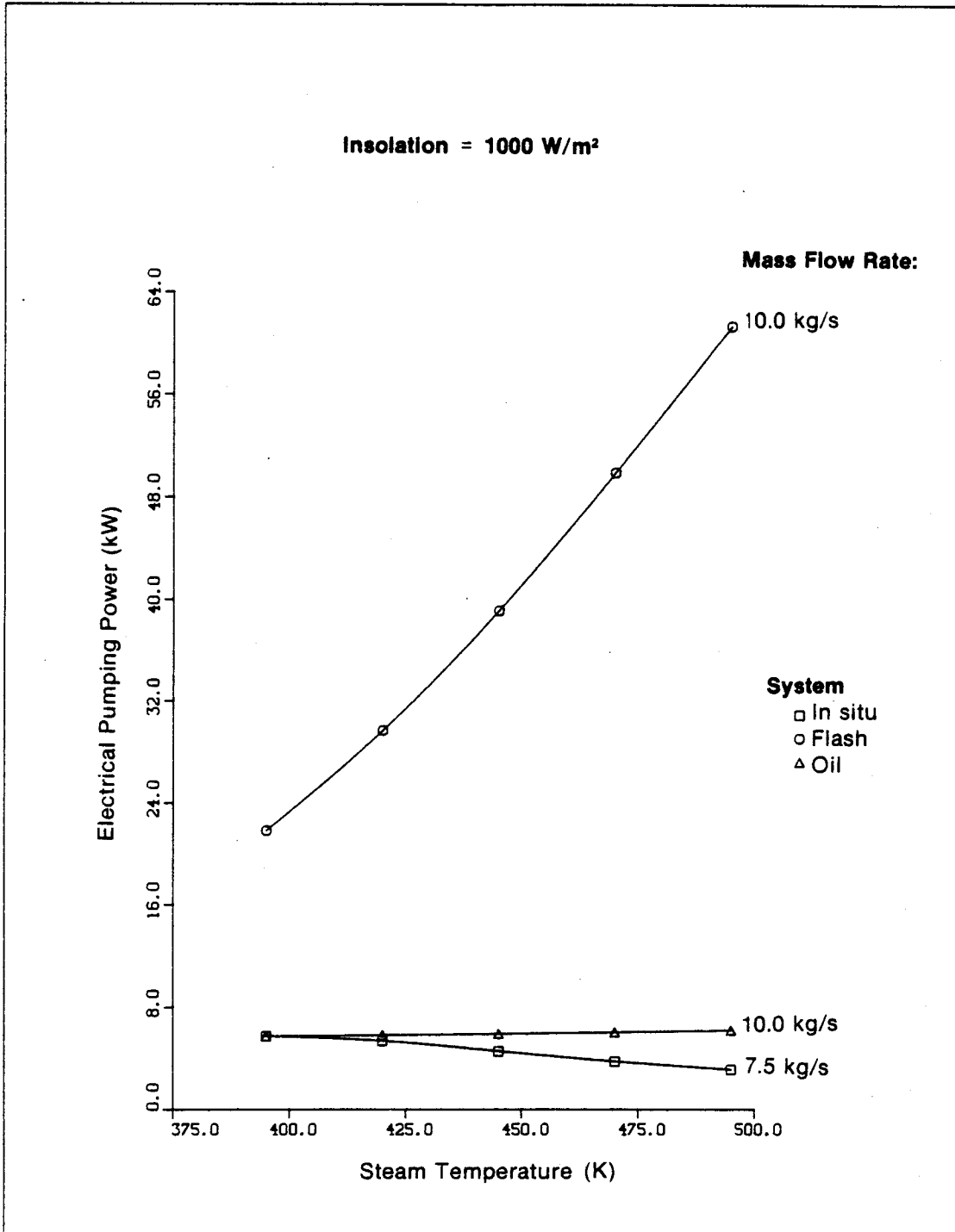
Figure 4-33. Electrical Pumping Power vs. Steam Temperature
(I = 1000 W/m^2)

In general, electric power consumed for pumping water in a direct-boiling system is similar but somewhat less than for the oil system. At the highest insolation and steam temperature levels, the flash system power consumption can be an order of magnitude higher. As insolation levels increase, corresponding increases in collector outlet temperature require higher pressures upstream of the flash valve to prevent boiling. This pressure is irreversibly dissipated across the flash valve. Pumping power for the oil system at a fixed mass flow rate will increase with incoming insolation because the reduction in viscosity cannot fully compensate for an increase in volumetric flow. Increases in exit quality raise the power requirements of the direct-boiling system at higher fluxes, but power consumption will fall as steam temperatures and therefore pressures increase.

4.2 LONG-TERM SYSTEM PERFORMANCE

To calculate long-term system performance, a number of procedures could have been used. One approach is to assume that the system performs in an essentially steady-state manner over the slowly varying diurnal and annual cycles. Then the steady-state predictions can be integrated over time for a specific location and known weather profile to yield the annual energy delivery. This general approach is currently employed in a number of detailed analysis tools for nonboiling systems (see Favell and Granjean 1980, or Klein 1979). Another approach which is simpler, albeit somewhat less precise, is to implement one of the long-term averaging techniques, while using the system response characterization defined by the detailed simulation model. This second approach was chosen for this analysis because it is simplified and economical.

The long-term averaging method developed by Rabl (1981) was used to predict the performance of collectors and collector systems on an annual basis. The procedure uses an assumed linear collector system performance model, along with a weather and insolation averaging procedure, to determine the annual performance of the system. The required inputs of the technique are the average daytime annual normal radiation, the latitude of the collector system, the annual average temperature, and the linearized operating parameters of the collector system. The average daytime fluxes are characterized in this study, and both the latitude and annual ambient temperature are simply selected.

Although an estimate of the average operating parameters for a system of collectors could be made based on the operating parameters of a single collector (see Appendix E), the most accurate and direct approach is to generate the required system operational characteristics from the detailed, steady-state model developed for this study. Hence, the approach selected develops separate operating characteristics for each system and each corresponding steam delivery temperature, for both the gross and net efficiency measures. For a specified system, steam delivery temperature, and nominal mass flow, a linear set of system performance characteristics was determined from a linear regression of system performance as a function of incident flux. As shown in Appendix E, this linearization provides very good, usable approximations. The most important results of the annual energy analysis are presented in Figs. 4-34 to 4-43.
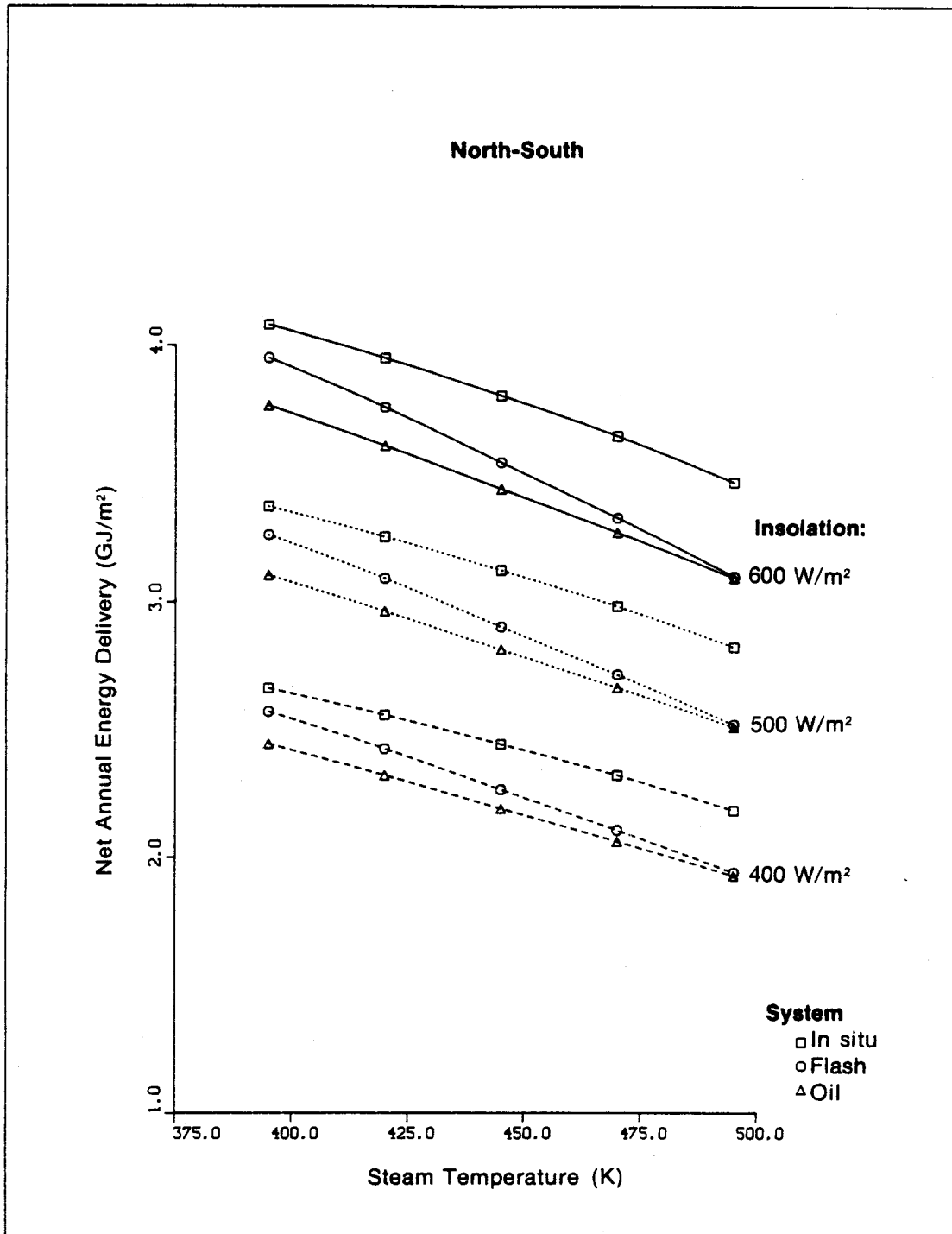
Figure 4-34. Net Annual Energy Delivery vs. Steam Temperature (North-South)
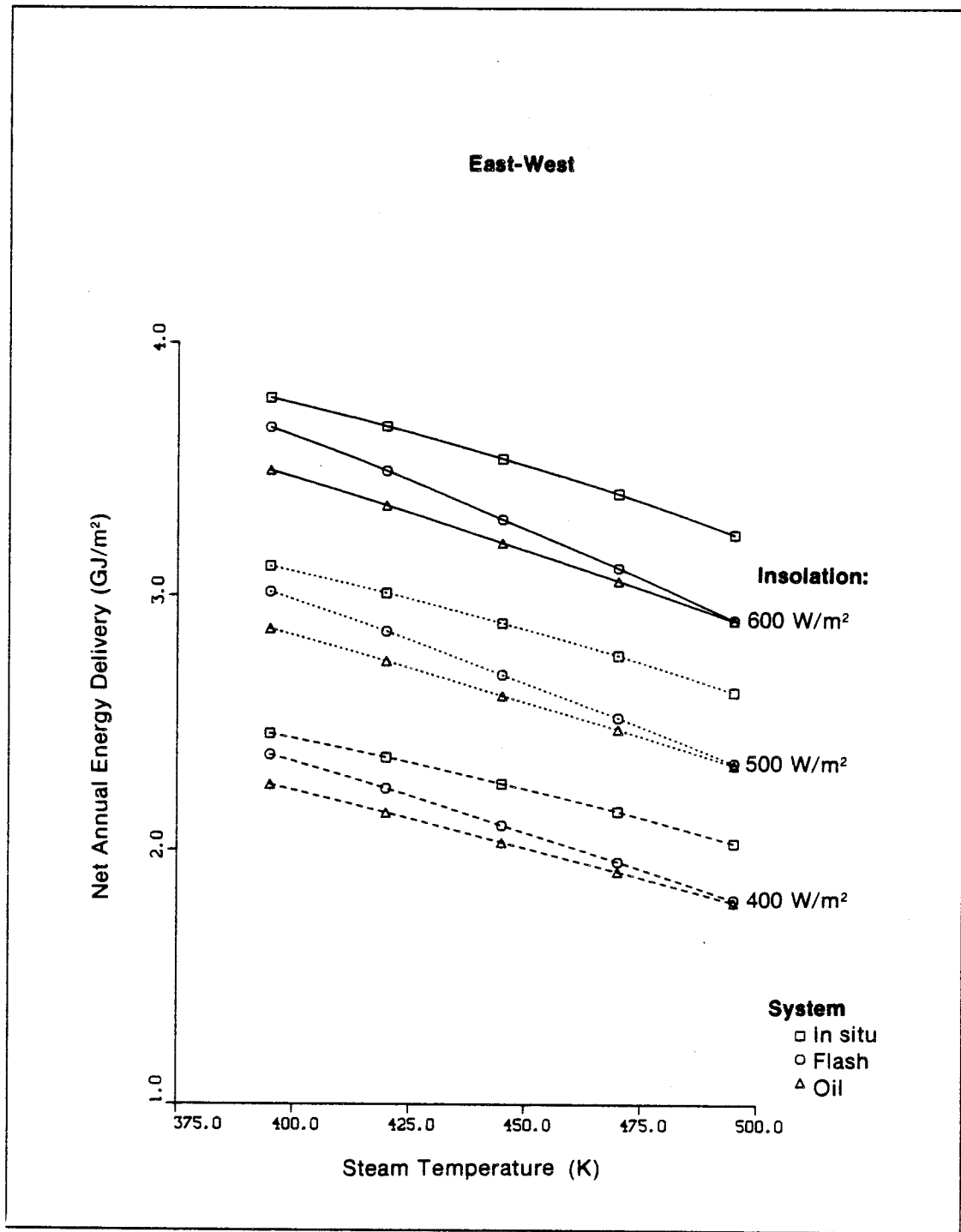
001025

East-West

Figure 4-35. Net Annual Energy Delivery vs. Steam Temperature (East-West)

56
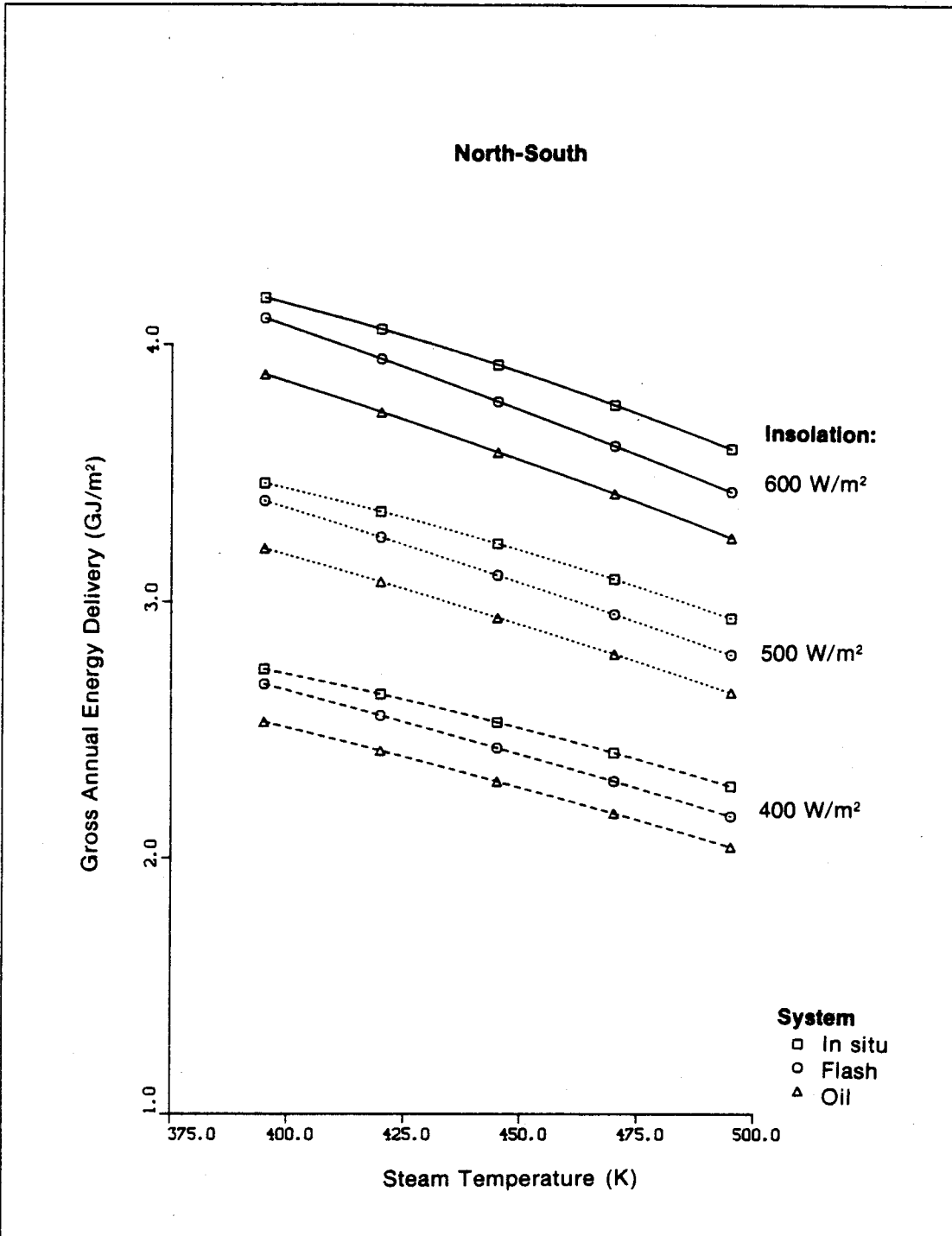
North-South

Figure 4-36. Gross Annual Energy Delivery vs. Steam Temperature (North-South)
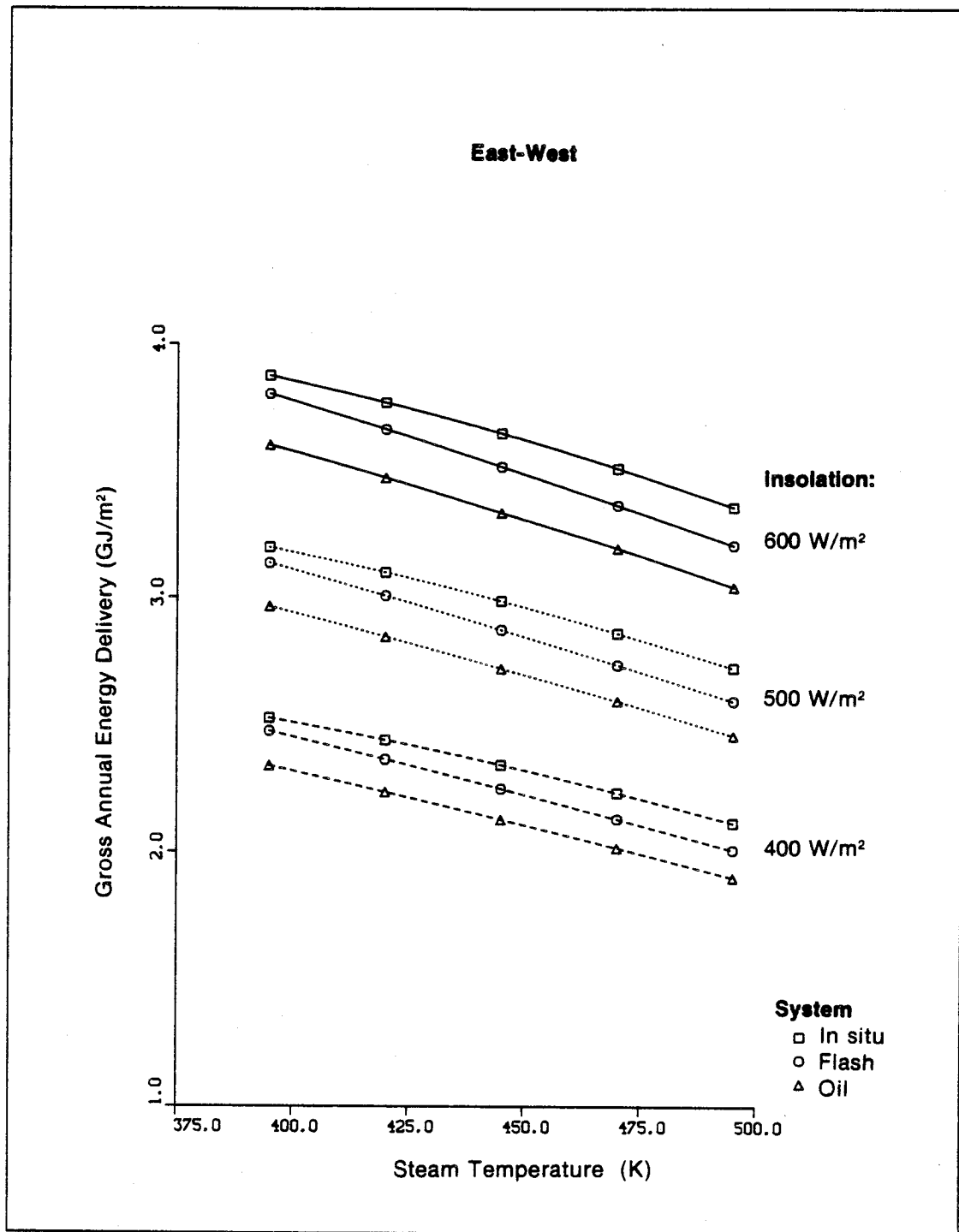
Figure 4-37. Gross Annual Energy Delivery vs. Steam Temperature (East-West)
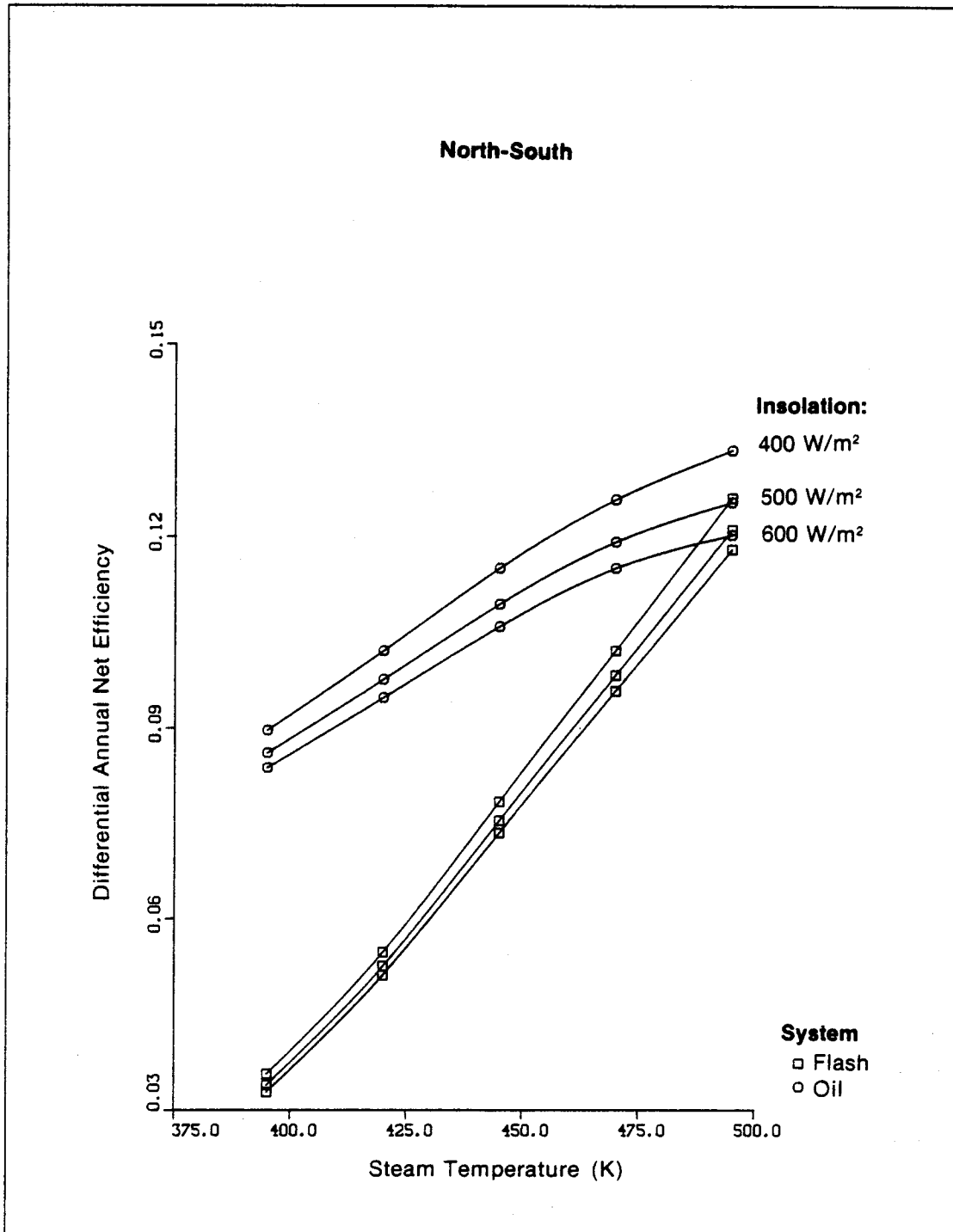
North-South

Figure 4-38. Relative Net Annual Delivered Energy Benefit Using In Situ Boiling vs. Steam Temperature (North-South)
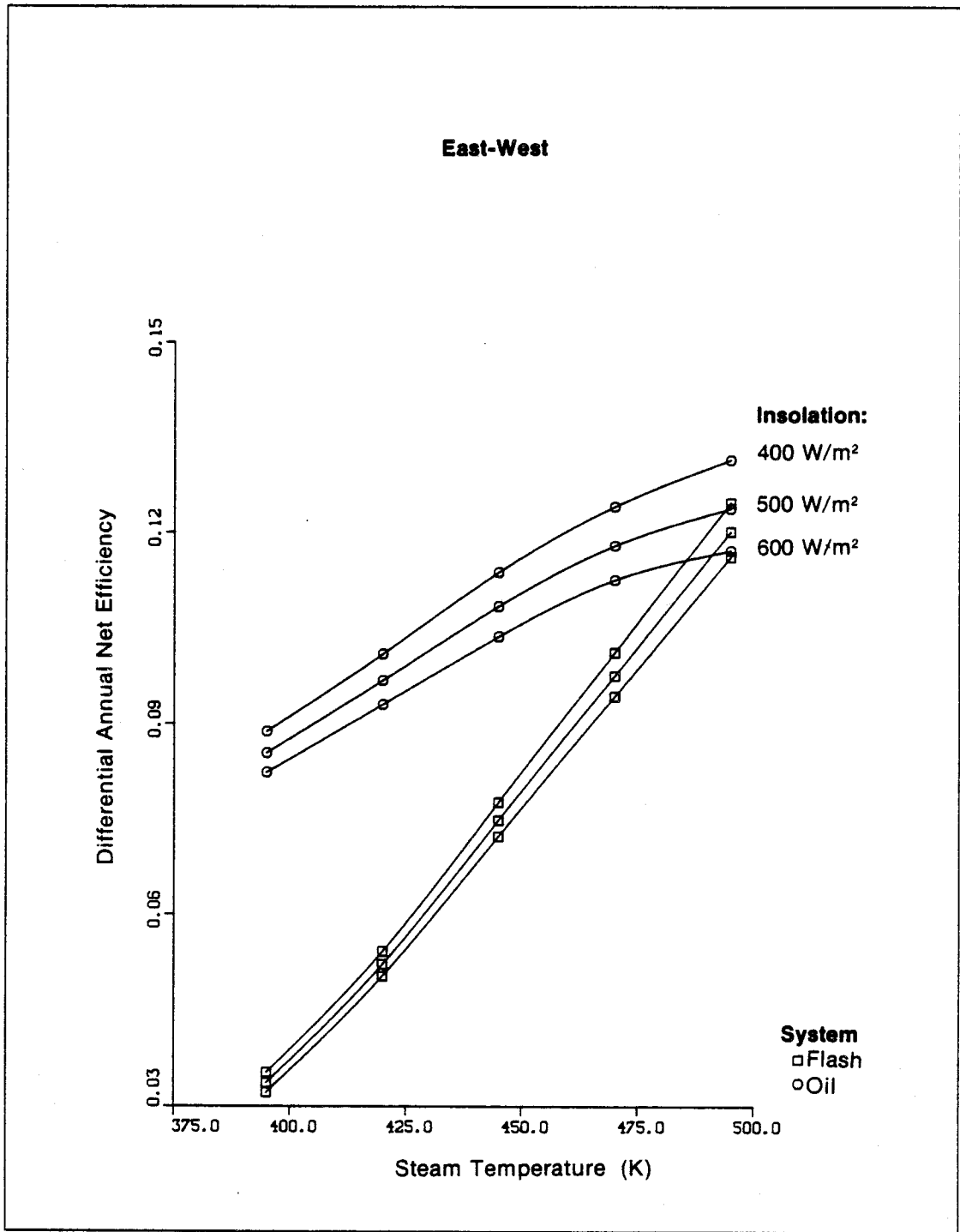
Figure 4-39. Relative Net Annual Delivered Energy Benefit Using In Situ
Boiling vs. Steam Temperature (East-West)

SERI
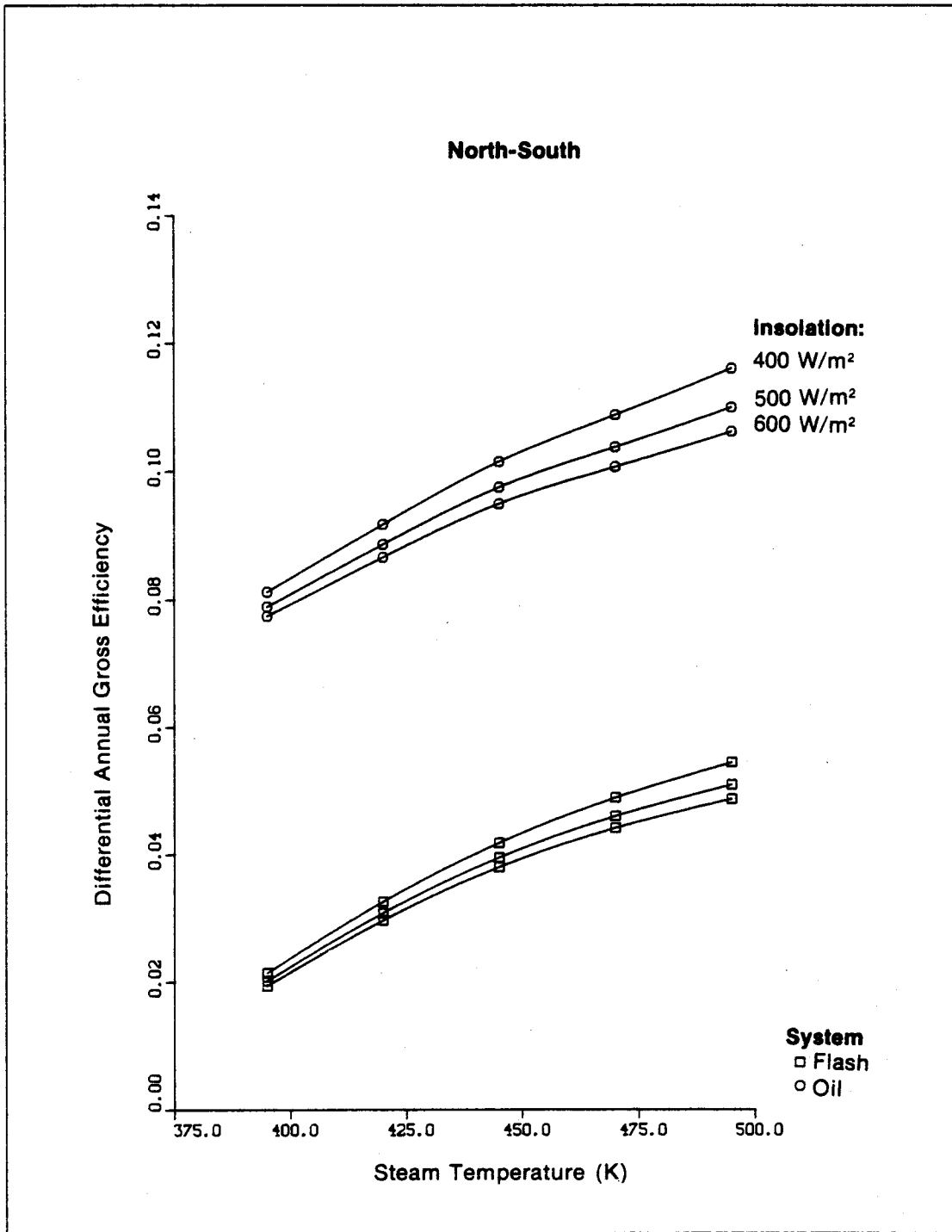
Figure 4-40.   Relative Gross Annual Delivered Energy Benefit Using
In Situ Boiling vs. Steam Temperature (North-South)
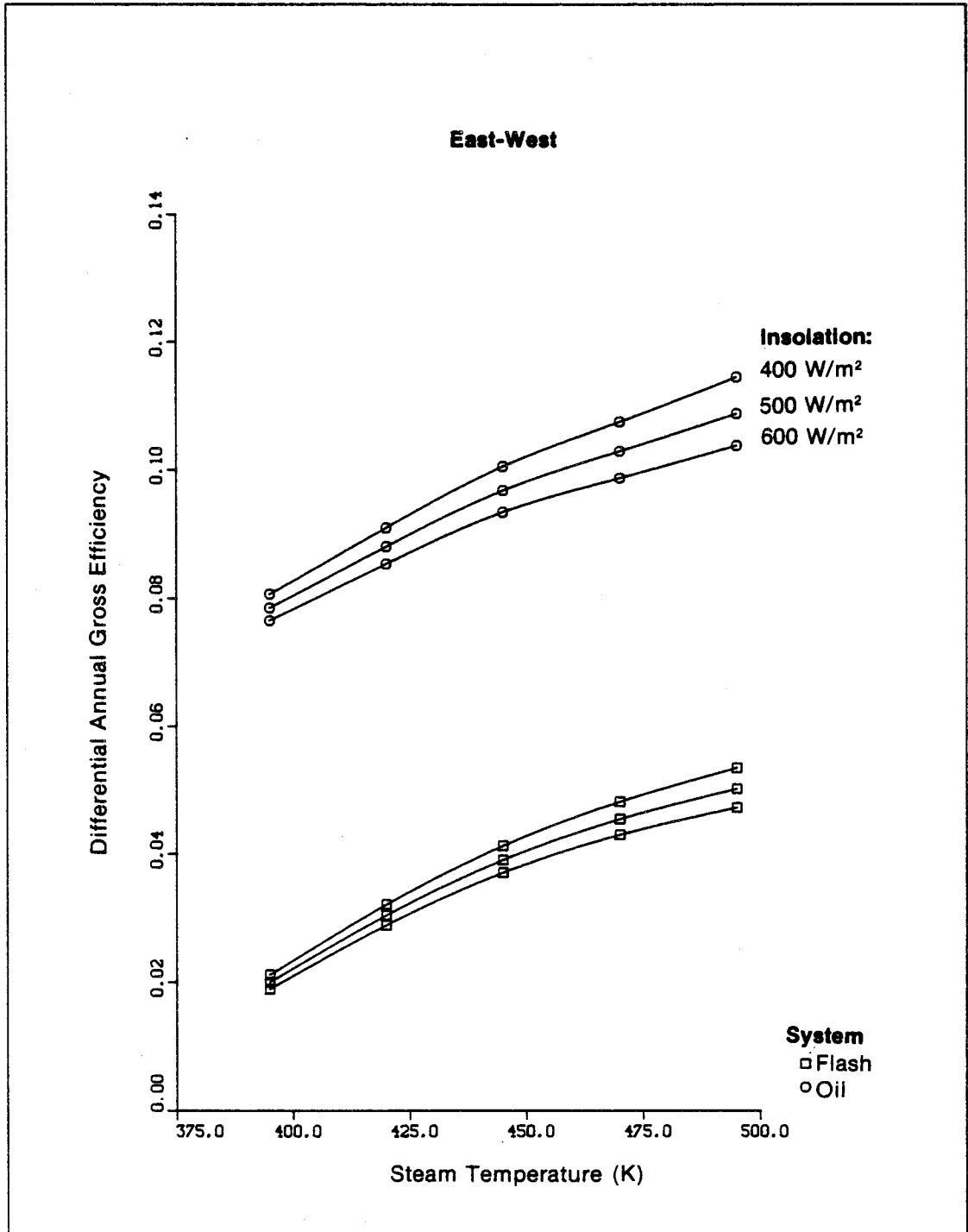
001031

East-West

Figure 4-41. Relative Gross Annual Delivered Energy Benefit Using In Situ
              Boiling vs. Steam Temperature (East-West)
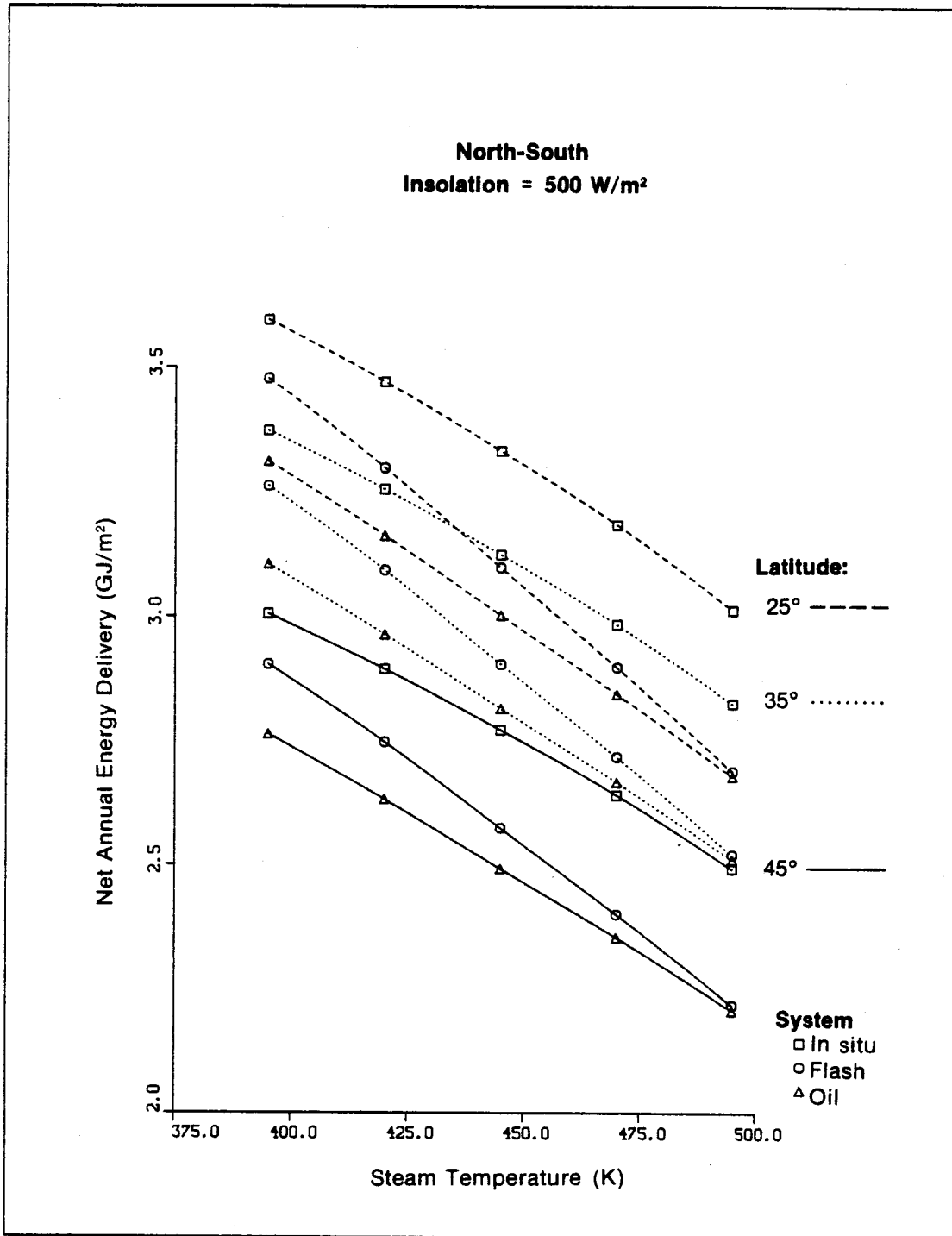
Figure 4-42. Effect of Latitude on Net Annual Energy Delivery
(North-South, I = 500 W/m^2)
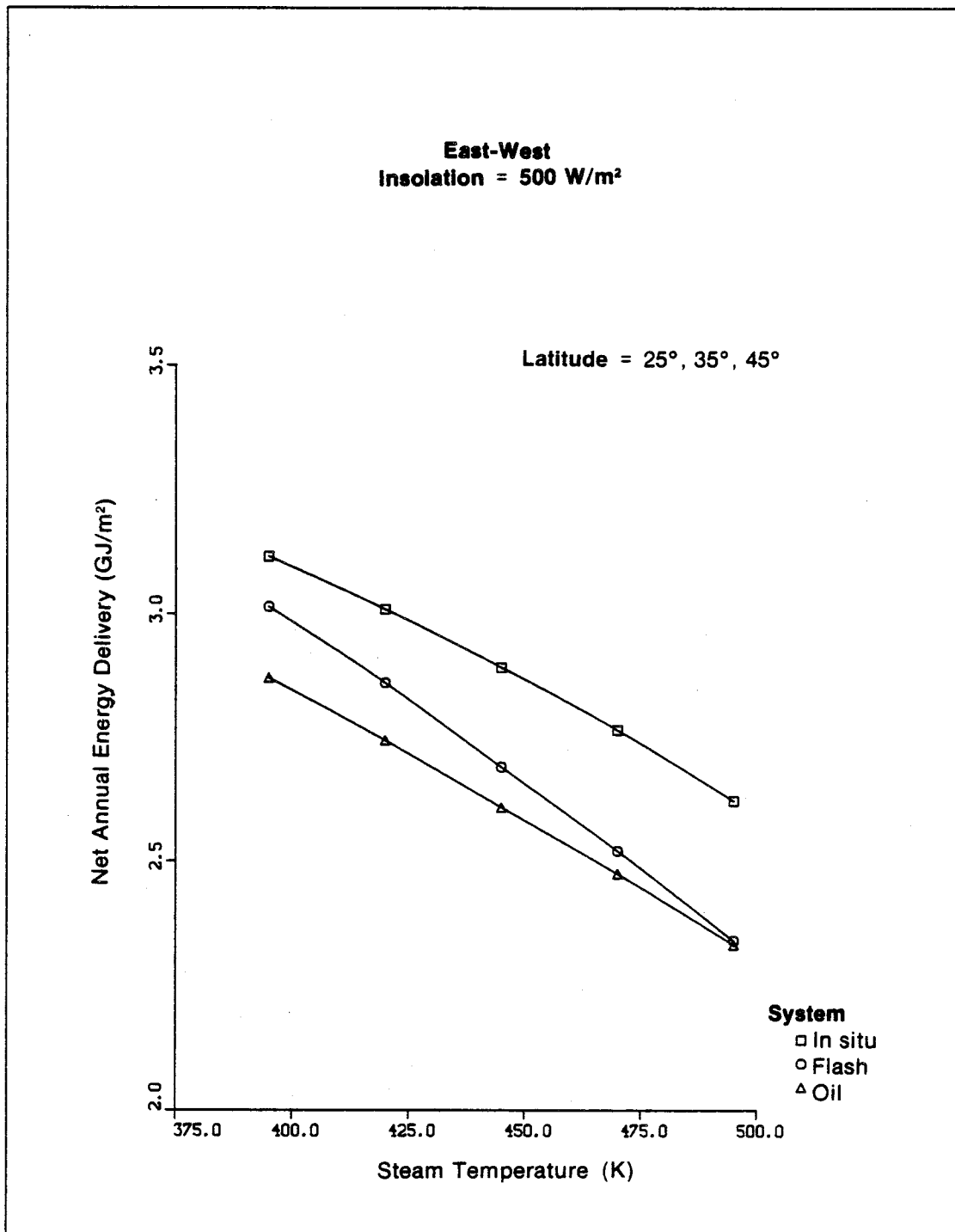
Figure 4-43. Effect of Latitude on Net Annual Energy Delivery (East-West, I = 500 W/m^2)

In Figs. 4-34 to 4-41, the annual energy delivery was calculated for a fixed latitude of 35°N, and a fixed annual average daytime ambient temperature of 287 K (14°C), typical parameters for a location such as Albuquerque, N. Mex. Three annual mean daytime normal solar radiation levels are also considered in these figures. At a latitude of 35°N, the highest average insolation level (600 W/m^2) considered would correspond to the climate such as Albuquerque; 500 W/m^2 would correspond to Lubbock, Tex.; and 400 W/m^2 would correspond to Oklahoma City, Okla. (It should be noted that mean daytime normal solar radiation levels in the northeastern and northwestern United States are about 300 W/m^2.) The energy delivery differences corresponding to east-west and north-south collector axis orientation for each of the three steam systems are also demonstrated. Figures 4-34 and 4-35 indicate the variation of annual delivered energy (per unit collector area) with steam temperature when the net efficiency measure is used. A similar trend is evident in Figs. 4-36 and 4-37 where gross energy delivered is considered; but the detrimental effect of pumping power for the flash system at high steam temperatures is not shown.

Figures 4-38 through 4-41 give a concise, overall picture of the relative benefits of using an in situ system in terms of net and gross system efficiency. The relative benefit is defined as the increase in annual energy delivered by the direct-boiling system over that of the flash (oil) system, divided by the annual energy delivered by the flash (oil) system:

$$\left(\frac{\Delta E}{E}\right)_{Flash} = \frac{E \ (Direct \ Boiling) - E \ (Flash)}{E \ (Flash)}$$

and

$$\left(\frac{\Delta E}{E}\right)_{Oil} = \frac{E \ (Direct \ Boiling) - E \ (Oil)}{E \ (Oil)} \ .$$

A number of conclusions can be drawn from these results, some of which can be anticipated from the steady-state analysis. As expected, the in situ system delivers the most energy on an annual basis. Over the range of steam temperatures investigated and the nearly optimal flow rates chosen, the net benefit over the oil system is from 9% to 13%; over the flash system the range is wider, from 3% to 12%, primarily because of the effect of pumping power. At even higher steam temperatures, the relative benefits of the in situ system would increase at a faster rate than the extrapolation of the trends shown in Figs. 4-38 and 4-39 would suggest. This increase arises because heat transfer oils are generally limited to 600 K and because the operating pressure of the flash system would require sturdier and heavier collector components.

Interestingly, the relative benefit of the in situ system increases with decreasing insolation. This trend was noted in Figs. 4-11 through 4-16 of the steady-state analysis. In addition, not only do north-south oriented troughs deliver more energy on an annual basis than east-west oriented troughs, but the relative benefit of the direct system over the other steam systems is slightly greater for the former orientation. Furthermore, as can be determined from the data presented in Fig. 4-42, the relative benefit of the in situ system for a north-south oriented field increases as latitude angle

increases even though annual energy collection decreases with a latitude angle increase. The annual energy calculation does not show any latitude dependence for an east-west oriented solar field. In short, the in situ system, compared to the flash and oil systems, has the greatest relative benefit when conditions for energy collection such as of increasing steam temperature and latitude and decreasing insolation (ambient temperature could be added) are least favorable. These results occur because the collector cut-off flux is lowest for the in situ system since it operates at the lowest temperature. (Not only is the in situ system more efficient, but it also operates over a longer period during the day; i.e., a more efficient system turns on a little earlier and off a little later.) For instance, in winter the daily insolation intercepted by a north-south orientated trough is less than half that intercepted daily in the summer, and ambient temperatures are lower. Thus, the relative benefit of the in situ system is higher in winter than in summer when insolation levels and ambient temperatures are greater. This effect tends to reduce the seasonal variation of energy collected by the in situ system compared to the flash and oil systems, and reduces the effect of increasing latitude.

4.3 RECEIVER PERFORMANCE RESULTS

As mentioned earlier, two different models, the simple efficiency analog and the detailed thermal network model, were used to simulate the performance of line-focus collectors. Appendix A gives a detailed discussion of each of these models. Implementation of either model provides essentially equivalent predicted results for the fluid transport state and energy delivery. The advantage of using the detailed model lies in the additional information provided by the thermal network, such as tube wall temperature profile, the glass envelope temperature, and the detailed energy balance from which losses can be studied.

Figures 4-44 to 4-46 illustrate the predicted bulk fluid temperature in the receiver as a function of position along its length for the three systems. The variation is provided for two flux levels and two temperatures. The advantage of the in situ system is clearly illustrated in terms of lower collector operating temperature. Note that the fluid temperature levels off, followed by a subsequent slight decrease in the in situ system. This decrease is caused by the pressure drop in the boiling region which in turn lowers the bulk saturation temperature of the two-phase fluid. Under some conditions, the fluid temperature near the receiver entrance of the flash system is lower than for the in situ system, which is caused by the higher baseline mass flow rate used in the flash system. For the same mass flow rate, the entrance temperature of the in situ system is slightly lower because of the increased steam exit quality and subsequent volume of makeup water.

Figures 4-47 through 4-50 illustrate various predicted fluid transport properties corresponding to the in situ system for two extreme flux and steam delivery levels, as a function of position along the receiver. Figure 4-47 illustrates the impact of steam temperature and flux on receiver fluid temperature. The smallest fluid temperature variations occur with low fluxes and with high steam temperatures. Figure 4-48 illustrates changes in steam
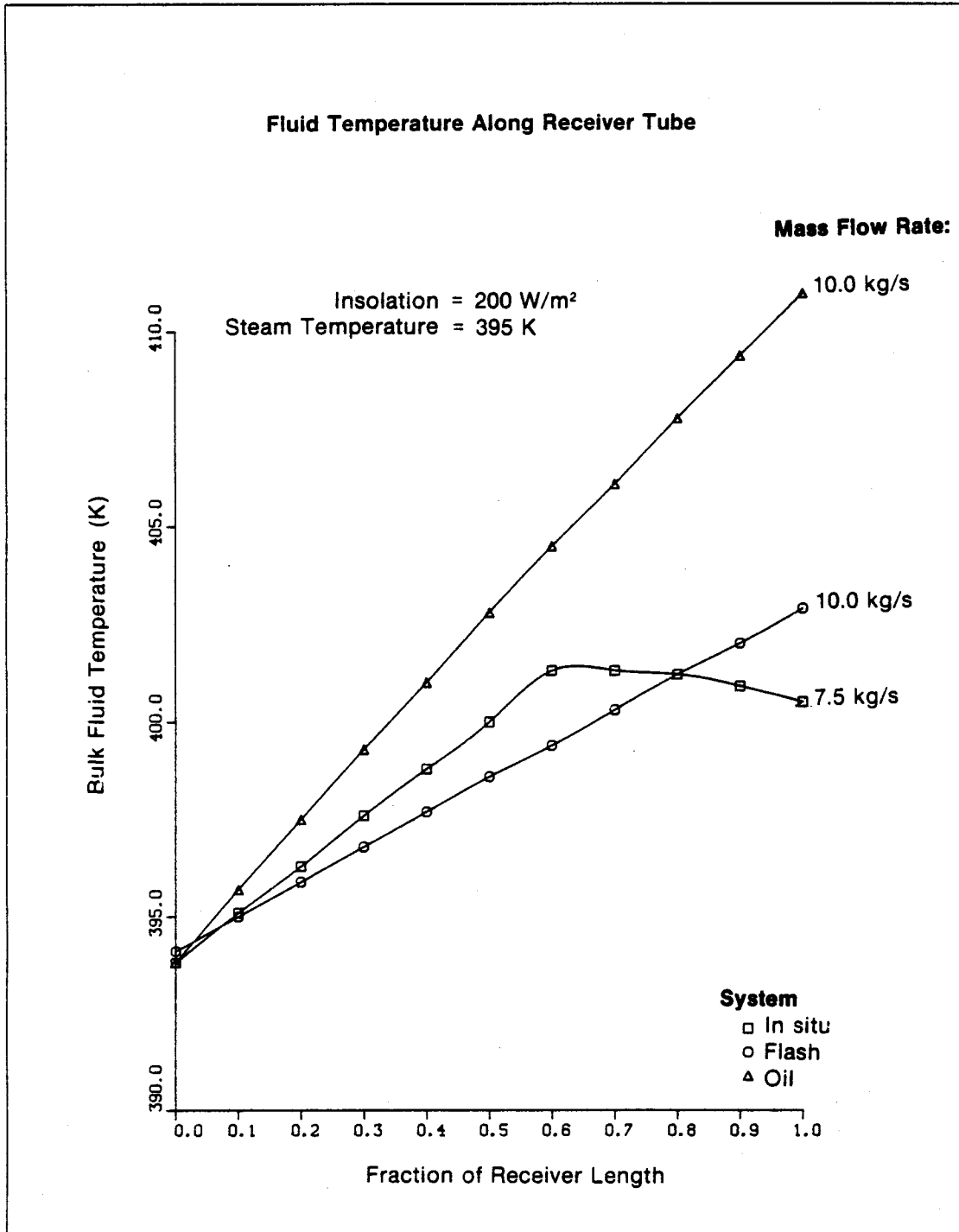
Figure 4-44. Bulk Fluid Temperature vs. Position Along Receiver (T_s = 395 K, I = 200 W/m²)

Fluid Temperature Along Receiver Tube
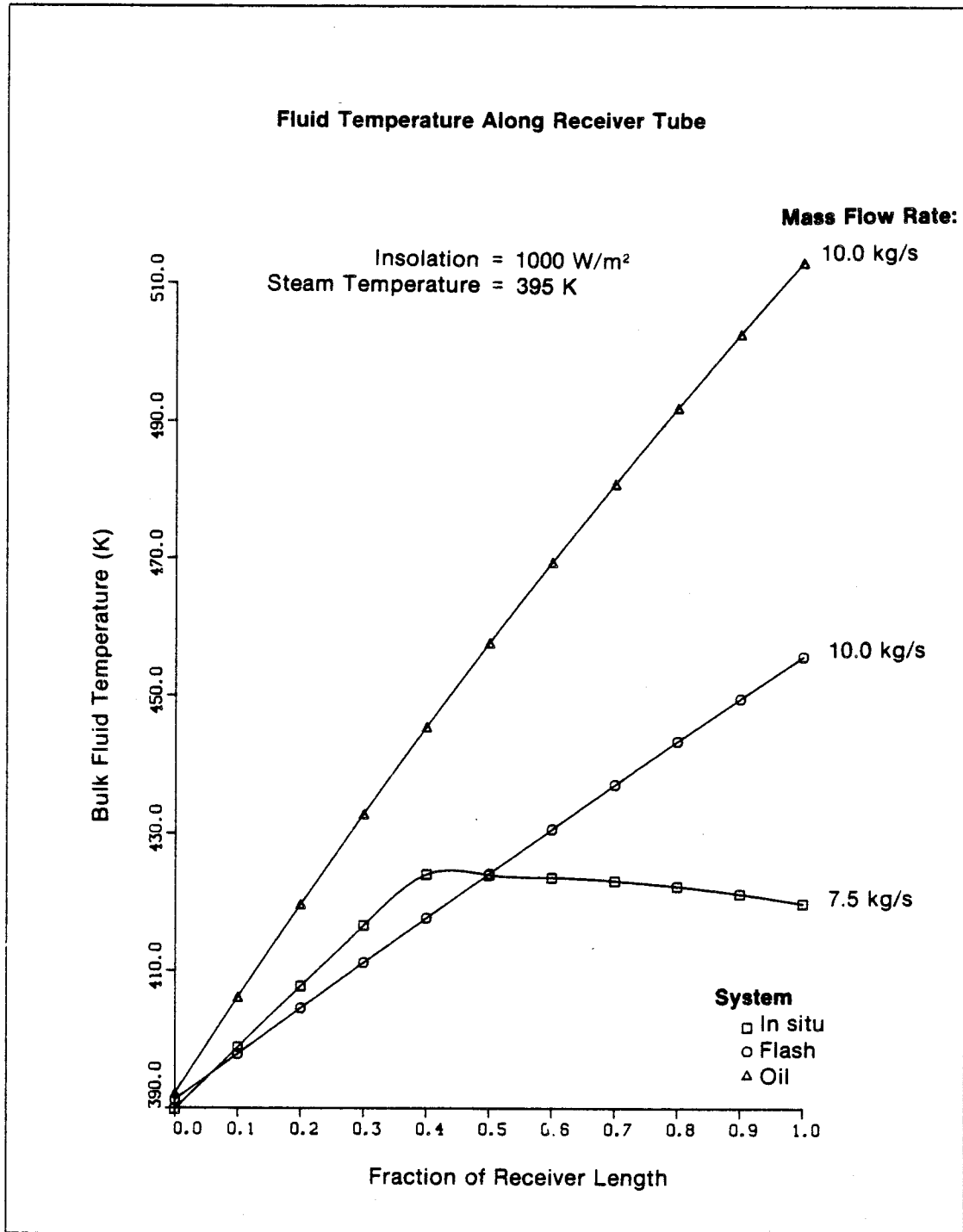
Figure 4-45. Bulk Fluid Temperature vs, Position Along Receiver
(T_s = 395 K, I = 1000 W/m^2)

SERI ⬤ ─────────────────────────────────────

001036

Fluid Temperature Along Receiver Tube

Insolation = 1000 W/m²
Steam Temperature = 495 K

Mass Flow Rate:

10.0 kg/s

10.0 kg/s

7.5 kg/s

System
□ In situ
○ Flash
△ Oil

Fraction of Receiver Length

Bulk Fluid Temperature (K)

590.0 565.0 540.0 515.0 490.0 465.0 440.0

0.0 0.1 0.2 0.3 0.4 0.5 0.6 0.7 0.8 0.9 1.0
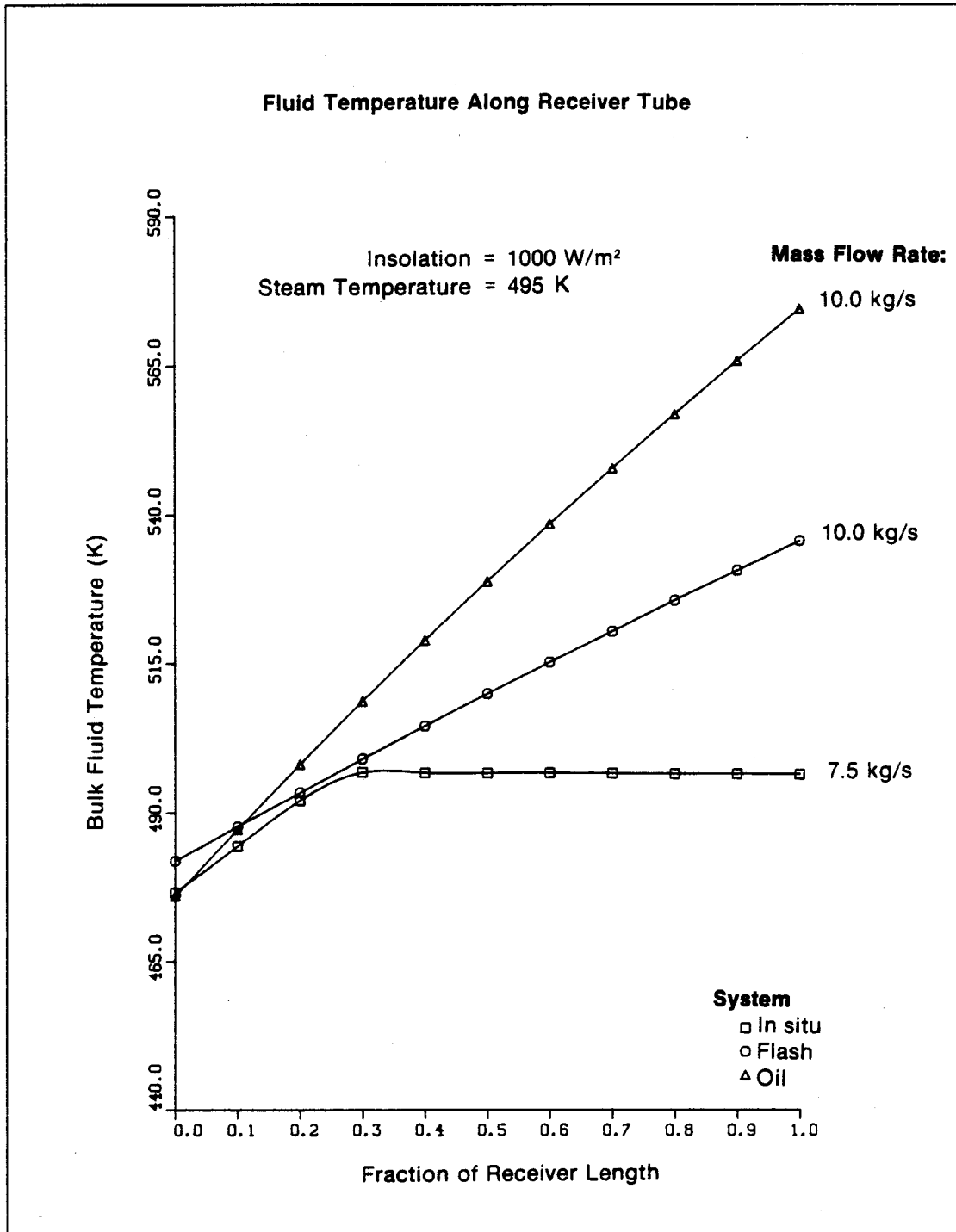
Figure 4-46. Bulk Fluid Temperature vs. Position Along Receiver
(T_s = 495 K, I = 1000 W/m²)
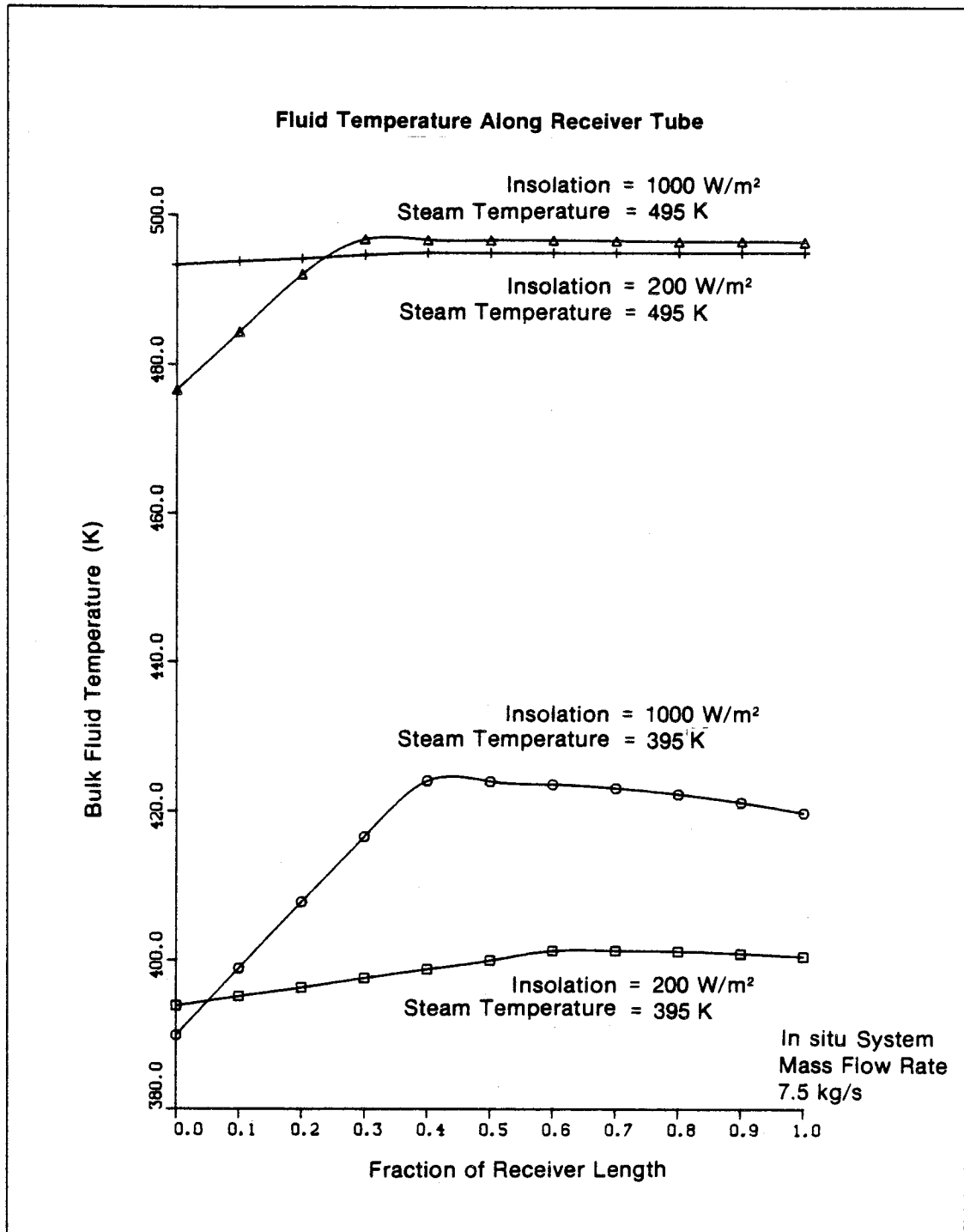
Figure 4-47. In Situ System Bulk Fluid Temperature vs. Position
Along Receiver

001038

Quality Change Along Receiver Tube

In situ System
Mass Flow Rate =
7.5 kg/s

Insolation = 1000 W/m²
Steam Temperature = 495 K

Insolation = 1000 W/m²
Steam
Temperature = 395 K

Insolation : 200 W/m²
Steam
Temperature = 395 K

Insolation = 200 W/m²
Steam
Temperature = 495 K

Quality

0.15
0.12
0.09
0.06
0.03
0.00

0.0 0.1 0.2 0.3 0.4 0.5 0.6 0.7 0.8 0.9 1.0

Fraction of Receiver Length
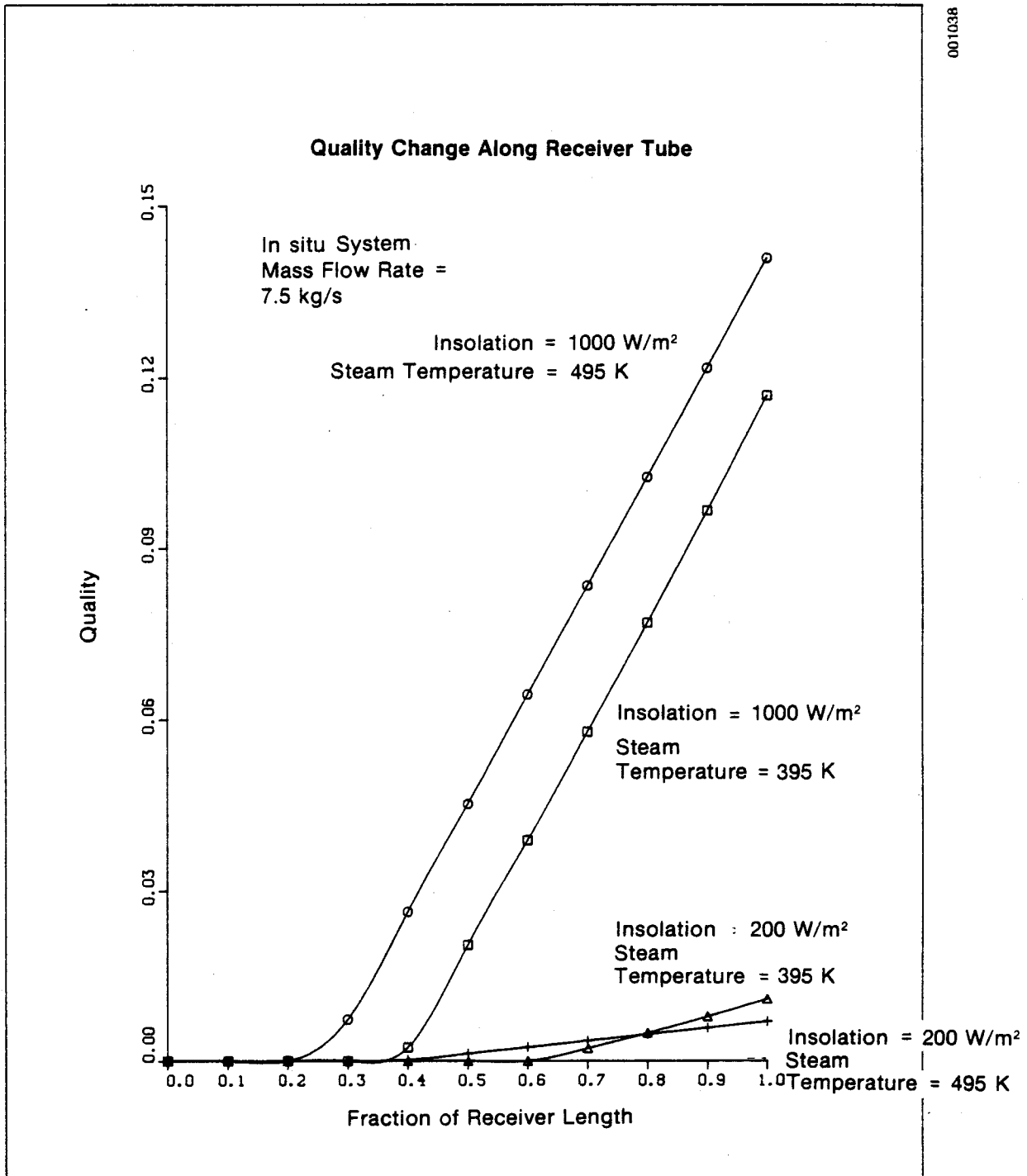
Figure 4-48. In Situ System Steam Quality vs. Position Along Receiver
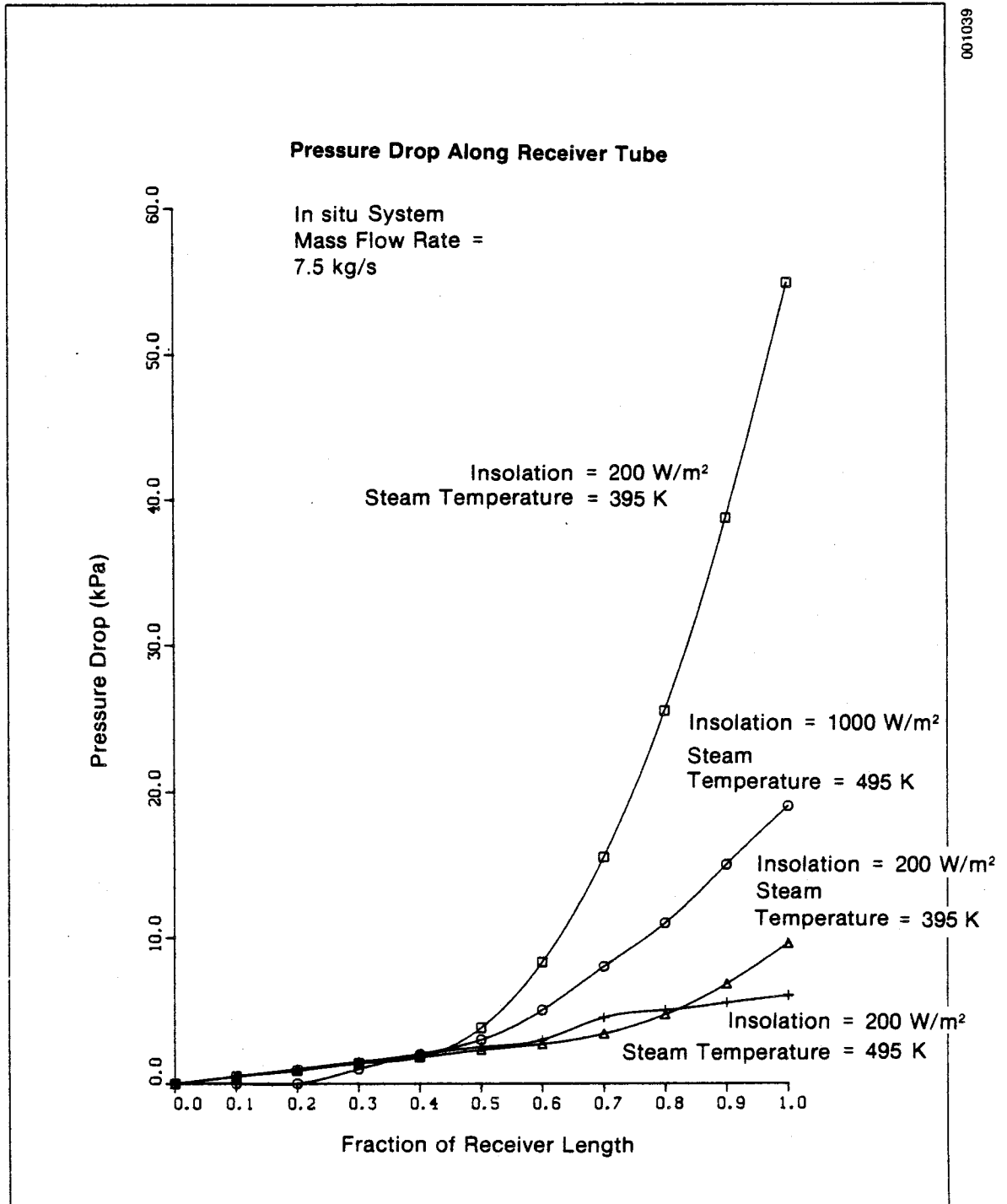
Figure 4-49. In Situ System Pressure Drop vs. Position Along Receiver
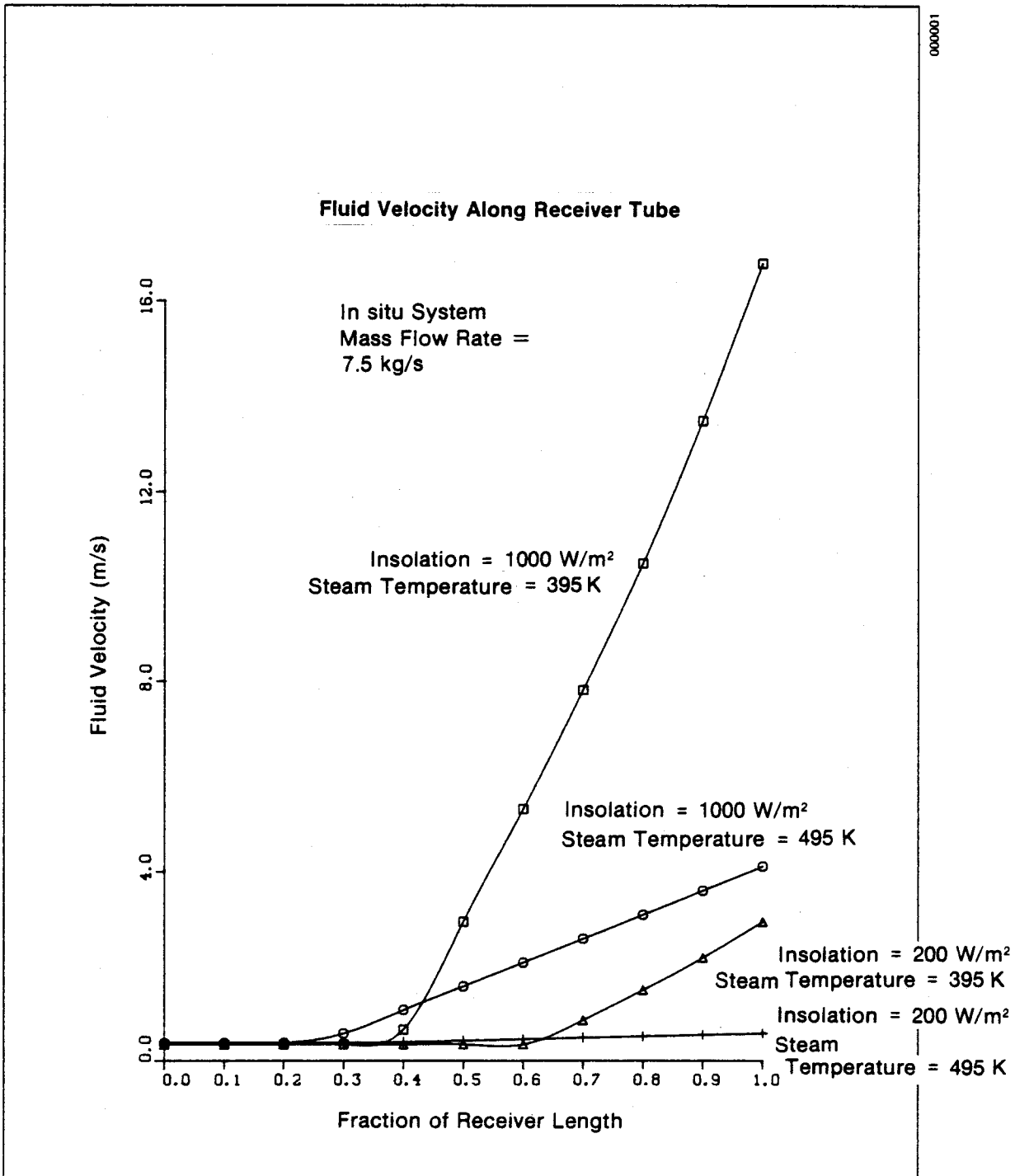
Figure 4-50. In Situ System Fluid Velocity vs. Position Along Receiver

SERI ⊛

quality along the receiver tube. For a fixed steam temperature, as radiative flux is increased, steam quality and the receiver length in which boiling occurs (effective boiling length) increases. Increasing steam temperature increases the effective boiling length even though final exit qualities into the separator are lower. This action results because the large frictional effects at low steam temperatures act to suppress boiling in the receiver. A considerable amount of flashing will occur in the outlet headers at low steam delivery pressures.

The predicted effects of steam delivery temperature and flux on bulk fluid pressure are seen in Fig. 4-49. Pressure drop is defined as the fluid pressure at the collector inlet minus the pressure at an arbitrary position along the collector. At low fluxes the pressure drop profiles are quite close regardless of steam delivery temperature, and their magnitudes are fairly small. As the flux increases the pressure drop profiles diverge dramatically with the largest pressure drop corresponding to the lowest steam temperatures. This action is caused by density considerations and velocity effects (shown in Fig. 4-50). The largest velocity increases occur at low steam temperatures and high fluxes because high fluxes produce higher qualities at the exit and also because at low steam temperatures the corresponding saturation pressures are lower and the bulk specific volumes and bulk velocities are comparatively higher.*

Finally, Figs. 4-51 through 4-53 show tube temperature (on the outer surface of the receiver tube) and bulk fluid temperature as a function of position along the receiver length for the three system types. The difference between the tube wall and bulk fluid temperatures is illustrated for a wider range of variables in Table A-2. The temperature scales for the three graphs are quite different. The close correlation of bulk and wall temperatures is seen in all cases with the difference between the tube and wall remaining nearly constant along the length, although there is a slight decrease in the difference as length increases due to the increase in Reynolds number. With the in situ system, the temperature rise in the subcooled liquid region followed by a slight temperature drop off in the boiling region due mainly to a pressure drop and the associated saturation temperature, is quite clearly seen in Fig. 4-51. The difference between the tube wall temperature and bulk fluid temperature for the oil system averages about 10 K compared to about 2 K for the water systems. At a given fluid temperature, this difference reduces the efficiency of an oil system by about 1% compared to the steam-flash and in situ systems.

---

*To illustrate this point, consider a high flux situation (1000 W/m^2), and then compare the specific volumes of the exit streams for the two steam temperatures. In this situation the bulk specific volume corresponding to T_s = 395 K, is approximately four times as large as that corresponding to T_s = 495 K.
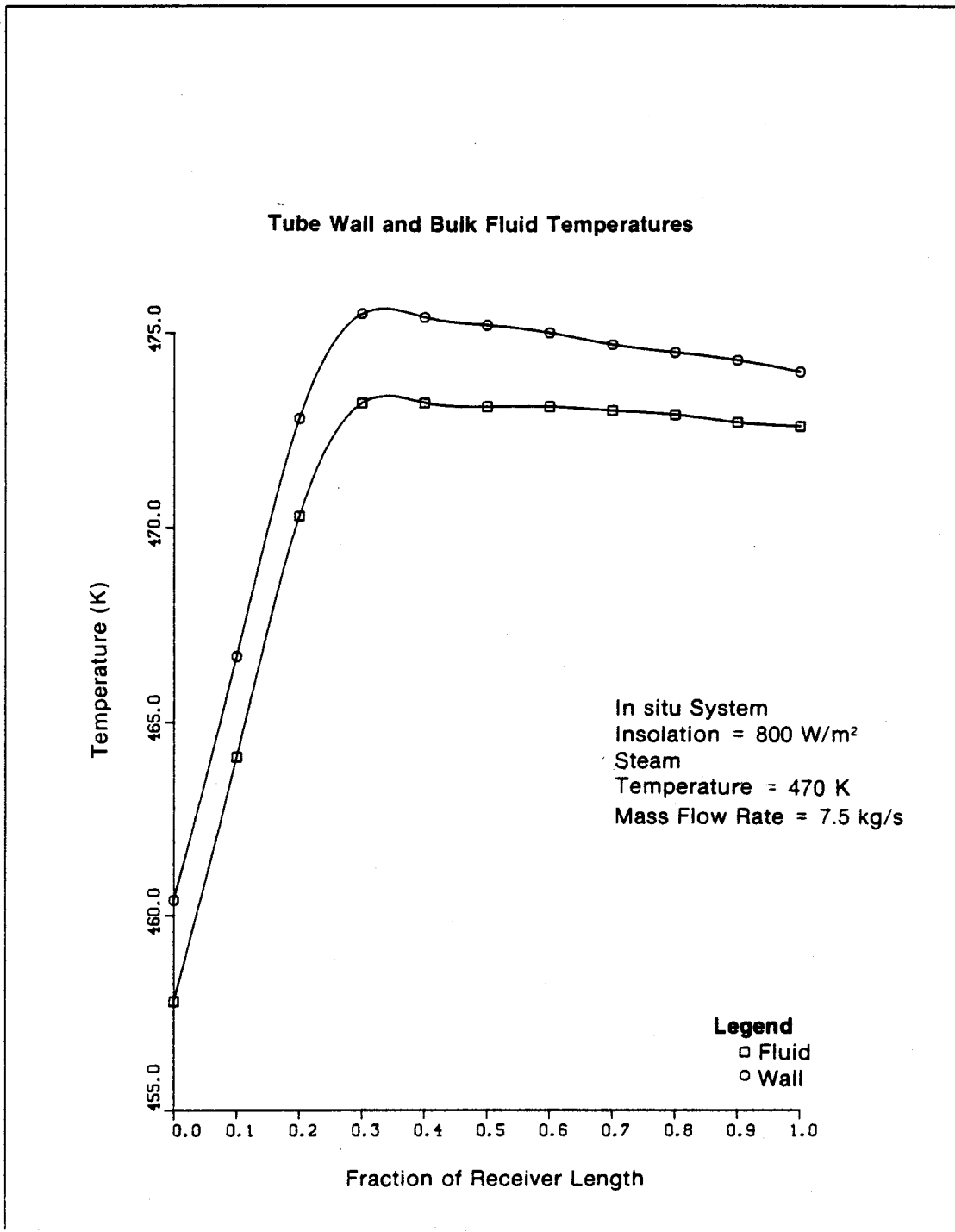
Figure 4-51. Tube Wall and Bulk Fluid Temperature vs. Position Along Receiver (In Situ System)
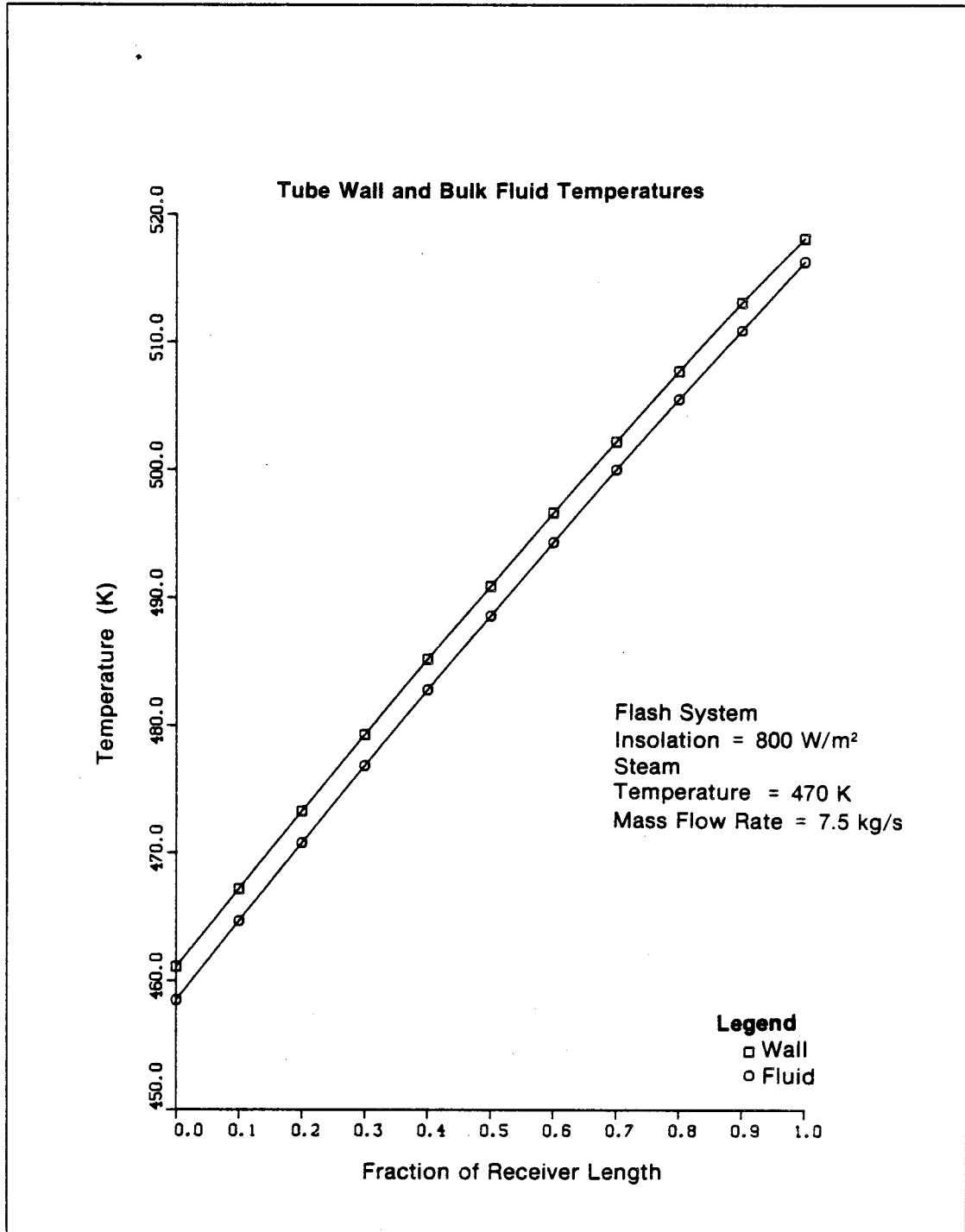
Figure 4-52. Tube Wall and Bulk Fluid Temperature vs. Position Along Receiver (Flash System)
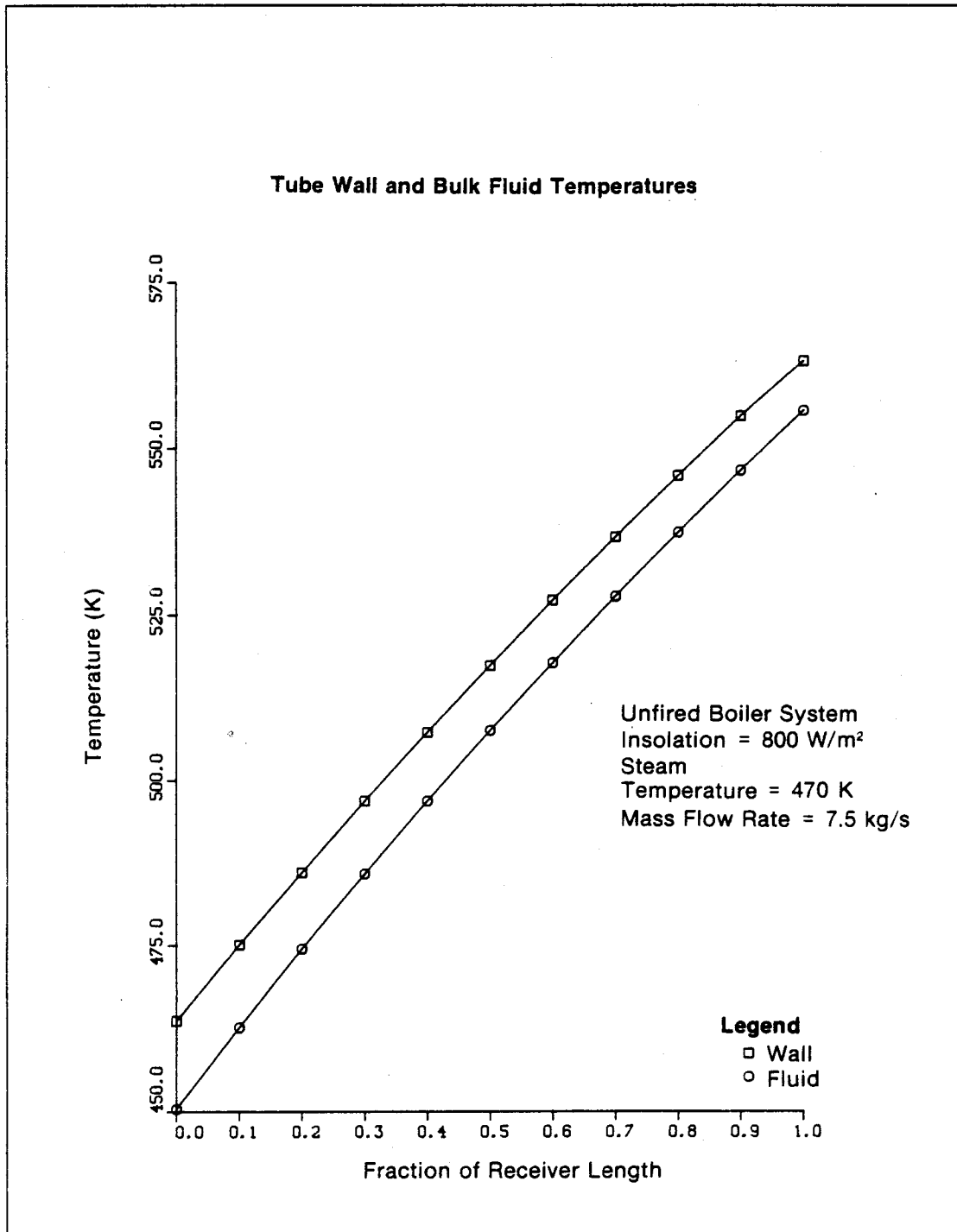
Figure 4-53. Tube Wall and Bulk Fluid Temperature vs. Position Along Receiver (Unfired Boiler System)

SERI ⚙ ─────────────────────────────────

SECTION 5.0

PRELIMINARY SYSTEM COST COMPARISON

A qualitative comparison of components that may result in overall construction and operating cost differences among the three competing solar steam-generating systems is shown in Table 5-1 and is discussed in the following sections.

Table 5-1. QUALITATIVE COST COMPARISON

| | System Type | | |
Component	Unfired Boiler	Steam Flash	Direct Boiling
Piping and insulation			
Pipe length	most	intermediate	least
Pipe diameter	same	same	least
Pipe schedule	same	same	same
Insulation thickness	most	intermediate	least
Pressure vessels			
	unfired boiler expansion tank	separator flash valve	separator
Pumps			
Capacity	same	same	least
Head	least	most	intermediate
Safety			
Explosion-proof equipment	yes	no	no
Liquid collection system	yes	no	no
Fire protection system	yes	no	no
Controls	least	most	intermediate
Maintenance			
Fluid makeup	yes	blowdown	blowdown
Corrosion	least	intermediate	most
Scale buildup	minimal	intermediate	most
Pumps	least	most	intermediate
Leakage	most	intermediate	least

5.1 COLLECTORS

The solar collectors in the three systems will probably be identical, since the receiver piping is designed to withstand the temperatures and pressures that will be encountered in each case.

SERI ❋

5.2 PIPING AND INSULATION

Field piping design should be similar in all three cases except that greater allowances must be made for thermal expansion of the oil system piping since this system tends to run at the highest temperature. Temperature limitations of the oil could limit the collector string length. To minimize field piping, the collector strings should be made as long as possible. The low operating pressure of the oil system will probably not allow any reduction in pipe schedules, since corrosion allowances must be maintained. Also, suppliers generally recommend the use of 300-lb flanges for maintaining required gasket compression to prevent leakage. For a given heat loss from field piping, the higher temperature oil system would require greater thicknesses of insulation. Flexhoses and safety pressure relief valves of high capacity must be chosen carefully in higher pressure water systems.

5.3 PRESSURE VESSELS

The unfired boiler and expansion tank are major costs in the oil system. The unfired boiler is a pressure vessel, and 90-10 copper-nickel tubes generally are specified to prevent corrosion. The boiler must be sized to accommodate the tube bundle and to provide sufficient disengaging space for the steam. The expansion tank usually is about 40% larger than the cold volume of the heat-transfer oil. A wide margin of safety is required since heat-transfer fluids have large coefficients of volumetric expansion. The tank is typically blanketed with nitrogen to prevent fluid degradation from contact with air. The tank is generally positioned so that the field drains back to it.

A water system requires a pressure vessel steam separator. The separator is sized to efficiently separate steam and to hold a volume of water to allow some running time if boiler feedwater is lost. The separator also can be used as heat storage for water circulation to prevent freezing. The flash valve is an additional component of the flash system.

5.4 PUMPS

The pumps for the oil system will be the least costly since they have low-head, high-volume design. However, an auxiliary, low-volume, positive displacement pump can be required to begin circulating the viscous fluid on cold days. The flash system pump will pump less volume than the oil pump but at a considerable pressure differential which makes for a costly pump. The direct steam-generating system should be intermediate between the two extremes of flow and pressure drop.

5.5 SAFETY

Oil systems could require explosion-proof electric equipment and a fire protection system because of the potential fire hazard. Safety valves must be vented to a collection system, to both collect the oil and prevent environmental contamination. An increased number of valves should be designed into the piping system to allow a greater isolation capability than would be required for a water system.

Leaks in high temperature water systems also present potential hazards. Flex-hoses are points of weakness in the piping system. Safety valves must be carefully vented to the atmosphere. Safety hazards can be minimized by restricting access to the solar system when it is operating.

5.6 CONTROLS

During operation the oil system should be the simplest and least costly to control. A small positive displacement pump could be required to initiate fluid movement during cold days. Control schemes that reduce electric power consumed by the pump for a flash system can be quite complicated. The control requirements for the in situ system should be more straightforward than for flash systems, and should only require sufficient inlet pressure drop to each collector string to ensure uniform flow distribution and adequate operating stability. Both water systems will require freeze protection mechanisms in cold climates.

5.7 MAINTENANCE

The flash system pump could be a high-maintenance component if high pressure steam is produced. Also, the flash valve is subject to erosion. Water systems are more subject to corrosion than oil systems. Overnight cool-down could draw air into the system. The potential of scale buildup is also present, especially for the in situ systems. Corrosion and fouling would be controlled by standard water treatment practices and by blowdown.

The major maintenance problem with the oil system is repairing leaks in the system. Flanges can be retightened somewhat, but once safety valves start to leak, they usually must be removed and reground. The reliability of mechanical seals tends to degrade at the upper operating temperature range of heat-transfer oils. Inventory of the oil must be maintained and its quality checked at regular intervals.

5.8 SYSTEM CAPITAL COST

A qualitative assessment of the items listed in Table 5-1 indicates that for a given collector field size, the oil system is the most expensive system. Assuming that the piping layout and insulation thickness were the same for each case, the major cost differences accrued to the oil system result from the increased cost of the pressure vessels and safety equipment. The difference between the two water systems is that the flash system requires a reducing valve and a more expensive pump.

Estimates presented by TRW, Inc., as part of the conceptual design for the Ore-Ida plant (Cherne et al. 1978), show that the capital cost of an oil system would exceed that of a flash system by over 10% for a 885-m^2 collector field. Assuming that the pump for a direct-boiling system of this size costs the same as a pump for an oil system and deleting the flash valve, the estimates indicate a direct-boiling system would cost almost 5% less than a steam-flash system. Thus, an oil system would cost about 15% more than a design

based upon the direct-boiling concept. Such figures are obviously based upon preliminary estimates, and only the construction of competing systems will provide definite cost data. However, the evidence that does exist indicates a potential savings in capital cost with a direct, steam-generating solar system over the other alternatives.

SECTION 6.0

FREEZE PROTECTION AND CORROSION

6.1 INTRODUCTION

A major disadvantage to using water in a solar system is the possibility of freezing during cold weather and damage to system components. Measures to combat freezing can cause significant thermal losses and increased electric power consumption (needed to drive circulating pumps or for heat tracing). Heat-transfer oils can be used as the collector fluid instead of water; but, as this analysis has shown, a considerable penalty is paid in reduced system efficiency and increased cost. Thus, there is considerable incentive to solve the freezing problem so that water can be used in the collector field for steam generation.

The map shown in Fig. 6-1 quantifies the extent of the freezing problem in the United States (U.S. Department of Commerce 1974). In the Gulf states and the coastal regions of California, freezing temperatures seldom occur during the year, and in Hawaii, freezing temperatures never occur. [Note that the map shows the number of days per year the minimum temperature falls below 0°C (32°F). It does not disclose how long freezing conditions persist.] East of the Rocky Mountains, freezing occurs for more than 120 days/yr only in the most northerly regions. West of the mountains, temperatures can fall below freezing for the majority of days in the year. Freezing is not a problem in tropical countries, which are major potential markets for solar equipment.

6.2 HEAT LOSS MECHANISM

Piping in solar systems should be carefully insulated to minimize the amount of exposed metal. Pipe supports should be isolated from the pipe surface. In colder climates, the circulating pump and associated fittings that are hard to insulate should be placed in a small pump house.

Using an idealized model, an insulated cylinder will cool to temperature T according to the following equation:

$$T = T_a + (T_i - T_a) \exp\left(-\frac{Ut}{MC_p}\right) ,$$

where

T_a is ambient temperature,
T_i is initial temperature of fluid in the pipe,
U is the heat loss coefficient per unit length of pipe,
t is time, and
MC_p is the heat capacity of the water-filled pipe.

Using the baseline data for the 3-in. inlet pipe to the collector field, which is covered with 2 in. of insulation, calculations show that it would take 33 h for the pipe to cool from 150°C to 0°C at an ambient temperature of -17.8°C (0°F). The heat capacity of the insulation is neglected, and the conductive

Figure 6-1. Mean Annual Number of Days Minimum Temperature 32°F and Below

heat loss coefficient is increased by 20% to account for radiative heat losses. Similar calculations for a suitably sized, well-insulated flash tank show that it would cool about 40°C over the same time period and under the same conditions.

These preliminary calculations illustrate that unless the solar system is shut down for an extended period of time, freezing should not be a problem for the transport piping or flash tank. This assumption presupposes that careful attention is paid to the insulation of exposed fittings and such items as sight-glasses. A small amount of electrical heat tracing could be employed at critical locations. Even if temperatures do fall to freezing, it is not a major cause for concern in large diameter piping. Ice formation proceeds from the outside of the pipe; without the insulating effect of the ice layer taken into account, the pipe discussed in the previous paragraph would take another 52 h to completely freeze. Damage is unlikely until freezing has taken place over a large fraction of the flow area.

Possible damage to collector-receiver components as the result of freezing, however, is a major concern with a water system. Under these same conditions, the receiver tubes would cool to freezing in about 2 h. Heat losses over this period would amount to about 1.8 GJ (1.7 million Btu) for the baseline system. This loss is considerable, since the heat capacity of the collector receiver tubes and fluid is about 50% of the total system heat capacity (excluding the separator). Thus, the ideal protection system would prevent freezing and would also minimize heat losses from the collector field.

6.3 FREEZE PROTECTION TECHNIQUES

Under normal circumstances, there is a large reservoir of heat in the insulated storage tank and field piping. Freeze protection systems draw on this heat by starting the circulation pump or a special, low-volume freeze protection pump to move hot fluid through the receiver tubes. Existing designs are extremely conservative and result in large heat losses. For instance, circulation is often initiated when ambient temperatures decrease to 4.4°C (40°F) and is prolonged for extended periods of time. With the collectors in the stow position and not radiating directly to the sky, there is little danger of freezing at this temperature. Reliable control schemes monitoring fluid temperatures within the receiver tube could greatly reduce the number of days when the freeze protection system is activated. Reducing overnight losses also will reduce the frequency of emergency conditions, requiring auxiliary heating to be brought on-line or draining the system because of depleted thermal storage. Control points for fluid temperatures only 1° or 2° C above freezing are possible. Microprocessor control systems could easily activate a freeze protection scheme to minimize heat loss and pump running time.

Regardless of the collector fluid, the receiver tube is a major source of overnight heat loss. Such losses and the danger of freezing conceivably could be reduced greatly by rotating the receiver tube from the stow position into an insulated enclosure. Applying this concept would require some redesign of the collector, but it could be cost-effective. Similar benefits would result from the successful development of an evacuated receiver tube. The success of these measures, together with an improved recirculation control scheme, would

remove many objections to using water as a heat transfer fluid in line-focus collectors.

In conclusion, the possibility of fluid freezing within system components is a significant but not insurmountable obstacle to using water in a line-focus collector field. Some basic research is needed to determine the most appropriate points for sensor location, and to gain a greater understanding of the effects of freezing conditions on a collector receiver tube. Such research would lead to more effective control schemes and greatly increase confidence in using water for solar heat transport. This research is needed as part of an overall program to demonstrate the feasibility and performance benefits of the direct-boiling, steam-generating concept.

6.4 CORROSION POTENTIAL

The open loop steam-flash and in situ systems are subject to corrosion as are conventional steam generators. Thus, conventional techniques to control corrosion (i.e., water treatment, deaeration, and corrosion allowances on piping) would be used. The system should be designed for full vacuum so that air cannot enter the system during overnight cooldown if the system pressure falls below atmospheric pressure.

Similarly, conventional techniques, such as mechanical or chemical cleaning, would be used to combat potential scaling problems. Scaling would increase the pressure drop of the direct-boiling system, but effects on thermal performance would be minimal, since scale can act as an effective site for bubble nucleation (Bergles et al. 1981).

SE꒓I ✷ ——————————————————————————————

SECTION 7.0

SYSTEM OPERATING STABILITY

The operating stability of a direct-boiling steam system is the major uncertainty when considering the technicial feasibility of the concept. System instabilities resulting from two-phase flow could conceivably lead to control problems, damage from vibration, or large temperature excursions of the receiver tube, which could damage the selective surface. To assess the likelihood of these difficulties occurring as well as the expected impact, the problem was investigated by Pederson and May (1982). This section summarizes investigations into the instability modes deemed most likely to occur along with the application of stability criteria to the full range of expected operating conditions, as predicted in the system performance analysis. Results of the stability analyses are encouraging; however, this issue must await experimental verification before it is resolved.

Pederson and May consider one representative tube of the parallel flow system to be uniformly heated and subject to an externally imposed constant pressure drop irrespective of mass flow rate. This latter condition incorporates the influence of the other tubes in the solar array. Using this model and appropriate stability criteria, five modes of flow instability with the greatest likelihood of occurring are assessed. The appropriate stability criteria are taken from the literature to establish necessary (but not sufficient) conditions for instabilities to occur, and are given in terms of flow parameters and thermal inputs. Three of the stability modes investigated are governed by the same necessary condition and are shown to have no effect over the range of expected system operating parameters. A fourth instability mode, density-wave oscillations, is a potential but unlikely problem. However, the necessary degree of inlet pressure restriction is easily determined from the corresponding stability criteria and can be set so as to guarantee the stability of the system. A fifth stability mode, flow-pattern transition instability, is possible, but apparently its impact does not warrant concern.

7.1 CLASSIFICATION OF INSTABILITIES

Instabilities are classified into two types: flow excursion and flow oscillation. In flow excursion, a slight peturbation can cause a drastic transient in the flow rate, after which a new equilibrium level is attained. The change is irreversible and can also produce an undesirable wall temperature excursion. In flow oscillation, the flow rate and pressure undergo periodic oscillations around a mean level after a slight perturbation. Flow oscillations may induce mechanical vibrations in components or system control problems that can affect local heat-transfer characteristics, possibly resulting in oscillatory wall temperatures or inducing dryout that leads to excessive wall temperatures. For purposes of an analytical discussion, instabilities are better classified into two broad categories: static or dynamic.

7.2 STATIC INSTABILITIES

Static instabilities can be predicted with the use of steady-state equations. Two static instabilities could affect the operation of the system: the Ledinegg instability (or flow excursion) and the flow-pattern transition instability.

7.2.1 Ledinegg Instability

The Ledinegg instability is characterized by a flow excursion, i.e., the flow rate in the channel suddenly changes to a new steady-state value. This instability can arise because the conditions of two-phase flow in a heated channel are bounded by the single-phase (gas and liquid) flow regions, which have greatly differing pressure-drop characteristics. This condition is illustrated in Fig. 7-1, showing one possible (and in this case, unstable) two-phase operating path of a heated channel. A conservative condition, necessary, but not sufficient, for the Ledinegg instability to arise is that

$$\frac{\partial (\Delta P)_{int}}{\partial G} \leqslant 0 \quad , \qquad\qquad (7\text{-}1)$$

where $(\Delta P)_{int}$ is the internal pressure drop of the heated channel, and G is the mass flux.
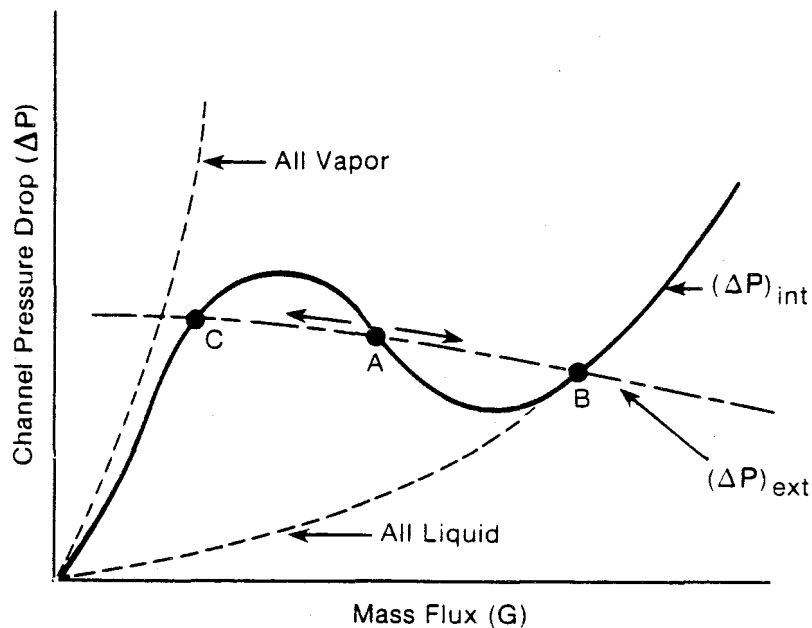
Figure 7-1. Two-Phase Pressure Drop Characteristics of a Heated Channel

7.2.2 Flow-Pattern Transition Instability

Flow-pattern transition instabilities apparently occur when flow conditions are close to the transition point between bubbly or slug flow and annular flow. A temporary reduction in flow rate or increase in heat flux may increase the vapor-generation rate sufficiently to change the flow pattern to

SERI ❀ ——————————————————————————————

annular flow with its characteristically lower pressure drop. The external pressure as exerted by the pump then tends to increase the flow rate, which can reduce the vapor-generation rate sufficiently to cause a reversion to bubbly or slug flow. Figure 7-2 shows the change in flow regime along the receiver tube for two sets of operating parameters which bound all conditions investigated in this study, superimposed on the flow regime map of Taitel and Dukler (1976). Annular flow conditions do exist in the receiver tube so that instabilities by the mechanism postulated above are possible. However, the literature indicates that flow-pattern transition instabilities will probably not cause mechanical or operational difficulties, especially with well-damped systems such as the one under investigation; but these instabilities could instigate other types of instability.

7.3 DYNAMIC INSTABILITIES

The three types of dynamic instabilities most likely to affect the operation of the present system are density-wave oscillations, acoustic (or pressure-wave) oscillations, and pressure-drop oscillations. Dynamic instabilities can occur in both single- and multiple-channel systems, with parallel channel situations presenting opportunities for additional interactions triggered by the basic mechanisms.

7.3.1 Density-Wave Oscillations

Density-wave oscillations are the most common oscillations observed and are the result of dynamic interactions between the flow rate, vapor-generation rate, and the pressure drop in the heated channel. Inlet-flow fluctuations in the single-phase region, when they reach the boiling region, are transformed into void-fraction fluctuations that travel with the flow along the channel, creating a dynamic pressure drop in the two-phase region. A necessary and conservative but not sufficient condition for a density-wave instability to occur, derived by Pederson from the literature, is given in terms of nondimensional subcooling (N_{sub}) and equilibrium phase change ($N_{pch,eq}$) numbers, by

$$\frac{N_{pch,eq} - N_{sub}}{2 \left(k_i + \frac{fL}{2d} + k_e \right) / \left[1 + \frac{1}{2} \left(\frac{fL}{2d} + 2k_e \right) \right]} \geqslant 1 \qquad (7\text{-}2)$$

where the subcooling number N_{sub}, and equilibrium phase-change number $N_{pch,eq}$ are defined as

$$N_{sub} = \frac{(h_f - h_i)}{h_{fg}} \frac{v_{fg}}{v_f} \ , \qquad (7\text{-}3)$$

and

10⁴ ─ annular / Bubbly region chart

Annular B **Bubbly**

Intermittent (Slug and Plug)

Wavy

Stratified

Lockhart-Martinelli Parameter X

K (left axis): 10^0 to 10^4
T or F (right axis): 10^{-3} to 10^1
X axis: 10^{-2} to 10^3
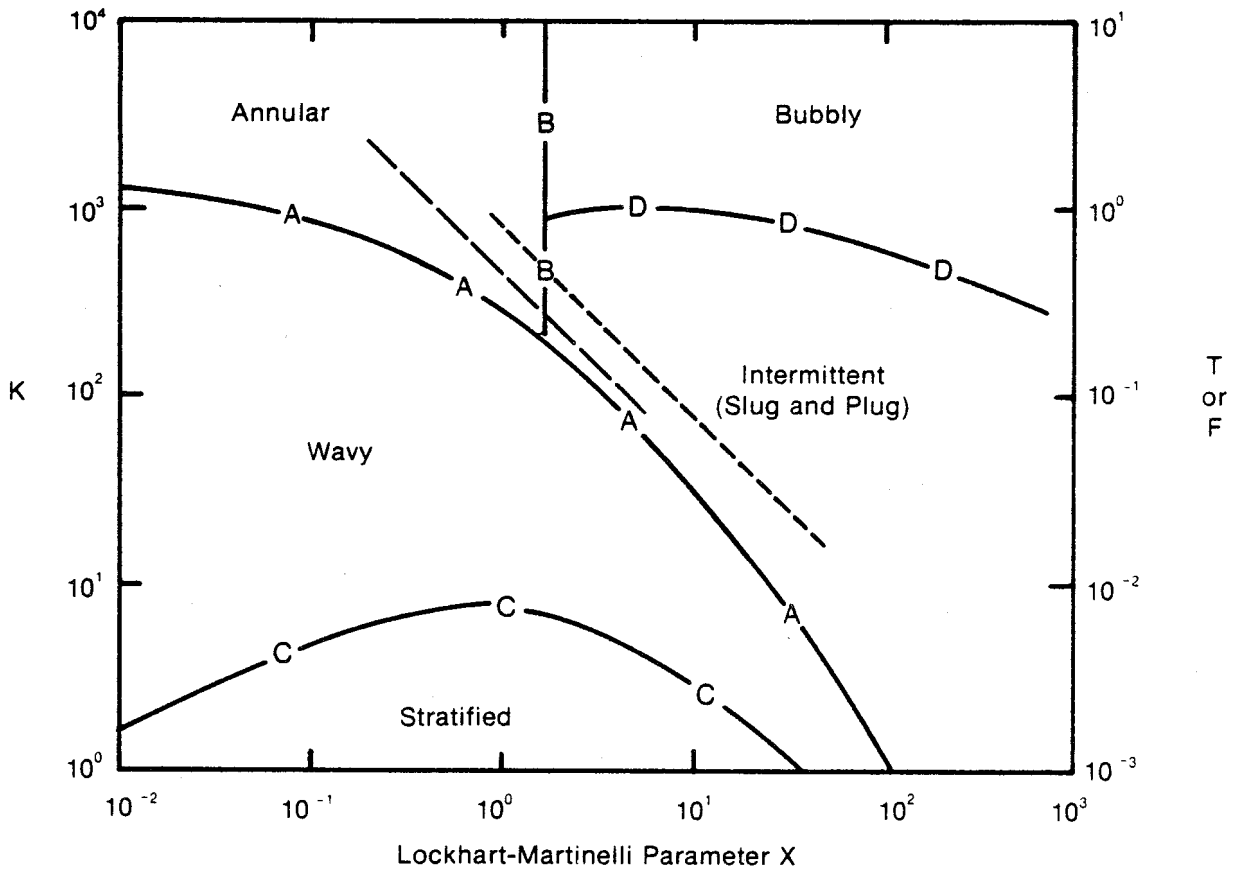
Curve: A & B   C   D
Coordinate: F vs. X   K vs. X   T vs. X

$$X = \left[\frac{(dP/dx)_{SL}}{(dP/dx)_{SG}}\right]^{1/2} \qquad F = \sqrt{\frac{\rho_g}{(\rho_f - \rho_g)}} \frac{V_{SG}}{\sqrt{dg \cos \alpha}}$$

$$T = \left[\frac{|(dP/dx)_{SL}|}{(\rho_f - \rho_g) g \cos \alpha}\right]^{1/2} \qquad K = \left[\frac{\rho_g V_{SG}^2 V_{SL}}{(\rho_f - \rho_g) v_f g \cos \alpha}\right]^{1/2}$$

- - - - - -   I = 1000 W/m², Tₛ = 495 K, m = 10 kg/s

────────   I = 1000 W/m², Tₛ = 395 K, m =   5 kg/s

Figure 7-2.   Flow-Pattern Transitions Along Receiver Tube on Generalized Flow Regime Map for Horizontal Two-Phase Flow (Taitel and Duckler 1976)

$$N_{pch,eq} = \frac{Q}{GA\,h_{fg}}\,\frac{v_{fg}}{v_f} \;, \tag{7-4}$$

and where h_i is the inlet enthalpy of the subcooled liquid, and Q is the total heat addition to the receiver. The liquid and vapor states are referenced to conditions at the outlet of the channel. The equilibrium exit quality $x_{e,eq}$ can be derived in terms of these variables:

$$x_{e,eq} = (N_{pch,\,eq} - N_{sub})\,\frac{v_f}{v_{fg}} \;. \tag{7-5}$$

The inlet and outlet restriction coefficients k_i and k_e are defined in terms of the inlet $(\Delta P)_i$ and exit $(\Delta P)_e$ pressure drops:

$$(\Delta P)_i = \frac{k_i u_i^2}{v_f} \;, \tag{7-6}$$

and

$$(\Delta P)_e = \frac{k_e u_e^2}{v_f} \;. \tag{7-7}$$

The stability line represented by Eq. 7-2 is based on the analysis of Ishii (1971) and confirmed by the experimental data of Saha et al. (1976). Its applicability is restricted to high subcooling numbers:

$$N_{sub} \geqslant \pi \;. \tag{7-8}$$

7.3.2 Acoustic Oscillations

Acoustic oscillations are due to disturbances propagated at the speed of sound within the channel. Such oscillations are not expected to cause harmful temperature excursions, but control problems and/or mechanical vibrations could be encountered. The threshold for acoustic oscillations occurs in the negative sloping region of the pressure drop, flow rate curve for a heated channel, and thus, Eq. 7-1 is a necessary but not sufficient condition for instability.

7.3.3 Pressure-Drop Oscillations

Pressure-drop oscillations arise from dynamic interactions between the inertia of the fluid in the channel and a compressible volume somewhere in the rest of the system. For the system under study, this compressible volume could be represented by a centrifugal circulating pump where flow varies with head, or the long receiver tubes may represent sufficient volume to initiate such oscillations. Again, Eq. 7-1 represents a necessary condition for such oscillations.

7.4 EVALUATION OF STABILITY CRITERIA

The stability criteria given by Eqs. 7-1 and 7-2 must still be evaluated to ascertain if potential stability problems should warrant concern. For the in situ boiling system under investigation, this evaluation is most easily accomplished numerically. The results of the numerical evaluation for the Ledinegg criteria are shown in Figs. 7-3 to 7-5, where differential pressure across the receiver string is plotted as a function of mass flow rate for the full range of flux and steam operating temperatures investigated in this study. By visual inspection it is clearly seen that the slope never becomes negative. Further, only the slightest inflection occurs at the low steam temperature, high flux case. Thus, the Ledinegg, acoustic oscillation, and pressure-drop oscillation instabilities can all be eliminated from concern according to this analysis.

However for density-wave instabilities, the situation is quite different. Results predicted from the criteria given by Eqs. 7-2 to 7-8 are illustrated in Figs. 7-6 to 7-7 as a function of mass flow rate over the range of incident flux levels and steam delivery temperatures. The term $F(k)$ is the denominator of the expression on the left-hand side of Eq. 7-2. These curves illustrate several points: the system becomes less stable with increasing radiation flux, with decreasing steam delivery temperature, and with decreasing mass flow. Over the bulk of the operating range considered, no density-wave instabilities should occur, especially at higher steam delivery temperatures [445 K (340°F) and above]* where the maximum benefits for the in situ system are predicted. Specifically, the direct generation of steam at 395 K (250°F) at the assumed inlet and outlet restrictions may produce density-wave oscillations. At 420 K (297°F), such oscillations could occur at flow rates of 7.5 kg/s or less and at insolations as low as 600 W/m^2; but in effect these three conditions form the boundary for density-wave oscillations.

To correct instabilities at low steam delivery temperatures and high flux conditions, more inlet orificing than was assumed for the baseline system may well be required. The required inlet orificing can be determined by setting the right-hand side of Eq. 7-2 equal to 1 and solving for k_e. For example, for the worst case of instability at a steam delivery temperature of 445 K (insolation 1000 W/m^2 and flow rate = 5 kg/s), the baseline system inlet pressure drop is 14.4 kPa (2.2 psi). The stability criteria indicate that a minimum inlet pressure drop of 23.3 kPa (3.4 psi) is required. For the overall worst case of instability considered [steam temperature = 395 K (250°F), flow rate = 5 kg/s, insolation = 1000 W/m^2], the baseline system pressure drop is 14.4 kPa (2.1 psi). For stability this would have to be increased to 137 kPa (20 psi) which could cause an unacceptable increase in electrical power consumption. However, there are other reasons, such as the possibility of erosion of system components due to high fluid velocities, that make application of the in situ concept inappropriate at very low steam pressures. Under these conditions the steam-flash system is particularly efficient. However the criterion given by Eq. 7-2 is a necessary, but not a sufficient condition. Hence density-wave instability may in fact not occur.

---

*The nominally optimal mass flow rate adopted for the baseline in situ system is 7.5 kg/s which is equivalent to 330 kg/m^{2}s.
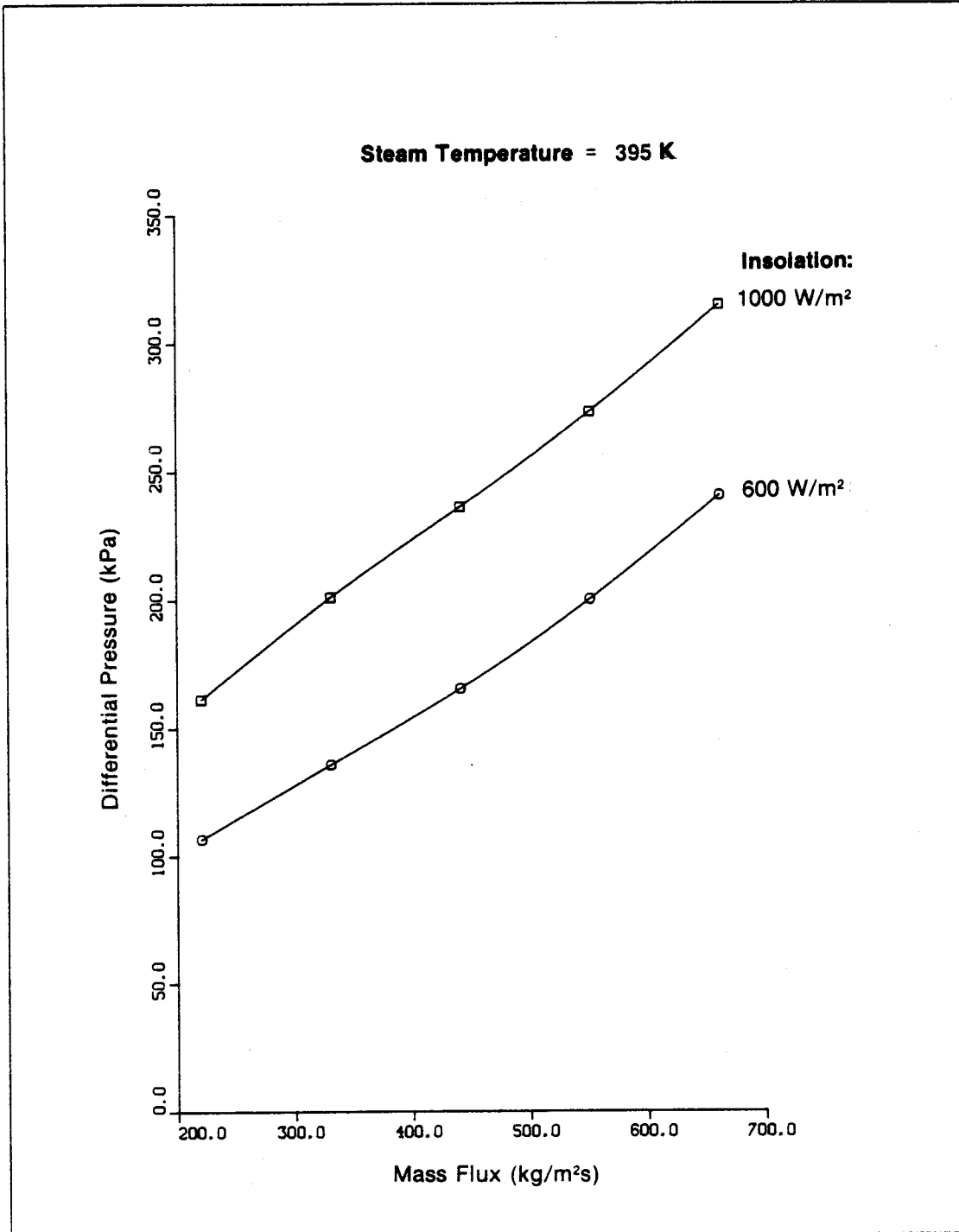
Figure 7-3. Differential Pressure Across Collector Row vs. Mass Flux
(T_s = 395 K)
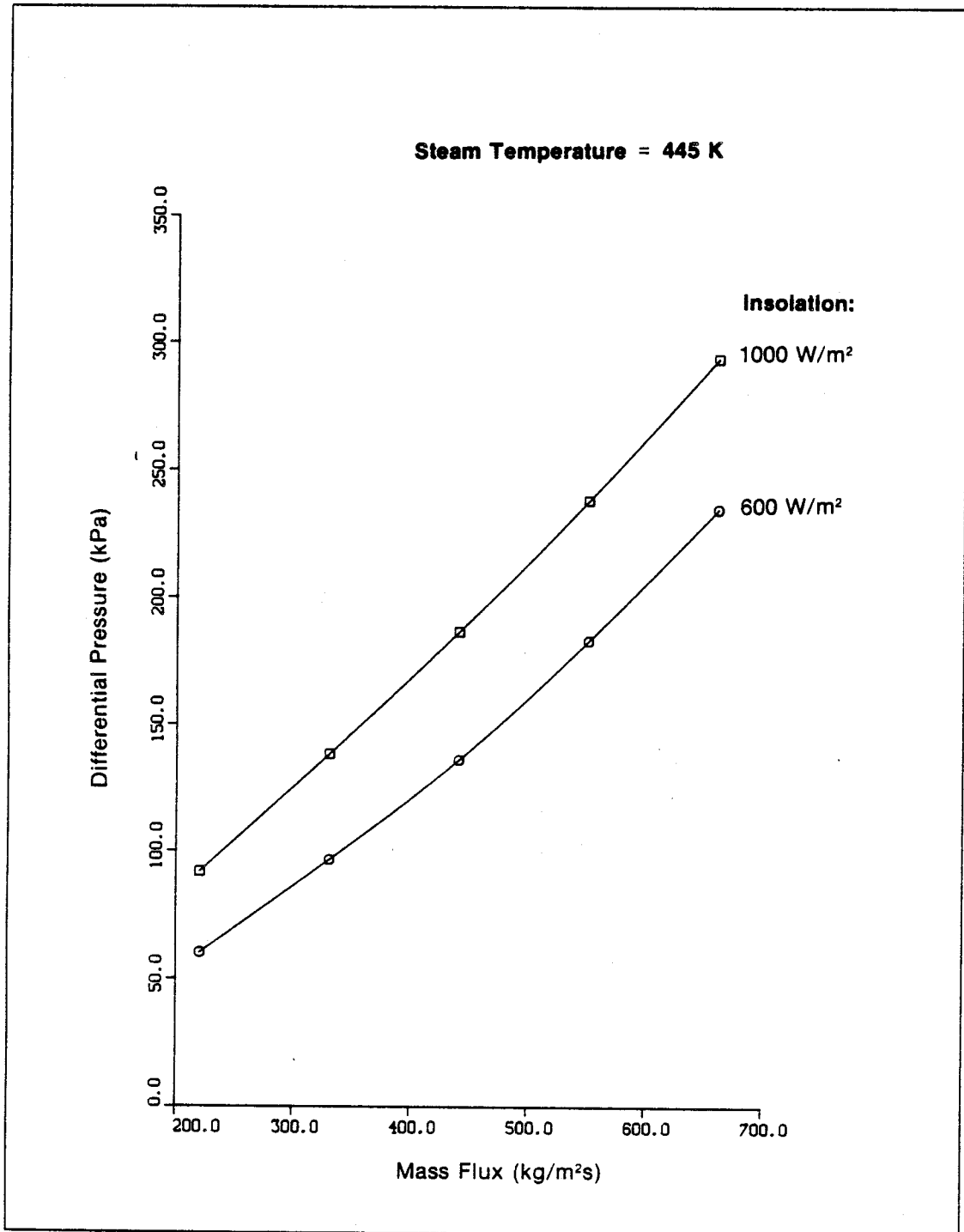
Figure 7-4. Differential Pressure Across Collector Row vs. Mass Flux (T_s = 445 K)
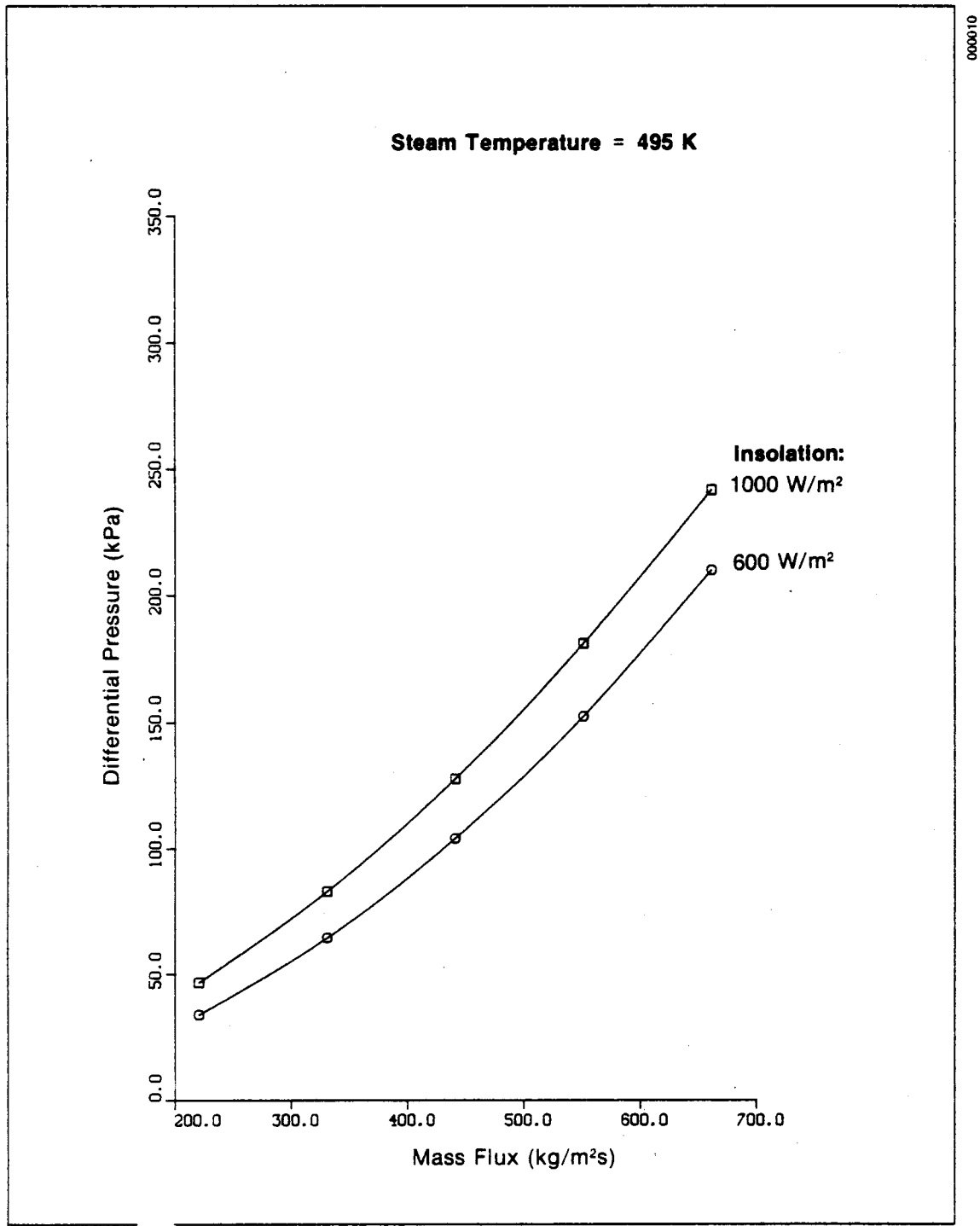
Figure 7-5.   Differential Pressure Across Collector Row vs. Mass Flux
(T_s = 495 K)
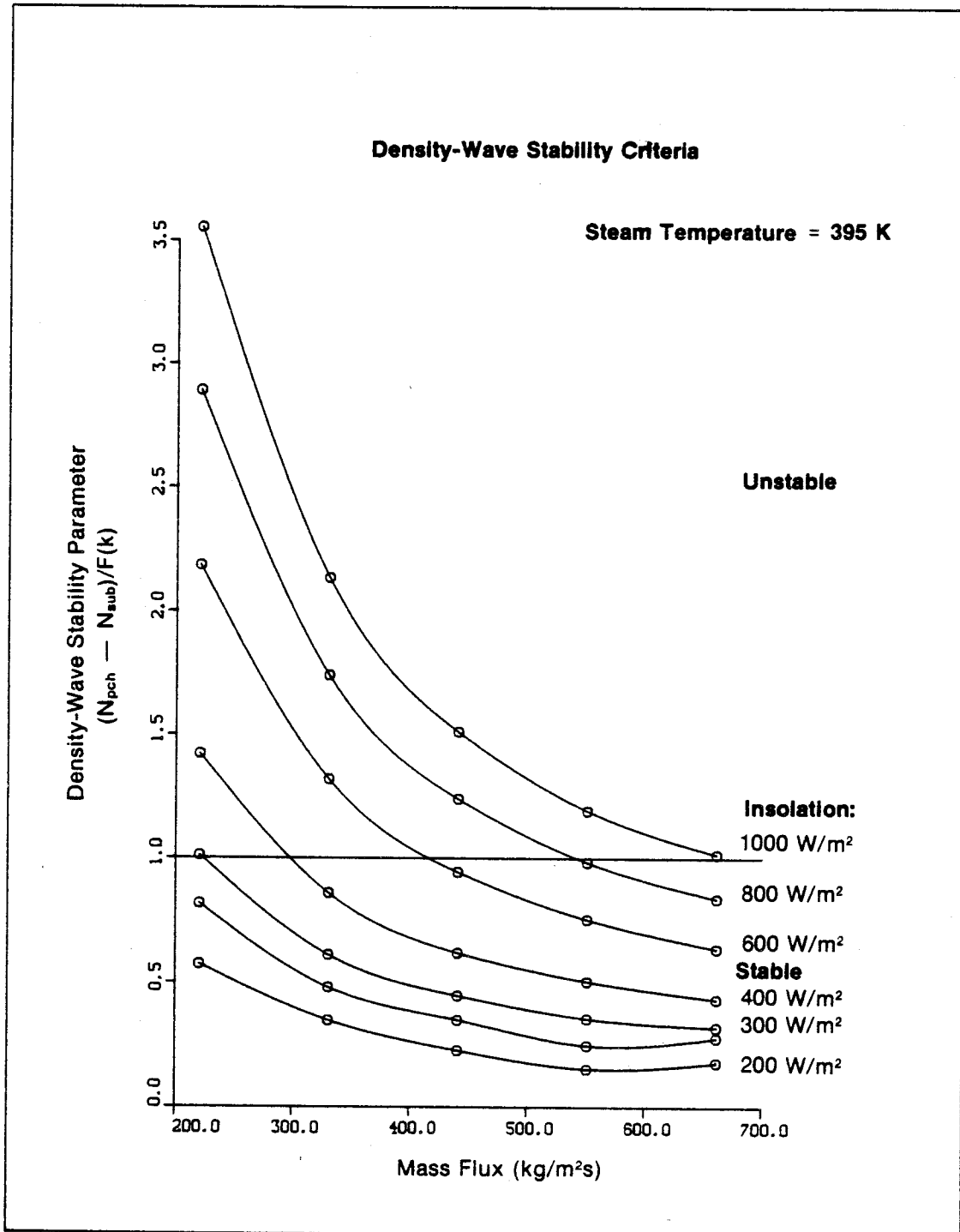
Figure 7-6. Density-Wave Stability Criteria vs. Mass Flux (T_S = 395 K)

96
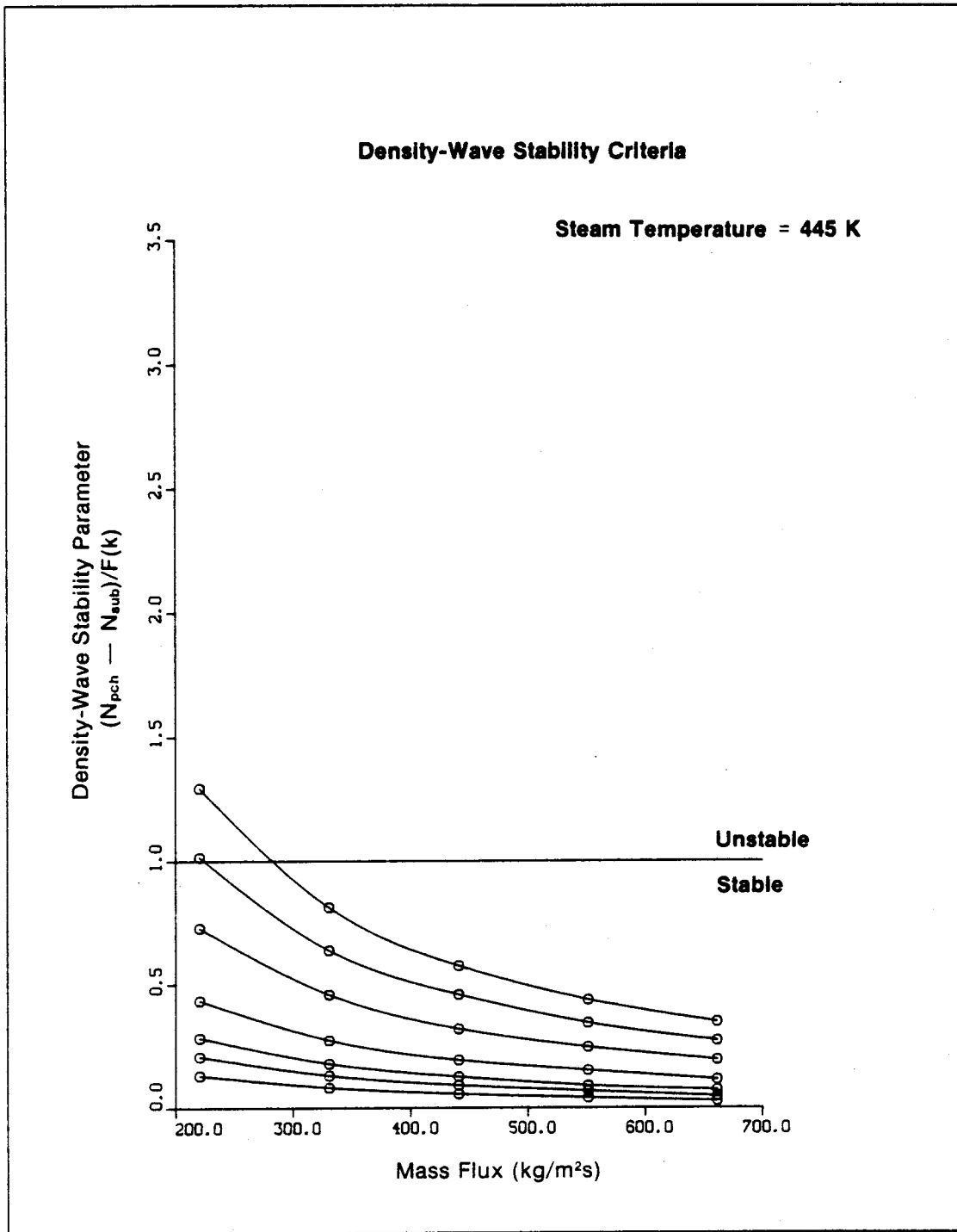
Figure 7-7. Density-Wave Stability Criteria vs. Mass Flux (T_s = 445 K)

000013

Density-Wave Stability Criteria

Steam Temperature = 495 K
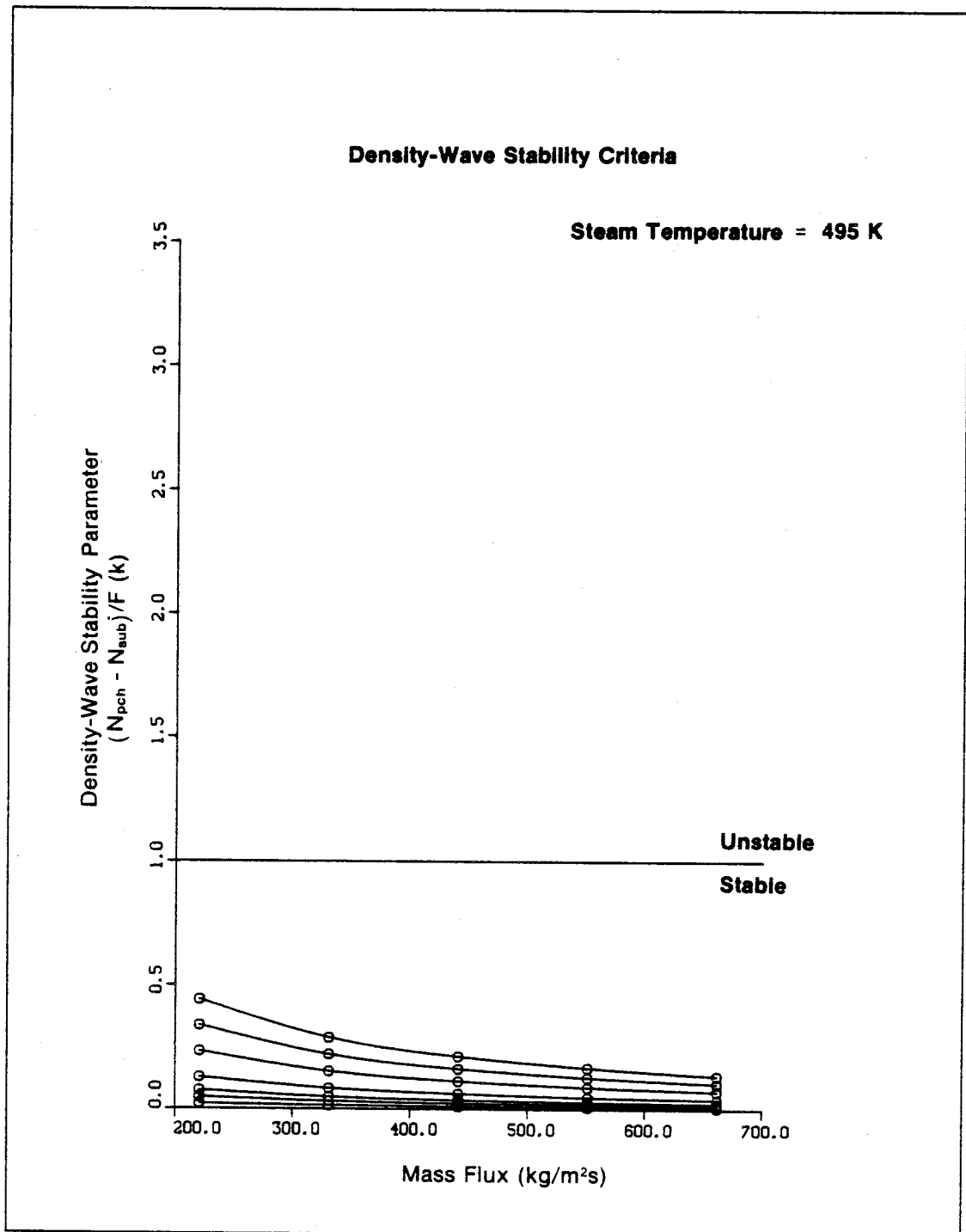
Figure 7-8. Density-Wave Stability Criteria vs. Mass Flux (T_s = 495 K)

Only testing can ultimately resolve this issue; an experimental program has been proposed by the authors to achieve this goal.

7.5 SUMMARY

The analysis presented in this chapter indicates that instabilities will not cause operational problems for a correctly engineered, direct steam-generating solar system. The tube wall should remain in liquid contact under all operating conditions. Thus, temperature excursions of the tube wall and consequent damage to the receiver selective surface are highly unlikely. As indicated in Sec. 2.4, even if dryout occurs, gravitational effects will expose only the top surface of the receiver tube; and the focus of the reflector is on the bottom of the receiver tube which will always be in liquid contact. Far from being a potential danger to the receiver selective surface, since deterioration of black chrome appears to be temperature dependent, the operation of an in situ system is less likely to affect the properties of the selective surface than the higher temperature operations of the steam-flash or unfired boiler systems.

Flow-pattern transition instabilities could arise, but the literature indicates that such effects will be minor. The characteristic pressure drop curve of the heated receiver tube is such that flow excursions, pressure-drop oscillations, and acoustic oscillations will not occur. The application of a conservative stability criterion indicates that density-wave oscillations could occur under the lowest steam pressures and flow rates, conditions which result in very high exit velocities from the receiver tube. Under these conditions the steam-flash system is probably a better choice to generate low-temperature steam, but the appropriate amount of inlet orificing can stabilize the in situ system even under these extremes.

There is an obvious need to confirm this analysis experimentally, and to demonstrate that instabilities that do occur can be corrected by minimal increases in system pressure drop. The analysis is critically dependent on the pressure drop characteristics at the inlet and outlet of the heated channel. Therefore the accumulation of such data would be a valuable asset toward the confirmation of this analysis.

SECTION 8.0

CONCLUSIONS AND RECOMMENDATIONS

This study investigated the important issues related to the direct generation of steam in the receiver tubes of line-focus solar collectors. Specifically, this study included: a literature survey of relevant experimental and analytical work on boiling; the development and implementation of a detailed system model to predict and compare the instantaneous and long-term thermal performance of systems based on the direct steam generation concept and conventional steam flash and unfired boiler alternatives; the application of the state-of-the-art stability criteria to the direct steam-generating system under investigation; a cursory cost analysis; and a discussion on pertinent operational issues such as freeze protection, corrosion, scaling, and safety.

8.1 CONCLUSIONS

8.1.1 Thermal Performance

Based on the analyses presented in this report the following conclusions can be reached.

- In terms of thermal performance, in situ systems will considerably outperform flash or oil systems over a wide range of operating conditions. In situ systems are most advantageous when compared with oil systems. More specificially direct-boiling systems should deliver from 9% to 13% more energy on an annual basis than competing oil systems. On an instantaneous basis, direct-boiling systems exhibit an efficiency advantage of 4% to 12% compared to oil and steam-flash systems.

- Performance advantages of in situ systems over the more conventional systems result from the synergistic effect of a number of phenomena including differences in collector operating temperature, heat-transfer coefficients, parasitic pumping power, and collector operating time. The major performance advantage over oil systems occurs due to lower collector operating temperature and a lower collector system cut-off temperature. Direct-boiling systems are more efficient than flash systems mainly because of much lower parasitic pumping power and lower collector operating temperatures especially at high fluxes. The lower collector temperatures inherent to the in situ system result from the nature of the latent heat transfer mechanism. Virtually no temperature differential over the steam delivery temperature is required for net energy delivery.

- In all of the parametric variations of mass flow rate, steam delivery temperature, and incident solar flux, the greatest impact on system performance occurred with solar flux variations. System efficiency drops off dramatically at low fluxes. Steam delivery temperature also has a significant impact. System performance has little dependence on mass flow rate when parasitics are not considered. When parasitics are considered, small but significant (2% to 3%) effects on system performance can be seen.

- Of the three system types considered, the in situ system is most nearly isothermal, at an average receiver temperature that is very close to or even less than the required steam temperature. Average receiver temperatures vary most with the oil systems, and can reach levels which are nearly 50 K higher than the required steam delivery temperature at the highest fluxes. The relative merit of the in situ system compared to the alternatives in terms of performance and pumping power increases with increasing steam temperature. The flash system is unsatisfactory for the production of steam in excess of about 2 MPa (290 psia) because of large pumping power consumption. At high steam temperatures, an oil system is limited by the breakdown temperature of the oil and the performance limit of the line-focus collector. On the other hand, the performance of a direct-boiling system at 250°C (500°F) or even 316°C (600°F) with advanced designs is satisfactory and is limited only by the mechanical integrity of the system at the flexhoses which are the weakest points. High exit qualities (up to perhaps 50%) are possible under such conditions. Clearly, the in situ concept would allow the application of line-focus collectors for the production of electric power at a relatively high thermodynamic efficiency.

- System performance is always dominated by the performance of the collector. System performance calculated using the detailed physical model of the collector developed in this study strongly agrees (within less than 1%) with a simplified model based on measured performance data.

- Because the in situ system is relatively more efficient at low flux levels, its benefits increase relative to the other systems with low ambient temperatures, areas of low insolation, elevated steam temperatures, high latitude applications, and north-south field orientation where lower net radiation levels are experienced compared to east-west orientations during an appreciable amount of the operating time.

8.1.2 Operating Stability

Stability criteria were developed for each of five types of instability which could result during operation of the in situ system. The instabilities were Ledinegg instability, flow-pattern transition instability, density-wave oscillations, acoustic oscillations and pressure-drop oscillations. Over the range of conditions considered in the study, only density-wave oscillations are likely to cause any concern.

Density-wave oscillations could mechanically vibrate system components. But from an application of the stability criteria, these density-wave oscillations are likely to occur only through a combination of very low steam temperatures and the lowest mass flow rates which result in the very highest exit qualities and steam velocities. Such conditions are not desirable applications of the direct-boiling concept, but in any case the oscillations can be subdued by adding more inlet orificing to each collector row resulting in a small increase in total system pressure drop. In fact, the inlet flow restriction required to give good interrow distribution is likely to alleviate all flow stability problems.

The possibility of tube dryout (burnout) appears nonexistent since large static flow excursions do not appear possible. Tube wall dryout could cause temperature increases of the tube wall with resulting damage to the receiver selective surface. In fact, degradation of the selective surface appears to be temperature dependent, and thus is more likely to occur using higher temperature steam-flash and oil systems.

8.1.3 Costs

- Initial costs for an in situ system may be reduced by as much as 15% when compared with an oil system because the unfired boiler, expansion tank, and oil costs are eliminated. Compared to a flash system, the flash valve can be eliminated and a smaller circulating pump can be used, resulting in a cost savings of about 5%.

- Potential additional cost reductions relating to piping, insulation, and safety assurance may be attained by appropriate optimization of the in situ system. The relative cost benefit of the in situ system increases with steam delivery temperature as increasing steam quality allows reductions in pipe sizes and auxiliary equipment. In total, the delivered cost of energy from an in situ solar steam system could be reduced by over 25% compared to an oil system.

8.1.4 Additional Comments

There are a number of additional conclusions that can be drawn from this study. These include:

- Ease of control is an advantage for direct-boiling systems over more conventional flash systems.

- Heat-transfer fluid handling and safety problems (including recurrent fire dangers) are greatly reduced by eliminating oil from the system.

- Direct-boiling systems offer another option (besides a steam-flash system) to food processors who will not use oil systems because of the potential for product contamination.

- Fluid freezing is not a major impediment to using water in a line-focus solar collector system. Through proper design and control, thermal heat losses can be minimized and freezing can be prevented.

- The dangers posed by high temperature water and steam systems are familiar to industry. The greatest hazards are from flexhoses and safety valves; these can be controlled by automated control procedures and by restricting personnel access to the operating collector field.

- Corrosion and scaling of the open loop steam systems can be controlled by standard industrial water treatment practices.

8.2 RECOMMENDATIONS

This study has analytically quantified the benefits of using the direct generation of steam in line-focus solar collectors. A timely, follow-up experimental program is warranted to fully demonstrate the feasibility of the concept and to confirm the conclusions of the study. In particular, it is strongly recommended that DOE/ SERI pursue the following research efforts.

- A comprehensive costing study should be undertaken to precisely define costs of the three competing solar system designs to more fully explain the economic benefit of using direct boiling. This study would consider the variation of capital costs with steam delivery temperature.

- Simple, low cost experiments can and should be run on SERAPH in FY 1982 to verify important performance and stability findings established in FY 1981, including the question of freeze protection.

- An IPH upgrade of an existing steam-flash project offers an excellent opportunity to demonstrate the concept at minimal cost. This should be pursued with the system user, collector supplier, and other interested parties.

- The analytical tools developed by SERI for this task are detailed and are state-of-the-art. They can and should be applied to other related solar phase-change and two-phase flow problems. Such development is being considered by DOE for flat-plate systems in air conditioning applications and for line-focus applications in power generation. The direct-boiling concept would generate electricity using line-focus technology at thermodynamic efficiencies comparable to pressurized-water nuclear reactors. Very high steam qualities (perhaps in excess of 50%) could be attained. This would allow considerable reductions in the size and cost of transport piping.

SECTION 9.0

REFERENCES

Acurex Corporation. 1980 (July). Quarterly Performance Report on Solar Production of Industrial Process Steam at Johnson and Johnson Plant. Sherman, TX.

Babcock and Wilcox Co. 1978. Steam—Its Generation and Use. 39th Edition. New York.

Baker, O. 1954. "Simultaneous Flow of Oil and Gas." Oil and Gas Journal. Vol. 53: pp. 185-195.

Beckman, W. A. 1978. "Duct and Pipe Losses in Solar Energy Systems." Solar Energy. Vol. 21: pp. 531-532.

Bergles, A. E.; Collier, J. G.; Delhaye, J. M.; Hewitt, G. F.; Mayinger, F. 1981. Two-Phase Flow and Heat Transfer in the Power and Process Industries. Washington, D.C.: Hemisphere Publishing Corp.

Bird, R. B.; Stewart, W. E.; Lightfoot, E. N. 1960. Transport Phenomena. New York: John Wiley and Sons.

Castle, J.; Su, W. 1980 (June). SERAPH Facility Capabilities. SERI/RR-632-702. Golden, CO: Solar Energy Research Institute.

Cherne, J. M.; Gelb, G. H.; Pinketon, J. D.; Paige, S. F.; Little, N. 1978 (Dec.). Conceptual Design Report: Solar Production of Industrial Process Steam at Ore-Ida Frozen Fried Potato Plant. Prepared under DOE Contract No. ET-78-C-03-2147. Redondo Beach, CA: TRW Energy Systems Group.

Crane Company. 1976. Flow of Fluids Through Valves, Fittings and Pipe. Technical Paper No. 410. New York.

DeWinter, F. 1975. "Heat Exchanger Penalties in Double-Loop Solar Water Heating Systems." Solar Energy. Vol. 17: pp. 335-337.

Dow Chemical Company. n.d. Dowtherm Handbook. Midland, MI.

Dukler, A. E.; Wicks, M.; Cleveland, R. G. 1964 (Jan.) "Frictional Pressure Drop in Two-Phase Flow: B. An Approach Through Similarity Analysis." AIChE Journal. Vol. 10 (No. 1): pp. 44-51.

Fand, R. M.; Morris, E. W.; Lum, M. 1977. "Natural Convection Heat Transfer From Horizontal Cylinders to Air, Water and Silicone Oil for Rayleigh Numbers Between 3×10^2 and 2×10^7." Int. J. Heat Mass Transfer. Vol. 20: pp. 1173-1184.

Favell, M. E.; Granjean, N. R. 1980 (Feb.). User's Manual for Computer Code SOLTES-1 (Simulator of Large Thermal Energy System). SAND-78-1315 (Revised). Albuquerque, NM: Sandia National Laboratories.

Gee, R; Gaul, H. W.; Kearney, D.; Rabl, A. 1980 (Mar.). Long-Term Average Performance Benefits of Parabolic Trough Improvements. SERI/TR-632-439. Golden, CO: Solar Energy Research Institute.

Gordon, J. M.; Rabl, A. 1981. "Design, Analysis and Optimization of Solar Industrial Process Heat Plants Without Storage." Submitted for publication.

Gupta, G. D. 1979 (Jan.). Conceptual Design Report for Solar Production of Industrial Process Steam Ranging in Temperature from 300°F to 550°F (Phase I). Prepared under DOE Contract No. ET-78-C-03-2199. Livingston, NJ: Foster Wheeler Development Corporation.

Hamel, B. B.; Brown, H. L. 1980 (Jan.). Total Energy, Steam Use and Boiler Profile for the Industrial Sector (SIC 20-39). Prepared for the Department of Energy under Contract E(11-1) 2862. Philadelphia, PA: Drexel University.

Harrison, T. D. 1980 (Nov.) Midtemperature Solar Systems Test Facility Predictions for Thermal Performance of the Solar Kinetics T-700 Solar Collector With FEK 244 Reflector Surface. SAND 80-1964/1. Albuquerque, NM: Sandia National Laboratories.

Hewitt, G. F.; Hall-Taylor, N. S. 1970. Annular Two-Phase Flow. Oxford: Pergamon Press.

Hickox, C. E.; Gartling, D. K. 1977 (Dec.). The Effects of Nonuniformities on Natural Convection in Annular Receiver Geometries. SAND 77-1641. Albuquerque, NM: Sandia National Laboratories.

InterTechnology Corporation. 1977. Analysis of the Economic Potential of Solar Thermal Energy to Provide Industrial Process Heat. 3 volumes. Warrenton, VA.

Ishii, M. 1971. "Thermally Induced Flow Instabilities in Two-Phase Mixtures in Thermal Equilibrium." Ph.D. Thesis. Atlanta, GA: School of Mechanical Engineering, Georgia Institute of Technology.

Kays, W. M. 1966. Convective Heat and Mass Transfer. New York: McGraw-Hill.

Kays, W. M.; Crawford, M. E. 1980. Convective Heat and Mass Transfer. 2nd edition. New York: McGraw-Hill.

Klein, S. 1979 (June). TRNSYS - A Transient System Simulation Program, Users' Manual. Report No. 3810. Madison, WI: Engineering Experiment Station, University of Wisconsin.

Kuehn, T. M.; Goldstein, R. J. 1978 (Nov.). "An Experimental Study of Natural Convection Heat Transfer in Concentric and Eccentric Horizontal Cylindrical Annuli." Trans. of ASME: Journal of Heat Transfer. Vol. 100 (No. 4): pp. 635-640.

Mandhane, J. M.; Gregory, G. A.; Aziz, K. 1974. "A Flow Pattern Map for Gas-Liquid Flow in Horizontal Pipes." Int. J. Multiphase Flow. Vol. 1; pp. 537-553.

Mandhane, J. M.; Gregory, G. A.; Aziz, K. 1977 (Oct.). "Critical Evaluation of Friction Pressure-Drop Prediction Methods for Gas-Liquid Flow in Horizontal Pipes." Journal of Petroleum Technology; pp. 1348-1358.

Martinelli, R. C.; Nelson, D. B. 1948 (Aug.). "Prediction of Pressure Drop During Forced-Circulation Boiling of Water." Transactions of ASME Journal of Heat Transfer. Vol. 70: pp. 695-702.

McClintock, R. B.; Silvestri, G. J. 1968. Formulations and Iterative Procedures for the Calculation of Properties of Steam. New York: The American Society of Mechanical Engineers.

Pederson, R. J.; May, E. K. 1982 (Mar.). Flow Instability During Direct-Steam Generation in a Line-Focus Solar Collector System. SERI/TR-632-1354. Golden, CO: Solar Energy Research Institute.

Rabl, A. 1981 (Jan.). Yearly Average Performance of the Principle Solar Collector Types. SERI/TR-631-716. Golden, CO: Solar Energy Research Institute.

Ratzel, A. C. 1979 (Sept.). Receiver Assembly Design Studies for 2-m 90° Parabolic-Cylindrical Solar Collectors. SAND 79-1026. Albuquerque, NM: Sandia National Laboratories.

Ratzel, A. C.; Sisson, C. E. 1980 (Oct.). Annular Solar Receiver Characteristics. SAND 79-1010. Albuquerque, NM: Sandia National Laboratories.

Saha, P.; Ishii, M.; Zuber N. 1976. "An Experimental Investigation of the Thermally Induced Flow Oscillations in Two-Phase Systems." J. Heat Transfer. Vol. 98: pp. 616-622.

Stauffer Chemical Company. 1979 (Oct.). Solar Production of Industrial Process Steam: Phase I Analysis and Design. Final design report prepared for U.S. Department of Energy under Contract No. EM-78-C-03-1882.

Stearns-Roger Services, Inc. 1981 (Jan.). Modular Industrial Solar Retrofit Sample Design and Sample Construction Specification. Albuquerque, NM: Sandia Laboratories.

Streeter, V. L. 1966. Fluid Mechanics. 4th edition. New York: McGraw-Hill.

Taitel, Y.; Dukler, A. E. 1976 (Jan.). "A Model for Predicting Flow Regime Transitions in Horizontal and Near Horizontal Gas-Liquid Flow." AIChE Journal. Vol. 22 (No. 1.): pp. 47-55.

Thom, J. R. S. 1964. "Prediction of Pressure Drop During Forced Circulation of Boiling Water." Int. J. Heat Mass Transfer. Vol. 7: pp. 709-724.

Tong, C. S. 1975. *Boiling Heat Transfer and Two-Phase Flow.* Huntington, NY: Robert Kreiger Publishing Co.

U.S. Department of Commerce. 1974. *Climatic Atlas of the United States.* Asheville, NC: National Climatic Center.

SERI ◈ ————————————————————————————————————

APPENDIX A

SYSTEM MODEL

The model described in this appendix was developed to predict the transport phenomena of two-phase flow in line-focus solar collector systems and to compare the relative engineering and system merits of using in situ boiling in line-focus receivers relative to the merits of steam-flash and unfired-boiler systems. The model provides a balance between simplicity, flexibility, and the detail needed to assess the specific phenomena of interest. Areas investigated using the model were pumping parasitics, piping heat loss and associated efficiency of line-focus components, the quality of steam generated in the receiver, and pressure drop across typical components. A brief description of the important aspects of the model follows.

A.1 THE MODEL

The model consists of a number of interconnected components used in typical IPH systems:

- a mixing manifold (1);

- a pump (1);

- collector manifolds (2), including flexhoses;

- water inlet and steam return lines from collectors;

- an expansion valve, a steam separator, and unfired boiler; and

- a collector model.

Assumptions pertinent to the individual components will be discussed later. However, the fundamental assumptions common to all components are

- steady-state operation;

- uniform, one-dimensional velocity profiles across pipe/collector cross sections; and

- uniform heat loss and gain from all cylindrical surfaces around the circumference.

A.2 FUNDAMENTALS

Variables derived from the system model include density, pressure, velocity, enthalpy, steam quality, and temperature, along with additional quantities such as Reynolds number and heat-transfer coefficients. The energy gains and/ or losses are determined and expressed in terms of enthalpy. Calculations proceed in sequential steps using known quantities at the inlet to a system component, or node, to determine conditions at the outlet.

The system computations for the water systems proceed as follows. The total mass flow (the sum of both makeup and return) is assumed constant for a particular set of input conditions. Initially, water delivered to the pump is assumed to be saturated water corresponding to the delivered steam temperature. The thermodynamic states at each component are calculated, and conditions at the outlet of the steam generator are compared with the assumed steam conditions. If the assumed input state and final output steam conditions do not agree, the mass flow of the makeup water, and the pressure increase across the system pump (both initially assumed to be zero) are adjusted to make the inlet and outlet saturated liquid properties agree. Only one or two successively improved estimates usually are needed to provide adequate agreement between assumed and calculated outlet conditions. Thus, for an assumed overall mass flow rate and an outlet steam temperature, the transport state at each node as well as the mass flow of steam and makeup water are determined. For the steam-flash case, successive adjustments are made to the pump outlet pressure to provide the necessary pressure to suppress boiling in the collector field prior to the flash valve.

The water/steam conditions at each node are determined from an analytical steam thermodynamic procedure developed by Brookhaven National Laboratory (McClintock and Silvestri 1968).* The routine provides a water/steam-state property vector for any two input parameters. For instance, if values of pressure and enthalpy are used as inputs to the procedure, the routine returns appropriate temperature, density, quality, and physical properties (such as conductivity, viscosity, and Prandtl number).

For the unfired-boiler system, an initial temperature for the oil entering the pump is assumed. The temperature of the oil around the loop is then calculated, and the final temperature of the oil exiting the heat exchanger is compared to the initial estimate. Successive iterations are made on this temperature until the required degree of accuracy is achieved.

A.3 BASIC RELATIONS

The appropriate form for the transport equation used in the model is determined from the statement of the First Law:

$$\Delta\left[m\left(H + \frac{1}{2}u^2 + gz\right)\right] = \Delta Q + \Delta W \quad , \tag{A-1}$$

where Δ denotes a change and m is the mass flow rate given by

$$m = \rho A u \quad . \tag{A-2}$$

Assuming constant density for any particular piping element, the total pressure drop can be expressed by

———————————————

*The version used in this study was adapted to the CDC computer system and provided to SERI by Gordon Miller of Sandia National Laboratories (SNL) at Livermore, CA.

SERI ●

$$\frac{\Delta P}{\rho} = - \Delta gz - \Delta \frac{1}{2} u^2 - \left(\frac{\Delta P}{\rho}\right)_{friction} + \left(\frac{\Delta P}{\rho}\right)_{pumping} \quad . \qquad (A-3)$$

The density used is the inlet density to the spatial zone of interest. Following the calculation of incremental pressure and enthalpy changes, the outlet density is calculated.

The first term on the right hand side of the equation represents pressure loss due to the decreased gravity head, and the second term represents pressure loss due to the kinetic energy loss. The third and fourth terms, in turn, represent the contribution to the pressure change from friction (and other irreversible effects) and from the pumping done on the fluid system. Since an enthalpy accounting procedure is used in the analysis, the appropriate expression for an enthalpy change across any component ΔH is given by

$$\Delta H = \frac{\Delta Q}{m} + \frac{\Delta W}{m} - g\Delta z - \frac{1}{2}\Delta u^2 \quad . \qquad (A-4)$$

Pressure drop for single-phase flow in tubes with uniform cross section is calculated using the previously described Colebrook formula. Generally, the solution procedure requires only two or three iterations before a high degree of accuracy is achieved. Pressure drop for two-phase flow is calculated using the Dukler no-slip model.

Additional pressure drops, resulting from the manifolds and flexhoses leading to the collector tubes, are prescribed. This is done empirically, since the design for each system can vary considerably, and an accurate analytical correlation could be quite cumbersome and computationally involved. The expression for the pressure drop leading from the main supply line to each collector line is

$$\frac{\Delta P}{\rho} = -g\Delta z - \frac{1}{2} k_1 u^2 |_{\substack{Supply \\ Line}} - \frac{1}{2} k_2' \left[\left(\frac{f}{d}\right)u^2\right]|_{\substack{Receiver \\ Tube\ Entrance}} \quad . \qquad (A-5)$$

The first term accounts for the difference in elevation from the supply line to the collector tube; the second term corresponds to the loss due to the header; and the third term accounts for the loss in the flexhose. Terms k_1 and k_2' are constants input by the user. Typically, k_1 has been determined so that for nominal system flow rates the second term yields a prescribed pressure drop.* The term k_2' allows the user to relate the pressure drop in the flexhose, to a corresponding pressure drop in an equivalent length of collector tube (near its entrance). Thus physically, k_2' represents the length of

---

*A value of 35 kPa (~5 psi) was used in the analysis.

the flexhose times the ratio of the pressure drop per unit length in the flex-hose to the pressure drop per unit length in the collector tube.*

The analytical expression assumed for the pressure drop leading from the collector to the main delivery line is similar to Eq. A-5:

$$\frac{\Delta P}{\rho} = g \Delta z - \frac{1}{2} k_3' \left(\frac{f}{d} u^2\right) \Big|_{\substack{\text{Receiver Tube} \\ \text{Exit}}} - \frac{1}{2} k_4 u^2 \Big|_{\substack{\text{Steam Delivery} \\ \text{Line}}} . \qquad \text{(A-6)}$$

Terms k_3' and k_4 are user input constants exactly analogous to k_2' and k_1, respectively.

A.4 SOLUTION/ITERATIVE PROCEDURE

A.4.1 Steam-Flash and Direct-Boiling Systems

With a given set of input conditions and an assumed constant mass flow rate and steam delivery temperature, the output states for each component are determined. If the final output steam temperature and steam mass output do not match the assumed initial values, then the pumping pressure and makeup mass flow are adjusted iteratively to obtain a better solution. The makeup mass flow and pumping pressure adjustment procedures are discussed below.

The makeup mass flow is equal to the amount of steam produced. Hence,

$$m \lambda = m x_m \qquad \text{(A-7)}$$
$$(\text{makeup mass flow} = \text{mass of steam produced})$$

where m is the total mass flow in the collector field, x_m is the quality of steam produced, and λ is the fraction of m supplied by the makeup stream. Furthermore, by considering an energy balance on the whole system, Q_{net} can be related to the steam mass flow by

$$Q_{net} = m x_m (h_g - h_m) = m(h_g - h_m)\lambda \quad , \qquad \text{(A-8)}$$

where h_g and h_m are the enthalpy of the delivered saturated vapor and the makeup liquid, respectively. On successive iterations, the estimate for the next assumed mass fraction (λ) of makeup water is simply the calculated quality from Eq. A-8.

---

*This pressure drop ratio has been determined from test data corresponding to nominal flow rates taken at SNLA, and the ratio is approximately 2.5 to 3.0 for Therminol heat-transfer fluid. The authors are not aware of similar data corresponding to water or steam.

The pumping pressure is adjusted by first assuming that the final outlet pressure (P_o) is a function of both the pump outlet pressure (P_p) and outlet quality (x_m). Thus,

$$P_o = P_o(P_p, x_m) \quad .$$

(A-9)

Differentiating gives

$$\Delta P_o = \left(\frac{\partial P_o}{\partial P_p}\right) \Delta P_p + \left(\frac{\partial P_o}{\partial x_m}\right) \Delta x_m \quad .$$

(A-10)

If the error between the desired and calculated outlet pressure is ΔP_o, the required adjustment to the pumping pressure is determined from Eq. A-10 by

$$\Delta P_p = \frac{\Delta P_o - \left(\frac{\partial P_o}{\partial x}\right) \Delta x_m}{\left(\frac{\partial P_o}{\partial P_p}\right)} \quad .$$

(A-11)

Computationally, the following procedure worked quite well. First, note that in the neighborhood of the solution

$$\left(\frac{\partial P_o}{\partial P_p}\right) = 1 \quad .$$

(A-12)

Then Eq. A-11 may be written (in the neighborhood of the solution) as

$$\Delta P_p = \Delta P_o - \left(\frac{\partial P_o}{\partial x_m}\right) \Delta x_m \quad .$$

(A-13)

Iteratively, the nth estimate for ΔP_p is expressed by

$$(\Delta P_p)_n = (\Delta P_o)_n - \left(\frac{\partial P_o}{\partial x}\right)_n \Delta x_n \quad .$$

(A-14)

Since $\left(\frac{\partial P_o}{\partial x}\right)_n$ is not easily evaluated but $\left(\frac{\partial P}{\partial x}\right)_{n-1}$ is already determined from the previous iteration, the iterative expression used is

$$\left(\Delta P_p\right)_n \simeq \left(\Delta P_o\right)_n - \left(\frac{\partial P}{\partial x}\right)_{n-1} \Delta x_n \quad ,$$

(A-15)

where

$$\left(\frac{\partial P}{\partial x}\right)_{n-1} = \frac{(\Delta P_o)_{n-1} - (\Delta P_p)_{n-1}}{\Delta x_{n-1}} = \frac{(P_o - P_p)_{n-1} - (P_o - P_p)_{n-2}}{x_{n-1} - x_{n-2}} \qquad (A-16)$$

and

$$\Delta x_n = x_n - x_{n-1} \quad . \qquad (A-17)$$

The new value of x is x_n calculated from Eq. A-8. As stated earlier, this value is equal to the makeup water mass flow fraction (λ) for the next iteration.

A.4.2 Unfired-Boiler System

When oil is circulated in the collector field, the solution iteration procedure is somewhat different than for the flash and in situ boiling systems which are essentially open systems. For the closed loop oil system, the collector field fluid inventory is constant, and the only energy exchanged is with that fluid through a heat exchanger boiler.

An initial temperature is assumed for the oil delivered to the pump suction for a fixed oil flow rate and incident flux. The energy gains and losses to the oil stream are calculated for the field components as described earlier. Now, the heated oil returning from the field passes through a boiler/heat exchanger, releasing its energy to generate steam. The output oil stream from the boiler/heat exchanger is then returned to the collector field. If the temperature of the oil exiting the boiler does not equal the previously assumed initial temperature, then this exit temperature is assumed to be the initial oil temperature for the next iteration. Successively better approximations are made until the assumed inlet and calculated outlet oil temperatures agree within the required range of accuracy.

The boiler/heat exchanger is modeled as a kettle boiler with a fixed heat-transfer area (input) and constant heat-transfer coefficients (inputs) corresponding to boiling and preheating, respectively. Perfect countercurrent heat transfer is also assumed. The amount of steam produced, as well as the areas allocated to boiling and preheating, and the output state of the oil at the boiler and at the preheated sections are determined by the code for a given makeup water temperature and desired saturated steam conditions. The heat transfer process is illustrated in Fig. A-1.
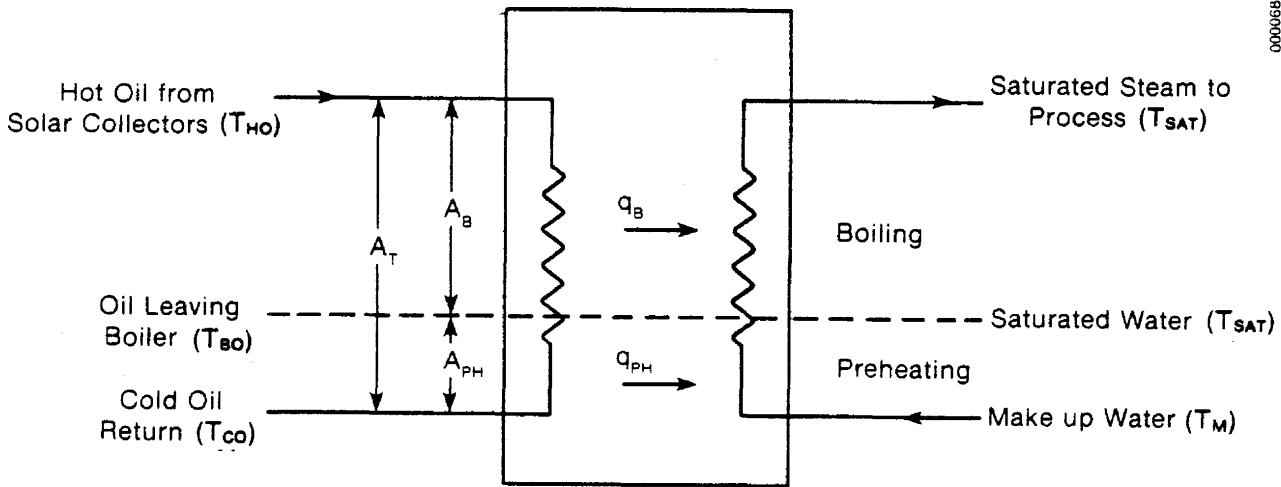
Figure A-1. Model of Unfired Boiler Steam Generator

The heat exchanged in the boiler region (q_B) is determined from three relations. First, q_B can be related to the oil mass flow (m_o), the average specific heat of the oil in the boiler region ($\overline{C_{po}}$), the hot oil temperature (T_{HO}), and the temperature of the oil at the exit of the boiler region (T_{BO}). Thus

$$q_B = m_o \, \overline{C_{po}} \, (T_{HO} - T_{BO}) \; . \tag{A-18}$$

Considering the water side of the boiler region, q_B can be determined from the mass flow of steam produced and the enthalpies of the saturated vapor (h_g) and saturated liquid (h_f), respectively. Thus,

$$q_B = m \, (h_g - h_f). \tag{A-19}$$

A third expression is determined for the boiler region by heat-transfer relations, resulting in

$$q_B = U_B \, A_B \, \overline{\Delta T_B} \; , \tag{A-20}$$

where U_B is the boiling heat-transfer coefficient (input and assumed constant) and A_B is the area allocated to boiling (to be determined). $\overline{\Delta T_B}$ is the log mean temperature difference across the boiler section of the heat exchanger defined by

$$\overline{\Delta T_B} = \left[(T_{HO} - T_{SL}) - (T_{BO} - T_{SL}) \right] / \ell n \left[(T_{HO} - T_{SL})/(T_{BO} - T_{SL}) \right] \; . \tag{A-21}$$

Equations A-18, A-20, and A-21 can be combined resulting in

$$T_{BO} = T_{SL} + (T_{HO} - T_{SL}) \exp \left(- \frac{U_B A_B}{m_o \overline{C_{po}}}\right) \quad . \tag{A-22}$$

Equations similar to those just derived for the boiler can then be developed for the preheater. Thus, heat transferred in the preheater (q_{PH}) may be expressed as

$$q_{PH} = m_o \overline{C_{po}}(T_{BO} - T_{CO}) \quad , \tag{A-23}$$

$$q_{PH} = m \overline{C_{pw}} (T_{SL} - T_M) \quad , \tag{A-24}$$

$$q_{PH} = U_{PH} A_{PH} \overline{\Delta T_{PH}} \quad , \text{ and} \tag{A-25}$$

$$\overline{\Delta T_{PH}} = [(T_{BO} - T_{SL}) - (T_{CO} - T_M)]/ \ell n \ [(T_{BO} - T_{SL})/(T_{CO} - T_M)] \quad . \tag{A-26}$$

Here, $\overline{C_{po}}$ and $\overline{C_{pw}}$ are the average specific heat of the oil and water, respectively, in the preheater. T_M is the makeup water temperature. The above four equations can be combined to give

$$T_{CO} = T_{BO} - (T_{BO} - T_M) \left[(1 - \exp D)/(\frac{m_o \overline{C_{po}}}{m \overline{C_{pw}}} - \exp D \ ) \right] \quad , \tag{A-27}$$

where D is defined by

$$D = U_{PH} A_{PH} \left(\frac{1}{m_o \overline{C_{po}}} - \frac{1}{m \overline{C_{pw}}}\right) \quad . \tag{A-28}$$

A final constraint equation needed for the areas is given by

$$A_T = A_B + A_{PH} \quad . \tag{A-29}$$

A solution for unknowns T_{BO}, T_{CO}, m, A_B, and A_{PH} can then be obtained. An initial value for A_{PH} is assumed, and a value for m is estimated based on the total energy gained by the collector system. Equations A-26, A-29, and A-22 are then solved for T_{BO} and T_{CO}. Using these values for T_{BO} and T_{CO}, two new estimates for m are obtained by solving Eqs. A-18, A-19, A-23, and A-26, respectively. The final new estimate is derived from the average of the two estimates. Having a new estimate for m, a new value for A_{PH} is determined from Eqs. A-24 and A-25. This process is repeated until successively better approximations for m and A_{PH} are determined along with calculated values for T_{BO} and T_{CO}. Usually only two or three iterations are required before a satisfactory solution is obtained.

A.5 DETERMINATION OF NUSSELT NUMBERS

Nusselt numbers corresponding to heat transfer in four different physical processes are used in the model: convective heat transfer associated with the flow in tubes, convective heat transfer in the annular region between the envelope and the absorber, and forced and natural convective heat transfer from convex cylindrical surfaces (i.e., the outer receiver tube and piping). The Nusselt number is defined in terms of a heat-transfer coefficient (h), a characteristic length (such as d, the diameter associated with flow in tubes), and the conductivity of the fluid (k):

$$Nu = hd/k(fluid) \quad . \tag{A-30}$$

Correlations to calculate Nusselt numbers corresponding to these conditions have been described previously.

A.6 DETAILED COLLECTOR MODEL

This model simulates both the transfer of solar energy incident on the collector to the working fluid and the thermal losses to the environment. Thus, it allows the complete determination of temperatures within the receiver tube assembly given the geometry, inlet fluid conditions, and solar radiation. The basic assumptions are that the heat flow is one dimensional, normal to the receiver axis, and uniform around the circumference. In addition, the tube is subdivided into an arbitrary number of discrete axial segments of length, Δx, over which the heat flux is assumed to be uniform. It is also assumed that there is no shading and the heat flux absorbed in a receiver increment Δx is reflected by a similar Δx length of reflective surface, i.e., end effects are neglected.

The thermal network analogy used to model the radial heat flow from the transport fluid through successive, resistive elements to the environment is depicted in Fig. A-2. Net conductances for an element of receiver length Δx are shown corresponding to the various radiative, convective, and conductive heat paths. The governing equations for the thermal network follow, and are given below in terms of heat flows (q), conductances (U), and temperature differences. The symbols in the energy balance equations and succeeding models in this Appendix are defined in Table A-1.

$$q_s = q_2 + q_3 + q_4 \quad , \text{ and} \tag{A-31}$$

$$q_{s,c} + q_3 + q_4 = q_5 + q_6 \quad , \tag{A-32}$$

where

$$q_1 = q_2 = \frac{U_1 U_2}{U_1 + U_2} (T_t - T_f) \quad , \tag{A-33}$$

$$q_3 = U_3(T_t - T_e), \tag{A-34}$$

$$q_4 = U_4(T_t - T_e), \tag{A-35}$$

q_6 ↑ q_5 ↑

T_{sky} ○ $T_{ambient}$ ○

Radiative
Conductance to
Sky (U_6)

Convective Conductance
to Ambient (U_5)

Glass Envelope (T_e) ○ ← $q_{s.c}$ Energy Absorbed by Envelope

q_3 ↑   ↑ q_4

Radiative Conductance
Across Air Gap (U_3)

Convective Conductance
Across Air Gap (U_4)

Outside Absorber
Tube (T_t) ○ ← q_s Incident Energy
on Absorber Tube

Tube Wall Conductance (U_2)
↓
q_2

Inside Absorber
Tube (T_{ti}) ○

Film Conductance (U_1)

Fluid (T_f) ○

↓ q_1

Figure A-2. Thermal Network of Receiver Tube of Parabolic Trough Solar Collector

118

SERI ❋

Table A-1. Definition of Symbols Used in Detailed Collector Model

Symbol	Definition (Units)
A_c	Aperture area of collector field (m^2)
d_i	Inner diameter of receiver tube (m)
d_o	Outer diameter of receiver tube (m)
d_{ei}	Inner diameter of glass envelope (m)
d_{eo}	Outer diameter of glass envelope (m)
F_{tg}	Radiation exchange factor between absorber and envelope (dimensionless)
k (air)	Thermal conductivity of ambient air (W/mK)
k (fluid)	Thermal conductivity of transport fluid (W/mK)
k (gas)	Thermal conductivity of gas between absorber tube and envelope (W/mK)
k (wall)	Thermal conductivity of absorber tube material (W/mK)
L	Length of absorber tube (m)
Nu (air)	Nusselt number for air adjacent to envelope external surface (dimensionless)
Nu (gas)	Nusselt number for gas between envelope and absorber tube (dimensionless)
Nu (fluid)	Nusselt number for transport fluid (dimensionless)
q_1	Rate of heat flow through boundary layer of transport fluid (W)
q_2	Rate of heat flow through absorber tube wall (W)
q_3	Rate of heat flow by radiation from absorber tube to envelope (W)
q_4	Rate of heat flow by convection from absorber tube to envelope (W)
q_5	Rate of heat flow by convection from envelope surface to ambient air (W)
q_6	Rate of heat flow by radiation from envelope to sky (W)
q_s	Rate of incident energy on absorber tube (W)
$q_{s,c}$	Rate of energy absorbed by envelope from incident energy (W)
Q_b	Incident solar heat flux (beam) (W/m^2)
T_a	Ambient air temperature (K)
T_e	Envelope temperature (K)
T_f	Fluid temperature (K)

Table A-1. Definition of Symbols Used in Detailed Collector Model (Concluded)

Symbol	Definition (Units)
T_t	Absorber tube, outer surface temperature (K)
T_{ti}	Absorber tube, inner surface temperature (K)
T_{sky}	Sky temperature (K)
U_1	Transport fluid film conductance (W/K)
U_2	Absorber tube conductance (W/K)
U_3	Conductance corresponding to radiative heat transfer between absorber tube and glass envelope (W/K)
U_4	Conductance corresponding to convective heat transfer between absorber tube and glass envelope (W/K)
U_5	Conductance corresponding to convective heat transfer between glass envelope and ambient air (W/K)
z	Height (m)
U_6	Conductance corresponding to radiative heat transfer between glass envelope and the sky (W/K)
α_e	Absorbtivity of glass envelope (dimensionless)
ε_e	Emissivity of glass envelope (dimensionless)
ε_t	Emissivity of absorber tube surface (dimensionless)
Δx	Element of absorber tube length (m)
ρ_c	Net reflectivity of collector surface (dimensionless)[a]
σ	Boltzman constant (W/m^2K^4)
τ_e	Transmittance of glass envelope (dimensionless)

[a]Includes optical errors.

$$q_5 = U_5(T_e - T_a), \tag{A-36}$$

$$q_6 = U_6(T_e - T_{sky}), \tag{A-37}$$

$$U_1 = \pi \Delta x \; Nu(fluid) \; k(fluid) \quad , \tag{A-38}$$

$$U_2 = \frac{2\pi \Delta x \; k(wall)}{\ell n(d_o/d_i)} \quad , \tag{A-39}$$

$$U_3 = \sigma\pi \, d_o \Delta x F_{tg}(T_t + T_e)(T_t^2 + T_e^2) \quad , \tag{A-40}$$

$$F_{tg} = \frac{1}{\dfrac{1}{\varepsilon_t} + \dfrac{d_o}{d_{ei}} \left(\dfrac{1}{\varepsilon_e} - 1 \right)} \quad , \tag{A-41}$$

$$U_4 = \pi \Delta x \; Nu(gas) \; k(gas) \quad , \tag{A-42}$$

$$U_5 = \pi \Delta x \; Nu(air) \; k(air) \quad , \text{ and} \tag{A-43}$$

$$U_6 = \sigma\pi \Delta x \; d_{eo} \; \varepsilon_e (T_e^2 + T_{sky}^2)(T_e + T_{sky}) \quad . \tag{A-44}$$

The energy balance equations are solved iteratively for T_i and T_e, since the conductances in general are also a function of T_t and T_e. For a particular increment the iteration is started by assuming a value for T_t and T_e, calculating the conductances, and then solving Eqs. A-31 and A-32 for a new set of T_t and T_e. The new values for T_t and T_e are then used to calculate a new set of conductances, and the procedure is repeated to the required degree of convergence. Usually only two or three iterations are required. Once a solution is obtained for the axial increment of interest, the iteration process is applied to the next segment, and the initial estimates for T_t and T_e are assumed as the corresponding values exiting from the previous segment.

A.7 SIMPLE COLLECTOR MODEL

The simple collector model is based upon the actual measured performance of a parabolic trough tested by SNLA and described in Sec. 3.1. As shown in Figs. A-3, A-4, and A-5 (for each system at the stated conditions) the results of the two models are almost indistinguishable. Such a close agreement may be coincidental with the choice of collector, but it does provide an additional degree of confidence in the detailed collector model. The simple model requires less computational time and thus is preferred for a wide range of parametric studies when details of heat transfer at the receiver are not required. However, all final results presented in this report were determined using the detailed collector model.
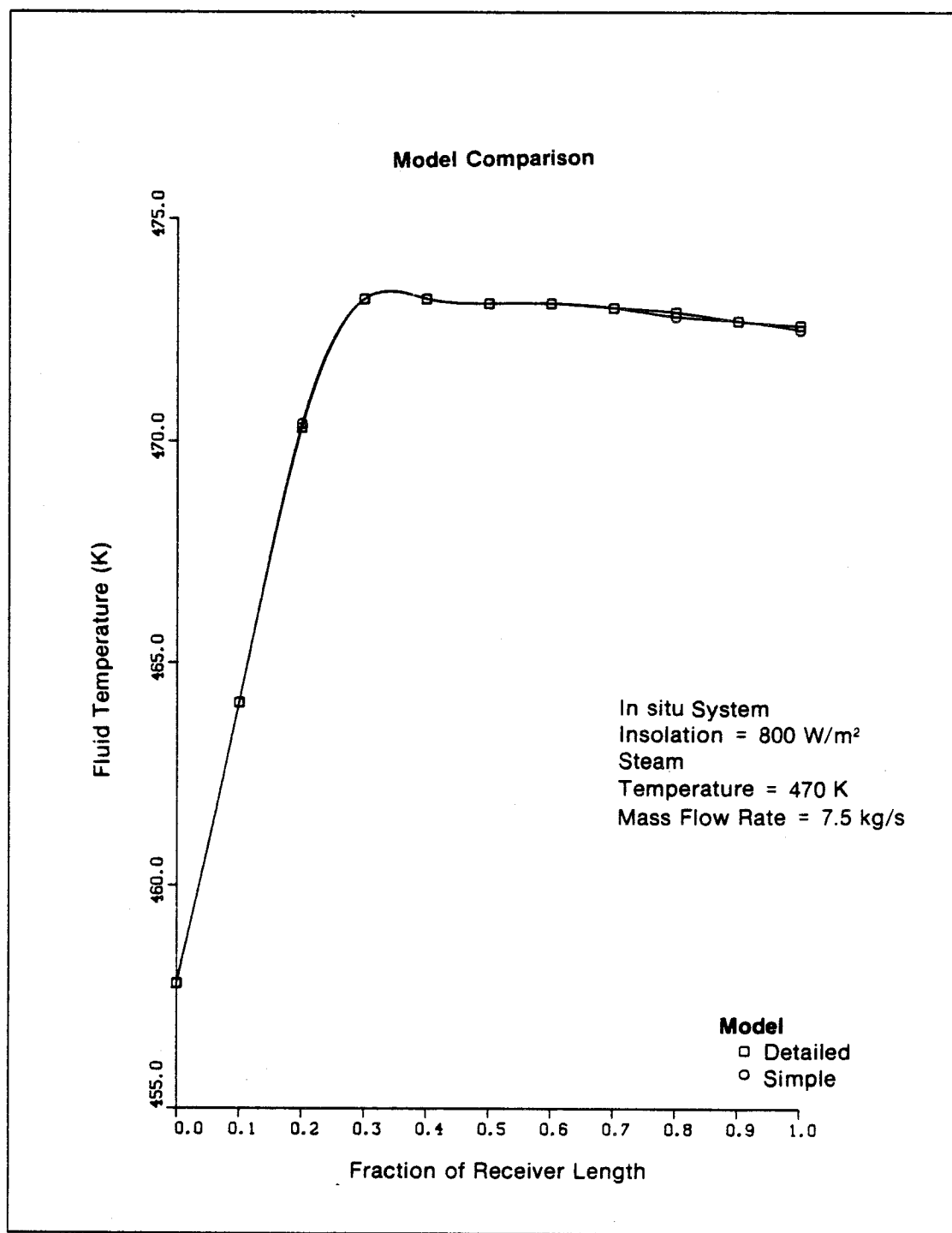
Figure A-3. Predicted Fluid Temperature vs. Position Along Receiver Using Simple and Detailed Collector Models (In Situ System)
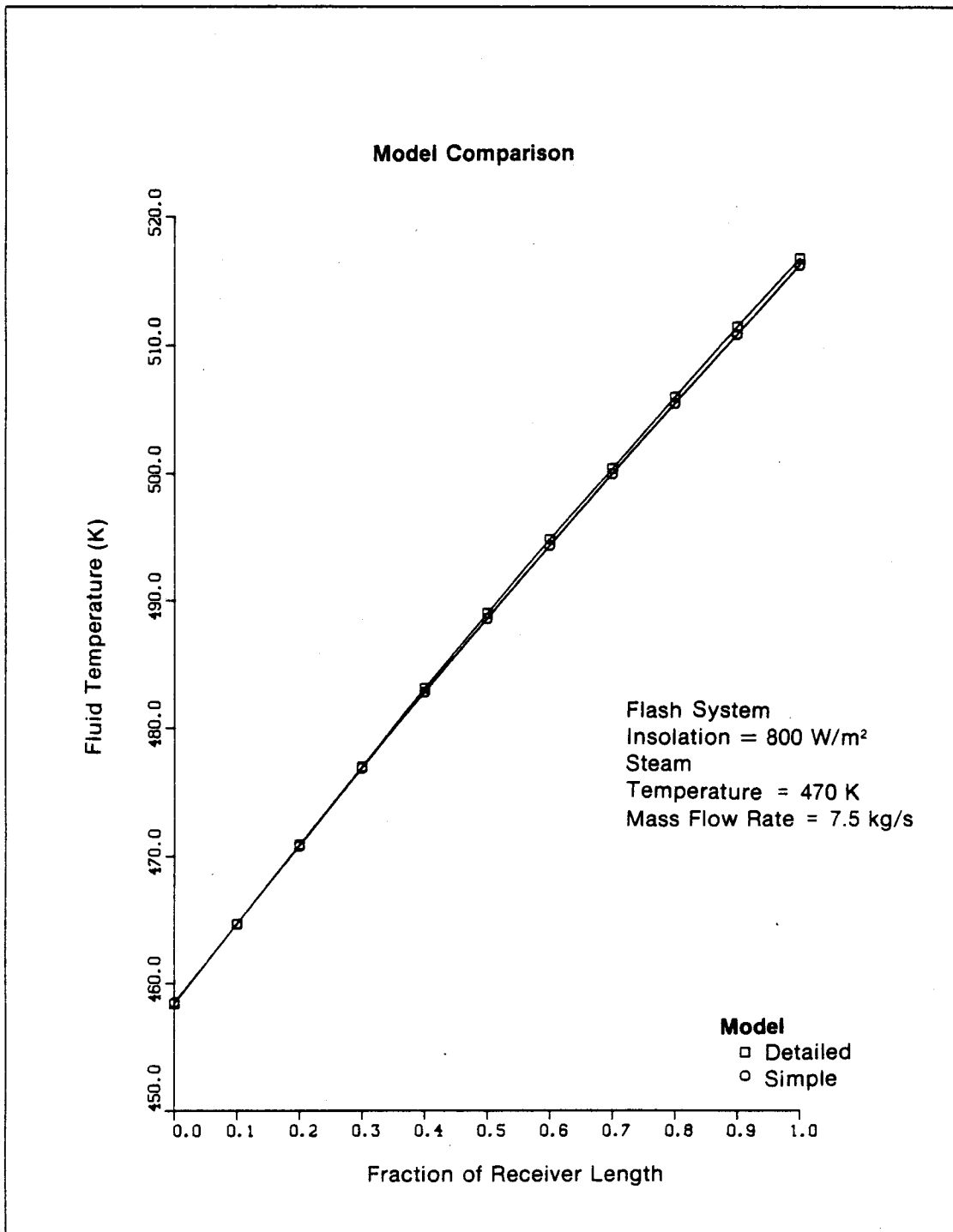
Figure A-4. Predicted Fluid Temperature vs. Position Along Receiver Using Simple and Detailed Collector Models (Flash System)
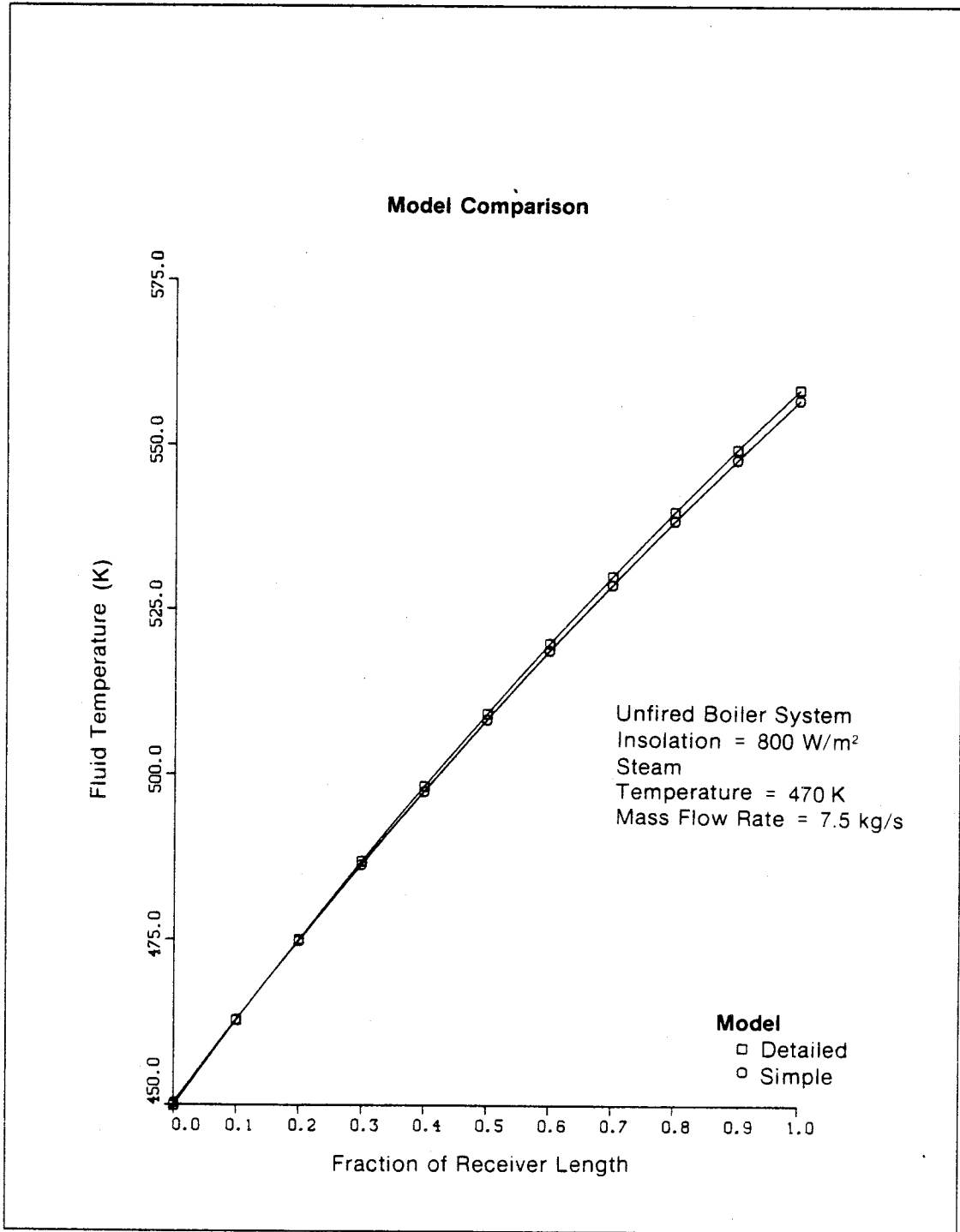
Figure A-5. Predicted Fluid Temperature vs. Position Along Receiver Using
Simple and Detailed Collector Models (Unfired Boiler System)

Figure A-3 illustrates why it is necessary to subdivide the receiver tube. Unlike a sensible heat process, the temperature profile for the in situ system is far from linear, and the average fluid temperature is higher than the average of the inlet and outlet temperatures. Using the average of the extreme temperatures would overestimate the performance of the direct-boiling collector.

The change of enthalpy (ΔH) along a segment of the collector is calculated from

$$\Delta H = \frac{\eta A_c I}{m} \frac{\Delta x}{L} \quad , \tag{A-45}$$

where L is the length of the collector string. The receiver tube is divided arbitrarily into 100 segments. The reported collector performance data are derived from test results using a heat-transfer oil and, in fact, are strictly valid only for that fluid. A fluid such as water with better heat-transfer characteristics than an oil would show higher performance than that reported because improved heat transfer would reduce the temperature of the receiver tube. This effect was illustrated in Figs. 4-51 to 4-53 and is documented for a larger range of variables in Table A-2. This effect is not accounted for in the simple collector model. As would be expected, the difference between the average receiver tube wall temperature (the figures show the outer surface) and the average bulk fluid temperature increases with increasing insolation (because since the overall resistance to heat transfer is relatively constant, the temperature differential is proportional to heat flux) and decreases with increasing steam temperature and mass flow rate (because of increasing Reynolds number). The increased difference between the tube wall and bulk fluid temperatures of the oil system compared to the direct-boiling system for a given fluid temperature accounts for about 1% of the reduced performance of the oil system.

Pressure drop across a segment of the collector is assumed to be the average of the pressure drop corresponding to the input and output states. Thus,

$$\Delta P_c = \frac{\Delta P_i/\Delta x + \Delta P_o/\Delta x}{2} \Delta x \quad . \tag{A-46}$$

Computationally, the enthalpy and pressure expressions are iteratively solved by initially assuming the outlet state is the input state. Equations A-45 and A-46 are used to obtain the final outlet states through successively better approximations.

A.8 HEAT LOSS TO ENVIRONMENT FROM TRANSPORT PIPING

The heat loss from the piping and manifolds is calculated using a thermal network similar to the network used for the detailed collector (see Fig. A-6), except that a single average fluid temperature over the length of the piping run (T_F) is assumed equal to the average of the inlet and outlet temperature in the piping length. The wall (T_W) and outer insulation surface temperatures (T_{INS}) are determined from the following energy balance equations:

Ambient

q_2 q_3

Convective Conductance
$(U_4 = \pi \times k_{air}\, Nu_{wind})$

Radiative Conductance
$[\,U_5 = \sigma\pi\epsilon_{ins} \times d_{oi}\,(T_{ins}^{2} + T_{sky}^{2})\,(T_{ins} + T_{sky})\,]$

Outside of
Insulation (T_{ins})

Insulation Conductance,
$U_3 = 2\pi \times k_i /\ln(d_{oi}/d_o)$

Inside of
Insulation

Wall Conductance
$[\,U_2 = 2\pi \times k_p /\ln(d_o/d_i)\,]$

Inside Pipe Wall (T_w)

Film Conductance
$(U_1 = \pi \times k_i Nu_i)$

Fluid (T_f)

q_1

x

r_i

r_o

r_{oi}
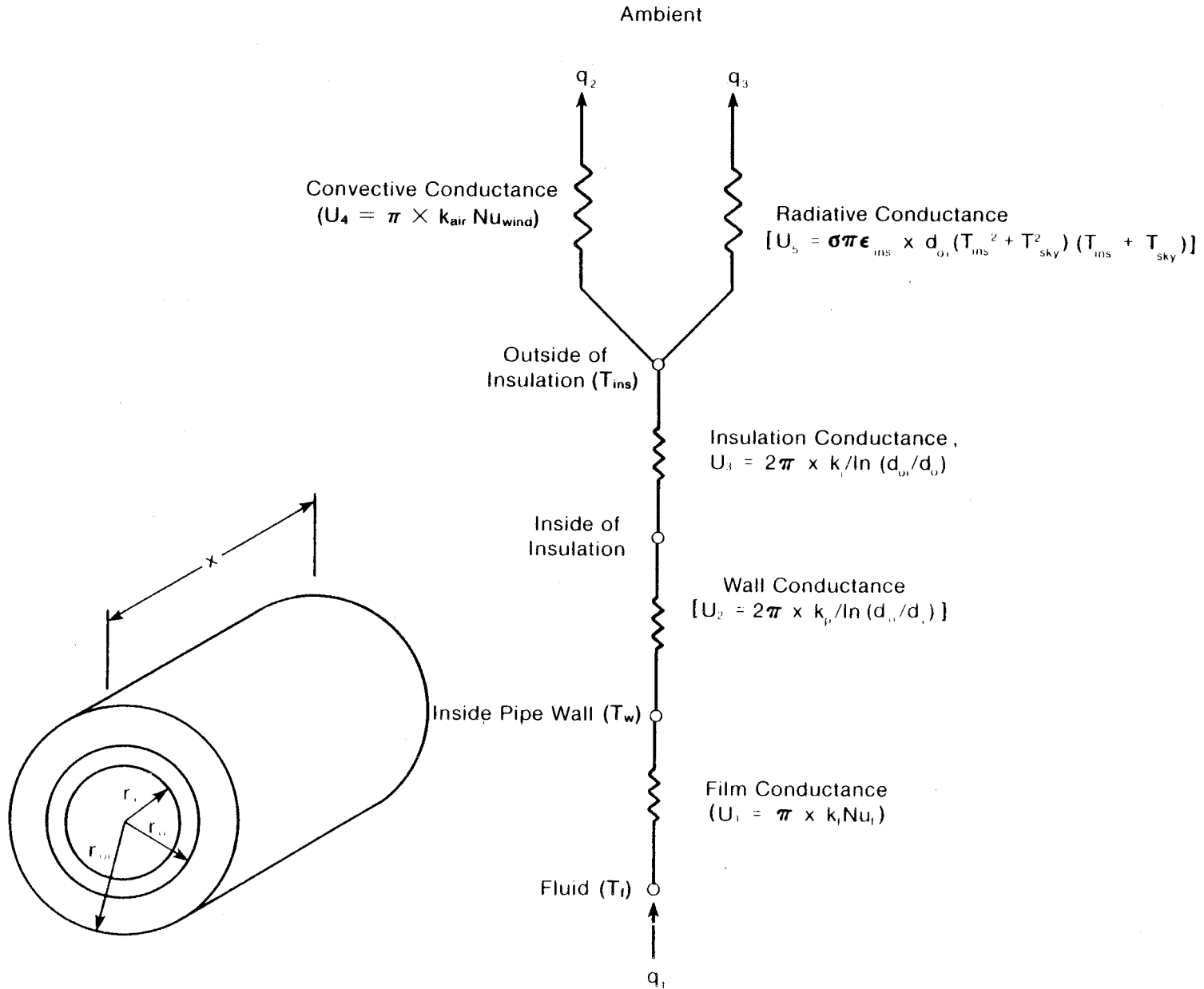
Table A-2. Receiver Tube and Fluid Temperatures

System	Insolation (W/m^2)	Steam Temperature (K)	Mass Flow Rate (kg/s)	Average Tube Wall Temperature (K)	Average Fluid Temperatue (K)	Difference (K)
In situ	1000	495	10	497.1	494.9	2.2
Flash				511.8	509.5	2.3
Oil				537.0	527.6	9.4
In situ	1000	495	7.5	496.4	494.0	2.4
Flash				517.0	514.2	2.8
Oil				546.0	534.2	11.8
In situ	1000	470	7.5	473.9	471.4	2.5
Flash				496.8	493.8	3.0
Oil				530.2	517.4	12.8
In situ	1000	395	7.5	418.2	415.5	2.7
Flash				436.9	433.2	3.7
Oil				486.8	470.5	16.3
In situ	800	470	7.5	473.2	471.1	2.1
Flash				490.5	488.2	2.3
Oil				516.1	506.0	10.1
In situ	600	470	7.5	472.4	470.8	1.6
Flash				484.2	482.6	1.6
Oil				502.0	494.7	7.3

$$q_1 = U_1 \ (T_F - T_W) = \frac{U_2 \ U_3}{U_2 + U_3} \ (T_W - T_{INS}) \quad , \text{ and} \qquad (A-47)$$

$$q_1 = q_2 + q_3 = U_1(T_F - T_W) = U_4(T_{INS} - T_A) + U_5(T_{INS} - T_{SKY}) \quad . \quad (A-48)$$

Since U_1, U_4, and U_5 are, in general, functions of unknown temperatures, estimates for T_{INS} and T_W are made in the calculation of U_1, U_4, and U_5. Then Eqs. A-47 and A-48 are solved for a new estimate of T_{INS} and T_W. The conductances are recalculated with each successively better estimate until the current and previous estimates agree to within the required accuracy. Then q_1 (Eq. A-47) can be calculated to determine heat loss from the piping length.

APPENDIX B

THERMAL-FLUID TRANSPORT CONSIDERATIONS

B.1 FLOW REGIMES IN HORIZONTAL, TWO-PHASE FLOW

The characteristic distributions of the liquid-gas interface of a fluid or fluids flowing in two phases are termed flow regimes. A commonly used classification of flow regimes for horizontal flow is illustrated in Fig. B-1 (Hewitt and Hall-Taylor 1970).
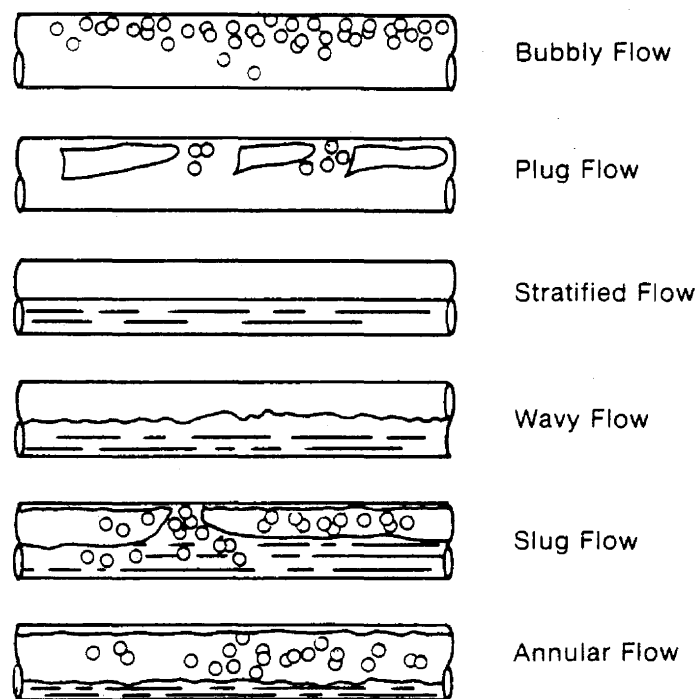
Figure B-1. Flow Patterns in Horizontal Flow

In bubbly flow, the gas phase is distributed in discrete bubbles within a liquid continuum. For horizontal flow the bubbles tend to collect in the upper part of the channel. As the gas flow is increased, the bubbles coalesce and plug flow develops. The bubbles are characteristically bullet-shaped but are somewhat asymmetric. The liquid layer separating the gas bubbles from the wall is thinner at the top of the channel than at the bottom.

For low liquid and gas velocities, the separation of the two phases is completed: the liquid flowing at the bottom of the channel and the gas at the top. As the gas velocity is increased in stratified flow, large surface waves build up on the liquid layer causing a transition to wavy flow. As the gas velocity is further increased in the wavy flow region, the waves eventually become large enough to reach the top of the channel. These waves are propagated at high velocity and wet the entire channel surface. The intermittent

slug-flow regime develops. Liquid droplets can be entrained in the vapor phase. As the gas velocity increases still further, the slugs become pierced with a gas core and the flow becomes essentially annular, with a thicker film at the bottom of the channel than at the top.

Predicting flow regimes is important because of the variation in fluid transport properties in different regions. Identification of the two-phase flow pattern also increases physical understanding and allows some general predictions to be made regarding the stability of the system.

Usually flow patterns are plotted on flow regime maps. Several maps have been proposed; for instance, Baker's diagram (1954) is an early map still widely used in the petroleum industry. The validity of a flow map is enhanced if the data on which it is based correspond closely to the desired application. The range of system variables considered in this study for boiling flow in the receiver tube of a parabolic trough solar collector was given in Table 3-1.

The map proposed by Taitel and Dukler (1976) was used to predict the flow regimes in this report. The map is based on a theoretical analysis of flow pattern transitions and was shown in Fig. 7-2. No differentiation is made between slug, plug, or elongated bubble flows, which are all considered variations of intermittent flow. Taitel and Dukler's map correctly predicts the trends of a map by Mandhane et al. (1974) which was based upon a large bank of air/water flow data. Taitel and Dukler's map, unlike Mandhane's map, correctly predicts the variation of transition boundaries for different fluid properties and thus is more applicable for steam/water flows.

To prevent burnout of the receiver tube, i.e., to ensure the tube wall remains completely wet at all times, operations should not be carried out in the stratified or wavy flow regimes. If the wall drys out, hot spots could result which would degrade the selective surface and produce instabilities from water flashing to steam upon contact with a hot, dry surface. Scale buildup is also more likely under such circumstances. Operations in the bubbly, intermittent, or annular flow regions will ensure that the tube wall is covered with a liquid film at all times. Taitel and Dukler also show that small degrees of inclination cause pronounced changes in transition boundaries. Downward inclinations cause the liquid to move more rapidly, have a lower level, and require higher gas and liquid flow rates to cause a transition from stratified flows. The intermittent flow region shrinks substantially. Conversely, flow at slight upward angles causes intermittent flow to take place over a much wider range of flow conditions. Using the in situ concept, the collector field should be designed with a slight upward slope. The map, however, cannot account for important variables, such as entrance effects (Hewitt and Hall-Taylor 1970).

B.2 HEAT-TRANSFER AND PRESSURE-DROP CORRELATIONS

B.2.1 Single-Phase, Pressure-Drop Correlations

The formula developed by Colebrook,

$$\frac{1}{\sqrt{f}} = -0.86 \, \ell n \left[\frac{\varepsilon/d}{3.7} + \frac{2.51}{Re\sqrt{f}} \right] \tag{B-1}$$

is used to determine the single-phase friction factor (Streeter 1966). The formula is written in terms of the Moody friction factor f, the Reynolds number Re, the inner diameter of the tube d, and the relative roughness of the tube surface ε. The pressure drop per unit length, $\Delta P / \Delta x$, is calculated from the relation

$$\frac{\Delta P}{\Delta x} = \frac{\rho f \, \bar{u}^2}{2d} \quad , \tag{B-2}$$

where $\bar{u}$ is the average liquid velocity over the conduit cross section and ρ is fluid density.

B.2.2 Two-Phase Flow, Pressure-Drop Correlations

Dukler et al. (1964) developed several correlations for frictional two-phase pressure drop by an approach employing similarity analysis. A particular case was based upon the homogeneous, no-slip model. This model assumes that the liquid and gas flow at equal velocities, and that the properties of the two-phase mixture can be defined in terms of properties of the liquid and gas, together with the volumetric void fraction, x_v, calculated from

$$x_v = \frac{x_m v_g}{x_m v_g + (1 - x_m) v_f} \quad , \tag{B-3}$$

where x_m is the mass quality and v_f and v_g are the liquid and gas specific volumes, respectively.

Using the assumption of homogeneous flow, the mixture no-slip density ρ_{NS} can be expressed in terms of the liquid ρ_f and gas ρ_g densities by

$$\rho_{NS} = \rho_f (1 - x_v) + \rho_g x_v \quad . \tag{B-4}$$

The mixture no-slip viscosity is defined similarly in terms of the liquid μ_f and gas μ_g viscosities:

$$\mu_{NS} = \mu_f (1 - x_v) + \mu_g x_v \quad . \tag{B-5}$$

Single-phase Reynolds number and friction factor relations, expressed in terms of properties of the mixture, are used to calculate two-phase frictional pressure drops. Thus, the Reynolds number of the mixture Re_{NS} is given by

$$Re_{NS} = \frac{Gd}{\mu_{NS}} \quad , \tag{B-6}$$

and the friction factor is calculated using the Colebrook relation for rough pipes:

$$\frac{1}{\sqrt{f_{NS}}} = 0.86 \, \ell n \left[\frac{\varepsilon/d}{3.7} + \frac{2.51}{Re_{NS}\sqrt{f_{NS}}} \right] \quad . \tag{B-7}$$

(The use of a friction factor for rough pipes introduces considerable conservatism into the pressure-drop correlation. For instance, two-phase frictional pressure drop increases on the order of 30%. Most experimental data is gathered and correlated using a "smooth" pipe friction factor.) Thus, the pressure drop per unit length of the mixture $(\Delta P/\Delta x)_{NS}$ is

$$\frac{\Delta P_{NS}}{\Delta x} = \frac{\rho_{NS} f_{NS} \, u^2_{NS}}{2d} \quad . \tag{B-8}$$

By comparison with experimental data, Dukler et al. (1964) show the validity of the simple, no-slip correlation. The correlation appears particularly appropriate for the calculation of pressure drop in the slug and plug flow regimes.

Using a large bank of experimental data, Mandhane et al. (1977) carried out a critical evaluation of the predictive methods available for the calculation of two-phase pressure drop in horizontal pipes. A series of recommended correlations, depending on the flow regime, was published. The Dukler (1964) correlation was judged as the best overall method to predict two-phase pressure drops. In addition, Dukler's correlation for the bubble and slug flow regimes rated very high in comparison with all the other correlations investigated, and it showed reasonable agreement for flow in the annular region.

Homogeneous flow can be assumed for low steam qualities and moderate pressures as considered in this study. Consequently, the Dukler correlation is appropriate under these conditions and is used to calculate two-phase pressure drops in this report.

The Dukler correlation can be extended to calculate pressure drop under boiling flow conditions that occur in the collector receiver tube. Average fluid properties are used over a specified length of tube. This assumption is particularly valid in this report when temperature increase per length of tube is relatively small. The work by J.R.S. Thom (1964) can be compared to calculations using the Dukler correlation. Thom generated a series of curves that directly calculate pressure drop from the onset of boiling to the outlet conditions in terms of liquid phase pressure drop. For instance, the two-phase pressure drop at 10% exit quality and 1724 kPa (250 psia) pressure is 6.3 times the liquid phase pressure drop. The difficulty with these correlations is that they were determined from data collected at conditions of high flux typical of steam generators. The effective friction factor for boiling in a parabolic trough receiver at very low heat flux should be somewhat lower. Also, the correlations are stated only at relatively high pressures. The original paper on which Thom based his work can be referenced for conditions of lower pressure (Martinelli and Nelson 1948).

As an example of the comparison between the no-slip and Thom correlations, consider the case of insolation equal to 1000 W/m², total collector flow rate equal to 7.5 kg/s, and steam delivery temperature equal to 470 K. Boiling occurs at 25% of the collector length, exit quality is 0.1417, and average pressure in the receiver tube is 1580 kPa (229 psia). Calculated pressure drop along the boiling length is 28 kPa (4.4 psi). The Thom multiplier is 9.2 and single-phase pressure drop is 38 Pa/m. This yields a total pressure drop of 28.8 kPa, similar to previous results.

Another important outcome of Thom's work is a method for calculating the degree of slip between the liquid and gas phases. Bernoulli's equation indicates that under a given pressure differential, lower density fluids travel faster than higher density fluids in a mixture. The slip ratio is the ratio of gas to liquid velocities. This ratio increases as pressure is reduced, is almost constant at a given pressure, and is independent of quality. Thus, at 14.7 psia and 250 psia, the slip ratios are 6.5 and 2.5, respectively. The slip ratio provides some meaning to the assumptions underlying the homogeneous model.

Because of the slip phenomenon, the no-slip model is a somewhat conservative method for predicting burnout. The area void fraction of the liquid phase is higher than would be predicted assuming homogeneous phases. As quality is increased, the ratio of phase velocities remains constant. However, the relative velocity between the phases is approximately proportional to quality.

The pressure drop correlations discussed apply only to calculations of frictional pressure drop and do not account for momentum or gravitational effects. In a horizontal tube, gravity has no effect. Pressure drop due to momentum changes can be stated as follows:

$$\Delta P_{acc} = G^2(u_o - u_i) , \qquad\qquad (B-9)$$

where G is the mass velocity, and u_o and u_i are the outlet and inlet fluid velocities, respectively.

Pressure differentials caused by momentum changes can be significant in industrial steam generators, where fluxes are high and tubes are short. However, in the cases considered here the opposite conditions apply, and the acceleration pressure drop is negligible compared to the frictional pressure drop.

The homogeneous model is extended to calculate pressure drop through singularities—bends, valves, etc. Bergles et al. (1981) conclude that while no correlation is generally applicable, the homogeneous model is adequate for several cases. Flow coefficients, as stated in Crane (1976), are used to calculate equivalent lengths of straight pipe.

B.2.3 Single-Phase Heat Transfer Inside Horizontal Cylinder

A formula by Kays and Crawford (1980, p. 243), valid for Prandtl numbers near 1.00, is used to calculate liquid phase, heat-transfer coefficients for water:

$$Nu = \frac{0.152 \ Re^{0.9}Pr}{0.833 \ [2.25 \ ln(0.114 \ Re^{0.9}) + 13.2 \ Pr - 5.8]} \quad . \qquad (B-10)$$

This formula for water, over the range of interest, gave values intermediate between the Dittus-Boelter equation and correlations proposed by Kays (1966, p. 173).

For heat-transfer oils at higher Prandtl numbers, a correlation by Petukhov is used (Kays and Crawford, 1980, p. 245):

$$Nu = \frac{RePr \ (C_f/2)}{1.07 + 12.7(Pr^{2/3} - 1) \ \sqrt{(C_f/2)}} \quad , \qquad (B-11)$$

and

$$\frac{C_f}{2} = (2.236 \ lnRe - 4.639)^{-2} \quad . \qquad (B-12)$$

All the equations above are for smooth pipe. They are corrected for the effects of surface roughness using a correlation from Kays and Crawford (1980, p. 271):

$$\frac{Nu}{Nu_{smooth}} = \left(\frac{C_f}{C_{f \ smooth}}\right)^n \quad , \qquad (B-13)$$

wheren $n = 0.68 \ Pr^{0.215}$. $\qquad (B-14)$

The friction factor for smooth pipe is calculated using Eq. B-12 and for rough pipes is calculated using the Colebrook relation. Surface roughness increases heat-transfer coefficients for water by about 15%. In the oil systems over a range of Reynolds numbers from 20,000 to 50,000, heat-transfer coefficients increase 12% to 25% due to surface roughness.

B.2.4 Boiling Heat-Transfer Correlation

Bergles et al. (1981) and Tong (1975) recommend the Chen correlation for the calculation of heat-transfer coefficients under conditions of two-phase, forced convection and saturated nucleate boiling. The overall two-phase, heat-transfer coefficient (h_{TP}) is the sum of components derived from macroscopic, forced convection heat transfer (h_c), and from microscopic convection through the liquid film by bubble nucleation (h_n). Thus

$$h_{TP} = h_c + h_n \quad , \qquad (B-15)$$

where

$$h_c = 0.023 \left[\frac{m(1 - x_m)d}{\mu_f} \right]^{0.8} \left[\frac{\mu_f C_{pf}}{k_f} \right]^{0.4} \left(\frac{k_f}{d} \right) F \; , \text{ and} \qquad \text{(B-16)}$$

$$h_n = 0.00122 \frac{k_f^{0.79} C_{pf}^{0.45} \rho_f^{0.49}}{\sigma^{0.5} \mu_f^{0.29} \Delta H_{fg}^{0.24} \rho_g^{0.24}} \Delta T_{SAT}^{0.24} \Delta P_{SAT}^{0.75} S \; . \qquad \text{(B-17)}$$

The driving force for nucleation is the degree of superheat between the pipe wall and the bulk fluid temperature. The model assumes that nucleation occurs when the bulk fluid temperature equals the saturation temperature. ΔT_{SAT} is the difference between the inside wall temperature and the bulk fluid temperature at saturation. ΔP_{SAT} is the difference in vapor pressures corresponding to the wall and bulk fluid temperatures at saturation. ΔH_{fg} is the latent heat of vaporization at the bulk fluid temperature. All other fluid properties are evaluated at bulk fluid conditions.

The parameter F is a function of the Martinelli parameter, X_{tt}. The parameter S is a function of the two-phase Reynolds number, Re_{TP}. Bergles et al. (1980) have curve fit the data of Chen.

$$F = 1 \text{ for } 1/X_{tt} \leqslant 0.1, \text{ and} \qquad \text{(B-18)}$$

$$F = 2.35 \; (1/X_{tt} + 0.213)^{0.736} \text{ for } 1/X_{tt} > 0.1, \qquad \text{(B-19)}$$

where

$$X_{tt} = \left(\frac{1 - x}{x} \right)^{0.9} \left(\frac{\rho_g}{\rho_f} \right)^{0.5} \left(\frac{\mu_f}{\mu_g} \right)^{0.1} \; , \qquad \text{(B-20)}$$

$$S = \frac{1}{1 + 2.53 \times 10^{-6} \; Re_{TP}^{1.17}} \; , \text{ and} \qquad \text{(B-21)}$$

$$Re_{TP} = Re_f \; F^{1.25} \; . \qquad \text{(B-22)}$$

B.2.5 Natural and Forced Convection Heat Loss from Horizontal Cylinder to Environment

Fand et al. (1977) tested various correlations of natural convection heat transfer from horizontal cylinders to various fluids. The correlation by Morgan was chosen as the most accurate correlation for heat transfer to air. This correlation is stated as

$$Nu_f = CRa_f^m \; , \qquad \text{(B-23)}$$

where the values of C and m depend upon the range of the Rayleigh number of the air, Ra_f, shown in Table B-1.

Table B-1. Morgan Correlation
for Natural Convec-
tion Heat Loss from
Horizontal Cylinders

Range of Ra_f	C	m
10^{-4} to 10^{-2}	0.675	0.058
10^{-2} to 10^{2}	1.02	0.148
10^{2} to 10^{4}	0.850	0.188
10^{4} to 10^{7}	0.480	0.250
10^{7} to 10^{12}	0.125	0.333

Both the Nusselt and Rayleigh numbers are evaluated using fluid properties at the mean film temperature. This correlation is used to calculate heat loss from the collector-receiver tube and fluid transport piping under conditions of no wind.

For heat transfer from piping and the receiver to the atmosphere under windy conditions, another correlation recommended by Morgan, and quoted in Kays and Crawford (1980), is used. The Nusselt number is based upon the cylinder diameter, and the Reynolds number is based upon cylinder diameter and upstream normal velocity; fluid properties are evaluated using a film temperature equal to the average of wall and free-stream values.

$$Nu = C_1 Re^{C_2} \quad .$$

(B-24)

The constants C_1 and C_2 are given in Table B-2.

Table B-2. Morgan Correlation for Forced
Convection Heat Loss from
Horizontal Cylinders

R_e		C_1	C_2
10^{-4}	to 4×10^{-3}	0.437	0.0895
4×10^{-3}	to 9×10^{-2}	0.565	0.136
9×10^{-2}	to 1	0.800	0.280
1	to 35	0.795	0.384
35	to 5×10^{3}	0.583	0.471
5×10^{3}	to 5×10^{4}	0.148	0.633
5×10^{4}	to 2×10^{5}	0.0208	0.814

SΞRI ❀ ──

B.2.6 Conductive and Convective Heat Transfer Across Annular Air Gap

A correlation by Kuehn and Goldstein (1978), which was also used by Gee et al. (1980), is used to calculate conductive and convective heat losses from the receiver tube to the glass cover through an air gap at atmospheric pressure. The Nusselt number for convection through the receiver boundary layer is

$$Nu_i = \frac{2}{\ln\left\{1 + \frac{2}{\left[\left(0.5\ Ra_i^{1/4}\right)^{15} + \left(0.12\ Ra_i^{1/3}\right)^{15}\right]^{1/5}}\right\}} \qquad (B-25)$$

The Rayleigh number Ra_i is based on the receiver outer diameter d_i and the difference between the wall temperature T_i and the bulk fluid temperature T_b. Fluid properties are evaluated at the average of these two temperatures.

Similarly, the Nusselt number for convection through the glass envelope boundary layer is

$$Nu_o = \frac{-2}{\ln\left\{1 + \frac{2}{\left[\left(Ra_o^{1/4}\right)^{15} + \left(0.12\ Ra_o^{1/3}\right)^{15}\right]^{1/15}}\right\}} \qquad (B-26)$$

The Rayleigh number Ra_o is based on the envelope inner diameter d_o and the difference between the envelope and bulk fluid temperatures, T_o and T_b, respectively. As before, fluid properties are calculated at the average of these two temperatures. The relation cannot be evaluated until T_b is known, found by equating heat transfer at each cylinder:

$$\frac{T_b - T_o}{T_i - T_b} = \frac{Nu_i}{Nu_o} \qquad (B-27)$$

An iterative procedure is employed to yield successively better estimates for the value of T_b.

The overall Nusselt number for convective heat transfer is

$$Nu_{conv} = \left[\frac{1}{Nu_i} + \frac{1}{Nu_o}\right]^{-1} \qquad (B-28)$$

The Nusselt number for conduction is

$$Nu_{cond} = \frac{2}{\ln\left(\frac{d_o}{d_i}\right)} \qquad (B-29)$$

These equations yield an overall Nusselt number of heat transfer between the receiver and glass envelope of

$$Nu = \left[(Nu_{cond})^{15} + (Nu_{conv})^{15} \right]^{1/15} \quad . \qquad (B-30)$$

APPENDIX C

PROPERTIES OF AIR

The equations used to calculate the properties of air as a function of absolute temperature are listed below. They are based upon those presented by Hickox and Gartling (1977).

$$\rho = \frac{353.4}{T} \ (kg/m^3) \ ,$$

$$\beta = \frac{1}{T} \ (1/K) \ ,$$

$$\mu = 1.459 \times 10^{-6} \left(\frac{T^{1.5}}{T + 110.4} \right) \ (kg/ms) \ ,$$

$$Cp = 937 + 0.191T \ (J/kgK) \ , \text{ and}$$

$$k = \frac{2.648 \times 10^{-3} \ T^{0.5}}{1 + \left(\frac{245.4}{T} \right) (0.1)^{-12/T}} \ (W/mK) \ .$$

SERI

APPENDIX D

PROPERTIES OF HEAT-TRANSFER FLUID

A heat-transfer fluid with properties similar to Therminol 60 was the most suitable fluid for this analysis. Therminol 60 has a somewhat lower temperature tolerance than such fluids as Therminol 66, which has been used in operating unfired-boiler systems, but it has much improved thermal transport characteristics. Curve fits of the physical properties for Therminol 60 were supplied by the manufacturer (and were converted to SI units):

$$\rho = 1191.6 - 0.6719 \, T \; (kg/m^3),$$

$$k = 0.1549 - 7.79 \times 10^{-5} \, T \; (W/m \; K),$$

$$C_p = 495.9 + 3.731 \, T \; (J/kg \; K), \text{ and}$$

$$\nu = 10^{-6} \times [10^{10^{(9.891 - 1.739 \, \ln T)}} - 0.79] \; (m^2/s).$$

APPENDIX E

METHODOLOGY FOR CALCULATING ANNUAL ENERGY DELIVERY

Annual energy delivery of the solar system is calculated using an approach similar to Rabl's (1981) long-term averaging method for predicting the yearly average performance of solar collectors. This technique can be extended to a collector system by using several parameters that are derived from an assumed constant inlet temperature and a linear expression (in temperature) for the instantaneous collector performance. This assumed expression for the collector performance is given by

$$(\dot{Q}_u)_{inst.} = F [\eta I - U(T_{if} - T_a)] \quad , \tag{E-1}$$

where $(\dot{Q}_u)_{inst.}$ is the instantaneous rate of useful energy delivered per unit area of the collector, F is the collector efficiency factor (F=1 when no heat exchanger is present), η is the optical efficiency, I is the incident solar radiation normal to the aperture, U is the overall collector heat loss term, and $(T_{if} - T_a)$ is the temperature difference between the inlet fluid temperature (T_{if}) and the outside ambient air temperature (T_a) as defined by Rabl (1981). The collector cut off flux (X)* can be described by the expression

$$X = \frac{U (T_{if} - T_a)}{\eta} \quad . \tag{E-2}$$

The annual energy delivered is then determined to have the form:

$$(Q_u)_{annual} = F\eta G(X, \overline{I}, L) \quad , \tag{E-3}$$

where G is a function as determined by Rabl (1981), $\overline{I}$ is the yearly average direct normal irradiance (kW/m^2) during daylight hours, and L (in radians) is the latitude at which the collector is located.

As mentioned earlier and as described in a recent publication (Gordon and Rabl 1981), the method can be extended to fields of collectors by appropriately modifying the parameters in the energy delivery equation for the collector to account for piping losses and the presence of a heat exchanger as exists in an unfired boiler system. Thus for a collector field, an equation analogous to Eq. E-1 can be written as

$$\frac{\dot{Q}_u}{I} = F[\eta' - \frac{U'}{I} (T_{fi} - T_a)] \quad , \tag{E-4}$$

where η' and U' are defined in terms of piping loss parameters, flow rates, and fluid heat capacities. Expressions for η' and U' are given in terms of η and U along with other systems parameters in Beckman (1978).

---

*The flux below which the collector cannot deliver useful energy.

In situations where U and the fluid heat capacities are functions of fluid phase and temperature, some complications arise; the system parameters investigated in this report are inconsistent with the idealizations in Gordon and Rabl's (1981) analysis. For example, the assumption of constant mass flow and constant field inlet temperature as assumed by Gordon and Rabl (1981) is not true for the systems studied here. The major reason for this difference is that the solar systems investigated are connected in parallel with the conventional steam generator. Hence, the makeup water mass flow rate will vary even though the collector field mass flow rate is constant. On the other hand, the inlet to the collector field, downstream of the mixing valve (the exit from the heat exchanger in an oil system), will experience constant mass flow, but the corresponding temperature will not be constant, although the temperature variation is fairly small.

To overcome these difficulties, a method for determining values for FU' and Fη' was defined. Specifically, Fη' and FU' were determined directly from steady-state calculations of system operations for each of the three systems. In this approach, a steam delivery temperature and a corresponding optimal flow rate for the specific system were first assumed. Then a corresponding set of system efficiencies for the fluid inlet temperature to the collector field, for various incident fluxes, was obtained from the calculated steady-state data. Consistent with the steady-state analysis presented in Sec. 4.0, two system efficiency measures were used: gross system efficiency, and net system efficiency, which includes the effects of parasitic pumping power. A linear regression was used to determine the best fit of these data corresponding to each particular steam temperature to produce an equation in the form of Eq. E-2. The data appear quite linear as can be seen in Figs. E-1, E-2, and E-3. Then for each of five steam temperatures, two system efficiency measures, and three system types, specific values of Fη' and FU' were determined. The annual energy delivery was then calculated from Eq. E-3 (as presented by Rabl 1981) where Fη is replaced by Fη' and X is replaced by X', and defined as

$$X' = \frac{FU'\,(T_{if} - T_a)}{F\eta'} \; . \tag{E-5}$$

Using Eq. E-3, two approaches were used to produce an effective inlet temperature for the annual energy calculation. In the first approach, the fluid inlet temperature was assumed to be the makeup water temperature (always constant) with the collector mass flow corresponding to the assumed average flux and required steam delivery temperature. With this approach, the numerical values for FU' and Fη' can be dramatically different from those values normally associated with the instantaneous collector efficiency. The second approach used the temperature just downstream of the mixing valve corresponding to the assumed average flux and required steam temperature.
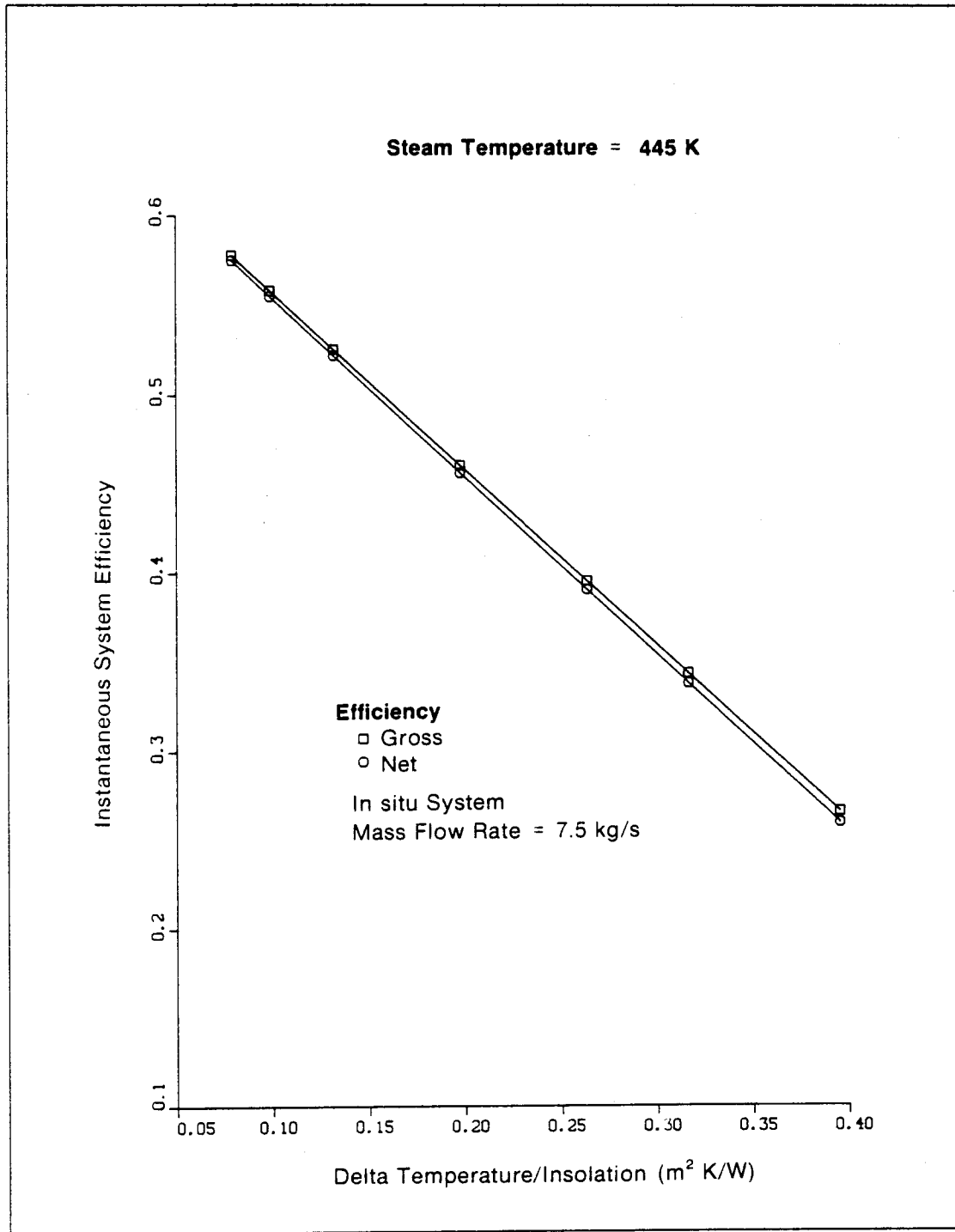
Figure E-1.   Instantaneous System Efficiency vs. $\Delta T/I$,
               (In Situ System, T_s = 445 K)

Steam Temperature = 445 K
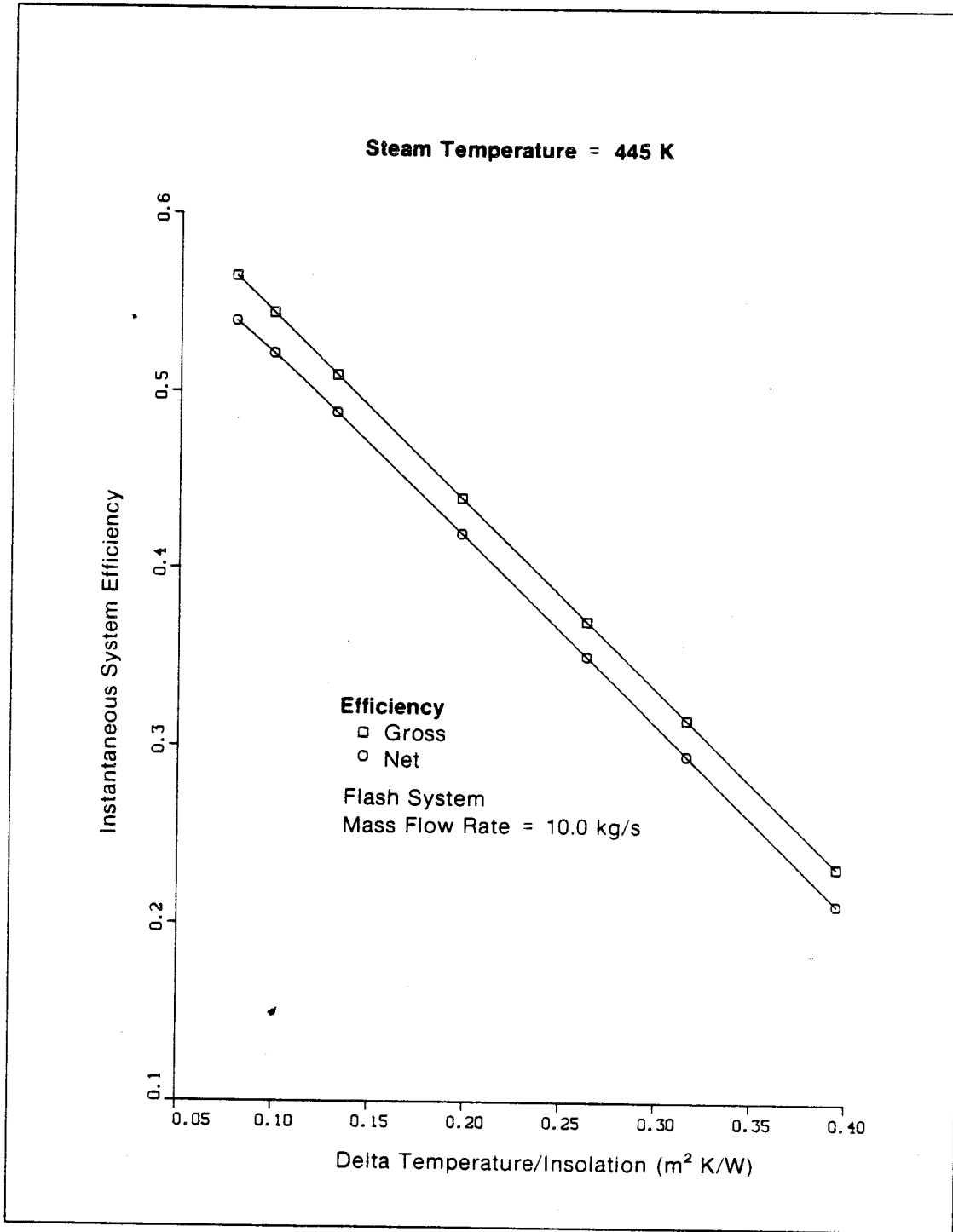
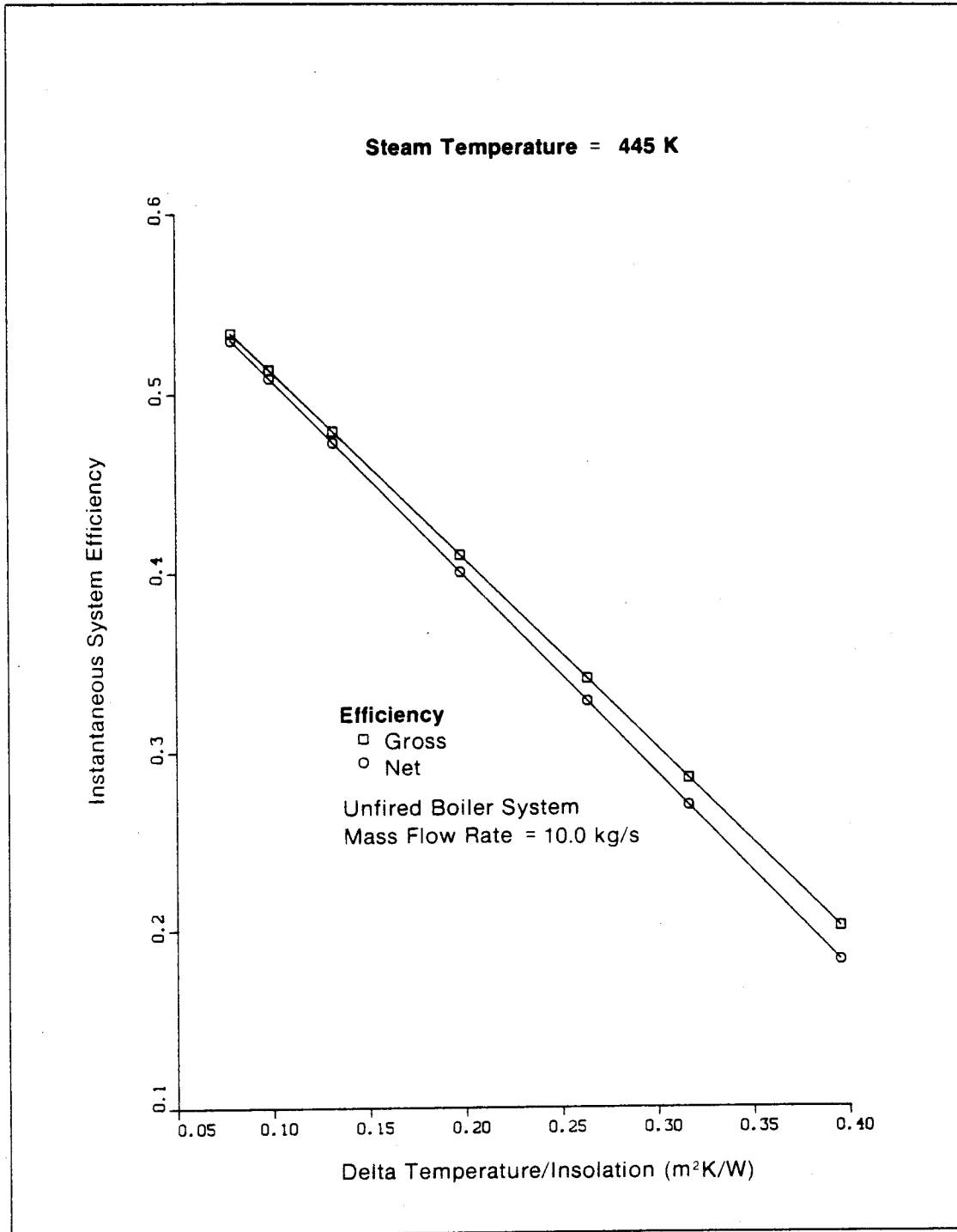Figure E-2. Instantaneous System Efficiency vs. $\Delta T/I$, (Flash System, T_s = 445 K)

Figure E-3. Instantaneous System Efficiency vs. $\Delta T/I$, (Unfired Boiler System, T_s = 445 K)

Predicted results of delivered annual energy, using each of the above measures of average inlet fluid temperature, were extremely close (differences of less than 0.5% were typically predicted for any given case). For several reasons, the results presented in this report were generated using the second procedure. First, the second approach yielded a slightly more conservative result (i.e., slightly less favorable to the in situ system). Second, the variation in inlet temperature showed only small variations, which indicates only a small departure from the constant inlet temperature assumption.

Each pair of system parameters corresponding to Eq. E-4, the modified cut-off flux defined by Eq. E-5, and the inlet temperature as determined by the above procedure, are given in Table E-1.

Table E-1. Performance Parameters for Various Systems and Steam Temperatures (T_a = 287 K, I = 0.5 kW/m²)

Steam Temperature (K)	In Situ System					Flash System				Oil System		
	F'	FU'	X (kW/m²)	T_{fi}	Fη'	FU'	X' (kW/m²)	T_{fi}	Fη'	FU'	X' (kW/m²)	T_{fi} (K)
Parameters Corresponding to Gross System Efficiency Measure												
395	0.641	0.472	0.078	393	0.630	0.505	0.085	393	0.610	0.530	0.092	393
420	0.644	0.482	0.097	416	0.625	0.510	0.106	417	0.610	0.536	0.114	416
445	0.647	0.493	0.117	440	0.619	0.518	0.129	441	0.610	0.545	0.136	440
470	0.649	0.507	0.138	464	0.612	0.524	0.153	465	0.610	0.551	0.159	463
495	0.649	0.521	0.161	488	0.604	0.531	0.178	490	0.612	0.567	0.186	487
Parameters Corresponding to Net System Efficiency Measure												
395	0.646	0.423	0.069	393	0.641	0.453	0.075	393	0.612	0.457	0.079	393
420	0.648	0.432	0.086	416	0.640	0.463	0.094	417	0.612	0.466	0.098	416
445	0.650	0.444	0.104	440	0.640	0.475	0.114	441	0.612	0.477	0.119	440
470	0.650	0.457	0.124	464	0.640	0.488	0.136	465	0.613	0.490	0.145	463
495	0.660	0.470	0.145	488	0.639	0.502	0.159	490	0.613	0.504	0.165	487

Document Control Page	1. SERI Report No. SERI/TR-253-1311	2. NTIS Accession No	3. Recipient's Accession No.

4. Title and Subtitle	5. Publication Date
Steam Generation in Line-Focus Solar Collectors: A Comparative Assessment of Thermal Performance, Operating Stability, and Cost Issues	April 1982
	6.

7. Author(s)	8. Performing Organization Rept. No.
L. M. Murphy, E. K. May	

9. Performing Organization Name and Address	10. Project/Task/Work Unit No.
Solar Energy Research Institute 1617 Cole Boulevard Golden, Colorado 80401	1006.00
	11. Contract (C) or Grant (G) No. (C) (G)

12. Sponsoring Organization Name and Address	13. Type of Report & Period Covered
	Technical Report
	14.

15. Supplementary Notes

16. Abstract (Limit: 200 words) The engineering and system benefits of using direct steam (in situ) generation in line-focus collectors are assessed in this report. The major emphasis of the analysis is a detailed thermal performance comparison of in situ systems with pressurized water systems (which utilize steam flash valves), and with oil systems (which utilize unfired boilers). The analysis model developed for this study is discussed in detail. An analysis of potential flow stability problems is also provided along with a cursory cost analysis and an assessment of freeze protection, safety, and control issues. Results indicated a significant thermal performance advantage over the more conventional oil and flash systems and the flow stability does not appear to be a significant problem. In particular, at steam temperatures of 220°C (430°F) under the chosen set of assumptions, annual delivered energy predictions indicate that the in situ system can deliver 15% more energy than an oil system and 12% more energy than a flash system, with all of the systems using the same collector field. Further, the in situ system may result in a 10% capital cost reduction. Other advantages include improvement in simpler control when compared with flash systems, and fluid handling and safety enhancement when compared with oil sytems.

17. Document Analysis

a. Descriptors Boiling ; Concentrating Collectors ; Cost ; Flow Rates ; Instability ; Low Temperature ; Medium Temperature ; Parabolic Collectors ; Parabolic Trough Collectors ; Performance ; Process Heat ; Solar Collectors ; Solar Flux ; Steam Generation ; Steam Generators ;

Identifiers/Open-Ended Terms: Line-Focus Solar Collectors ; Unfired Boilers ; Steam-Flash Systems

c. UC Categories
59b, 59c, 62e

18. Availability Statement	19. No. of Pages
National Technical Information Service U.S. Department of Commerce 5285 Port Royal Road Springfield, Virginia 22161	171
	20. Price $8.00

Form No. 8200-13 (6-79)